NITROGEN-DONOR LATE TRANSITION METAL COMPLEXES AS ETHYLENE OLIGOMERIZATION CATALYSTS

BY

GEORGE SIMBA NYAMATO

SUBMITTED IN FULFILMENT OF THE ACADEMIC REQUIREMENTS FOR THE DEGREE OF DOCTOR OF PHILOSOPHY IN CHEMISTRY IN THE COLLEGE OF AGRICULTURE, ENGINEERING AND SCIENCE,
UNIVERSITY OF KWAZULU-NATAL
PIETERMARITZBURG

Supervisor: Dr. Stephen O. Ojwach

December 2015

DECLARATION

I, **George Simba Nyamato** declare that;

1. The research reported in this thesis, "**Nitrogen-donor late transition metal complexes as ethylene oligomerization catalysts"** except where otherwise indicated, is my original research.
2. This thesis has not been submitted for any degree or examination at any other university.
3. This thesis does not contain other persons' data, pictures, graphs or other information, unless specifically acknowledged as being sourced from other persons.
4. This thesis does not contain other persons' writing, unless specifically acknowledged as being sourced from other researchers. Where other written sources have been quoted, then:
    a. Their words have been re-written but the general information attributed to them has been referenced.
    b. Where their exact words have been used, then their writing has been placed in italics and inside quotation marks and referenced.
5. This thesis does not contain text, graphics or tables copied and pasted from the Internet, unless specifically acknowledged, and the source being detailed in the thesis and in the References sections.

Signed: …….Date…….

As the candidate's supervisor I have approved this thesis for submission.

Name: …… Signed: ……. Date: ……..…

DEDICATION

This thesis is dedicated to my wife Kerubo- thanks dear for not losing faith in me.

ACKNOWLEDGEMENTS

My profound gratitude to my supervisor, Dr. Stephen O. Ojwach for his patience, guidance and support throughout the course of this project. Your insights and enthusiasm in my study gave me much hope. To Dr. Matthew P. Akerman, thank you for the X-ray crystallography analyses.

I am very grateful to the University of KwaZulu-Natal for financial assistance, without which all these could not have been possible. To the staff in the School of Chemistry and physics, University of KwaZulu-Natal, thank you for your support. To my colleagues in the catalysis research group, thank you for your friendship, support and the great moments we shared.

A special word of thanks to my parents and siblings who supported and encouraged me. Most of all I want to thank my wife, Kerubo-you have been the wind beneath my wings; thank you my dear. To our juniors, Nyamato and Moraa, thanks for your patience and understanding.

PREFACE

Over the past few years, interest has grown in developing a new generation of catalysts with greater selectivity for the desired range of linear α-olefins. At the center of these developments have been late transition metal complexes. The architecture of the ligands in the complex structures plays a crucial role. Although the interplay between electronic and steric properties of the ligands have long been recognized as essential in determining the catalytic performance of these complexes, accurate predictions still remain a major challenge. The main areas of interest are catalyst activity, selectivity and stability. The quest to strike a balance between these key catalyst properties underlies the rationale of this research study. This thesis is made up of seven chapters.

Chapter 1 covers the introduction of olefin catalysis; highlighting the industrial manufacture and commercial applications of olefins and the role played by late-transition metals in these processes. **Chapter 2** reviews the relevant literature on late transition metal catalysts towards ethylene oligomerization reactions. Recent developments associated with late-transition metal complexes, in particular nickel(II), cobalt(II), iron(II) and palladium(II) complexes, are discussed.

Chapter 3 describes the syntheses of 2-(chloromethyl)-6-(pyrazol-1-ylmethyl)pyridine nickel(II), cobalt(II) and iron(II) complexes and their catalytic behaviour in ethylene oligomerization reactions. The study focused on the role of co-catalyst and solvent in ethylene oligomerization reactions using $EtAlCl_2$ and MAO co-catalysts and toluene, hexane and

chlorobenzene solvents. The findings of this chapter have been published in *J. Mol. Catal. A: Chem*., **2014**, 394, 274-282.

Chapter 4 focuses on the syntheses of nickel(II), cobalt(II) and iron(II) complexes of the N^N^O (pyrazolyl)-(phosphinoyl)pyridine ligands and their evaluation as catalysts in ethylene oligomerization reactions. It is noteworthy to point out that the initial target was to synthesize N^N^P phosphine ligands, but these attempts were hampered by *in situ* oxidation of the ligands resulting in the formation of N^N^O phosphinite ligands. Nevertheless, these complexes formed active catalysts in ethylene oligomerization reactions upon activation with $EtAlCl_2$, methylaluminoxane (MAO) and trimethylaluminium ($AlMe_3$) as co-catalysts. The findings of this chapter have been published in *J. Organometal. Chem., **2015**, 783, 64-72.*

Chapter 5 deals with the syntheses of new palladium(II) complexes of potential hemi-labile (imino)pyridine ligands. The generation of the active catalysts for ethylene oligomerization reactions and the use of ^1H NMR spectroscopy and theoretical calculations using density functional theory (DFT) studies to rationalize the reactivity trends of these palladium(II) complexes are described. The findings of this chapter have been published in *Organometallics **2015**, DOI: 10.1021/acs.organomet.5b00860.*

Chapter 6 reports attempts to circumvent hydrolysis of the (imino)pyridine ligands synthesized in chapter 5, when used to prepare their nickel(II) complexes, by reducing the imine ligands to their analogous amines. The syntheses, molecular structures of these new (amino)pyridine nickel(II) complexes and their behavior as ethylene oligomerization catalysts are discussed.

Finally, general conclusions on the key findings of this study and the future prospects are presented in **Chapter 7**.

RESEARCH OUTPUTS

This thesis is based on the following original publications and conference presentations.

Publications:

I. **Nyamato, G. S**.; Ojwach, S. O.; Akerman, M. P. Unsymmetrical (pyrazolylmethyl)-pyridine metal complexes as catalysts for ethylene oligomerization reactions: Role of solvent and co-catalyst in product distribution. *Journal of Molecular Catalysis A: Chemical* ***2014****, 394, 274–282.*

II. **Nyamato, G. S**.; Alam, M. G.; Ojwach, S. O.; Akerman, M. P. (Pyrazolyl)-(phosphinoyl)pyridine iron(II), cobalt(II) and nickel(II) complexes: Synthesis, characterization and ethylene oligomerization studies. *Journal of Organometallic Chemistry* **2015**, 783, 64-72.

III. **Nyamato, G. S**.; Ojwach, S. O.; Akerman, M. P. Packing forces in dichloridobis(3,5-diphenyl-1*H*-pyrazole-*k*N^2)cobalt(II) dichloromethane hemisolvate. *Acta Cryst*. **2014**, C70, 780-783.

IV. **Nyamato, G. S**.; Ojwach, S. O.; Akerman, M. P. (Imino)pyridine palladium(II) complexes: Experimental, theoretical studies and as ethylene oligomerization catalysts. *Organometallics* **2015***,* DOI: 10.1021/acs.organomet.5b00860.

V. **Nyamato, G. S**.; Alam, M. G.; Ojwach, S. O.; Akerman, M. P. Nickel(II) complexes bearing pyrazolylpyridines: Synthesis, structures and ethylene oligomerization reactions. *Applied Organometallic Chemistry* 2015, DOI: 10.1002/aoc.3402.

VI. **Nyamato, G. S**.; Ojwach, S. O.; Akerman, M. P. Ethylene oligomerization studies by nickel(II) complexes chelated by (amino)pyridine ligands: Experimental and density functional theory studies. Manuscript submitted to *Dalton Transactions.*

Conference presentations:

I. George S. Nyamato, Stephen O. Ojwach and Matthew P. Akerman. *(Imino)pyridine palladium(II) complexes: Experimental, theoretical studies and as ethylene oligomerization catalysts*. SACI INORG 2015, Rhodes University, South Africa, **28th June -2nd July 2015**.

II. George S. Nyamato, Stephen O. Ojwach and Matthew P. Akerman. *Unsymmetrical (pyrazolylmethyl)pyridine metal complexes as catalysts for ethylene oligomerization reactions: Role of solvent and co-catalyst in product distribution*. College of Agriculture, Engineering and Science Post-graduate Research Day, UKZN, **27th Oct. 2014**.

III. George S. Nyamato and Stephen O. Ojwach. *Synthesis and characterization of new pyrazolylpyridine late transition metal complexes*. College of Agriculture, Engineering and Science Post-graduate Research Day, UKZN, **01 Nov. 2013**.

ABSTRACT

Compounds 2-(chloromethyl)-6-((3,5-dimethyl-1H-pyrazol-1-yl)methyl)pyridine (**L1**) and 2-(chloromethyl)-6-((3,5-diphenyl-1H-pyrazol-1-yl)methyl)pyridine (**L2**) were prepared by phase transfer catalyzed alkylation of 2,6-bis(chloromethyl)pyridine and the appropriate pyrazolyl units. Ligands **L1** and **L2** were reacted with iron(II), cobalt(II) and nickel(II) to form their respective metal complexes [$NiCl_2$(**L1**)] (**1**), [$NiBr_2$(**L1**)] (**2**), [$CoCl_2$(**L1**)] (**3**), [$FeCl_2$(**L1**)] (**4**), [$NiBr_2$(**L2**)] (**5**), and [$CoCl_2$(**L2**)] (**6**). Solid-state structures of **5** and **6** confirmed the bidentate coordination modes of **L1** and **L2** and formation of monometallic compounds. Complexes **1-6** formed active catalysts for the oligomerization of ethylene reactions when activated with either $EtAlCl_2$ or methylaluminoxane (MAO) as co-catalysts. The catalytic activities of complexes **1-6** and the products formed largely depended on the co-catalyst and solvent system. While activation with $EtAlCl_2$, in toluene produced Friedel-Crafts toluene-alkylated products, the use of hexane and chlorobenzene gave predominantly C_4 and C_6 oligomers. On the other hand, activation with MAO in toluene led to the formation of mainly C_4, C_6 and C_8 oligomers.

The second type of ligands that were synthesized were 2-((3,5-dimethyl-1H-pyrazol-1-yl)methyl)-6-((diphenylphosphinoyl)methyl)-pyridine (**L3**) and 2-((3,5-diphenyl-1H-pyrazol-1-yl)methyl)-6-((diphenylphosphinoyl) methyl)pyridine (**L4**). Ligands **L3** and **L4** were reacted with iron(II), cobalt(II) and nickel(II) salts to afford complexes [$NiCl_2$(**L3**)] (**7**), [$NiBr_2$(**L3**)] (**8**), [$CoCl_2$(**L3**)] (**9**), [$FeCl_2$(**L3**)] (**10**), [$NiBr_2$(**L4**)] (**11**), and [$CoCl_2$(**L4**)] (**12**). Molecular structures of complexes **7**, **11** and **12** were confirmed by single crystal X-ray crystallography to contain one tridentate bound N^N^O **L3** and **L4** ligands. Complexes **7-12** formed active catalysts in ethylene oligomerization reactions upon activation with $EtAlCl_2$, methylaluminoxane (MAO)

or trimethylaluminium ($AlMe_3$) as co-catalysts to produce C_4 as the major product as well as C_6 and C_8 oligomers.

Another set of potential hemi-labile ligands, 2-methoxy-N-(1-(pyridin-2-yl)ethylidene)-ethanamine (**L5**), 2-methoxy-N-((pyridin-2-yl)methylene)ethanamine (**L6**), 3-methoxy-N-((pyridin-2-yl)methylene)propan-1-amine (**L7**), N,N-diethyl-N-((pyridin-2-yl)methylene)-ethane-1,2-diamine (**L8**), N-((6-bromopyridin-2-yl)methylene)-2-methoxyethanamine (**L9**) and 2-((pyridin-2-yl)methylene-amino)ethanol (**L10**) were synthesized by condensation of the appropriate aldehydes and the corresponding amines. Reactions of ligands **L5-L9** with [PdCl(Me)(cod)] afforded the corresponding palladium(II) complexes [PdCl(Me)(**L5**)] (**13**), [PdCl(Me)(**L6**)] (**14**), [PdCl(Me)(**L7**)] (**15**), [PdCl(Me)(**L8**)] (**16**) and [PdCl(Me)(**L9**)] (**17**). Molecular structures of **13** and **14** confirmed the bidentate coordination modes of **L5** and **L6** and formation of monometallic compounds. Treatment of the neutral complexes **13-17** with one molar equivalent of $Na[BAr_4]$ (Ar = 3,5-$(CF_3)_2C_6H_3$) led to *in situ* formation of the corresponding cationic compounds $[Pd(Me)(\mathbf{L5})]^+$ (**13a**), $[Pd(Me)(\mathbf{L6})]^+$ (**14a**), $[Pd(Me)(\mathbf{L7})]^+$ (**15a**), $[Pd(Me)(\mathbf{L8})]^+$ (**16a**) and $[Pd(Me)(\mathbf{L9})]^+$ (**17a**). In the presence of ethylene, the catalyst systems **13-17**/MAO and **13a-17a** exhibited modest catalytic activities in selective ethylene dimerization producing mainly butenes. ^1H NMR spectroscopy and DFT studies provided valuable insight into the role of ligand architecture on ethylene-coordination to the palladium(II) metal center, catalytic activities and stabilities of the resultant catalysts.

Attempts to react (amino)pyridine ligands **L5-L10** with $[NiBr_2(DME)]$ were futile due to possible hydrolysis of the imine group in the ligands. Analyses of the products by ^1H NMR

spectroscopy confirmed ligand hydrolysis due to the signal observed at 9.00 ppm, associated with the aldehyde proton. Thus, the (amino)pyridine ligands N-(2-methoxyethyl)-1-(pyridin-2-yl)ethanamine (**L5a**), 2-methoxy-N-((pyridin-2-yl)methyl)-ethanamine (**L6a**), N,N-diethyl-N-((pyridin-2-yl)methyl)ethane-1,2-diamine (**L8a**) and 2-((pyridin-2-yl)methylamino)ethanol (**L10a**) were obtained by reducing their corresponding imine compounds **L5, L6, L8** and **L10**. Reactions of the (amino)pyridine ligands **L5a**, **L6a**, **L8a** and **L10a** with [$NiBr_2$(DME)] afforded nickel(II) complexes, [$NiBr_2$(**L5a**)$_2$] (**18**), [$NiBr_2$(**L6a**)$_2$] (**19**), [$NiBr_2$(**L8a**)$_2$] (**20**) and [$NiBr_2$(**L10a**)$_2$] (**21**), respectively. Molecular structures of **19** and **21** confirmed the formation of these bis(chelated)nickel(II) complexes. When complexes **18-21** were activated with $EtAlCl_2$ and MAO, highly active oligomerization catalysts were formed producing mostly ethylene dimers (C_4), in addition to trimmers (C_6) and tetramers (C_8). The catalytic performance was substantially affected by the ligand environment regarding the pendant oxygen- and nitrogen-donor groups, and the substituent on the ligand framework. Better activities were observed with $EtAlCl_2$ as co-catalyst than with MAO. Theoretical studies provided valuable insight into the reactivity of these complexes.

TABLE OF CONTENTS

LIST OF FIGURES

LIST OF SCHEMES

LIST OF TABLES

ABBREVIATIONS

COD	1,5-cyclooctadiene
d	Doublet
DCM	Dichloromethane
DME	Dimethoxyethane
ESI	Electron spray ionization
GC	Gas chromatography
GC-MS	Gas chromatography-mass spectrometry
HDPE	High density polyethylene
IR	Infrared spectroscopy
J	coupling constant
L	Ligand
LDPE	Low density polyethylene
LLDPE	Linear low density polyethylene
m	Multiplet
MAO	Methylaluminoxane
MHz	Megahertz
MMAO	Modified methylaluminoxane
MS	Mass spectrometry
NMR	Nuclear Magnetic Resonance
Ph	Phenyl
ppm	Parts per million
py	Pyridine

pz	Pyrazole
r.t.	Room temperature
s	Singlet
SHOP	Shell Higher Olefin Process
t	Triplet
TMA	Trimethylaluminium
TOF	Turn over frequency
TON	Turn over number
δ	Chemical shift

CHAPTER 1

Introduction to the synthesis and applications of olefins and role of transition metal catalysts

1.1. General introductory remarks

Linear α-olefins are important feedstocks in the manufacture of a wide range of industrial and domestic chemicals due to their capacity to undergo a number of transformations such as hydrogenation, hydroformylation, copolymerization, isomerization, oligomerization and polymerization.[1, 2] Ethylene oligomerization is the primary source of α-olefins with the Shell higher olefin process (SHOP) alone manufacturing over one million tonnes of α-olefins annually.[3] Short chain linear α-olefins (1-butene, 1-hexene and 1-octene) are strategic targets in industrial chemistry since they permit the formation of co-polymers with good tear resistance, besides other desirable properties.[4]

Linear α-olefins produced by ethylene oligomerization have the advantage of yielding biodegradable products compared to the branched olefins,[5] but most industrial processes produce these α-olefins non-selectively, frequently not matching the market demand. In these processes, significant amount of branched internal olefins are produced that, in most cases, are undesirable and often not easy to separate, hence avoided commercially. Consequently, improved methods of producing short chain linear α-olefins are desired.

Estimates indicate that the global annual average growth for linear α-olefins is at a rate of 3.3% in the period 2012-2020.[6] Moreover, the worldwide demand for short chain linear α-olefins (C_4-

C_8) is already at 40%; growing faster than those in the C_{12}^+ range.[7] Thus, the development of highly selective catalysts for the formation of the desired short chain α-olefins from ethylene, which could circumvent the typical broad Schulz-Flory distributions usually observed in ethylene oligomerization reactions, is a topic of significant and applied importance.[8] In this regard, transition metal homogeneous catalysis opens doors to the design and development of selective oligomerization processes.[6]

This chapter looks at a general overview of the syntheses and industrial applications of olefins and the significant role played by transition metals as ethylene oligomerization and polymerization catalysts.

1.2. Industrial commercial processes for ethylene oligomerization reactions

α-Olefins can be produced by cracking of paraffins, dehydrogenation of paraffins, dehydration of alcohols, and ethylene oligomerization. Although the cracking of paraffins still finds widespread application for the synthesis of ethylene, the first three processes generally no longer play an important role in the preparation of α-olefins.[8] Ethylene is a readily available feedstock, and there are three core technologies that oligomerize ethylene to linear α-olefins which are owned and operated at a world-scale.[7]

1.2.1. The Chevron Philips process

In the Chevron Philips process (formerly Gulf), α-olefins are synthesized from ethylene using Ziegler catalysts.[9] The process employs two basic steps to the olefin synthesis: Chain-growth and displacement.[10] In this process, only a catalytic amount of triethylaluminium is used and a

number of chain-growth displacement sequences take place on each aluminium bond during each pass through reactor. During displacement, straight chain α-olefins are produced due to little isomerization that takes place under the reaction conditions. One characteristic of this single-step process is the broad Schulz–Flory carbon number distribution of the ethylene oligomers produced.[10]

1.2.2. The INEOS process

The INEOS process is a combination of stoichiometric and catalytic chain-growth reactions, and the products have a poison distribution with a relative narrow distribution of olefins and an increased branching of olefins in the higher fraction (C_{14}–C_{18}).[8, 10, 11] Like the Chevron Philips process, the INEOS process also employs Ziegler catalysts. It uses three basic steps of triethylaluminium synthesis, chain growth and displacement to synthesize α-olefins from ethylene.[11, 12]

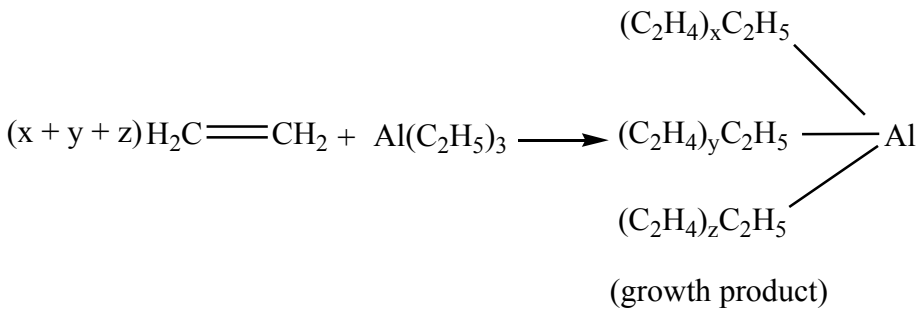

Scheme 1.1: Catalytic ethylene addition in the INEOS process[12, 13]

The active triethylaluminium catalyst is prepared by reductive alkylation of aluminium powder using hydrogen and ethylene. Ethylene chain-growth occurs catalytically through stepwise addition to the three alkyl groups of triethylaluminium (Scheme 1.1).[13] Chain-growth is

regulated by controlling temperature and ethylene addition, yielding a broad carbon number range.[12]

1.2.3. The Shell higher olefin process (SHOP)

The Shell higher olefin process (SHOP), discovered in 1977, is a chemical process used for the production of linear α-olefins by oligomerization of ethylene.[14] It uses phosphine-donor nickel(II) complexes of the type depicted in Figure 1.1. Compared to the other processes, the SHOP process is the most complex but quite exceptional because it affords ethylene oligomers whose composition is adjusted to the desired products through consecutive isomerization and metathesis steps.[15]

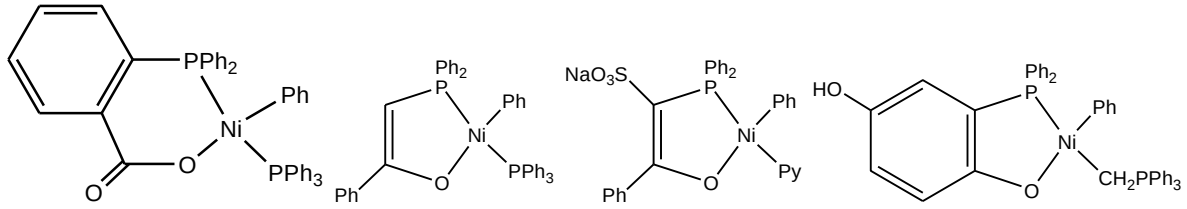

Figure 1.1: Examples of SHOP catalysts for ethylene oligomerization reactions[14, 15]

As explained by Keim,[3] the oligomerization reaction is carried out in a polar solvent e.g. in reactor 1 (Figure 1.2). The phases are then separated in the second step and the catalyst recirculated. Directly marketable α-olefins are separated by distillation in step 3 and the non-marketable portion undergoes olefin isomerization in reactor 4, and eventually olefin metathesis in reactor 5. The metathesis step enables the low and high boiling range internal olefins to be disaproportionated into a wide variety of more useful olefins. Annually, over one million tons of α-olefins are produced using the Shell higher olefin process.[3]

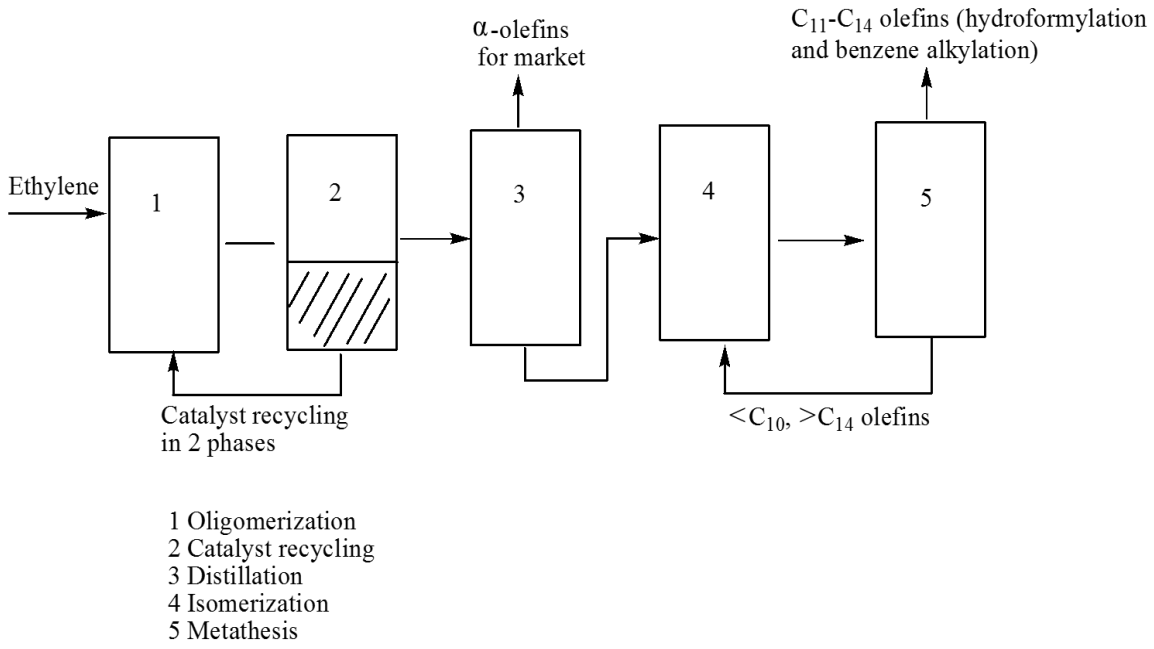

Figure 1.2: Flow diagram of the SHOP production plant.[3]

Distinguished by its tremendous flexibility, and by combining olefin isomerization, metathesis and distillation, SHOP can produce a wide range of linear even-numbered α-olefins and linear internal mono-olefins. As illustrated in a typical statistical distribution of a mixture of linear α-olefins in Scheme 1.2,[16] separation is required in order to isolate the desired α-olefins. Considering the high cost involved with separating mixtures of olefins, coupled with the inevitable consequence of limiting the yield of a given olefin, selective formation of specific short-chain linear α-olefins by circumventing the typical Shultz-Flory distribution is of remarkable significance. Furthermore, despite the remarkable success of the SHOP process, the high reaction temperature of 80-120 °C and pressure (70-140 bar) are not commercially desirable.[17]

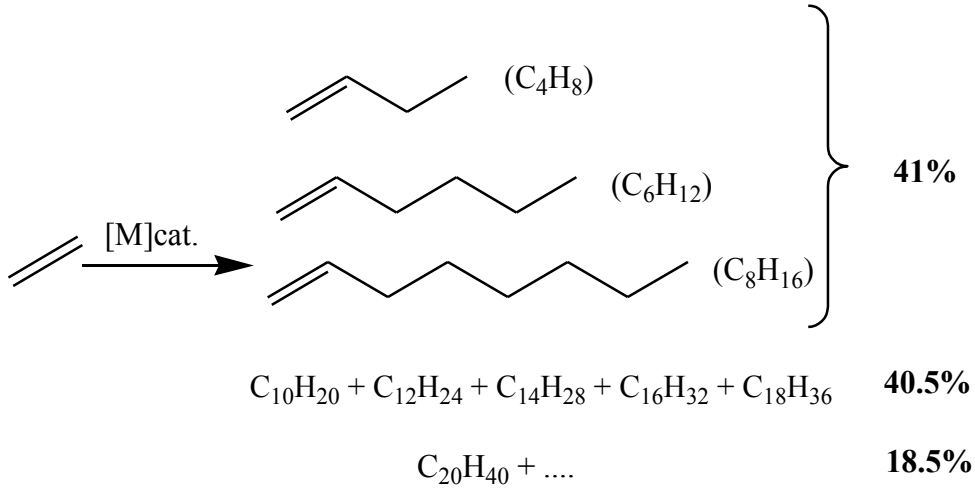

Scheme 1.2: Typical distribution of linear α-olefins in the SHOP non-selective industrial ethylene oligomerization process[16]

The increasing market demand for a 'selective' olefin instead of a range of linear α-olefins has led to increased interest in the design and development of selective ethylene oligomerization processes. Consequently, selective dimerization, trimerization and tetramerization of ethylene have received much attention in the recent past.[6] Thus, in addition to the above "*full range*" processes of ethylene oligomerization, are the "*on-purpose*" technologies of Sasol[3, 11] and Chevron Phillips,[18] which selectively synthesize short chain α-olefins.

1.2.4. The Sasol Fischer-Tropsch process

Sasol uses the Fisher–Tropsch process for making olefins from synthesis gas, which is obtained from coal or natural gas and has achieved selective trimerization of ethylene to 1-hexene and tetramerization of ethylene to 1-octene.[3] Besides, while most of the current commercial plants produce even-numbered alpha-olefins based on ethylene oligomerization, the coal-based synthetic fuels plant of Sasol is the only producer of 1-pentene in commercial quantities.[3]

1.2.5. Chevron Phillips trimerization process

This process, based on chromium catalysts, can selectively trimerizes ethylene to 1-hexene with high selectivity.[7] The fundamental difference between this system and the conventional ethylene oligomerization catalysts lie in its ability to form metallacycles as depicted in Scheme 1.3.[19, 20] The first metallacycle consists of a five membered ring made up of two ethylene molecules. Being thermodynamically stable, the five membered ring remains intact long enough for another ethylene monomer to insert resulting in a seven membered metallacycle. Decomposition of the seven membered ring, courtesy of reductive elimination, yields 1-hexene.

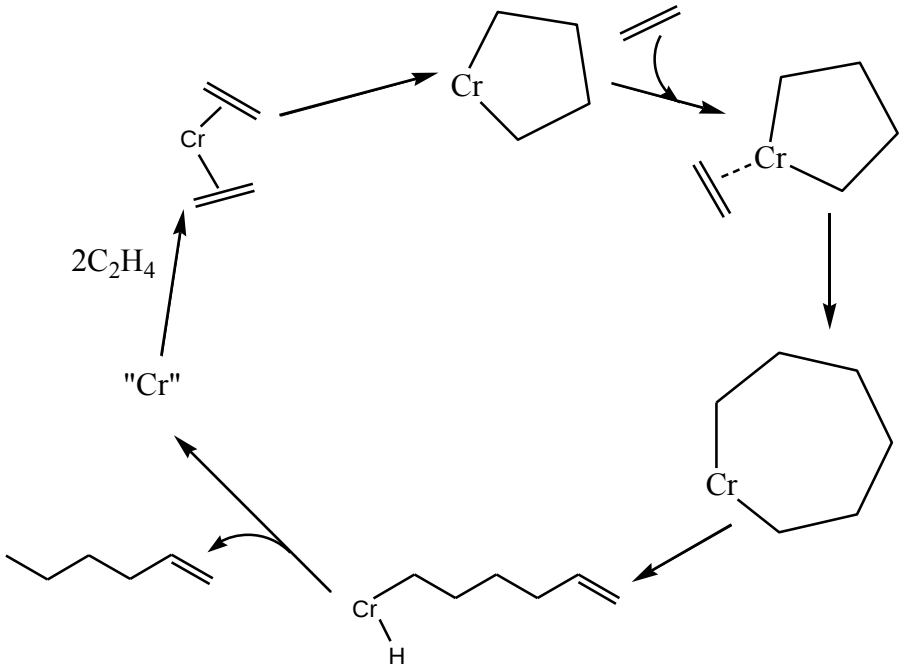

Scheme 1.3: Ethylene trimerization via chromium metallacycles[19, 20]

1.3. α-Olefin derivatives and their applications

Oligomerization of ethylene to linear α-olefins dominates the market for homogeneous-catalyzed oligomerization.[21] Linear α-olefins are important feedstocks for the chemical industry that have found applications as comonomers for polyethylene production, oxo-alcohols used in

detergents and plasticizers, and for the production of poly-α-olefins for the synthetic lubricant pool.[1, 6] In addition, they are also starting materials for other important chemicals like propylene, amines and acids, as shown in Scheme 1.4.[1,11]

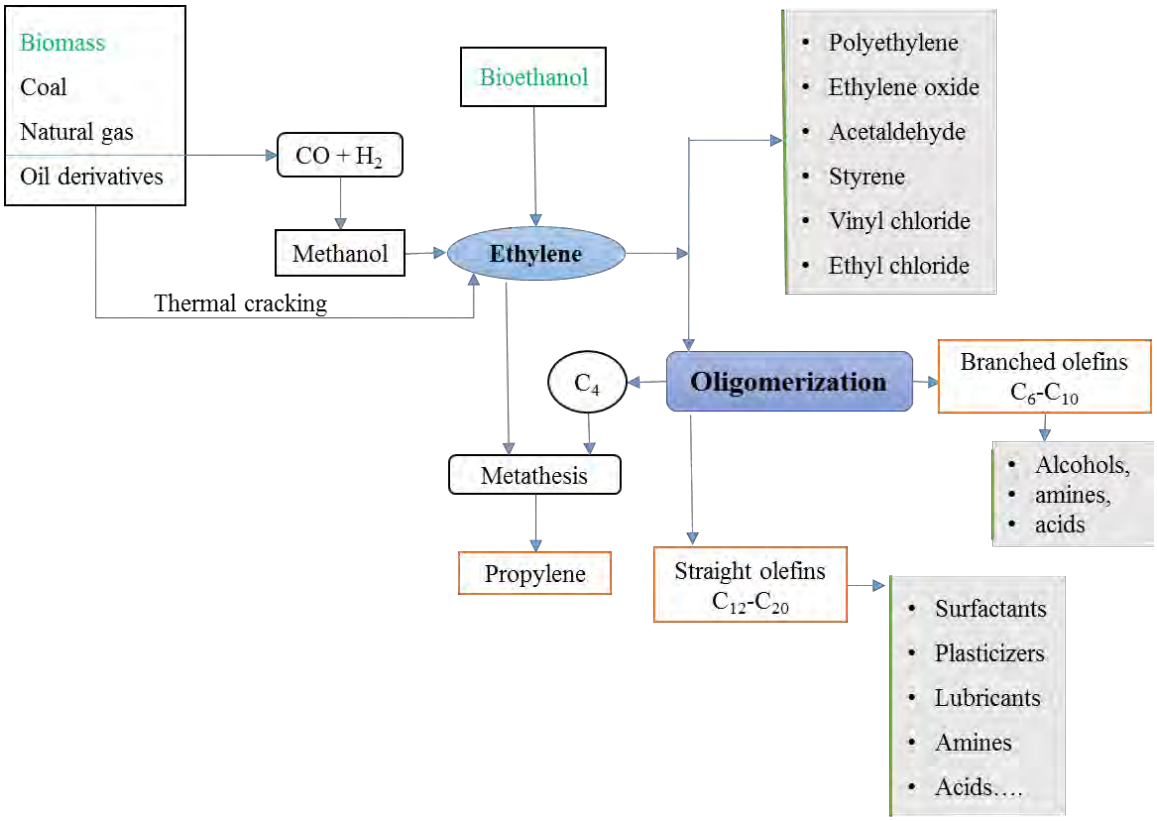

Scheme 1.4: Chart depicting the various ethylene feed-stocks and major derivatives.[1]

An sp^2 hybridized model of carbon-carbon double bond explains the extensive commercial application of α-olefins. According to the model, the carbon-carbon double bond comprises of a strong σ-bond and a weaker π-bond. Because of the high electron density due to the overlapping of the π-π bond of the two carbon atoms, the double bond is susceptible to electrophilic attack. Thus, α-olefins are more reactive than their corresponding internal olefins due to the ease of access of the double bond, which is at the terminal position compared to the sterically hindered internal olefins.

1.3.1. Polyolefins

Polyolefins are the dominant consumers of olefins due to their inherent properties and wide range of applications, with much of these olefins used for the production of linear low-density polyethylene (LLDPE), as is evident from Figure 1.3.[21, 22] LLDPE has better mechanical strength and processability than high-density polyethylene (HDPE), a feat achieved by controlling the amount of short-chain branching in the polymer through co-monomer addition.[23] For example, HDPE uses 2–4% of comonomer (C_4–C_6), while LLDPE uses 8–10 % of co-monomer (C_4–C_8).

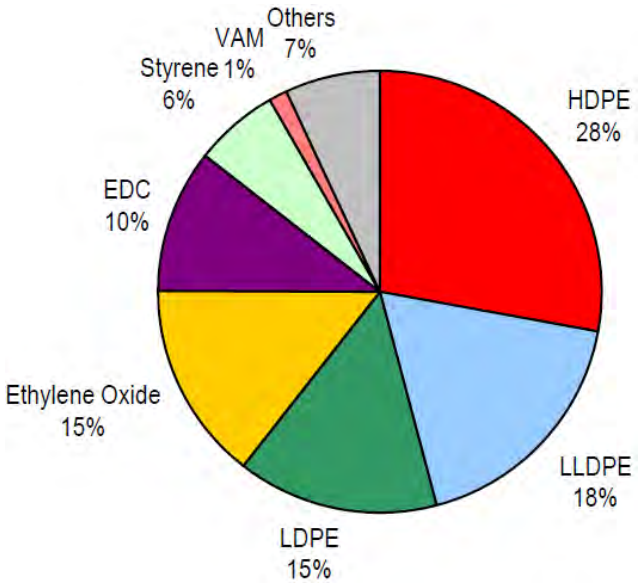

Figure 1.3: Ethylene end-uses 2013.[24]

1-butene is still the most used co-monomer in the production of LLDPE (more flexible and resilient PE), and to a lesser extent HDPE.[6] However, 1-hexene and 1-octene have become more desirable because of the excellent properties they impart on the co-polymer product, such as higher stress-crack resistance and ability to withstand tearing.[7] For example, 1-hexene incorporated LLDPE produces tougher thinner film than would be produced with 1-butene

(Figure 1.4). Incorporation of 1-octene, on the other hand, produces the highest quality products in terms of surface finish, transparency and resistance to tearing.[7]

LDPE waste disposal bags

LDPE film for wrapping foods

HDPE water pipes

HDPE Water tank

Figure 1.4: Examples of polyethylene-end products and their applications.

The LLDPE are used mainly for film packaging, dispensing bottles or wash bottles, electrical insulation and waste disposal bags, while the HDPE are blow-molded to make drums, storage tanks, and building and construction pipes (Figure 1.4).

1.3.2. Plasticizers, detergents and lubricants

Linear α-olefins find wide application in the detergent and fuel industry, given that they are components of plasticizers e.g. phthalates, through hydroformylation (C_6-C_{10}), detergents through sulphonation/arylation (C_{12}-C_{16}) and lubricants through oligomerization (C_{10}-C_{12}).[1] For example, olefins are reacted with benzene to form linear alkyl benzenes which are then sulfonated to linear alkyl benzyl sulfonates; an industrial and household detergent. Furthermore, besides C_{14} being used in the manufacture of detergents, it is also preferred as on-land drilling fluid lubricant instead of diesel or kerosene due to its biodegradable nature and being less toxic and irritating to the skin.[25] In addition, higher olefins, C_{16}-C_{18}, are used as lubricating fluids, hydrophobes in oil-soluble surfactants and as synthetic drilling fluid base in off-shore synthetic drilling fluids.

1.3.3. Conversion of olefins to industrial chemical intermediates

Homogeneous and heterogeneous catalysts play an important role in the conversion of olefins to more useful industrial products;[26] for example, reaction of olefins with carbon monoxide to produce commercially useful aldehydes, alcohols and ketones (Scheme 1.5). Carboxylic acids can be prepared by the reaction of olefins with water and carbon monoxide in the presence of transition metal catalysts such as $Ni(CO)_4$, $Co_2(CO)_8$ and $HPtCl_6$.[27, 28] Carbon monoxide and an alcohol can also be added to olefins, in the presence of metal catalysts such as tin(II) chloride and either palladium(II) or platinum(II) complexes, to produce esters through hydroesterification.[29] Another important reaction in the chemical industry is the oxidation of α-olefins. For example, ethylene glycol, prepared by the oxidation of ethylene to ethylene oxide followed by hydrolysis of the oxide over a silver catalyst at 250 °C to ethylene glycol, finds

wide applications in various fields such as, in the manufacture of polyesters, antifreeze and coolant in automobile industry.[30-32]

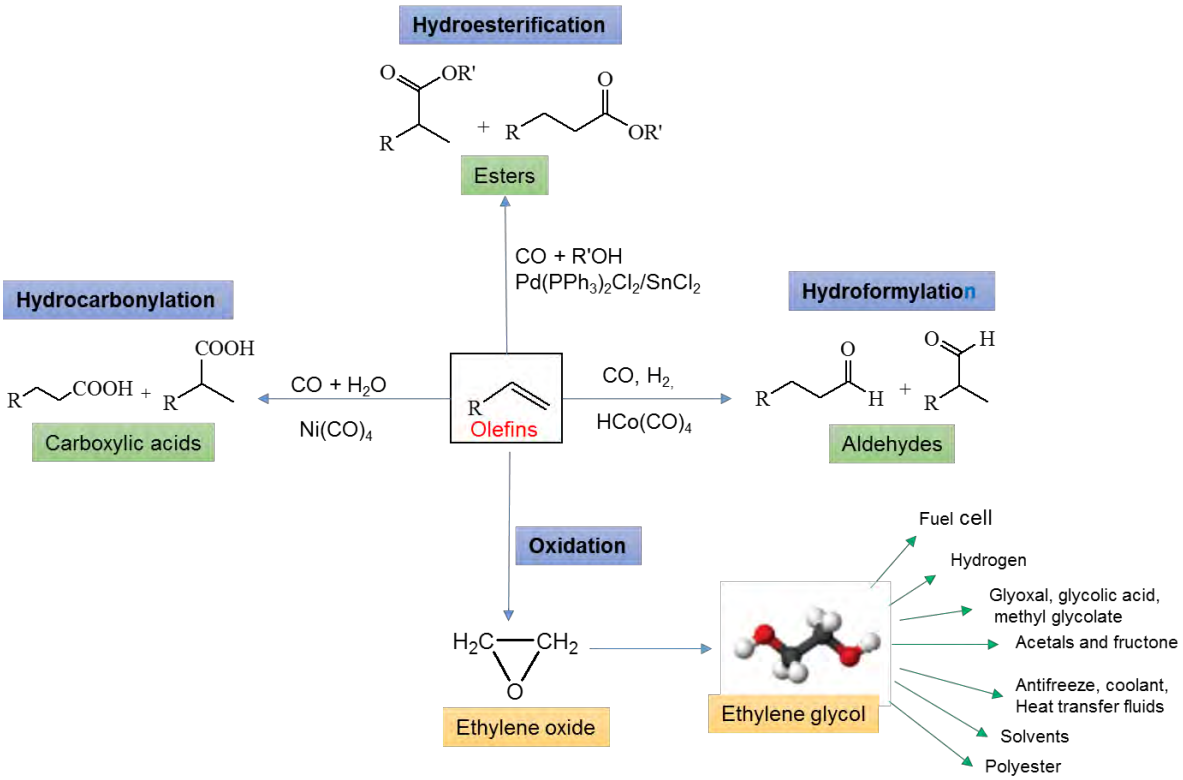

Scheme 1.5: Synthetic conversions of olefins to industrial products[26, 29-32]

1.4. Transition-metal based catalysts for ethylene oligomerization and polymerization reactions

1.4.1. Early-transition metal catalysts

In the 1950s, it was discovered by Karl Ziegler that trialkylaluminium-activated titanium-based catalyst was highly active for α-olefin polymerization.[33-35] Furthermore, Giulio Natta made use of this catalyst to polymerize propylene into crystalline polypropylene.[36] This work, as illustrated in Scheme 1.6, led to the commercialization of the Ziegler-Natta catalysts, which are still the basis of major industrial polymerization processes.[37]

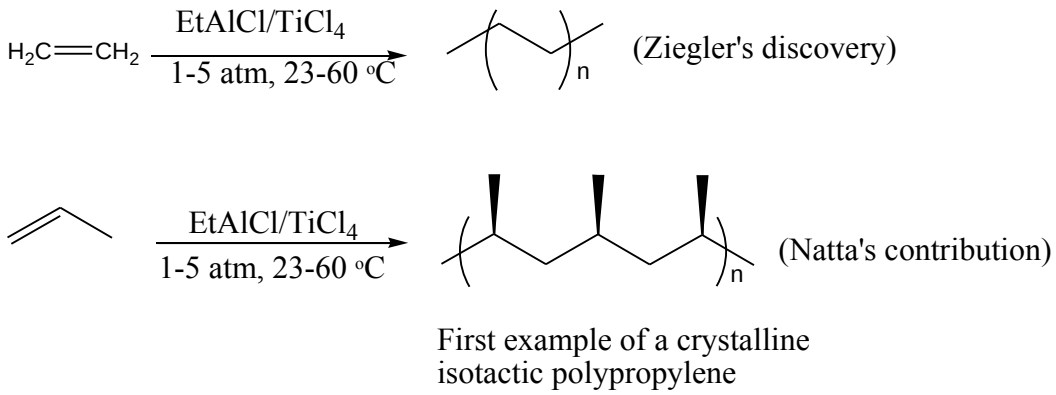

Scheme 1.6: Ziegler and Natta's work[37]

Despite their great success in the production of polyolefins, the Ziegler-Natta catalysts suffer from a number of limitations. For example, investigation of their reaction mechanism is hampered by their heterogeneous nature and the catalysts have multiple active sites which lead to non-uniform incorporation of comonomers in the resultant copolymers.[38] To address these limitations, homogeneous Group 4 metallocene systems of type **1.1** (Figure 1.5) were developed[39] which could polymerize virtually any α-olefins, including several cyclic olefins.[40] However, they suffered from the inability to produce stereo-regular polymers. Consequently, *ansa*-metallocenes, depicted by example **1.2**, with uniform active species were developed that could allow the control of polymer microstructure. In spite of the ability of these metallocene catalysts permitting the production of polymers with low polydispersities, as well as rational design of new catalysts owing to their homogeneous, and single-site feature, early-transition metal catalysts suffer from intolerance to polar monomers due to their highly electron deficient nature.[41]

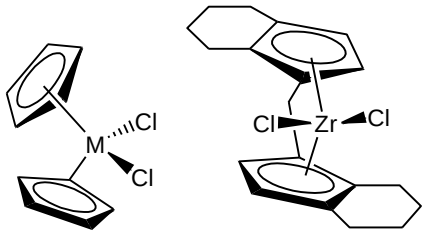

1.1 **1.2**

Figure 1.5: Representative Group 4 metallocenes[39]

1.4.2. Late-transition metal catalysts

To overcome the drawbacks of early-transition metal catalysts, much effort and focus has been directed towards late-transition metal systems in the design and development of new catalysts. Late transition metals are functional group tolerant, making them particularly attractive for designing catalysts for copolymerization with polar functional groups.[38] Furthermore, the cationic late-transition metal catalysts can be highly electrophilic which can allow a higher rate of olefin insertion. These characteristics have been explored in the works of Brookhart's group on α-diimine nickel(II) and palladium(II) complexes, as effective catalysts for ethylene oligomerization and polymerization reactions.[42, 43] Following this seminal work of Brookhart *et al*. in 1995,[42] much effort has been devoted to the design of other late-transition metal catalysts.[44, 45]

The discovery in 1998, for example, by Brookhart *et al.*[46] and Gibson *et al.*[47] of the highly active five coordinate 2,6-bis(imino)pyridine iron(II) and cobalt(II) complexes gave great promise in the use of late-transition metal complexes as catalysts for ethylene oligomerization and polymerization and spurred intense interest in the search of other suitable ligand designs. These complexes, when activated with MAO, are highly active for ethylene oligomerization and their

ligand design permits high precision in the control of the microstructure and hence the properties of the resulting products.[48]

Over the years, much research effort has been devoted to the development of new transition metal complexes and to the study of their catalytic behaviour towards ethylene. However, during the last recent years, interest has shifted towards the development of a new generation of late transition metal catalysts aimed at more selective routes to these desired α-olefins.[6, 44] This has been motivated by the soaring demand for linear α-olefins within the C_4-C_{10} range, almost half of which are used for the formation of polyethylene and polypropylene products.[49] Studies have clearly demonstrated that even minor variations in the steric and electronic properties of these ligands and the geometrical constraints they impose on the metal can lead to great changes in their catalytic reactivity such as oligomerization versus polymerization, initial activity (TOF), productivity (TON) as well as catalyst stability and lifetime.[45, 50]

Thus ligand microstructure, especially adapted to the nature of the metal, plays a key role in the development of desirable catalysts.[45] However, the identification and fine-tuning of the parameters that influence catalytic activity and selectivity of suitable catalysts continues to pose a challenge. In chapter 2, a review of the development of late transition metals in homogeneous ethylene oligomerization and polymerization catalysis will be discussed. Recent advances in ethylene oligomerization, as well as important facets of the process will be highlighted, illustrating the influence of a diverse range of ligand systems on the performance of late transition metal oligomerization catalysts.

1.5. References

1. Finiels, A.; Fajula, F.; Hulea, V., *Catal. Sci. Technol.* **2014**, *4*, 2412-2426.
2. Malgas-Enus, R.; Mapolie, S. F., *Inorg. Chim. Acta* **2014**, *409*, 96-105.
3. Keim, W., *Angew. Chem. Int. Ed.* **2013**, *52*, 12492-12496.
4. Kissin, Y. V., *Kirk-Othmer Encyclopedia of Chemical Technology* **2005**.
5. Kurokawa, H.; Miura, K.; Yamamoto, K.; Sakuragi, T.; Sugiyama, T.; Ohshima, M.-a.; Miura, H., *Catalysts* **2013**, *3*, 125-136.
6. Breuil, P.-A. R.; Magna, L.; Olivier-Bourbigou, H., *Catal. Lett.* **2015**, *145*, 173-192.
7. Forestière, A.; Olivier-Bourbigou, H.; Saussine, L., *Oil Gas Sci. Technol.* **2009**, *64*, 649-667.
8. Speiser, F.; Braunstein, P.; Saussine, L., *Acc. Chem. Res.* **2005**, *38*, 784-793.
9. Ziegler, K.; Holzkamp, E.; Breil, H.; Martin, H., *Angew. Chem.* **1955**, *67*, 541-547.
10. Lappin, G.; Nemec, L.; Sauer, J.; Wagner, J., *Higher Olefins*; *Kirk-Othmer Encyclopedia of Chemical Technology*. In Wiley & Sons, Inc.: New York, NY, USA: 2000.
11. Vogt, D., Oligomerisation of Ethylene to Higher Linear R-Olefins. In *Applied Homogeneous Catalysis with Organometallic Compounds*, Cornils, B., Hermann, W. A., Eds: New York, 1996; Vol. 1.
12. Lappin, G., *Alpha olefins applications handbook*. CRC Press: 1989.
13. ChemSystems *Apha Olefins PERP06/07-5*; 2008; pp 1-11.
14. Lutz, E., *J. Chem. Educ.* **1986**, *63*, 202-203.
15. Skupinska, J., *Chem. Rev.* **1991**, *91*, 613-648.
16. Elowe, P. R., PhD Thesis, *California Institute of Technology*, 2009.

17. Britovsek, G. J.; Mastroianni, S.; Solan, G. A.; Baugh, S. P.; Redshaw, C.; Gibson, V. C.; White, A. J.; Williams, D. J.; Elsegood, M. R., *Chem. Eur. J.* **2000**, *6*, 2221-2231.

18. Dixon, J. T.; Green, M. J.; Hess, F. M.; Morgan, D. H., *J. Organomet. Chem.* **2004**, *689*, 3641-3668.

19. Zilbershtein, T. M.; Kardash, V. A.; Suvorova, V. V.; Golovko, A. K., *Appl. Catal. A: Gen.* **2014**, *475*, 371-378.

20. Briggs, J. R., *J. Chem. Soc., Chem. Commun.* **1989**, 674-675.

21. Ye, J.; Jiang, B.; Wang, J.; Yang, Y.; Pu, Q., *J. Polym. Sci., Part A: Polym. Chem.* **2014**, *52*, 2748-2759.

22. Vasile, C.; Pascu, M., *Practical guide to polyethylene*. Smithers Rapra Publishing: 2005.

23. Xie, G.; Zhang, X.; Li, T.; Li, L.; Liu, G.; Zhang, A., *J. Mol. Catal. A: Chem.* **2014**, *383*, 121-127.

24. NexantThinking, C. P. R.-. *Ethylene. PERP 2013-4*; Nexant: 2013.

25. Ojwach, S. O., PhD Thesis, *University of Johannesburg*, 2008.

26. Beller, M.; Bolm, C., *Transition metals for organic synthesis*. Wiley-VCH: 1998.

27. Wender, I.; Pino, P., *Organic Synthesis via Metal Carbonyls*, Vol. 2. In Wiley, New York: 1977.

28. Kehoe, L.; Schell, R., *J. Org. Chem.* **1970**, *35*, 2846-2848.

29. Parshall, G.; Ittel, S., *Homogeneous catalysis*. Wiley, New York, **1992**.

30. Chen, L.-F.; Guo, P.-J.; Qiao, M.-H.; Yan, S.-R.; Li, H.-X.; Shen, W.; Xu, H.-L.; Fan, K.-N., *J. Catal.* **2008**, *257*, 172-180.

31. Yin, A.; Guo, X.; Dai, W.; Fan, K., *Chem. Commun.* **2010**, *46*, 4348-4350.

32. Yue, H.; Zhao, Y.; Ma, X.; Gong, J., *Chem. Soc. Rev.* **2012**, *41*, 4218-4244.

33. Ziegler, K., In *Organometallic Chemistry* (ed. Zeiss, H.); Reinhold: New York, **1960,** p *194*.

34. Martin, H., In *Ziegler Catalysts, Recent Scientific Innovations and Technological Improvements.* G. Fink, R. M. ülhaupt, H. H. Brintzinger ed. Springer-Verlag Berlin, 1995; pp 15-34.

35. Albizzati, E.; Galimberti, M., *Catal. Today* **1998**, *41*, 159-168.

36. Natta, G., *J. Polym. Sci.* **1959**, *34*, 21-48.

37. Boor, J., *Ziegler-Natta catalysts and polymerizations*. Academic Press: New York, 1979.

38. Camacho, D. H.; Guan, Z., *Chem. Commun.* **2010**, *46*, 7879-7893.

39. Kaminsky, W., *J. Polym. Sci., Part A: Polym. Chem.* **2004**, *42*, 3911-3921.

40. Makio, H.; Prasad, A. V.; Terao, H.; Saito, J.; Fujita, T., *Dalton Trans.* **2013**, *42*, 9112-9119.

41. Aaltonen, P.; Fink, G.; Löfgren, B.; Seppälä, J., *Macromolecules* **1996**, *29*, 5255-5260.

42. Johnson, L. K.; Killian, C. M.; Brookhart, M., *J. Am. Chem. Soc.* **1995**, *117*, 6414-6415.

43. Johnson, L. K.; Mecking, S.; Brookhart, M., *J. Am. Chem. Soc.* **1996**, *118*, 267-268.

44. Wang, S.; Sun, W.-H.; Redshaw, C., *J. Organomet. Chem.* **2014**, *751*, 717-741.

45. Boudier, A.; Breuil, P.-A. R.; Magna, L.; Olivier-Bourbigou, H.; Braunstein, P., *Chem. Commun.* **2014**, *50*, 1398-1407.

46. Small, B. L.; Brookhart, M.; Bennett, A. M., *J. Am. Chem. Soc.* **1998**, *120*, 4049-4050.

47. Britovsek, G. P.; Gibson, V.; McTavish, S.; Solan, G.; White, A. P.; Williams, D.; Kimberley, B.; Maddox, P., *Chem. Commun.* **1998**, 849-850.

48. Wegner, M. M.; Ott, A. K.; Rieger, B., *Macromolecules* **2010**, *43*, 3624-3633.

49. Ma, J.; Feng, C.; Wang, S.; Zhao, K.-Q.; Sun, W.-H.; Redshaw, C.; Solan, G. A., *Inorg. Chem. Front.* **2014**, *1*, 14-34.

50. Zhang, W.; Sun, W.-H.; Redshaw, C., *Dalton Trans.* **2013**, *42*, 8988-8997.

CHAPTER 2

Literature review of late-transition metal complexes as catalysts in ethylene oligomerization reactions

2.1. Background information

Late-transition metal catalyzed ethylene oligomerization to higher olefins has witnessed significant attention over decades leading to several breakthroughs that are of prime importance to both academia and industry.[1-4] In recent years, the focus has been on designing new ligand frameworks geared towards enhancing activity and selectivity through catalyst and process developments.[4, 5] The importance of catalyst design towards ethylene oligomerization, which revolves around the design of new ancillary ligands, is underscored by the amount of resources that have been used and numerous reviews that have appeared over the years.[1-4, 6, 7]

This chapter presents a review of the relevant literature on late transition metal catalysts, in particular nickel(II), cobalt(II), iron(II) and palladium(II) complexes that have been designed for homogeneous catalysis in ethylene oligomerization reactions. Recent advances in ethylene oligomerization, highlighting the complex and diverse roles played by a wide range of ligand systems on the performance of late-transition metal complexes in ethylene oligomerization reactions will be discussed.

2.2. Late-transition metal catalysts for ethylene oligomerization reactions

2.2.1. Nickel(II) complexes in ethylene oligomerization reactions

Since the first discovery of the ‘‘nickel effect’’ by Ziegler in the 1960s,[8, 9] nickel still continues to be one of the most studied metals in the field of late transition metal olefin oligomerization and polymerization catalysis.[10] In this respect, a wide variety of multifunctional ligand designs have been reported such as those with P^O, P^N or N^O donor atoms that introduce variable electronic effect on the metal center and ultimately influence the catalytic activities of such complexes.[11, 12]

2.2.1.1. Nickel(II) catalyst systems based on P^O and P^N ligands

The first example of late transition metal catalyzed oligomerization of ethylene was reported by Keim and co-workers in the late 1960s and used neutral Ni complexes of P^O-chelating ligands. These systems are excellent catalysts for the oligomerization of ethylene to short-chain α-olefins.[13, 14] The P^O chelating ligand controls the selectivity of the catalyst in ethylene oligomerization while ligands like PPh_3 stabilize the nickel(II) complex. These catalysts form the basis of the Shell higher olefin process (SHOP); a very successful multi-stage industrial homogeneous catalytic process.[15] The design of SHOP catalysts, such as of type **2-I** (Figure 2.1), is based on the strong propensity of late-transition metals to undergo β-hydride elimination on the central metal thereby inducing oligomerization of ethylene.[16] The functional-group tolerance of the nickel(II) catalyst is demonstrated by the fact that it allows the use of 1,4-butanediol, a polar solvent. Given that the α-olefins formed are insoluble in the alcohol, phase separation takes place allowing simple isolation of the products.[17] In addition, the SHOP-type catalysts have also been shown to be effective for olefin polymerization.[18]

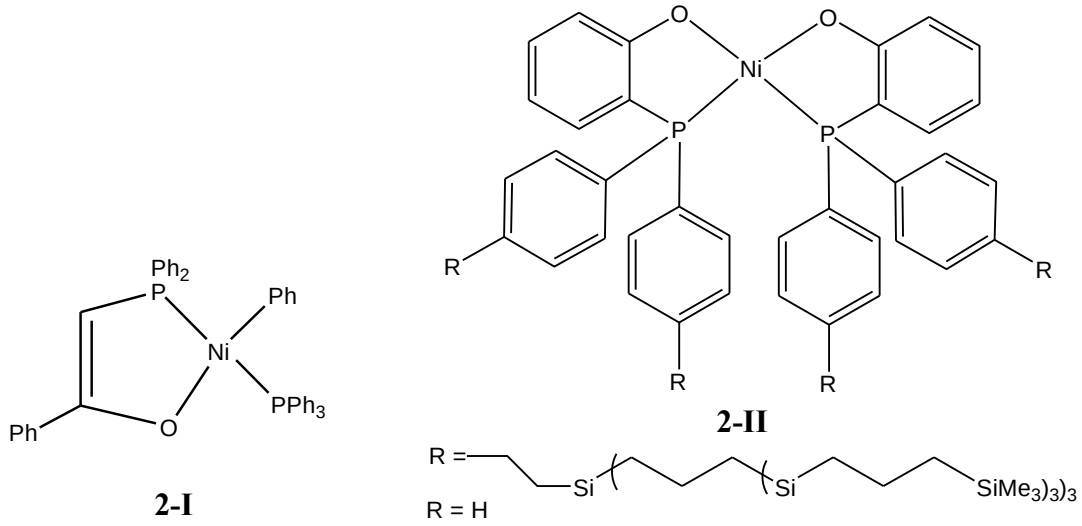

Figure 2.1: Nickel(II) complexes bearing P^O ligands[15, 19]

To date, much focus has been directed towards the design of ethylene oligomerization catalysts based on P^O and P^N ligands that can rival the SHOP catalysts. For example, nickel(II) dendrimer based catalyst **2-II** (Figure 2.1) has been used to oligomerize ethylene giving a Schulz-Flory distribution of oligomers.[19] In another example, Braunstein *et al*.[20] investigated the catalytic properties of complexes of type **2-III** (Figure 2.2) bearing phosphino ligands. The complexes catalyze ethylene oligomerization upon activation with $EtAlCl_2$, producing mainly C_4 and C_6, as well as marginal amounts of C_8 and C_{10} oligomers. Lower catalytic activities are obtained on substituting the sulfur on the azoline ring with the oxygen atom. The same trend is observed on using MAO as the co-catalyst, with enhanced selectivity for C_4 (75.3–89.1%).[20] Using pyridyl-phosphine complexes of type **2-IV**, the activity is influenced by the size of the bite angle, producing C_4 as the predominant product, upon activation with MAO, as well as small quantities of C_6-C_{10} oligomers.[21]

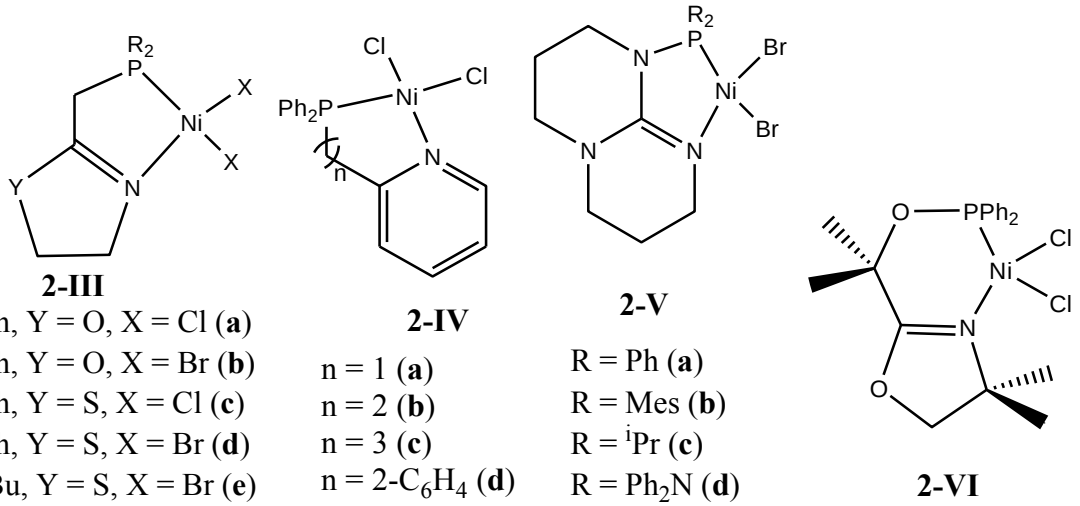

2-III

R = Ph, Y = O, X = Cl (**a**)
R = Ph, Y = O, X = Br (**b**)
R = Ph, Y = S, X = Cl (**c**)
R = Ph, Y = S, X = Br (**d**)
R = ^{t}Bu, Y = S, X = Br (**e**)

2-IV

n = 1 (**a**)
n = 2 (**b**)
n = 3 (**c**)
n = 2-C_6H_4 (**d**)

2-V

R = Ph (**a**)
R = Mes (**b**)
R = ^{i}Pr (**c**)
R = Ph_2N (**d**)

2-VI

Figure 2.2: Nickel(II) complexes with P^N ligands[20, 21]

Complexes **2-V**, chelated by *N*-phosphino guanidine on the other hand, give moderate activity when $EtAlCl_2$ is used as the co-catalyst to afford C_4 and C_6 as the main products and small amounts of C_8. Complex **2-V(d)**, bearing the weakest σ-donor phosphine, is the least active (1.58 x 10^3 molC_2H_4 .mol^{-1}Ni.h^{-1}) while complex **2-V(c)** containing the strongest σ-donor phosphine is the most active (6.34 x 10^3 mol.C_2H_4.mol^{-1}Ni.h^{-1}).[20] In addition, complex **2-VI**, bearing a phosphinite group (-$OPPh_2$), has also been shown to form active catalysts in ethylene oligomerization upon activation with $EtAlCl_2$. There is remarkable improvement of catalytic activity of complex **2-VI** on increasing the co-catalyst concentration from 2 equiv. to 6 equiv., although this is accompanied by a decline in selectivity for C_4.[20]

In another related study, catalyst systems **2-VII** - **2-X** (Figure 2.3) were used as precatalysts in ethylene oligomerization reactions using $AlEtCl_2$ and MAO as co-catalysts.[22] Activation of the complexes with $EtAlCl_2$ forms highly active catalysts in ethylene oligomerization to produce C_4 as the major product. The dinuclear complex **2-VIII** is the most active while **2-IX(a)** registers

the best selectivity for butenes (97%) using 2 equiv. of $AlEtCl_2$. All the complexes (**2-VII** to **2-X)** show low to moderate selectivities for 1-butene, ranging from 13-72%.[22]

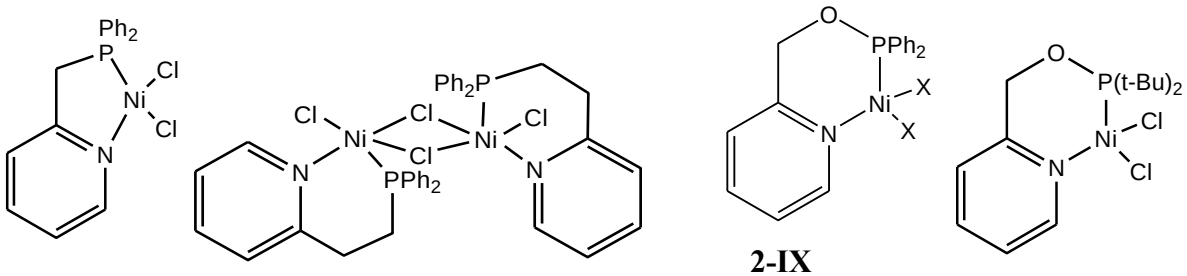

2-VII **2-VIII** **2-IX** X = Cl (**a**); X = Br (**b**) **2-X**

Figure 2.3: Nickel(II) complexes based on pyridyl P^N ligands[22]

2.2.1.2. Nickel(II) catalysts based on α-diimine ligands

Since the discovery of α-diimine nickel(II) complexes **2-XI** (Figure 2.4) as active catalysts for ethylene polymerization by Brookhart and co-workers,[23] much focus has been directed towards related α-diimine systems and their derivatives.[10, 16, 17, 24, 25] This has been aided by the ease with which the steric and electronic properties of these α-diimine ligands can be varied.[26, 27]

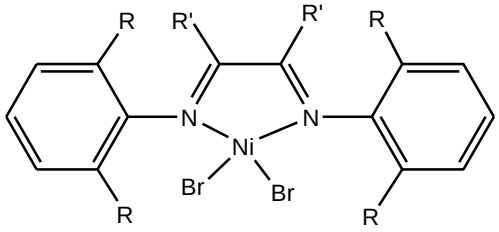

R = H, Me, i-Pr; R' = H, Me

2-XI

Figure 2.4: Brookhart's α-diimine nickel(II) complexes[23]

This advantage was further exploited by the Brookhart group in their design of nickel(II) complexes **2-XII** and **2-XIII** (Figure 2.5) bearing α-diimine ligands without bulky ortho-aryl substituents.[28, 29] Activation of these nickel(II) dibromide complexes with MAO or Et_2AlCl, in

toluene, generates active cationic catalysts *in-situ* that catalyze ethylene oligomerization with a Schulz-Flory distribution of linear α-olefins.

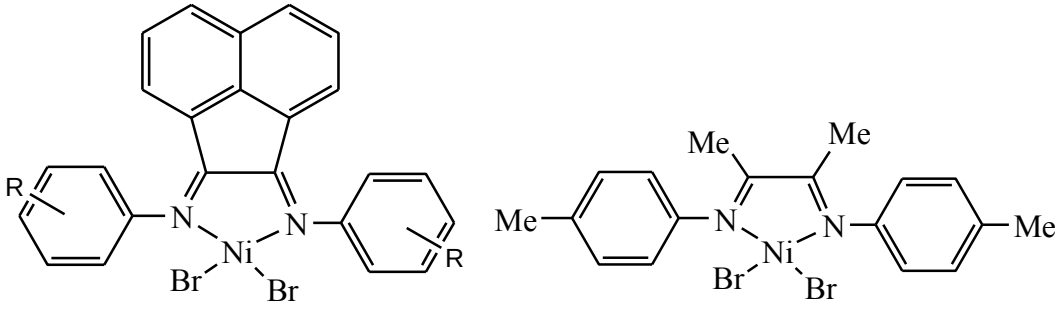

R = 4-CF_3, 4-H, 4-Me, 4-OMe

2-XII **2-XIII**

Figure 2.5: Nickel(II) based system bearing diimine ligands lacking bulky o-aryl substituents[28, 29]

Stemming from Brookhart's work, a new set of bis-α-diimine nickel(II) complexes of type **2-XIV** (Figure 2.6) were recently reported,[5] which when activated with methyl aluminoxane (MAO) as a co-catalyst, form highly active catalysts in ethylene oligomerization reaction. The dinickel(II) complexes favor the formation of mainly butenes, with high selectivity for 1-butene. Small amounts of hexenes and octenes are formed, as well as trace amounts of polyethylene for complexes **2-XIV(a)** and **2-XIV(c)**.

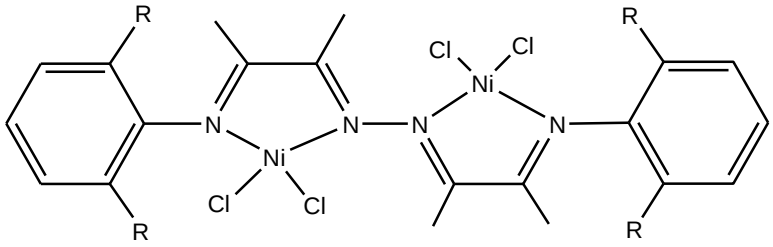

2-XIV

R = Me (**a**), R = Et (**b**), R = ^{i}Pr (**c**)

Figure 2.6: Dinickel(II) complexes bearing bis-α-diimine ligands[5]

2.2.1.3. Pyridyl(imine) based nickel(II) catalysts

The quest for active oligomerization catalysts has seen enormous efforts being devoted to ligand modification, with the hope that the new ligand systems will possess the potential to induce high catalytic activities and improved product selectivities.[30] For example, 2-iminopyridyl nickel(II) complexes of type **2-XV** (Figure 2.7) catalyze ethylene oligomerization and polymerization reactions with activities as high as 9.30 x 10^6 g oligomer.mol.$^{-1}$Ni.h^{-1} for ethylene polymerization. With increase in steric hindrance of the substituent group at the *ortho* position of the phenyl group, polymers are produced.[31-33]

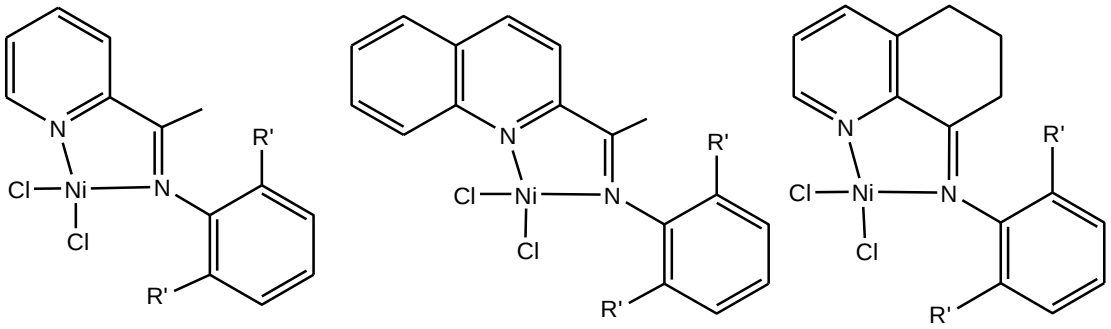

2-XV **2-XVI** **2-XVII**

Figure 2.7: *N,N*-bidentate nickel(II) dichloride complexes[33-35]

Modification of the ligand design in **2-XV** by introducing a benzene ring fused to the pyridine ring as in nickel(II) complexes of type **2-XVI** results in catalysts that exhibit higher catalytic activities than **2-XV** in ethylene oligomerization (10^6 g oligomer.mol.$^{-1}$Ni.h^{-1}), forming mainly butenes.[35] However, the nickel(II) complexes of type **2-XVII** containing fused cycloalkanonylpyridines exhibit high catalytic activities in ethylene polymerization reactions without formation of any oligomers.[34, 36] Moreover, fusion of the cycloketonyl group to pyridine leads to higher ethylene polymerization activity than the (imino)pyridylnickel(II) complexes of type **2-XV**.

In another related work, nickel(II) complexes of type **2-XVIII** (Figure 2.8) bearing 2-(1-aryliminoethylidene)quinoline ligands have been shown to form highly active catalysts for selective ethylene dimerization.[37]

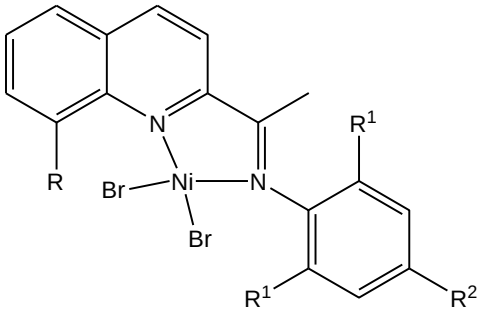

2-XVIII

R = Me, R^1 = Me, R^2 = H (**a**) R = Me, R^1 = Et, R^2 = Me (**e**)
R = Me, R^1 = Et, R^2 = H (**b**) R = Me, R^1 = $CH(Ph)_2$, R^2 = Me (**f**)
R = Me, R^1 = ^{i}Pr, R^2 = H (**c**) R = Me, R^1 = ^{i}Pr, R^2 = NO_2 (**g**)
R = Me, R^1 = Me, R^2 = Me (**d**)

Figure 2.8: *N,N*-bidentate nickel(II) dibromide complexes[37]

The catalytic behaviour of these nickel(II) complexes is affected by the nature of substituents on the quinoline and phenyl moieties. For example, using Et_2AlCl as a co-catalyst, high catalytic activities of up to 2.4×10^6 g oligomer.mol.$^{-1}$Ni.h^{-1} in ethylene dimerization reaction are obtained using complexes of type **2-XVIII(a-c)**. Increasing steric bulk, as in complexes **2-XVIII(d)** and **2-XVIII(e**), show enhanced catalytic activities compared to **2-XVIII(a)** and **2-XVIII(c)**, respectively. This has been attributed to better solubility of **2-XVIII(d**) and **2-XVIII(e)** due to the additional methyl group in the complexes.[37]

Subsequent to the studies on α-diimine complexes, a related class of pyridine diimine compounds were reported by Sun *et al*.[38] The nickel(II) catalysts (**2-XIX** and **2-XX**) bearing 2-carboxylate-6-iminopyridine ligands (Figure 2.9) have been shown to be highly active in

ethylene oligomerization reaction, to produce mainly C_4–C_8 oligomers as main products upon activation with MAO. Consistent with previous reports, bulky substituents on the aryl ring results in the formation of small amounts of polyethylene.[38]

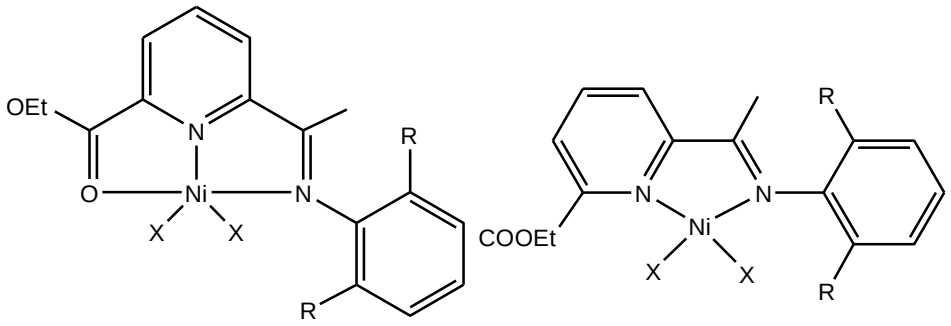

2-XIX **2-XX**

R = Me, Et, *i*-Pr, F, Cl, Br; X = Br, Cl

Figure 2.9: Nickel(II) complexes with 2-carboxylate-6-iminopyridine[38]

In a related work, Sun *et al*.[39] reported the syntheses of a series of nickel(II) complexes of type **2-XXI** ligated by 2-(1-methyl-2-benzimidazole)-6-(1-aryliminoethyl)pyridine ligands (Figure 2.10). When activated using Et_2AlCl as a co-catalyst, all the nickel(II) complexes form active catalysts in ethylene oligomerization reactions showing good catalytic activities of up to 5.87 $\times 10^5$ g oligomer.mol.$^{-1}$Ni.h^{-1} atm^{-1}, to produce mainly butenes and hexenes. In this report, complexes containing electron-withdrawing halide substituents on the aryl ring show higher catalytic activities than those bearing alkyl substituents. This is attributed to enhanced electrophilicity of the metal center by the electron-withdrawing groups at the *ortho*-position of the aryl rings.[39] Lai and co-workers[40] also reported an unsymmetrically bulky substituted nickel(II) complexes of type **2-XXII** (Figure 2.10) which favor ethylene dimerization, producing 1-butene (98.6%) and small amounts of 1-hexene.

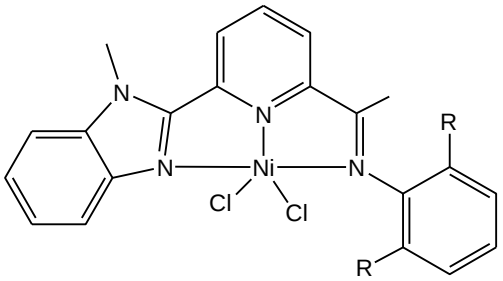

2-XXI

R = Me, Et, i-Pr, Cl, Br

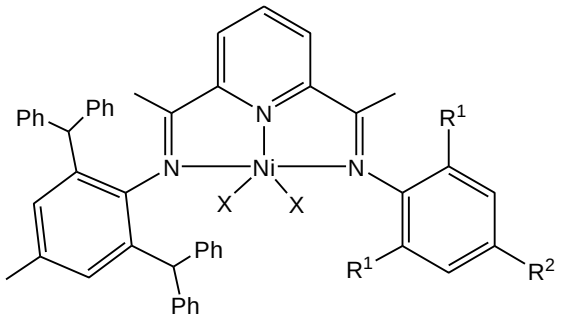

2-XXII

X = Br; R^2 = H; R^1 = Me (**a**), Et (**b**), *i*-Pr (**c**)
X = Br; R^2 = Me; R^1 = Me (**d**), Et (**e**)
X = Cl; R^2 = H; R^1 = Me (**f**), Et (**g**), *i*-Pr (**h**)
X = Cl; R^2 = Me; R^1 = Me (**i**), Et (**j**)

Figure 2.10: Pyridine diimine nickel(II) complexes[39, 40]

2.2.1.4. Nickel(II) catalyst systems based on N^O ligands

The design of ethylene oligomerization catalysts has also witnessed the use of numerous nickel(II) complexes bearing bidentate N^O ligands with promising results.[22, 41-47] For example, upon activation with MAO, DIBALH or $AlEt_3$, complexes of type **2-XXIII** (Figure 2.11) exhibit considerable catalytic activities and selectivities in ethylene oligomerization reactions. Interestingly, the unsubstituted oxazoline and aryl rings (**2-XXIII(a)**) exhibit higher catalytic activity of up to 5.51 x 10^5 g prod.mol^{-1}Ni.h.$^{-1}$

Moreover, activation using MAO favor the formation of C_6 (85%) and afford the highest catalytic activities.[48] On the other hand, complexes of type **2-XXIV** form exclusively C_4 with high selectivity for 1-C_4 (99%). The best catalytic activity is obtained on using complex **2-XXIV(e)**. Substitution of R^1 with Cl as in **2-XXIV(b)** or Me group as in **2-XXIV(c**) results in reduced catalytic activities.[49]

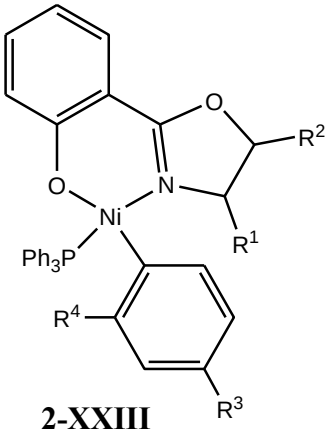

2-XXIII

$R^1 = R^2 = R^3 = R^4 = H$, (**a**)
$R^1 = R^2 = R^3 = R^4 = Me$, (**b**)
$R^1 = R^2 = R^3 = H$, $R^4 = Me$, (**c**)
$R^1 = R^3 = R^4 = H$, $R^2 = Me$, (**d**)
$R^1 = Ph$, $R^2 = R^3 = R^4 = H$, (**e**)
$R^1 = Ph$, $R^2 = R^3 = H$, $R^4 = Me$, (**f**)

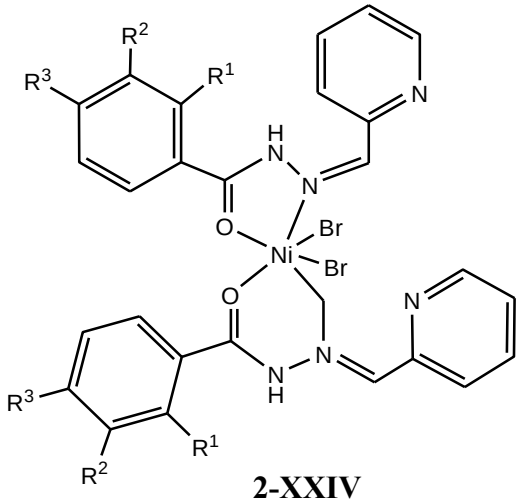

2-XXIV

$R^1 = R^2 = R^3 = H$, (**a**)
$R^1 = Cl$, $R^2 = R^3 = H$, (**b**)
$R^1 = Me$, $R^2 = R^3 = H$, (**c**)
$R^1 = R^3 = H$, $R^2 = OMe$, (**d**)
$R^1 = R^2 = H$, $R^3 = Me$, (**e**)

Figure 2.11: Nickel(II) complexes of N^O ligands[48, 49]

The nickel(II) complex **2-XXV** (Figure 2.12) is however inactive when activated with less than 6 equiv. of $EtAlCl_2$. On increasing the concentration of $EtAlCl_2$ to 10 equiv., appreciable catalytic activities of 45 000 mol.C_2H_4/mol.Ni.h are obtained, to produce mainly C_4 and C_6 oligomers and small amounts of C_8.[50]

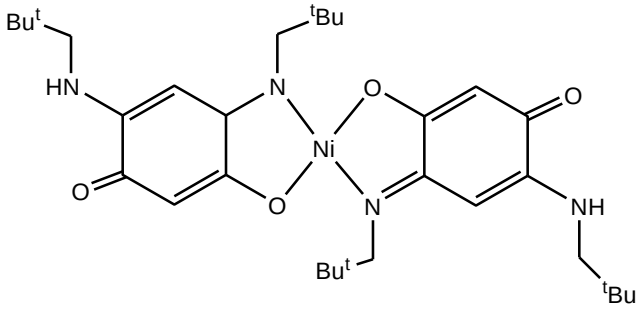

2-XXV

Figure 2.12: Bis(benzoquinonemonoimine) nickel(II) complex[50]

2.2.1.5. Pyrazolyl based nickel(II) catalysts

Since the first report in 1999 on pyrazolyl palladium(II) catalysts for ethylene oligomerization and polymerization, albeit with very low activity by Jordan and co-workers,[51] a number of nickel(II) pyrazolyl based compounds have been explored for ethylene oligomerization and polymerization reactions. For example, Casagrande, Jr. and co-workers[52] also explored a series of nickel(II) complexes of type **2-XXVI** (Figure 2.13) bearing bis(pyrazolyl) ligands.

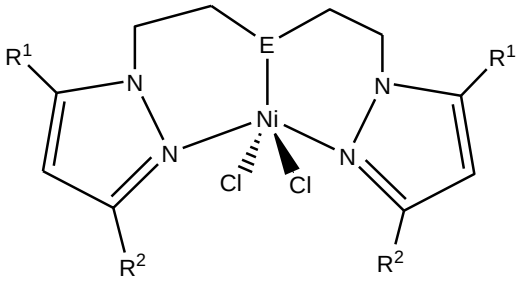

2-XXVI

E = NH, R^1=R^2 = Me, n = 0 (**a**) E = O, R^1= H, R^2 = ^{t}Bu, n = 2 (**d**)
E = O, R^1=R^2 = Me, n = 2 (**b**) E = S, R^1=R^2 = Me, n = 2 (**e**)
E = O, R^1=H, R^2 = Ph, n = 2 (**c**)

Figure 2.13: Pyrazolyl nickel(II) complexes[52]

Depending on the ligand framework, these complexes show high catalytic activities in ethylene oligomerization reactions upon activation with MAO. For example, complex **2-XXVI(e)** containing a sulfur-bridged ligand gives the highest TOF compared to the complexes bearing N- and O-based ligands **2-XXVI(a-d)**. However, these complexes of type **2-XXVI(a-d)** exhibit high selectivities for butenes and 1-butene (87.3-87.8%).

In another related work, Darkwa *et al.*[53] developed (pyrazolyl)amine nickel(II) complexes of type **2-XXVII** (Figure 2.14) which are highly active towards ethylene oligomerization reactions to mainly 1-butene and 1-hexene. Complex **2-XXVII(c)** exhibits the highest catalytic activity

producing mainly butenes and hexenes; as high as >90% selectivity for 1-butene and 1-hexene. In addition, the dibromide complex **2-XXVII(b)** gives a much higher amount of C_8–C_{20} (48%) compared to compositions reported for **2-XXVII(a)** and **2-XXVII(c)** (<2%).

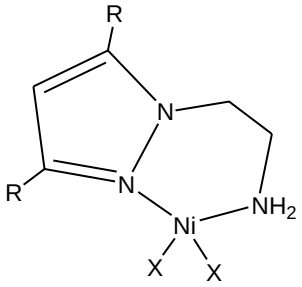

2-XXVII

R = Me, X = Cl (**a**) R = Me, X = Br (**c**)
R = H, X = Br (**b**)

Figure 2.14: (Pyrazolyl) nickel(II) complexes[53]

2.2.1.6. Friedel-Crafts alkylation by nickel(II) catalysts

The first report on Friedel-Crafts alkylation of pre-formed oligomers by toluene solvent was reported by Dyer *et al*.[54] They observed that nickel(II) complexes of type **2-XXVIII(b-d)** of *N*-phosphinoguanidine ligands, (Figure 2.15) when activated by $EtAlCl_2$, form C_4, C_6 and C_8 oligomers. Under identical conditions, [7-(diphenylphosphino)-1,5,7-triazabicyclo[4.4.0]-dec-5-ene]nickel(II) dibromide complex **2-XXVIII(a)** promotes *in situ* Friedel–Crafts alkylation of toluene solvent by the pre-formed oligomers to form alkyltoluenes. Only small amounts of oligomers (<1 wt%) are obtained suggesting that the Ph_2P-substituted ligand is an indispensable factor in initiating Friedel-Crafts reaction in this system. Furthermore, reaction of **2-XXVIII(a)** in dichloromethane or chlorobenzene only forms small quantities of butenes and hexenes without the occurrence of Friedel-Crafts reactions.

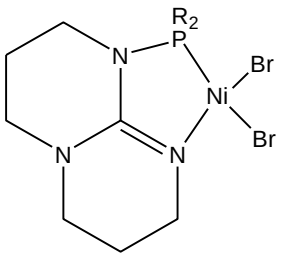

2-XXVIII

R= Ph (**a**); Mes(**b**); *i*Pr$_2$N(**c**); Ph$_2$N(**d**)

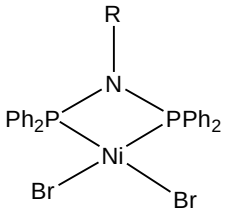

2-XXIX

R= $CH_2(C_6H_5)$, $CH_2(C_4H_3O)$, $CH_2(C_4H_3S)$, $CH_2(C_5H_4N)$,$CH_2CH_2(C_4H_3S)$

Figure 2.15: *N*-Phosphino guanidine and bis(phosphanyl)amine nickel(II) complexes[54, 55]

In a follow up work, Song and co-workers[55] reported nickel(II) complexes of type **2-XXIX** (Figure 2.15) which, upon activation using $EtAlCl_2$ or MAO, catalyze oligomerization of ethylene to mainly butene (96 mol%) and small amounts of hexene oligomers at -40 °C. In contrast, increasing the reaction temperature to 50 °C results in the formation of trace amounts of oligomers. The main products formed being alkyltoluenes that consist of ethyltoluenes, butyltoluenes and hexyltoluenes.

Ojwach *et al.*[56] encountered the same phenomenon in their work on nickel(II) complexes **2-XXX-2-XXXII** (Figure 2.16) of the symmetrical 2,6-bis(pyrazol-1-ylmethyl)pyridine and 2-(pyrazol-1-ylmethyl)pyridine ligands. Activation of these nickel(II) complexes with $EtAlCl_2$ results in oligomerization of ethylene to C_4-C_8 oligomers, which subsequently undergo complete alkylation by the toluene solvent, to form alkyltoluenes. Activities as high as 15 660 kg products.mol.$^{-1}$Ni.h^{-1} are obtained. These complexes, however, do not promote direct alkylation of ethylene to toluene solvent to form ethyltoluenes.

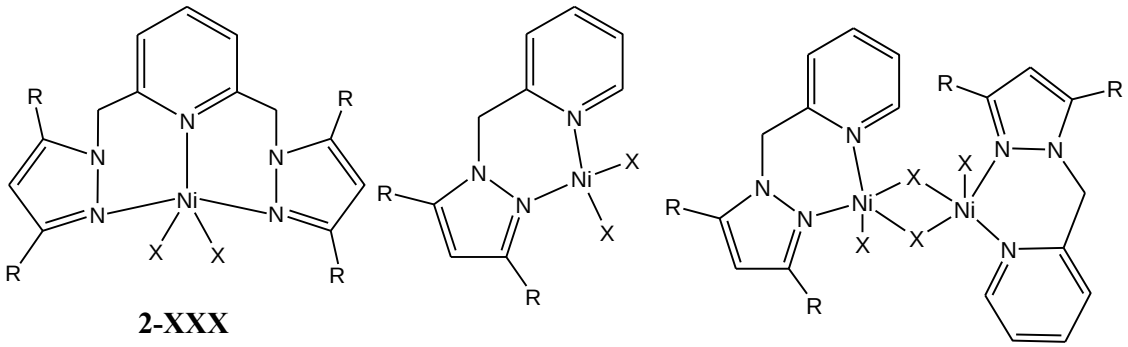

2-XXX

R = Me, X = Cl (**a**)
R = Me, X = Br (**b**)
R = ^{t}Bu, X = Cl (**c**)
R = ^{t}Bu, X = Br (**d**)

2-XXXI

R = ^{t}Bu, X = Cl (**a**)
R = ^{t}Bu, X = Br (**b**)

2-XXXII

R = Me, X = Cl (**a**)
R = Me, X = Br (**b**)

Figure 2.16: (Pyrazol-1-ylmethyl)pyridine nickel(II) complexes[56]

In a follow-up work, Ainooson *et al*.[57] reported pyrazolyl nickel(II) bromide complexes **2-XXXIII** and **2-XXXIV** (Figure 2.17) which upon activation using $EtAlCl_2$, produces active catalysts for ethylene oligomerization reactions with catalytic activities as high as 4 329 kg oligomer.mol.$^{-1}$Ni.h^{-1}. Using complex **2-XXXIII**, mainly butenes (57%) and hexenes (43%) are produced, of which a combined 20% are subsequently alkylated to toluene. Complex **2-XXXIV**, on the other hand, catalyzes ethylene to produce mainly butenes (90%) and hexenes (10%) which are then completely converted to the corresponding alkyltoluenes. In terms of catalytic activity, complex **2-XXXIII** is more active (4, 197 kg oligomer.mol.$^{-1}$Ni.h^{-1}) than complex **2-XXXIV** (78 kg oligomer.mol.$^{-1}$Ni.h^{-1}), under the same reaction conditions. Thus, the difference in catalytic activities and product distribution exhibited by these complexes underscores the role of the ligand in ethylene oligomerization reactions. It's noteworthy to point out that both complexes do not catalyze Friedel-Crafts alkylation of the ethylene monomer.

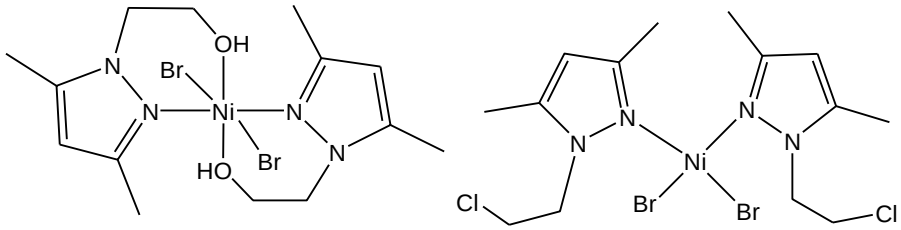

2-XXXIII **2-XXXIV**

Figure 2.17: (Pyrazolyl) nickel(II) dibromide complexes[57]

In a related study, Budhai *et al*.[58] showed that nickel(II) complexes **2-XXXV** and **2-XXXVI** (Figure 2.18), upon activation with $EtAlCl_2$, catalyze oligomerization of ethylene to mainly 1-butene and 1-hexene oligomers, most of which are subsequently alkylated to toluene used as solvent in these reactions. Only < 5% oligomers are obtained with these complexes. Moreover, these complexes also catalyze Friedel-Crafts reaction of ethylene monomer to produce ethyltoluenes in the product mixture.

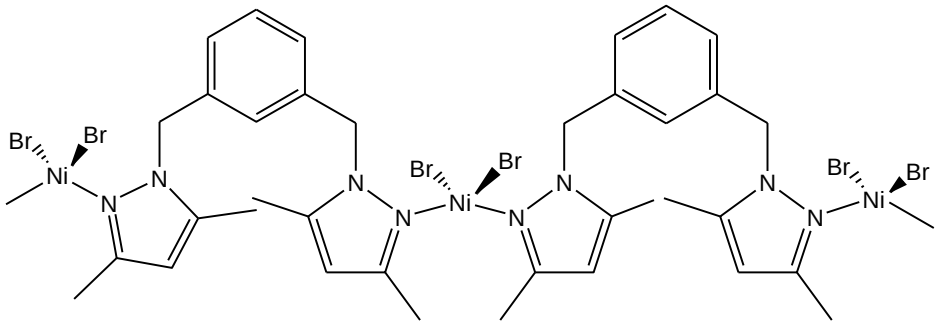

2-XXXV

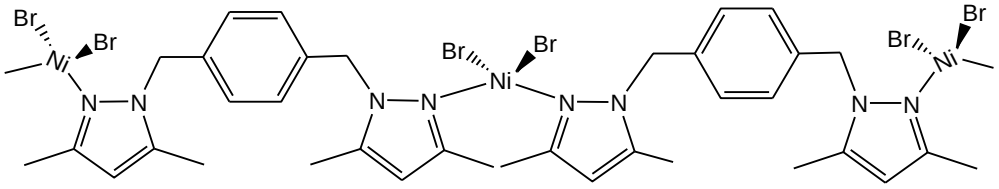

2-XXXVI

Figure 2.18: (Pyrazolyl) nickel(II) complexes[58]

Recently, Obuah and co-workers also reported Friedel-Crafts alkylation when investigating nickel(II) dibromide complexes of type **2-XXXVII** and **2-XXXVIII** that incorporate pyridine and pyrrole rings, respectively (Figure 2.19).[59] These complexes, upon activation with $EtAlCl_2$, catalyze ethylene oligomerization to form butene and hexene oligomers which are subsequently alkylated to the toluene solvent. However, unlike in the work by Ojwach *et al*.[56] where all the pre-formed oligomers are subsequently alkylated to toluene, these complexes only selectively alkylate butene to produce butyl-butyltoluenes. On using MAO as the co-catalyst, these complexes catalyze ethylene polymerization, forming high density polyethylene. This highlights the role of co-catalyst in this type of reactions. Moreover, these nickel(II) dibromide complexes (**2-XXXVII** and **2-XXXVIII**) also demonstrate the role of solvent in ethylene oligomerization and polymerization reactions given that when the reactions are conducted in chlorobenzene, butenes, hexenes and branched polyethylenes are formed.

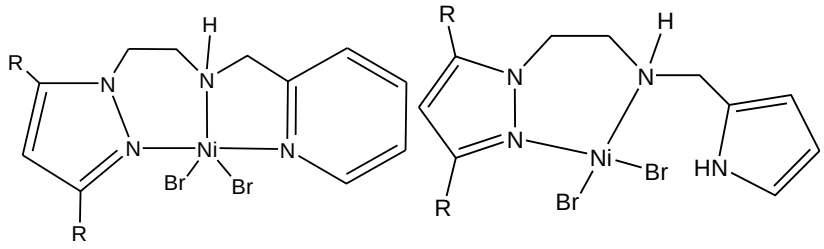

2-XXXVII
R = Me (**a**); R = ^{t}Bu (**b**)

2-XXXVIII
R = Me, ^{t}Bu

Figure 2.19: (Pyrazolyl)-pyridine and pyrazolyl-pyrrole nickel(II) complexes[59]

2.2.2. Iron(II) and cobalt(II) complexes as catalysts in ethylene oligomerization reactions

In the quest to discover other catalysts that can rival Brookhart's α-diimine nickel(II) and palladium(II) olefin oligomerization and polymerization catalysts, investigations have been extended to other metal centers such as iron(II) and cobalt(II). In 1998, the groups of Brookhart[60] and Gibson[61] independently reported cationic 2,6-bis(arylimino)pyridyl iron(II) and cobalt(II)

active complexes of type **2-XXXIX** (Figure 2.20) that form active catalysts in ethylene oligomerization and polymerization reactions, upon activation with MAO. This work triggered an ‘‘iron age’’ in ethylene oligomerization and polymerization research. It has been shown that these late transition metal catalysts offer several advantages over the metallocenes, ranging from the ease of preparation and handling, to the use of low-cost metals with negligible environmental impact, and facile-tuning of their catalytic activity through tailoring of the ligand architecture.[60, 61]

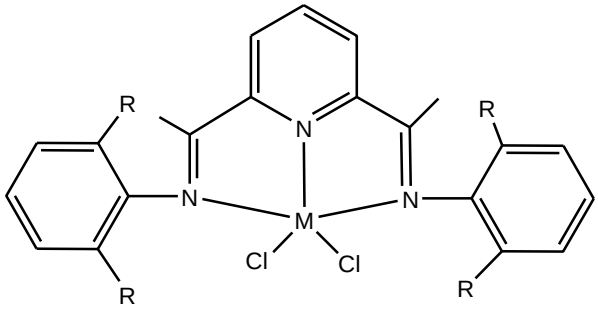

2-XXXIX
M = Fe, Co
R = *i*Pr, Me

Figure 2.20: 2,6-Bis(arylimino)pyridyl iron(II) and cobalt(II) active catalysts[60, 61]

The ability to fine tune the ancillary ligand set is perhaps one of the most attractive features of this catalyst design, making it possible to vary product distribution from oligomers to polymers. The complexes exhibit high catalytic activities in ethylene oligomerization and polymerization reactions, producing linear polyethylenes as well as oligomers. Introduction of bulky aryl-substituents in the *ortho* positions slows the rate of chain transfer relative to chain growth to afford high molecular weight polymers.[62]

The influence of steric bulk has been shown to be more pronounced in the iron(II) complexes compared to their cobalt(II) analogues. For example, the less sterically bulk methyl group on the aryl rings remarkably enhances the catalytic activity of the iron(II) catalyst in ethylene oligomerization reactions. Surprisingly high turnover frequencies (TOF), as high as several millions per hour have been reported for the iron(II) catalysts under optimized conditions.[60] In addition, this reduced steric crowding around the iron(II) metal center results in the formation of linear α-olefins (>99%).

The reports of the groups of Brookhart[60] and Gibson[61] have stimulated considerable interest in iron(II) and cobalt(II) complexes, bearing neutral tridentate N^N^N ligands, as precursors in ethylene oligomerization reactions.[63-66] Most notable is the report by Bianchini *et al.*[2] on bimetallic iron(II) and cobalt(II) complexes bearing 2,6-bis(imino)pyridine ligands **2-XL** and **2-XLI** (Figure 2.21).

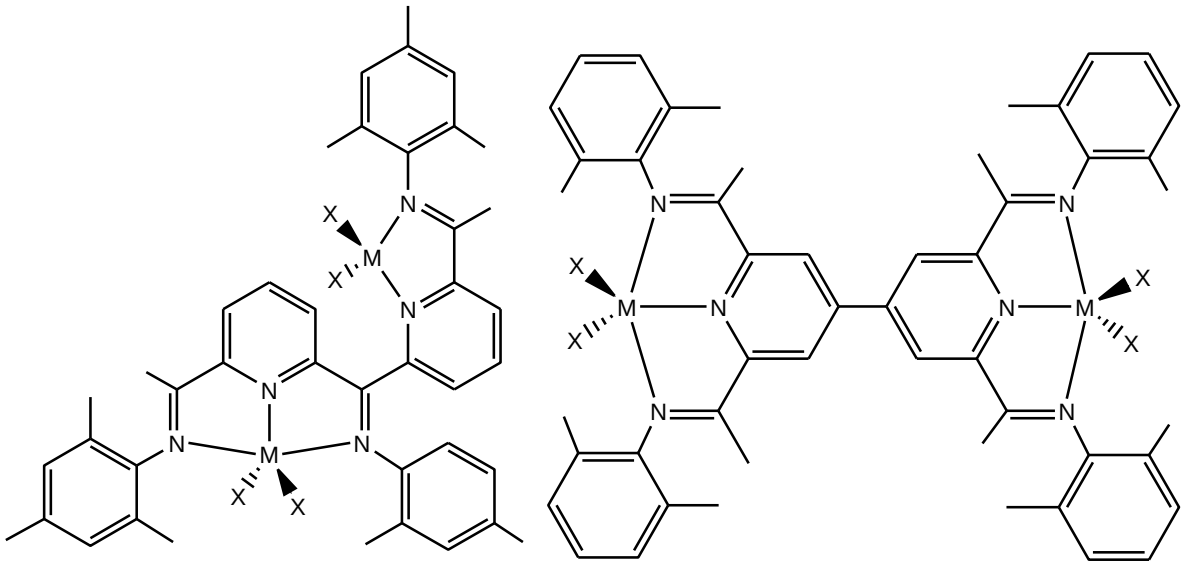

2-XL **2-XLI**

M = Co, Fe; X = Br, Cl

Figure 2.21: Iron(II) and cobalt(II) complexes bearing 2,6-bis(imino)pyridine ligands[2]

These complexes, upon activation with MAO, generate active catalysts in ethylene oligomerization reactions to produce α-olefins in the range C_4-C_{14}. The dinuclear cobalt(II) complexes are particularly active, exhibiting activities of up to 61 000 kg oligomer.mol.$^{-1}$Co.h^{-1} compared to typical mononuclear systems which display activities of about 1 000 kg oligomer.mol.$^{-1}$Co.h^{-1}. Ironically, cobalt(II) catalyst of type **2-XL**, for example, displays exceptionally high catalytic activity in ethylene polymerization of 64 000 kg PE.mol.$^{-1}$Co.h^{-1}.[67, 68] In addition, Sun and co-workers reported iron(II) and cobalt(II) catalysts chelated by N-(1-(6-(quinoxalin-2-yl)pyridine-2-yl)ethylidene)benzenamines of type **2-XLII** and 2-(1-(2,4-bis((di(4-fluorophenyl)-methyl)-6-methylphenylimino)ethyl)-6-(1-(arylimino)ethyl)pyridine ligands **2-XLIII** (Figure 2.22).[69] In both systems, the iron(II) complexes show higher catalytic activities in ethylene oligomerization and polymerization, as well as, improved thermal stability upon activation with MAO than their cobalt(II) analogues.

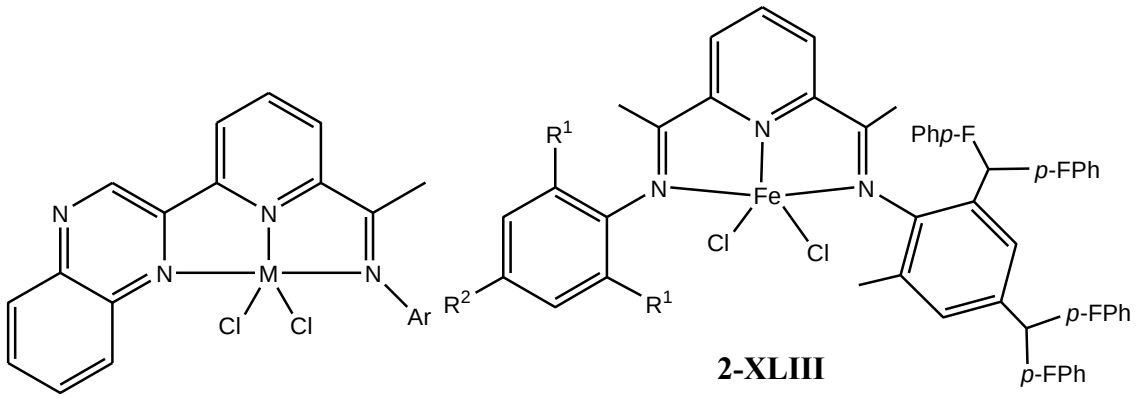

2-XLII
M= Fe, Co

2-XLIII
R^1 = Me, Et, iPr,
R^2 = H, Me

Figure 2.22: Iron(II) and cobalt(II) complexes bearing N-(1-(6-(quinoxalin-2-yl)pyridine-2-yl)ethylidene)benzenamines[69]

In another study by Bahuleyan *et al*.[70] on tridentate cobalt(II) complexes of type **2-XLIV** (Figure 2.23) bearing pendant donor modified α-diimine ligands, it has been shown that the catalytic

behaviour of these complexes are significantly affected by the ligand environment. Increasing the steric demands of the substituent group at the *ortho*-position of the aryl group considerably enhances catalytic activities towards ethylene oligomerization upon activation with MAO. For example, the activity of **2-XLIV(c)**, bearing isopropyl substituents is 9.4×10^4 g oligomer.mol^{-1}Co.h^{-1} compared to that of complex **2-XLIV(b**) containing an ethyl substituent of 8.2×10^4 g oligomer.mol^{-1}Co.h^{-1}. Both of these complexes are more active than **2-XLIV(a**) containing a less sterically demanding methyl substituent (7.3×10^4 g mol^{-1}(Co) h^{-1}).

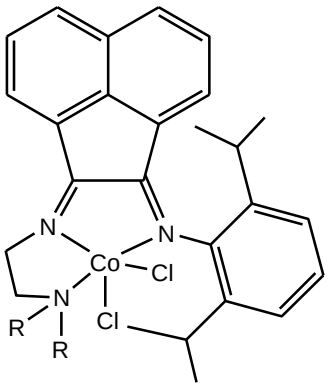

2-XLIV

R = Me (**a**); R = Et (**b**); R = *i*-Pr (**c**)

Figure 2.23: α-Diimine cobalt(II) complexes[70]

Generally, iron(II) complexes have been found to exhibit higher catalytic activities in ethylene oligomerization reactions compared to the cobalt(II) based complexes, with high selectivities towards linear α-olefins.[71-73] In spite of the efforts that have been directed towards enhancing the catalytic performance of these iron(II) and cobalt(II) catalysts, none of the new ligand designs has given rise to systems capable of oligomerizing ethylene with similar or higher activities than Brookhart's bis(imino)-pyridine iron(II) complexes (10^8 g oligomer.mol.$^{-}$

^{1}catalysts.h.$^{-1}$atm^{-1}. Nevertheless, there is more promise in the less investigated environmental friendly iron(II) and cobalt(II) complexes as ethylene oligomerization catalysts.[4, 73]

2.2.3. Palladium(II) complexes as catalysts in ethylene oligomerization reactions

2.2.3.1. Neutral palladium(II) complexes

Literature reports describing the application of neutral palladium(II) complexes in ethylene oligomerization reactions are few, a factor that has been attributed to the low catalytic performance of these palladium(II) systems.[74] One such example is the report by Moss *et al*.[75] on palladium(II) α-diimine containing dendritic wedges (**2-XLV**) as ethylene oligomerization catalysts (Figure 2.24) which upon activation using MAO (400 equiv.) forms C_4-C_{14} oligomers.

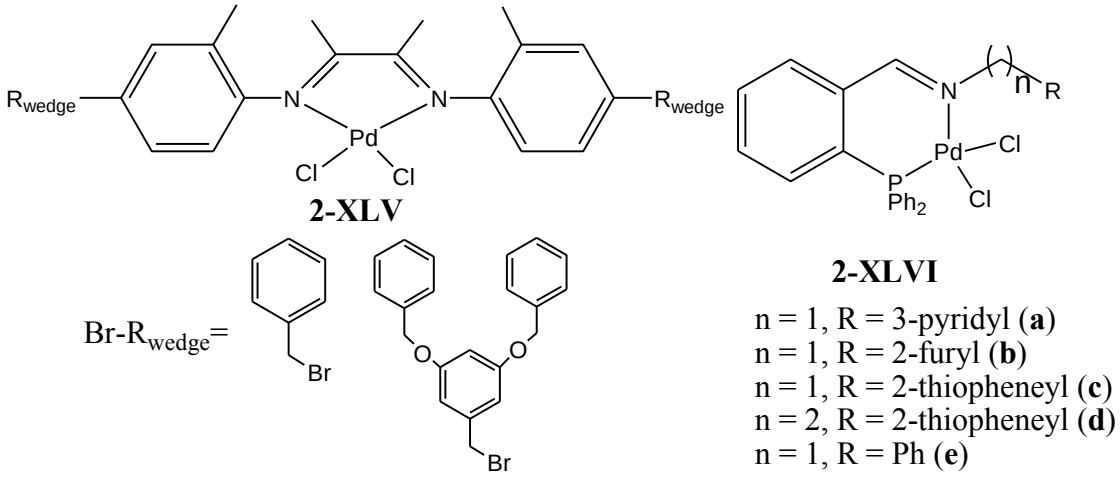

Figure 2.24: Neutral palladium(II) complexes containing dendritic wedges (**2-XLV**) and *P^N* Schiff-base (**2-XLVI**) ligands[74, 75]

Smith and co-workers also reported neutral palladium(II) complexes **2-XLVI** chelated by 2-phosphinobenzaldimino ligands (Figure 2.24) which favor ethylene dimerization (with minimal amounts of hexenes, <3%) upon activation with $EtAlCl_2$ as co-catalyst.[74] The catalytic behaviour

of these complexes is affected by the reaction conditions such as co-catalyst/pre-cursor molar ratio, ethylene pressure, reaction temperature and time. For example, higher catalytic activities are obtained on increasing Al/Pd molar ratio from 10 to 50 while no catalytic activity is obtained at reduced Al/Pd of 4.

Recently, Revankar *et al*.[76] reported ethylene oligomerization studies using binuclear palladium(II) catalysts **2-XLVII** bearing bis-α-diimine ligands (Figure 2.25). All the complexes exhibit high catalytic activities in ethylene oligomerization reactions when activated with ethylaluminum sesquichloride (EASC) or MAO as co-catalysts to produce C_4-C_{20} oligomers. Activities of up to 1 218.4 kg oligomer.mol.$^{-1}$Pd.bar.$^{-1}$h^{-1} are obtained using EASC. The ligand environment influences the catalytic performance of these palladium(II) complexes with complexes bearing bulky isopropyl groups forming the most active catalysts.

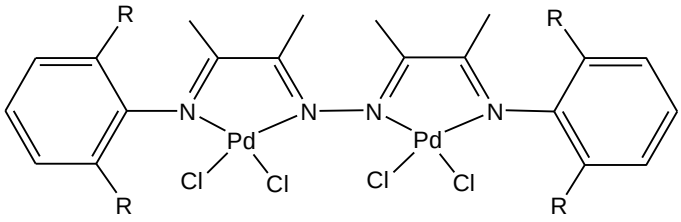

2-XLVII

R = Me (**a**), R = Et (**b**), R = ^{i}Pr (**c**)

Figure 2.25: Binuclear bis-α-diimine palladium(II) complexes[76]

2.2.3.2. Cationic palladium(II) complexes as ethylene oligomerization catalysts

In the neutral systems discussed above, the active cationic species are generated *in situ* upon activation with co-catalysts such as MAO, $EtAlCl_2$ etc. On the other hand, cationic palladium(II) complexes can be isolated using well defined halide abstractors such as $NaBAr_4$ and stabilized by weak coordinating donor solvents, such as MeCN, which can be readily displaced by an

incoming ethylene monomer. In spite of the enormous efforts that have been devoted to improve the catalytic activities of these palladium(II) based catalysts, the outcome in most cases has been low or inactive systems.[21] For example, Kress and co-workers reported ethylene oligomerization using cationic palladium(II) catalysts of type **2-XLVIII** based on unsymmetrical α-diimine ligand (Figure 2.26).[77] The catalyst is efficient in ethylene oligomerization with an average activity of 150 kg oligomer.mol.$^{-1}$Pd.h^{-1} and gives a Schulz–Flory distribution of oligomeric products (C_4-C_{20}).

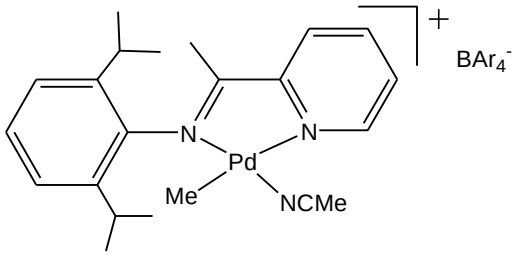

2-XLVIII

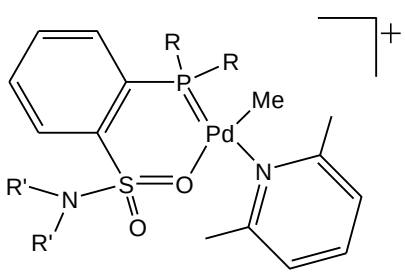

2-XLIX

R = Ph, R' = Cy (**a**)
R = o-OMePh, R' = Cy (**b**)
R = Cy, R' = Cy (**c**)
R = *i*Pr, R' = Cy (**d**)
R = Ph, R' = Me (**e**)
R = *i*Pr, R' = Me (**f**)

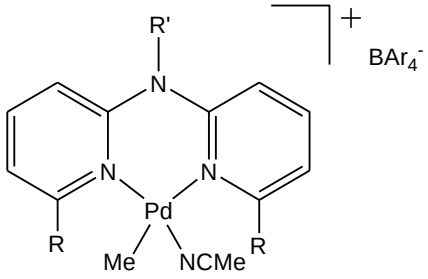

2-L

R = H, R' = Me (**a**)
R = H, R' = Bn (**b**)
R = H, R' = MeCy (**c**)
R = H, R' = Np (**d**)
R = Me, R' = Me (**e**)

Figure 2.26: Examples of cationic palladium(II) complexes evaluated for ethylene oligomerization[77-79]

In a recent report,[79] palladium(II) complexes of type **2-XLIX** (Figure 2.26) bearing phosphine-sulfonamide ligands have been developed that catalyze ethylene oligomerization to mainly

butenes and hexenes. In a similar study, cationic palladium(II) complexes of type **2-L** anchored on *N*-alkyl 2,2′-dipyridylamine ligands have also been shown to favor the formation of exclusively butenes.[78] However, the catalytic activities of these complexes are significantly low, with the highest TOF ($n_{ethylene}$ consumed/(n_{Pd} h)) value of 7.4 h^{-1} obtained for complex **2-L$_d$**.

2.2.3.3. Hemi-labile palladium(II) systems

The term ‘‘hemi-labile’’ was introduced about 36 years ago by Rauchfuss,[80] however, the phenomenon itself had been observed earlier.[81] Hemi-lability arises in hetero-multidentate ligands which can partly and reversibly dissociate from the metal center to which they are coordinated. The dissociation of one of the donor groups generates a coordination site at the metal center that allows for coordination of an incoming substrate.[82] Ideally, the incoming monomer should be more strongly coordinating than the hemi-labile moiety.

Literature reports[83-89] detail numerous applications of this phenomenon which has strong relevance in homogeneous catalysis in which the main role of the hemi-labile system is to stabilize the active cationic species, thus enhancing the stability of the catalyst. For example, Liu *et al*.[88] have shown that the hemi-labile ether donor of complex **2-LI** (Figure 2.27) is easily replaced by a weakly coordinating ligand such as MeCN. Complex **2-LI** catalyzes the conversion of ethylene into C_4-C_{16} oligomers with activities of up to 4.95 x 10^{-2} g $mm^{-1}h^{-1}$.

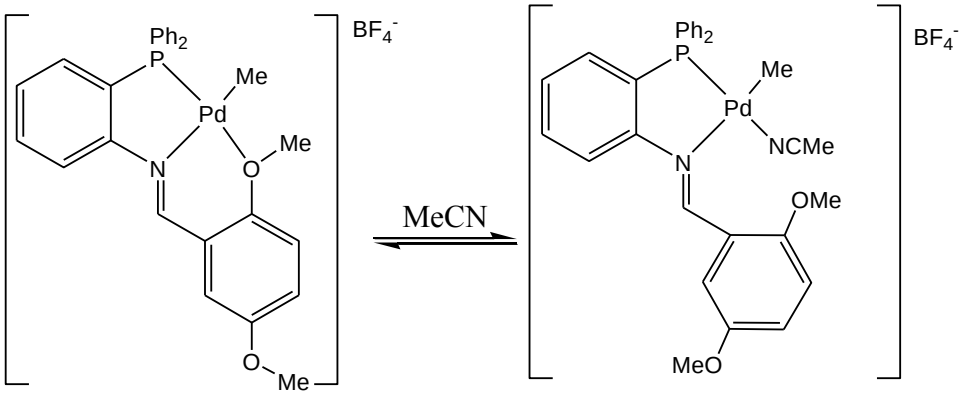

2-LI

Figure 2.27: Hemi-labile cationic palladium(II) complexes containing P^N^O ligand[88]

In another related example, Onani and co-workers[87] reported palladium(II) complexes of type **2-LII** (Figure 2.28) containing furan or thiophene hemi-labile groups which catalyze polymerization of ethylene though with very low activities. From Density Functional Theory (DFT) calculations, competition between ethylene monomer and the furan or thiophene groups for the vacant active site upon halide abstraction, hinders ethylene coordination to the palladium(II) center, thus resulting in negligible activities.

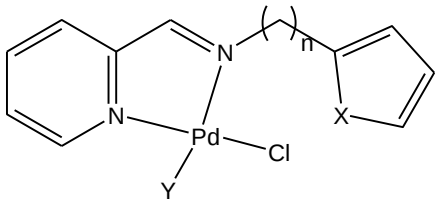

2-LII

X= O, S;Y= Cl, Me
n= 1, 2

Figure 2.28: Hemi-labile pyridyl-imine palladium(II) complexes[87]

In summary, the seminal work of Brookhart and co-workers on nickel(II) aryl-substituted α-diimine catalysts and subsequent iron(II) complexes bearing tridentate 2,6-bis(imino)pyridine

reported independently by the groups of Brookhart and Gibson proved to be a milestone in the development of late-transition metal based catalysts in ethylene oligomerization reactions. Much effort has been directed towards catalyst modification in order to enhance both activity and selectivity. To achieve this goal, further exploration is required.

2.3. Rationale of study

Ethylene is a readily available feedstock, and its oligomerization for the production of higher olefins is one of the most significant processes of transition-metal catalysis. During the last twenty years, the design and development of new ligand systems has been essential for the improvement of olefin oligomerization catalysts. Homogeneous catalysts permit good flexibility in the reactions given that their high activity and selectivity at low concentration levels (ppm) makes it possible to minimize costs resulting from catalyst consumption and spent catalyst disposal.[90]

The production of lighter linear olefins such as C_4-C_8 is achieved predominantly by metal-catalyzed oligomerization of ethylene, which more often than not leads to a distribution of α-olefins with different chain lengths that frequently does not match the market demand. Despite the advances made in selective oligomerization of ethylene, such as selective tetramerization of ethylene to 1-octene by Sasol Technology South Africa,[15] the identification and fine-tuning of the parameters that control the activity and selectivity of the metal catalysts still constitute a major challenge. Consequently, a considerable number of studies still need to be done on ethylene oligomerization reactions, targeting a narrow product distribution and improvement of activity in order to meet the souring commercial demand for α-olefins in the C_4-C_{10} range. This

project therefore aimed at designing late transition metal catalysts that are not only active but also selective in ethylene oligomerization reactions.

2.4. Objectives

From the rationale above, the objectives of this study can be formulated as follows:

1. To synthesize and characterize new (pyrazolyl)pyridine cobalt(II), iron(II) and nickel(II) complexes and study their ability to catalyze ethylene oligomerization reactions. This was aimed at gaining insight into the role of the pyrazolyl unit in controlling the catalytic activities of these metal complexes.

2. To synthesize and characterize (pyrazolyl)phosphine cobalt(II), iron(II) and nickel(II) complexes and evaluate them as ethylene oligomerization catalysts to further understand the behavior of mixed P^N donor systems. However, due to *in situ* oxidation of (pyrazolyl)phosphine ligands to their corresponding phosphinite ligands, cobalt(II), iron(II) and nickel(II) complexes bearing N^N^O (pyrazolyl)(phosphinoyl)-pyridine ligands were evaluated as catalysts in ethylene oligomerization reactions.

3. To synthesize and characterize new palladium(II) complexes bearing (imino)pyridine ligands containing potential hemilabile ether or amino pendant donor groups and study their ability to catalyze ethylene oligomerization reactions.

4. Attempts to synthesize nickel(II) complexes bearing the (imino)pyridine ligands were unsuccessful, possibly due to hydrolysis. Thus, the ligands were reduced to their respective

amines and the resultant new pyridinamine nickel(II) complexes were investigated for their ability to catalyze ethylene oligomerization reactions.

5. To employ theoretical and spectroscopic methods to interrogate the observed catalytic trends and offer more insight on rational ligand and catalyst design tailored for specific product distribution in ethylene oligomerization reactions.

Chapters 3-6 describes the results of the work done to achieve the above objectives, while the overall conclusions are summarized in Chapter 7.

2.5. References

1. Skupinska, J., *Chem. Rev.* **1991**, *91*, 613-648.
2. Bianchini, C.; Giambastiani, G.; Rios, I. G.; Mantovani, G.; Meli, A.; Segarra, A. M., *Coord. Chem. Rev.* **2006**, *250*, 1391-1418.
3. Mecking, S., *Coord. Chem. Rev.* **2000**, *203*, 325-351.
4. Boudier, A.; Breuil, P.-A. R.; Magna, L.; Olivier-Bourbigou, H.; Braunstein, P., *Chem. Commun.* **2014**, *50*, 1398-1407.
5. Netalkar, S. P.; Netalkar, P. P.; Sathisha, M.; Budagumpi, S.; Revankar, V. K., *Catal. Lett.* **2014**, *144*, 181-191.
6. Bianchini, C.; Giambastiani, G.; Luconi, L.; Meli, A., *Coord. Chem. Rev.* **2010**, *254*, 431-455.
7. Gibson, V. C.; Redshaw, C.; Solan, G. A., *Chem. Rev.* **2007**, *107*, 1745-1776.

8. Fischer, K.; Jonas, K.; Misbach, P.; Stabba, R.; Wilke, G., *Angew. Chem. Int. Ed.* **1973**, *12*, 943-953.
9. Ziegler, K.; Gellert, H.; Holzkamp, E.; Wilke, G., *Chem.* **1954,** *35*, 321.
10. Gao, R.; Sun, W.-H.; Redshaw, C., *Catal. Sci. Technol.* **2013**, *3*, 1172-1179.
11. Ortiz de la Tabla, L.; Matas, I.; Palma, P.; Á varez, E.; Cámpora, J., *Organometallics* **2012**, *31*, 1006-1016.
12. Wang, S.; Sun, W.-H.; Redshaw, C., *J. Organomet. Chem.* **2014**, *751*, 717-741.
13. Hirose, K.; Keim, W., *J. Mol. Catal.* **1992**, *73*, 271-276.
14. Keim, W.; Kowaldt, F. H.; Goddard, R.; Krüger, C., *Angew. Chem. Int. Ed.* **1978**, *17*, 466-467.
15. Keim, W., *Angew. Chem. Int. Ed.* **2013**, *52*, 12492-12496.
16. Ittel, S. D.; Johnson, L. K.; Brookhart, M., *Chem. Rev.* **2000**, *100*, 1169-1204.
17. Mecking, S., *Angew. Chem. Int. Ed.* **2001**, *40*, 534-540.
18. Klabunde, U.; Mulhaupt, R.; Herskovitz, T.; Janowicz, A.; Calabrese, J.; Ittel, S., *J. Polym. Sci., Part A: Polym. Chem.* **1987**, *25*, 1989-2003.
19. Müller, C.; Ackerman, L. J.; Reek, J. N.; Kamer, P. C.; van Leeuwen, P. W., *J. Am. Chem. Soc.* **2004**, *126*, 14960-14963.
20. Chavez, P.; Rios, I. G.; Kermagoret, A.; Pattacini, R.; Meli, A.; Bianchini, C.; Giambastiani, G.; Braunstein, P., *Organometallics* **2009**, *28*, 1776-1784.
21. Flapper, J.; Kooijman, H.; Lutz, M.; Spek, A. L.; van Leeuwen, P. W.; Elsevier, C. J.; Kamer, P. C., *Organometallics* **2009**, *28*, 1180-1192.
22. Kermagoret, A.; Braunstein, P., *Organometallics* **2007**, *27*, 88-99.
23. Johnson, L. K.; Killian, C. M.; Brookhart, M., *J. Am. Chem. Soc.* **1995**, *117*, 6414-6415.

24. Speiser, F.; Braunstein, P.; Saussine, L., *Acc. Chem. Res.* **2005**, *38*, 784-793.

25. Zhang, W.; Sun, W., *Prog. Chem.* **2005**, *17*, 310-319.

26. Dieck, H. T.; Svoboda, M.; Greiser, T., *Z. Naturforsch B: Chem. Sci.* **1981**, *36*, 823-832.

27. van Asselt, R.; Elsevier, C. J.; Smeets, W. J. J.; Spek, A. L.; Benedix, R., *Recl. Trav. Chim. Pays B.* **1994**, *113*, 88-98.

28. Killian, C. M.; Johnson, L. K.; Brookhart, M., *Organometallics* **1997**, *16*, 2005-2007.

29. Svejda, S. A.; Brookhart, M., *Organometallics* **1999**, *18*, 65-74.

30. Wang, S.; Du, S.; Zhang, W.; Asuha, S.; Sun, W.-H., *ChemistryOpen* **2015**, 4, 328-334.

31. Laine, T. V.; Piironen, U.; Lappalainen, K.; Klinga, M.; Aitola, E.; Leskelä, M., *J. Organomet. Chem.* **2000**, *606*, 112-124.

32. Sun, W.-H.; Song, S.; Li, B.; Redshaw, C.; Hao, X.; Li, Y.-S.; Wang, F., *Dalton Trans.* **2012,** *41*, 11999-12010.

33. Yue, E.; Zhang, L.; Xing, Q.; Cao, X.-P.; Hao, X.; Redshaw, C.; Sun, W.-H., *Dalton Trans.* **2014**, *43*, 423-431.

34. Hou, X.; Cai, Z.; Chen, X.; Wang, L.; Redshaw, C.; Sun, W.-H., *Dalton Trans.* **2012**, *41*, 1617-1623.

35. Song, S.; Xiao, T.; Wang, L.; Redshaw, C.; Wang, F.; Sun, W.-H., *J. Organomet. Chem.* **2012**, *699*, 18-25.

36. Zhang, L.; Hao, X.; Sun, W.-H.; Redshaw, C., *ACS Catalysis* **2011**, *1*, 1213-1220.

37. Song, S.; Li, Y.; Redshaw, C.; Wang, F.; Sun, W.-H., *J. Organomet. Chem.* **2011**, *696*, 3772-3778.

38. Tang, X.; Sun, W.-H.; Gao, T.; Hou, J.; Chen, J.; Chen, W., *J. Organomet. Chem.* **2005**, *690*, 1570-1580.

39. Hao, P.; Zhang, S.; Sun, W.-H.; Shi, Q.; Adewuyi, S.; Lu, X.; Li, P., *Organometallics* **2007**, *26*, 2439-2446.

40. Lai, J.; Hou, X.; Liu, Y.; Redshaw, C.; Sun, W.-H., *J. Organomet. Chem.* **2012**, *702*, 52-58.

41. Delferro, M.; McInnis, J. P.; Marks, T. J., *Organometallics* **2010**, *29*, 5040-5049.

42. Hu, T.; Tang, L.-M.; Li, X.-F.; Li, Y.-S.; Hu, N.-H., *Organometallics* **2005**, *24*, 2628-2632.

43. Shi, Q.; Zhang, S.; Chang, F.; Hao, P.; Sun, W.-H., *C. R. Chim.* **2007**, *10*, 1200-1208.

44. Song, D.-P.; Wang, Y.-X.; Mu, H.-L.; Li, B.-X.; Li, Y.-S., *Organometallics* **2011**, *30*, 925-934.

45. Wang, C.; Friedrich, S.; Younkin, T. R.; Li, R. T.; Grubbs, R. H.; Bansleben, D. A.; Day, M. W., *Organometallics* **1998,** *17*, 3149-3151.

46. Younkin, T. R.; Connor, E. F.; Henderson, J. I.; Friedrich, S. K.; Grubbs, R. H.; Bansleben, D. A., *Science* **2000**, *287*, 460-462.

47. Kermagoret, A.; Braunstein, P., *Dalton Trans.* **2008**, 1564-1573.

48. Zhao, W.; Qian, Y.; Huang, J.; Duan, J., *J. Organomet. Chem.* **2004**, *689*, 2614-2623.

49. Hou, J.; Sun, W.-H.; Zhang, D.; Chen, L.; Li, W.; Zhao, D.; Song, H., *J. Mol. Catal. A: Chem.* **2005**, *231*, 221-233.

50. Taquet, J.-p.; Siri, O.; Braunstein, P.; Welter, R., *Inorg. Chem.* **2004**, *43*, 6944-6953.

51. Tsuji, S.; Swenson, D. C.; Jordan, R. F., *Organometallics* **1999**, *18*, 4758-4764.

52. Ajellal, N.; Kuhn, M. C.; Boff, A. D.; Hörner, M.; Thomas, C. M.; Carpentier, J.-F.; Casagrande, O. L., *Organometallics* **2006**, *25*, 1213-1216.

53. Ainooson, M. K.; Guzei, I. A.; Spencer, L. C.; Darkwa, J., *Polyhedron* **2013**, *53*, 295-303.

54. Dyer, P. W.; Fawcett, J.; Hanton, M. J., *Organometallics* **2008**, *27*, 5082-5087.

55. Song, K.; Gao, H.; Liu, F.; Pan, J.; Guo, L.; Zai, S.; Wu, Q., *Eur. J. Inorg. Chem.* **2009**, *2009*, 3016-3024.

56. Ojwach, S. O.; Guzei, I. A.; Benade, L. L.; Mapolie, S. F.; Darkwa, J., *Organometallics* **2009**, *28*, 2127-2133.

57. Ainooson, M. K.; Ojwach, S. O.; Guzei, I. A.; Spencer, L. C.; Darkwa, J., *J. Organomet. Chem.* **2011**, *696*, 1528-1535.

58. Budhai, A.; Omondi, B.; Ojwach, S. O.; Obuah, C.; Osei-Twum, E. Y.; Darkwa, J., *Catal. Sci. Technol.* **2013**, *3*, 3130-3135.

59. Obuah, C.; Omondi, B.; Nozaki, K.; Darkwa, J., *J. Mol. Catal. A: Chem.* **2014**, *382*, 31-40.

60. Small, B. L.; Brookhart, M., *J. Amer. Chem. Soc.* **1998**, *120*, 7143-7144.

61. Britovsek, G. J.; Mastroianni, S.; Solan, G. A.; Baugh, S. P.; Redshaw, C.; Gibson, V. C.; White, A. J.; Williams, D. J.; Elsegood, M. R., *Chem. Eur. J.* **2000**, *6*, 2221-2231.

62. Tempel, D. J.; Johnson, L. K.; Huff, R. L.; White, P. S.; Brookhart, M., *J. Am. Chem. Soc.* **2000**, *122*, 6686-6700.

63. Sun, W. H.; Zhao, W.; Yu, J.; Zhang, W.; Hao, X.; Redshaw, C., *Macromol. Chem. Phys.* **2012**, *213*, 1266-1273.

64. Wang, S.; Li, B.; Liang, T.; Redshaw, C.; Li, Y.; Sun, W.-H., *Dalton Trans.* **2013**, *42*, 9188-9197.

65. Zhang, W.; Wang, S.; Du, S.; Guo, C. Y.; Hao, X.; Sun, W. H., *Macromol. Chem. Phys.* **2014**, *215*, 1797-1809.

66. Zhao, W.; Yu, J.; Song, S.; Yang, W.; Liu, H.; Hao, X.; Redshaw, C.; Sun, W.-H., *Polymer* **2012**, *53*, 130-137.

67. Görl, C.; Alt, H. G., *J. Mol. Catal. A: Chem.* **2007**, *273*, 118-132.

68. Small, B. L.; Rios, R.; Fernandez, E. R.; Carney, M. J., *Organometallics* **2007**, *26*, 1744-1749.

69. Sun, W.-H.; Hao, P.; Li, G.; Zhang, S.; Wang, W.; Yi, J.; Asma, M.; Tang, N., *J. Organomet. Chem.* **2007**, *692*, 4506-4518.

70. Bahuleyan, B. K.; Ahn, I. Y.; Appukuttan, V.; Lee, S. H.; Ha, C.-S.; Kim, I.; Suh, H., *Macromol. Res.* **2010**, *18*, 701-704.

71. Karam, A. R.; Catarí, E. L.; López-Linares, F.; Agrifoglio, G.; Albano, C. L.; Díaz-Barrios, A.; Lehmann, T. E.; Pekerar, S. V.; Albornoz, L. A.; Atencio, R., *Appl. Catal. A: Gen.* **2005**, *280*, 165-173.

72. Small, B. L.; Brookhart, M.; Bennett, A. M., *J. Am. Chem. Soc.* **1998**, *120*, 4049-4050.

73. Sun, W.-H.; Zhang, S.; Zuo, W., *C. R. Chim.* **2008**, *11*, 307-316.

74. Mogorosi, M. M.; Mahamo, T.; Moss, J. R.; Mapolie, S. F.; Slootweg, J. C.; Lammertsma, K.; Smith, G. S., *J. Organomet. Chem.* **2011**, *696*, 3585-3592.

75. Blom, B.; Overett, M. J.; Meijboom, R.; Moss, J. R., *Inorg. Chim. Acta* **2005**, *358*, 3491-3496.

76. Netalkar, S. P.; Budagumpi, S.; Abdallah, H. H.; Netalkar, P. P.; Revankar, V. K., *J. Mol. Struct.* **2014**, *1075*, 559-565.

77. Meneghetti, S. P.; Lutz, P. J.; Kress, J., *Organometallics* **1999**, *18*, 2734-2737.

78. Swarts, A. J.; Zheng, F.; Smith, V. J.; Nordlander, E.; Mapolie, S. F., *Organometallics* **2014**, *33*, 2247-2256.

79. Zhang, Y.; Cao, Y.; Leng, X.; Chen, C.; Huang, Z., *Organometallics* **2014**, *33*, 3738-3745.

80. Jeffrey, J. C.; Rauchfuss, T. B., *Inorg. Chem.* **1979**, *18*, 2658-2666.

81. Braunstein, P.; Matt, D.; Mathey, F.; Thavard, D., *J. Chem. Res.* **1978**, 232-233.

82. Braunstein, P., *Bull. Japn. Soc. Coord. Chem.* **2014**, *63*, 19-28.

83. Deckers, P. J.; Hessen, B.; Teuben, J. H., *Angew. Chem. Int. Ed.* **2001**, *40*, 2516-2519.

84. Zhang, W.-H.; Chien, S. W.; Hor, T. A., *Coord. Chem. Rev.* **2011**, *255*, 1991-2024.

85. George, J., *J. Chem. Soc. Chem. Commun.* **1993**, 1632-1634.

86. Mecking, S.; Keim, W., *Organometallics* **1996**, *15*, 2650-2656.

87. Motswainyana, W. M.; Ojwach, S. O.; Onani, M. O.; Iwuoha, E. I.; Darkwa, J., *Polyhedron* **2011**, *30*, 2574-2580.

88. Shi, P.-Y.; Liu, Y.-H.; Peng, S.-M.; Liu, S.-T., *Organometallics* **2002**, *21*, 3203-3207.

89. Braunstein, P., *J. Organomet. Chem.* **2004**, *689*, 3953-3967.

90. Forestière, A.; Olivier-Bourbigou, H.; Saussine, L., *Oil Gas Sci. Technol.* **2009**, *64*, 649-667.

CHAPTER 3

Unsymmetrical (pyrazolylmethyl)pyridine metal complexes as catalysts for ethylene oligomerization reactions: Role of solvent and co-catalyst in product distribution

This chapter is adapted from the paper published in *J. Mol. Catal. A: Chem*. 394 (2014) 274-282 and is based on the experimental work of the first author, George S. Nyamato. The contributions of the first author include syntheses of the ligands and complexes, ethylene catalysis and drafting of the manuscript.

3.1. Introduction

Late-transition metal complexes containing nitrogen donor ligands have continued to receive attention as α-olefin oligomerization and polymerization catalysts[1] since the discovery by Brookhart and co-workers that α-diimine late transition metal complexes form active catalysts for olefin oligomerization and polymerization reactions.[2-6] Significant amount of research has been directed towards the design and development of other late transition metal nitrogen-donor complexes as ethylene polymerization[7-9] and oligomerization catalysts.[10-13]

The role of ligands in transition metal catalyzed ethylene oligomerization reactions is reaching new frontiers with recent discoveries of Dyer *et al*.[14] that nickel(II) complexes of *N*-phosphino guanidine ligands and $EtAlCl_2$ as a co-catalyst promote *in situ* Friedel–Crafts alkylation of toluene solvent by the preformed oligomers. Until then, most ethylene oligomerization reactions catalyzed by nickel(II) complexes were reported to give mostly ethylene oligomers irrespective of the co-catalysts and solvent used. Well known examples include Shell higher olefin process P^O nickel(II) catalysts,[15-17] α-diimine complexes

discovered by Brookhart and co-workers[2, 3] and nitrogen and phosphine donor nickel(II) catalysts developed by Braunstein.[18-21]

As a follow up to the Dyer report, Song *et al*.[22] reported the oligomerization of ethylene to butene, hexene and octene followed by subsequent Friedel-Crafts alkylation of the toluene solvent using nickel(II) complexes and $EtAlCl_2$ or MAO as co-catalysts. Our first reports of this phenomenon were using (pyrazol-1-ylmethyl)pyridine[23] and (pyrazolylmethyl)benzene nickel(II) complexes[24] that catalyze ethylene oligomerization to mainly C_4 and C_6 fractions followed by subsequent Friedel-Crafts alkylation of the toluene solvent. More recently, Obuah *et al*.[25] reported that pyrazolylamine nickel(II) complexes when activated with $EtAlCl_2$ in toluene oligomerize ethylene to butenes and hexenes accompanied by selective Friedel-Crafts alkylation of toluene solvent by butenes to butyltoluene, dibutyltoluene and tributyltoluene products. On the other hand, reactions in chlorobenzene solvent using $EtAlCl_2$ as a co-catalyst produced butenes, hexenes as well as branched polyethylene. In these findings, the use of MAO as a co-catalyst in toluene solvent produced exclusively higher density polyethylene. From these accounts, it is clear that Friedel-Crafts alkylation of the pre-formed oligomers is more complex than initially thought to be initiated by use of excess $EtAlCl_2$ co-catalyst and toluene solvent. It is therefore apparent that in addition to the reaction solvents and co-catalyst used, ligand design also plays a major role in these Friedel-Crafts reactions.

As part of our continued study of pyrazolyl nickel(II) complexes as catalyst for ethylene oligomerization and polymerization reactions, we report here a simple modification of the bis(pyrazolylmethyl)pydine ligand we previously reported.[23] The aim is to further gain insight into the role of the pyrazolyl unit in controlling the catalytic activities of these

nickel(II) complexes. Herein, we describe the synthesis of 2-(chloromethyl)-6-(pyrazol-1-ylmethyl)pyridine nickel(II), cobalt(II) and iron(II) complexes and their catalytic activities in ethylene oligomerization reactions. The effects of co-catalyst and solvent have been investigated using $EtAlCl_2$ and MAO co-catalysts and toluene, hexane and chlorobenzene solvents.

3.2. Experimental section

3.2.1. Materials and methods

All synthetic manipulations were performed using standard Schlenk techniques under a nitrogen atmosphere. Solvents were dried by distillation prior to use, and tetrabutylammonium bromide, ethylaluminium dichloride ($EtAlCl_2$, 1.8M in toluene), ethylaluminium dichloride ($EtAlCl_2$, 1.0M in hexane), methylaluminoxane (10 wt.% in toluene), 3,5-dimethylpyrazole, dibenzoylmethane, hydrazine hydrate, thionyl chloride, 2,6-bis(hydroxymethyl)pyridine, and metal halides were obtained from Sigma-Aldrich and used as received. The starting materials 2,6-bis(chloromethyl)pyridine,[26] and 3,5-diphenylpyrazole[27] were synthesized following literature procedures. ^{1}H NMR and $^{13}C\{^{1}H\}$ NMR spectra were recorded on a Bruker 400 MHz spectrometer in $CDCl_3$ solution at room temperature using tetramethylsilane as an internal standard, and chemical shifts are reported in ppm. Elemental analyses were performed on a Thermal Scientific Flash 2000 while ESI-mass spectra were recorded on an LC premier micro-mass spectrometer. Magnetic moments of the complexes were determined using Evans balance. GC analyses were performed using a Varian CP-3800 gas chromatograph equipped with a CP-Sil 5 CB (30 m × 0.2 mm × 0.25 µm) capillary column while GC‑MS analyses were performed on a Shimadzu GC‑MS-QP2010.

3.2.2. Syntheses of (pyrazolylmethyl)pyridine ligands and their metal complexes

*3.2.2.1. 2-(chloromethyl)-6-((3,5-dimethyl-1H-pyrazol-1-yl)methyl)pyridine (**L1**)*

Ligand **L1** was prepared by dissolving 2, 6-bis(chloromethyl)pyridine (1.83 g, 10.4 mmol) and 3,5-dimethylpyrazole (1.00 g, 10.4 mmol) in toluene (30 mL) followed by addition of 40% aqueous NaOH (12 mL) and 40% aqueous tetrabutylammonium bromide (5 drops). The reaction mixture was refluxed for 24 h after which the organic layer was separated from the aqueous layer and washed three times with deionised water. The organic layer was dried over anhydrous Na_2SO_4 and reduced under vacuum. Purification was done by column chromatography using hexane/diethyl ether (3:2) solvent mixture to afford **L1** as a white solid. Yield: 0.64 g (26%). ^{1}H NMR ($CDC1_3$): δ 2.19 (s, 3H, CH_3, pz); 2.24 (s, 3H, CH_3, pz); 4.64 (s, 2H, CH_2-Cl); 5.33 (s, 2H, CH_2-N); 5.88 (s, 1H, pz); 6.72 (d, 1H, 3-py, $^3J_{HH}$ = 8.0 Hz); 7.34 (d, 1H, 5-py, $^3J_{HH}$ = 8.0 Hz); 7.61(dd, 1H, 4-py, $^3J_{HH}$ = 8.0 Hz). $^{13}C\{^1H\}$ NMR ($CDC1_3$): δ 11.08 (3-pz-CH_3), 13.43 (5-pz-CH_3), 46.54 (CH_2-Cl), 54.18 (CH_2-N), 105.80 (4-pz-C), 120.30 (3-py-C), 121.4 (5-py-C), 138.12 (5-pz-C), 139.96 (4-py-C), 148.10 (3-pz-C), 156.20 (6-py-C), 157.20 (2-py-C). ESI-MS: *m*/*z* (%) 258 [$(M + Na)^+$, (^{35}Cl) 100%], 260 [$(M + Na)^+$, (^{37}Cl) 49%]. Anal. Calcd. for $C_{12}H_{14}ClN_3 \cdot 0.5CH_2Cl_2$: C, 53.97; H, 5.44; N, 15.11. Found: C, 53.41; H, 5.21; N, 15.00.

*3.2.2.2. 2-(chloromethyl)-6-((3,5-diphenyl-1H-pyrazol-1-yl)methyl)pyridine (**L2**)*

Ligand **L2** was prepared from 2,6-bis(chloromethyl)pyridine (3.0 g, 17.04 mmol) and 3,5-diphenylpyrazole (3.75 g, 17.04 mmol) following the procedure described for **L1.** The crude product was purified by column chromatography on silica gel using petroleum ether to diethyl ether (2:1) to give **L2** as an analytically pure white solid. Yield: 1.7 g (28%). ^{1}H NMR ($CDC1_3$): δ 4.66 (s, 2H, CH_2-Cl); 5.55 (s, 2H, CH_2-N); 6.73 (s, 1H, pz); 6.94 (d, 1H, 3-py, $^3J_{HH}$ = 8.0 Hz); 7.34 (dd, 2H, 4-ph, $^3J_{HH}$ = 8.0 Hz); 7.37(dd, 4H, 3-ph, $^3J_{HH}$ = 8.0 Hz);

7.44 (d, 4H, 2-ph, $^{3}J_{HH}$ = 8.0 Hz); 7.66 (dd, 1H, 4-py, $^{3}J_{HH}$ = 8.0 Hz); 7.88 (d, 1H, 5-py, $^{3}J_{HH}$ = 8.0 Hz). $^{13}C\{^{1}H\}$ NMR ($CDC1_3$): δ 46.60 (CH_2-Cl), 54.92 (CH_2-N), 103.84 (4-pz-C), 120.61(3-py-C), 121.46 (5-py-C), 125.75(3-pz-ph-2C), 127.56 (3-pz-ph-4C), 127.89 (5-pz-ph-4C), 128.23 (5-pz-ph-2C), 128.67 (3-pz-ph-3C), 128.83 (5-pz-ph-3C), 130.24(5-pz-ph-1C), 133.35 (3-pz-ph-1C), 138.09 (4-py-C), 146.08 (5-pz-C), 151.51(3-pz-C), 156.16 (6-py-C), 157.53 (2-py-C). ESI-MS: *m/z* (%) 282 [(M + Na)$^+$, (^{35}Cl) 100%], 284 [(M + Na)$^+$, (^{37}Cl) 56%]. Anal. Calcd for $C_{22}H_{18}ClN_3$: C, 73.43; H, 5.04; N, 11.68. Found: C, 73.94; H, 4.60; N, 11.92.

*3.2.2.3. [{2-(chloromethyl)-6-((3,5-dimethyl-1H-pyrazol-1-yl)methyl)pyridine}$NiCl_2$] (**1**)*

Complex **1** was prepared by adding a solution of $NiCl_2$ (0.11 g, 0.85 mmol) in dichloromethane (15 mL) to a solution of **L1** (0.20 g, 0.85 mmol) in dichloromethane (15 mL). The resultant solution was stirred for 24 h to give a green precipitate which was isolated by filtration, washed with ethanol and diethyl ether to afford complex **1** as a green solid. Yield: 0.12 g (65%). ESI-MS: *m/z* (%) 329 (M$^+$-Cl, 88%). Anal. Calcd for $C_{12}H_{14}ClN_3NiCl_2$ CH_2Cl_2: C, 34.68; H, 3.58; N, 9.33. Found: C, 34.95; H, 3.66; N, 10.06. μ_{eff} = 3.64 BM.

Complexes **2**-**4** were prepared following the procedure described for **1**.

*3.2.2.4. [{2-(chloromethyl)-6-((3,5-dimethyl-1H-pyrazol-1-yl)methyl)pyridine}$NiBr_2$] (**2**)*

[$NiBr_2$] (0.19 g, 0.85 mmol) and **L1** (0.20 g, 0.85 mmol). Pale purple solid. Yield: 0.30 g (78%). ESI-MS: *m/z* (%) 373 (M$^+$-Br, 97%). Anal. Calcd for $C_{12}H_{14}ClN_3NiBr_2{\cdot}CH_2Cl_2$: C, 28.96; H, 2.99; N, 7.79. Found: C, 29.26; H, 3.35; N, 8.37. μ_{eff} = 3.92 BM.

*3.2.2.5. [{2-(chloromethyl)-6-((3,5-dimethyl-1H-pyrazol-1-yl)methyl)pyridine}$CoCl_2$] (**3**)*

[$CoCl_2$] (0.06 g, 0.42 mmol) and **L1** (0.10 g, 0.42 mmol). Recrystallization from CH_2Cl_2-hexane solution gave **3** as an analytically pure blue solid. Yield: 0.13 g (84%). ESI-MS: *m*/*z* (%) 328 (M^+-Cl, 68%). Anal. Calcd for $C_{12}H_{14}ClN_3CoCl_2$: C, 39.43; H, 3.86; N, 11.49. Found: C, 39.09; H, 3.91; N, 11.00. μ_{eff}= 4.27 BM.

*3.2.2.6. [{2-(chloromethyl)-6-((3,5-dimethyl-1H-pyrazol-1-yl)methyl)pyridine}$FeCl_2$] (**4**)*

[$FeCl_2.4H_2O$] (0.08 g, 0.42 mmol) and **L1** (0.10 g, 0.42). Brown solid. Yield: 0.13 g (82%). ESI-MS: *m*/*z* (%) 326 (M^+-Cl, 32%). Anal. Calcd for $C_{12}H_{14}ClN_3FeCl_2.1.5CH_2Cl_2$: C, 33.10; H, 3.50; N, 8.58. Found: C, 33.58; H, 3.35; N, 9.40. μ_{eff}= 5.28 BM.

*3.2.2.7. [{2-(chloromethyl)-6-((3,5-diphenyl-1H-pyrazol-1-yl)methyl)pyridine}$NiBr_2$] (**5**)*

To a solution of $NiBr_2$ (0.12 g, 0.56 mmol) in dichloromethane (15 mL) was added a solution of **L2** (0.20 g, 0.56 mmol) in dichloromethane (15 mL). The resultant solution was stirred for 48 h to give a deep blue solution. Slow evaporation of the solvent gave a light violet solid which upon recrystallization from CH_2Cl_2-hexane solution afforded purple crystals suitable for single-crystal X-ray analysis. Yield: 0.22 g (67%). ESI-MS: *m*/*z* (%) 498 (M^+-Br, 30%). Anal. Calcd for $C_{22}H_{18}Br_2ClN_3Ni.1.5CH_2Cl_2$: C, 39.99; H, 3.00; N, 5.95. Found: C, 40.38; H, 2.91; N, 6.37. μ_{eff}= 3.88 BM.

*3.2.2.8. [{2-(chloromethyl)-6-((3,5-diphenyl-1H-pyrazol-1-yl)methyl)pyridine}$CoCl_2$] (**6**)*

Compound **6** was prepared in a similar manner to **5** using [$CoCl_2$] (0.07 g, 0.56 mmol) and **L2** (0.2 g, 0.56 mmol). Recrystallization from CH_2Cl_2-hexane solution led to the formation of blue crystals suitable for single-crystal X-ray analysis. Yield: 0. 20 g (72%). ESI-MS: *m*/*z*

(%) 453 (M^+-Cl, 67%). Anal. Calcd for $C_{22}H_{18}Cl_3CoN_3 \cdot 2CH_2Cl_2$: C, 43.70; H, 3.36; N, 6.37. Found: C, 43.71; H, 3.90; N, 6.25. μ_{eff} = 4.50 BM.

3.2.3. X-ray crystallography

X-ray data collection for compounds **5** and **6** were recorded on a Bruker Apex Duo diffractometer equipped with an Oxford Instruments Cryojet operating at 100(2) K and an Incoatec microsource operating at 30 W power. For both structures the data were collected with Mo Kα (λ = 0.71073 Å) radiation at a crystal-to-detector distance of 50 mm. The data collections were performed using omega and phi scans with exposures taken at 30 W X-ray power and 0.50° frame widths using APEX2.[28] The data were reduced with the programme SAINT[28] using outlier rejection, scan speed scaling, as well as standard Lorentz and polarisation correction factors. A SADABS semi-empirical multi-scan absorption correction[28] was applied to the data. Direct methods, SHELXS-97[29] and WinGX[30] were used to solve both structures. All non-hydrogen atoms were located in the difference density map and refined anisotropically with SHELXL-97.[29] All hydrogen atoms were included as idealized contributors in the least squares process. Their positions were calculated using a standard riding model with C–$H_{aromatic}$ distances of 0.95 Å and U_{iso} = 1.2 U_{eq} and C–$H_{methylene}$ distances of 0.99 Å and U_{iso} = 1.2 U_{eq}.

3.2.4. General procedure for ethylene oligomerization reactions

Ethylene oligomerization reactions were carried out in a 400 mL stainless steel Parr reactor equipped with a mechanical stirrer, temperature controller and an internal cooling system. In a typical experiment, the reactor was preheated to 100 °C *in vacuo* and cooled to room temperature. The catalyst precursor (10.0 μmol) was transferred into a dry Schlenk tube under nitrogen and toluene (20 mL) was added using a syringe. An appropriate amount of

co-catalyst ($EtAlCl_2$ or MAO) was then introduced into the Schlenk tube containing the pre-catalyst to form the active catalytic system. The resultant solution was then transferred *via* cannula into the reactor. Additional toluene solvent (60 mL) was also transferred *via* cannula into the reactor, and the reactor was then flushed three times with ethylene and the desired pressure and temperature was set and the reaction started. After the reaction time, the reactor was cooled to -10 °C using a bath of ice/liquid nitrogen and excess ethylene vented off. The reaction was then quenched by addition of 10% HCl (5mL). A portion of the reaction mixture was sampled for GC and GC-MS analyses to determine the oligomer by comparison to the standard authentic samples. The amount of products formed was determined by mass difference of 80 mL toluene (69.60 g) and mass of final solution.

3.3. Results and discussion

3.3.1. Synthesis of (pyrazolylmethyl)pyridine ligands and their metal complexes

Ligands 2-(chloromethyl)-6-((3,5-dimethyl-1H-pyrazol-1-yl)methyl)pyridine (**L1**) and 2-(chloromethyl)-6-((3,5-diphenyl-1H-pyrazol-1-yl)methyl)pyridine (**L2**) were prepared by phase transfer catalyzed alkylation of 2,6-bis(chloromethyl)pyridine and the appropriate pyrazolyl unit following literature procedure[31] (Scheme 3.1).

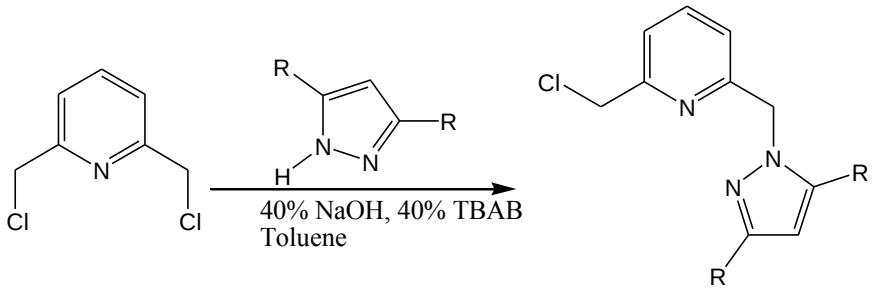

R = Me, (**L1**)
R = Ph, (**L2**)

Scheme 3.1: Synthesis of (pyrazolylmethyl)pyridine ligands

The formation of both ligands **L1** and **L2** suffered from the formation of their respective bis(pyrazolyl)pyridine compounds but analytically pure compounds were obtained after purification by column chromatography on silica gel as white solids. All the compounds were characterized by a combination of ^{1}H, $^{13}C\{^{1}H\}$ NMR, mass spectrometry, microanalyses and for complexes **5** and **6**, single-crystal X-ray diffraction and the analytical data are in agreement with the proposed structures. For example, two singlet signature peaks of the Cl-CH_2 and N-CH_2 linker protons of **L1** (Figure 3.1) were observed at 4.64 ppm and 5.33 ppm, respectively, while for **L2**, these two CH_2 linker protons were observed as singlets at 4.66 ppm and 5.55 ppm, respectively; indicating the unsymmetrical nature of both ligands.

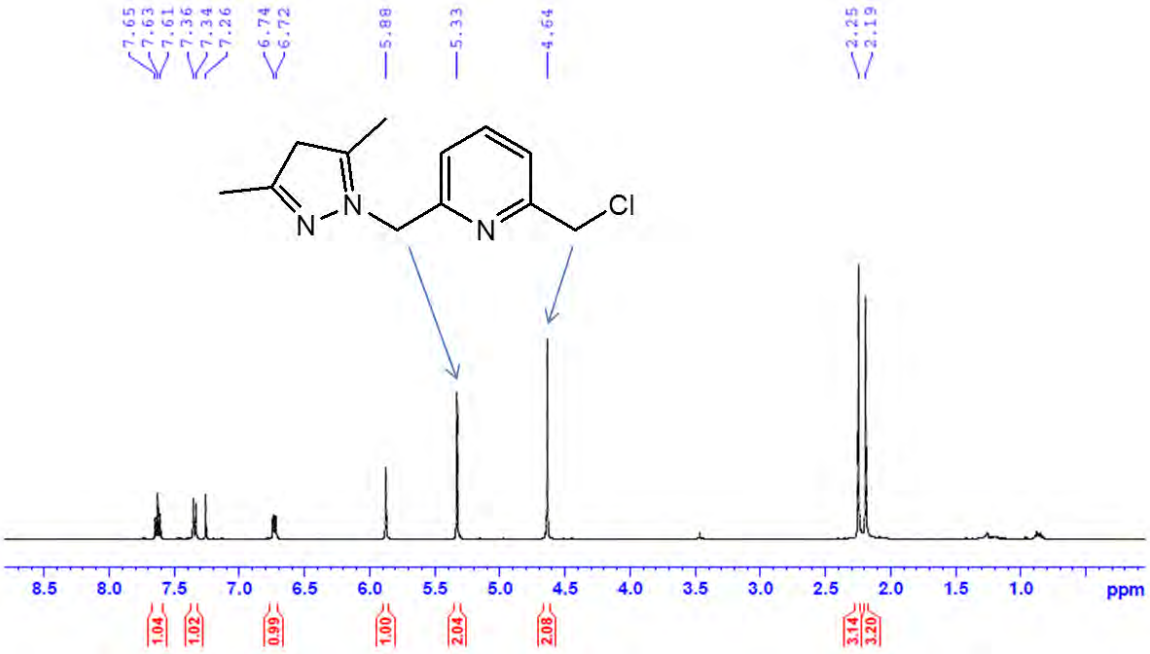

Figure 3.1: ^{1}H NMR spectrum of **L1** showing its unsymmetrical nature

This is contrary to the one signal reported for the CH_2 linker protons at 5.47 ppm for the symmetrical compound 2,6-bis(pyrazol-1-ylmethyl)pyridine, but comparable to the two singlet peaks reported for 2-chloromethyl-6-(pyrazol-1-ylmethyl)pyridine in which a singlet for the Cl-CH_2 protons was observed at 4.63 ppm and another singlet for N-CH_2 protons was observed at 5.47 ppm.[31]

$^{13}C\{^{1}H\}$ NMR data for both ligands, **L1** and **L2**, were consistent with the ^{1}H NMR data. For example, in the **L1** spectrum, two signals at 46.54 ppm and 54.18 ppm assigned to the two CH_2 linker carbons were observed while in the **L2** spectrum, they were observed at 46.60 ppm and 54.92 ppm. Mass spectrometry data of both ligands, **L1** (M^+ = 235) and **L2** (M^+ = 359), show m/z = 258 and m/z = 382, respectively, which correspond to sodium coordinated molecular ions that are very much in good correlation with the proposed structures.

Reactions of **L1** and **L2** with the appropriate metal salts in a 1:1 mole ratio in dichloromethane afforded the corresponding nickel(II), iron(II) and cobalt(II) metal complexes **1-6** in moderate yields (Scheme 3.2).

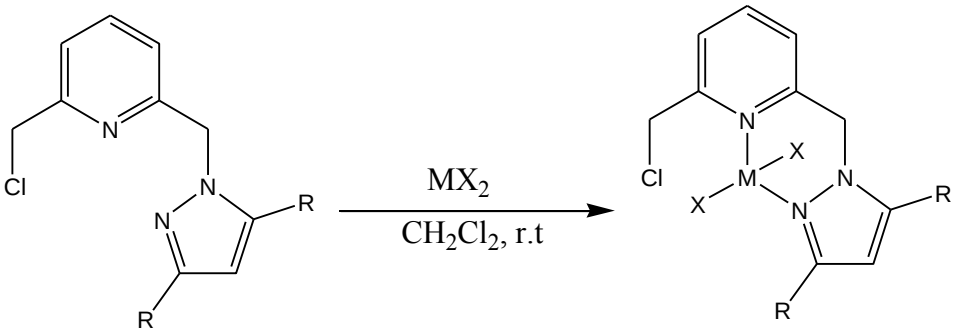

R = Me, (**L1**)
R = Ph, (**L2**)

R = Me, M = Ni, X = Cl, (**1**)
R = Me, M = Ni, X = Br, (**2**)
R = Me, M = Co, X = Cl, (**3**)
R = Me, M = Fe, X = Cl, (**4**)
R = Ph, M = Ni, X = Br, (**5**)
R = Ph, M = Co, X = Cl, (**6**)

Scheme 3.2: Synthesis of (pyrazolylmethyl)pyridine nickel(II), cobalt(II) and iron(II) complexes

Due to the paramagnetic nature of complexes **1-6**, NMR was not useful in their structural characterization. The complexes were thus characterized by magnetic moment measurements, elemental analyses, mass spectrometry and single crystal X-ray analyses for **5** and **6**. The magnetic moments of the nickel(II) complexes **1, 2** and **5** were recorded as 3.64

BM, 3.92 BM and 3.88 BM, respectively. These values were effectively higher than the expected spin only value of 2.83 BM for nickel(II) complexes. However, they fall within the expected range for high spin nickel(II) complexes of 2.9-4.2 BM.[32]

Similarly, the magnetic moments of cobalt(II) complexes **3** and **6** and the iron(II) complex **4** were obtained as 4.27 BM, 4.50 BM and 4.90 BM, respectively, and fall within the expected range for cobalt(II) and iron(II) complexes with three and two unpaired electrons, respectively.[33]

Mass spectrometry also proved useful in establishing the formation and identity of the complexes. A typical mass spectrum of the complexes exhibited loss of a halide ligand followed by the metal fragment to give the corresponding sodium coordinated ligand signal as the base peak (Figure 3.2). The elemental analyses data of **1-6** were consistent with one ligand motif per metal atom as proposed in Scheme 3.2.

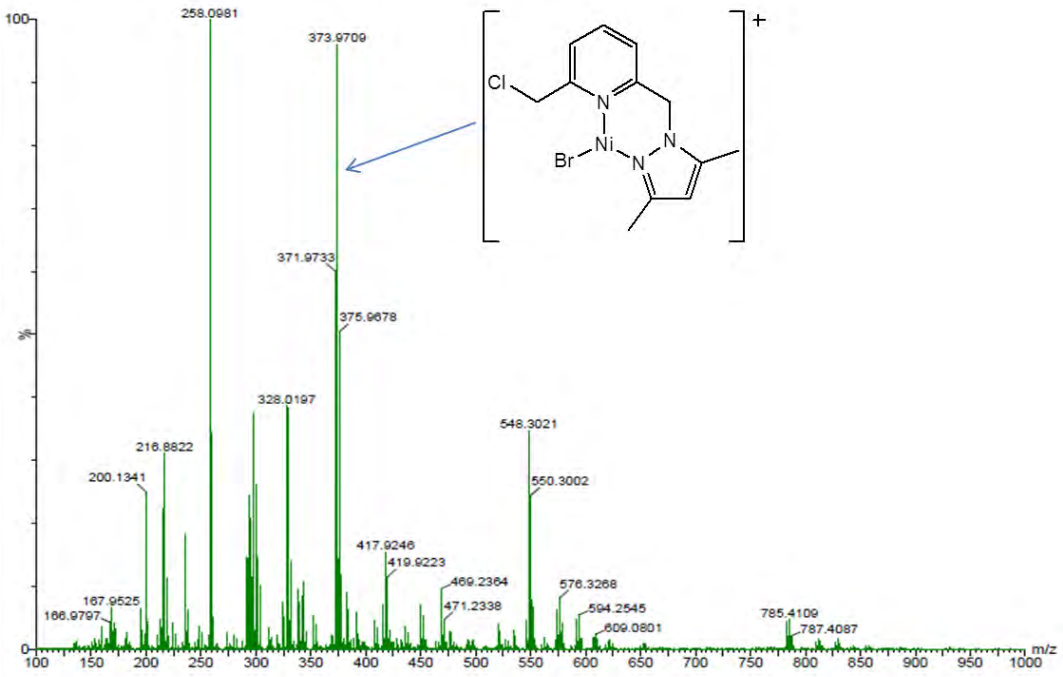

Figure 3.2: Mass pectrum of complex **2** showing the m/z = 373 (M^+-Br).

3.3.2. Molecular structures of complexes 5 and 6

Single crystals of complexes **5** and **6** suitable for X-ray analyses were grown by slow evaporation of dichloromethane/hexane solutions. The molecular structures of **5** and **6** are shown in Figures 3.3 and 3.4, respectively, while their crystallographic data and structure refinement parameters are given in Table 3.1.

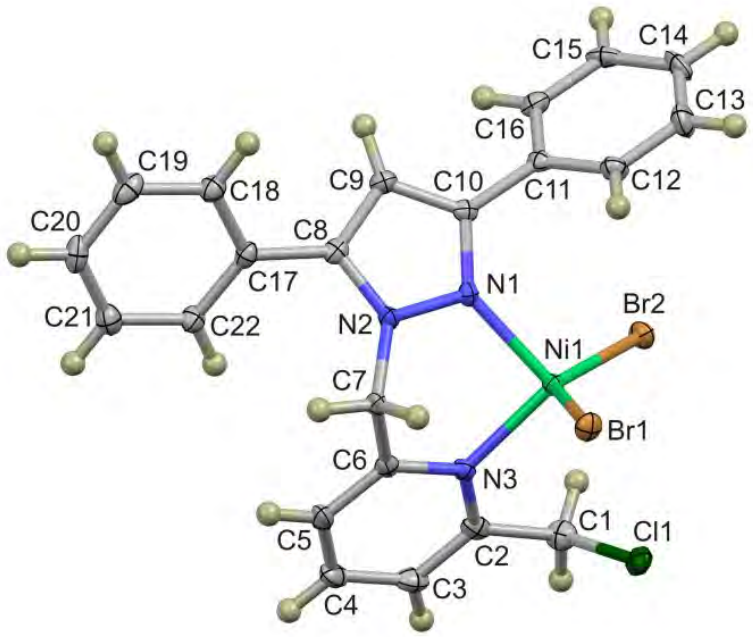

Figure 3.3: Molecular structure diagram of **5** shown with 50% probability ellipsoids. Selected bond lengths [Å] and angles [°]: Ni(1)-N(1), 2.013(3); Ni(1)-N(3), 2.043(3); Ni(1)-Br(1), 2.3866(6); Ni(1)-Br(2), 2.3653(6); C(1)-Cl(1), 1.820(4); N(1)-Ni(1)-N(3), 93.6(1); N(1)-Ni(1)-Br(1), 101.07(9); N(1)-Ni(1)-Br(2), 107.07(9); N(3)-Ni(1)-Br(1), 103.62(9); N(3)-Ni(1)-Br(2), 115.82(9); Br(1)-Ni(1)-Br(2), 128.98(2).

The nickel(II) complex **5** adopts a distorted tetrahedral coordination geometry which comprises the bidentate N_2-donor ligand and two bromide ligands. The large ionic radius of the bromide ion leads to steric strain which manifests as a large Br–Ni–Br bond angle of 128.98°. This angle is significantly larger than those previously reported by Ojwach *et al.* for closely related structures which range from 118.32(1) to 121.57(1).[23] All the bond lengths

describing the coordination sphere compare favorably with those previously reported.[23] The phenyl ring substituents are not coplanar with the pyrazole ring; the C9–C10–C11–C12 and C9–C8–C17–C22 torsion angles measure 130.2(4) and 140.0(4)°, respectively. It would seem that the current configuration minimizes steric repulsion between the phenyl rings and the methylene hydrogen atoms and the bromide ligands.

Complex **6** exhibits a similar distorted tetrahedral geometry with the coordination sphere of the cobalt(II) occupied by the pyridine and pyrazole nitrogen atoms of the bidentate ligand and two chloride ligands. A Mogul structural search[34] shows that the bond lengths between the cobalt(II) ion and the ligand nitrogen donor atoms are comparable to related structures.

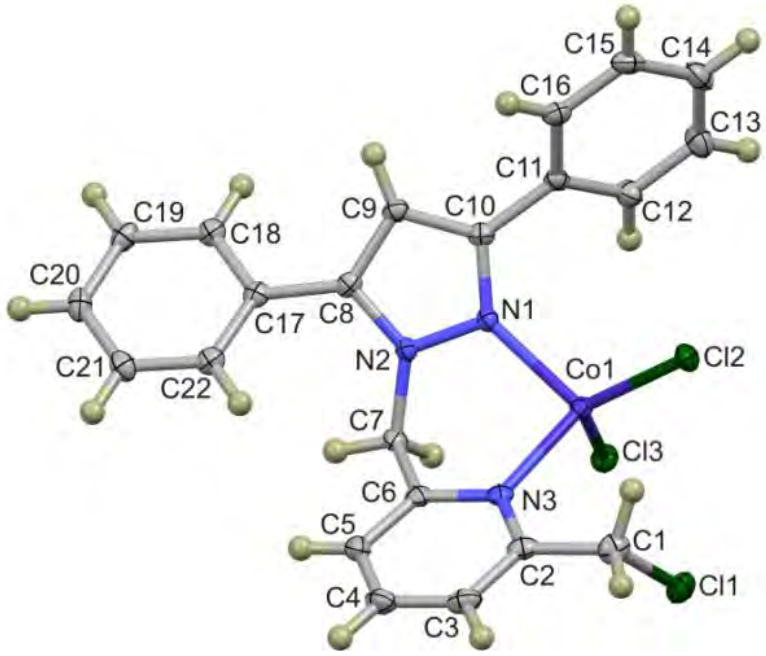

Figure. 3.4: Molecular structure diagram of **6** shown with 50% probability ellipsoids. Selected bond lengths [Å] and angles [°]: Co(1)-N(1), 2.0347(13); Co(1)-N(3), 2.0799(14); Co(1)-Cl(3), 2.2402(5); Co(1)-Cl(2), 2.2524(5); C(1)-Cl(1), 1.803(2); N(1)-Co(1)-N(3), 93.71(5); N(1)-Co(1)-Cl(3), 111.71(4); N(1)-Co(1)-Cl(2), 103.71(4); N(3)-Co(1)-Cl(2), 105.86(4); N(3)-Co(1)-Cl(3), 115.76(4); Cl(3)-Co(1)-Cl(2), 121.887(18).

Table 3.1: Crystal data collection and structure refinement parameters for complexes **5** and **6**

Crystal Data	**5**	**6**
Chemical formula	$C_{22}H_{18}Br_2ClN_3Ni$	$C_{22}H_{18}Cl_3CoN_3$
Molar Mass (g mol^{-1})	578.37	489.67
Crystal system, space group	Monoclinic, $P2_1/n$	Monoclinic, $P2_1/n$
Temperature (K)	100(2)	100(2)
a, *b*, *c* (Å)	8.4928(5), 14.1962(8), 17.4974(10)	8.244(1), 14.134(2), 17.642(2)
α, β, γ (°)	α = γ = 90°, β = 96.128(3)	α = γ = 90°, β = 97.496(2)
V ($Å^3$)	2097.5(2)	2038.1(4)
Z	4	4
Radiation type	Mo *K*α	Mo *K*α
μ (mm^{-1})	4.88	1.25
Crystal size (mm)	0.18 × 0.10 × 0.06	0.12 × 0.10 × 0.06
Data collection		
Diffractometer	Bruker Apex Duo CCD diffractometer	
Absorption correction	Multi-scan, *SADABS*, Bruker 2012	
T_{min}, T_{max}	0.474, 0.759	0.865, 0.929
No. of Measured, independent and observed [$I > 2\sigma(I)$] reflections	15673, 4017, 3410	21357, 4218, 3887
R_{int}	0.031	0.026
Refinement		
$R[F^2 > 2\sigma(F^2)]$, $wR(F^2)$, *S*	0.032, 0.082, 1.06	0.023, 0.059, 1.02
No. of reflections	4017	4218
No. of parameters	262	262
No. of restraints	0	0
H-atom treatment	H atom parameters constrained.	
$\Delta\rho_{max}$, $\Delta\rho_{min}$ (e $Å^{-3}$)	0.89, –0.52	0.32, –0.41

3.3.3. Evaluation of the metal complexes as catalysts for ethylene oligomerization reactions

Complexes **1-6** were investigated as potential ethylene oligomerization catalysts using $EtAlCl_2$ or MAO as co-catalyst in three different solvents; toluene, hexane and chlorobenzene. In all cases, the complexes showed appreciable catalytic activities up to 2 460 kg product.mol.$^{-1}$catalyst.h^{-1}. A notable observation was the dependence of product distribution on the nature of the co-catalyst and solvent used. Major products observed included butenes, hexenes, octenes and toluene-alkylated products from the preformed oligomers. In the subsequent sections, we present detailed analyses of the products and discussion of our findings.

*3.3.3.1. Ethylene oligomerization reactions catalyzed by **1-6** using $EtAlCl_2$ as a co-catalyst*

We first investigated ethylene oligomerization reactions, catalyzed by complexes **1-6**, using $EtAlCl_2$ as a co-catalyst in toluene solvent. Table 3.2 shows a summary of the data obtained for all the catalysts. Detailed analyses of the oligomer products obtained were carried out using GC (Figures 3.5 and 3.6), ^{1}H NMR spectroscopy and GC-MS. A combination of these data revealed the formation of toluene-alkylated C_2, C_4 and C_6 products and no traces of olefins. For example, a typical ^{1}H NMR spectrum (Figure 3.7) showed that the oligomerization products were mainly aromatic compounds due to the presence of peaks observed at around 7.00 ppm. No signature peaks between 5-6 ppm corresponding to the olefin oligomers were recorded. Further analyses of the products by GC-MS confirmed that these ethylene oligomerization products were alkyl-toluenes of C_2 and the preformed C_4 and C_6 oligomers. As an illustration, a molecular mass of 176.08 corresponding to hexyl-toluene was observed (Figure 3.8).

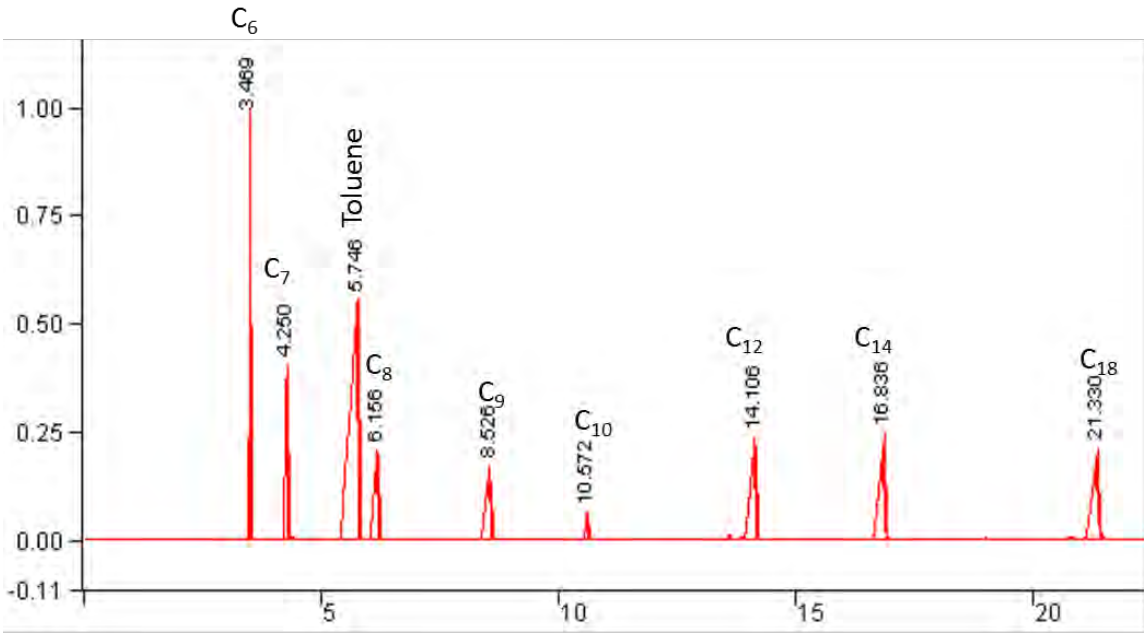

Figure 3.5: Gas chromatogram of authentic standards in toluene

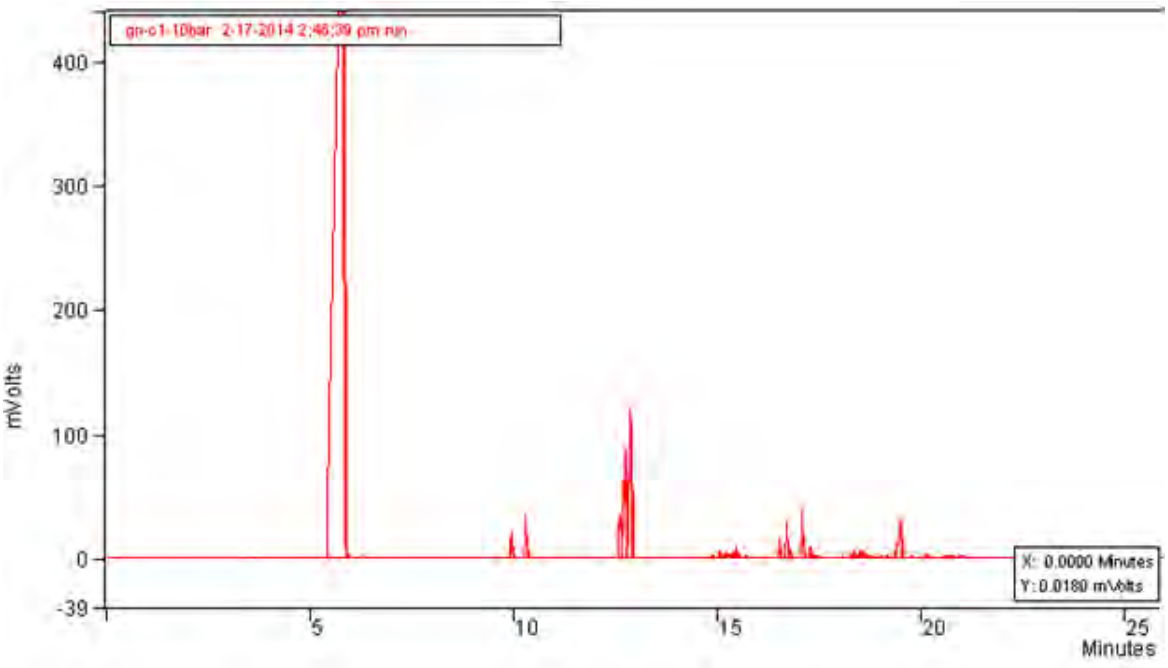

Figure 3.6: Typical chromatogram of products obtained using catalyst **1**, Al:Ni ratio of 250:1, temperature = 30 °C, pressure = 10 bar, time = 1 h, solvent = toluene.

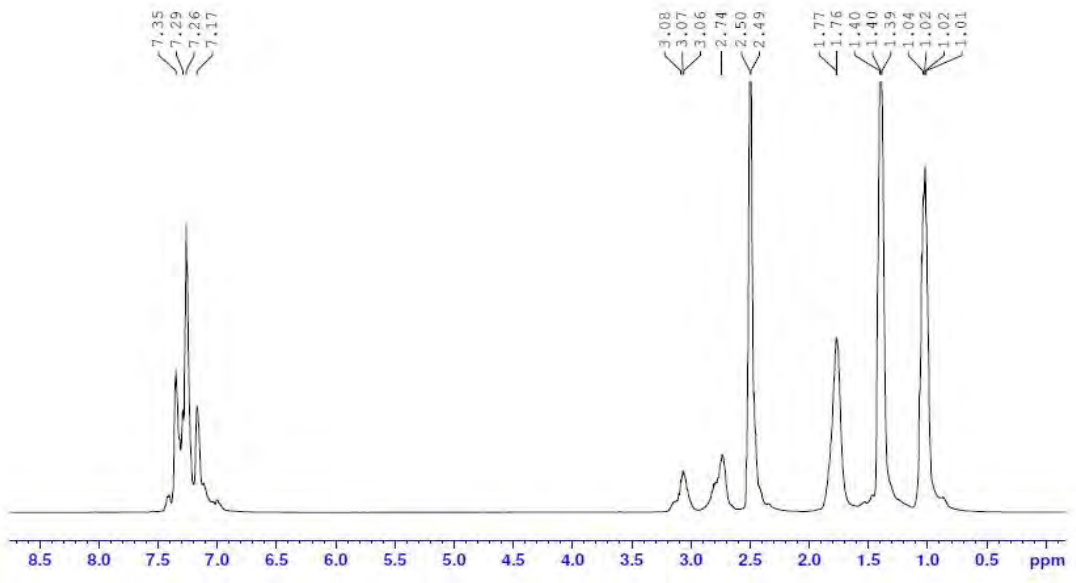

Figure 3.7: ^{1}H NMR spectrum of the products of catalyst **1** from the reaction at Al:Ni ratio of 250:1, temperature = 30 °C, pressure = 10 bar, time = 1 h, solvent = toluene. The absence of signals at around 5-6 ppm indicates the absence of any alkenes in the mixture. The presence of aromatic and alkyl signals confirms the presence of alkylated toluenes.

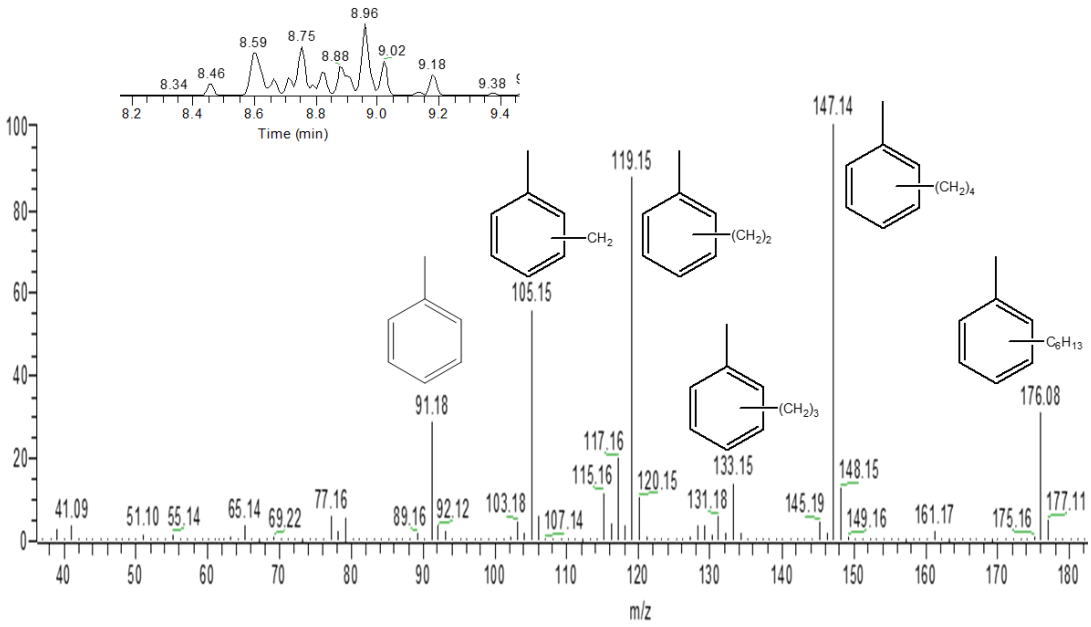

Figure 3.8: Mass spectrum of the product C_6H_{13}-toluene regioisomers obtained from catalyst **1**, $EtAlCl_2$:Ni ratio of 250:1, temperature = 30 °C, pressure = 10 bar, time = 1 h, solvent = toluene. M^+= 176.08 corresponds to the molecular ion mass of the hexylmethylbenzene at retention time of 8.96 min.

As is evident from Figure 3.8, the fragmentation pattern corresponds with the fragmentation of hexane; the loss of the first CH_3 results in the peak at 161.17 and subsequent loss of CH_2 leads to the observed peak at 147.14. Further fragmentations of CH_2 groups resulted in the observed peaks at 133.15, 119.15 and 105.15. The last CH_2 fragmentation resulted in the peak at 91.18, which corresponds to a toluene molecule. From these characterization data, we can conclude that the products from oligomerization of ethylene by **1-6** when using $EtAlCl_2$ as a co-catalysts were alkyl-toluenes and not higher olefins. Scheme 3.3 shows the distribution of the alkyl-toluene products obtained. Thus, the pre-formed oligomers underwent *in situ* Friedel-Crafts alkylation of the toluene solvent used. GC-mass spectra of the oligomers also showed more than one peak for each product corresponding to the possible ortho-, para- and meta-alkyl-toluenes in addition to branched products.[24]

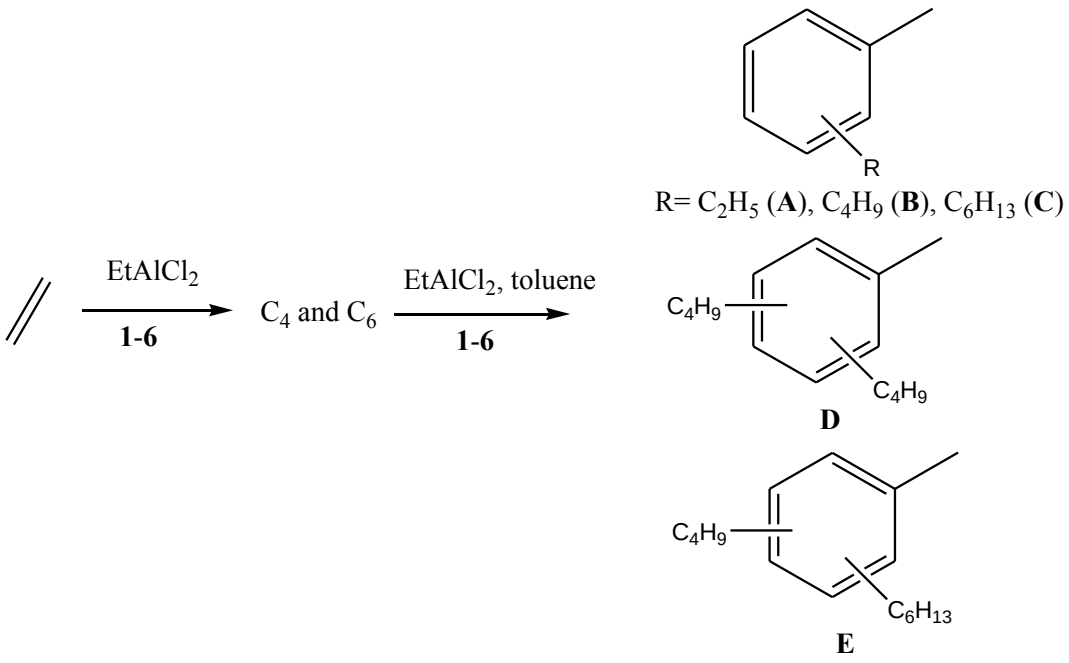

Scheme 3.3: Ethylene oligomerization and subsequent Friedel-Crafts alkylation of toluene with complexes **1-6**, and $EtAlCl_2$ as co-catalyst

The Friedel-Crafts alkylation of toluene solvent used in the oligomerization of ethylene using $EtAlCl_2$ as a co-catalyst has been previously reported.[14, 23-25, 35, 36] For example, in our initial findings, we reported oligomerization of ethylene to give C_4, C_6, and C_8 alkenes, followed by subsequent Friedel-Crafts alkylation of the toluene solvent to alkylated toluene products using (pyrazol-1-ylmethyl)pyridine nickel(II) catalysts.[23] In this current work, we also observed Friedel-Crafts alkylation of ethylene as a parallel reaction to oligomerization reactions. This can be alluded to the reduced catalytic activities exhibited by **1-6** in comparison to the previously reported (pyrazolylmethyl)pyridine catalysts. Consistent with these current data is the work of Budhai *et al*.[24] who reported similar alkylation of toluene by the pre-formed olefins.

These results suggest that other than the co-catalyst and toluene solvent, the nature of the pre-catalyst used also plays a role in the Friedel-Crafts alkylation of the formed oligomers. In deed there are numerous reports in literature in which only C_4, C_6 and C_8 oligomer are obtained when $EtAlCl_2$ in toluene is used as a co-catalyst.[37-40] However, in reports that do not produce Friedel-Crafts alkylated products, lower Al/Ni ratios were used. For instance, Braunstein and co-workers[37] have employed Al/Ni ratio of 10-20 in the ethylene oligomerization reactions catalyzed by pyridyl-triaxle nickel(II) catalysts. It can thus be argued that higher Al/Ni ratios of about 250 could also account for the occurrence of Friedel-Crafts alkylation reactions in our systems.

Table 3.2: Ethylene oligomerization data for **1-6** in using $EtAlCl_2$ as co-catalyst in toluene.[a]

Entry	Catalyst	Pressure (bar)	Time (h)	T_{min}/T_{max} (°C)[b]	Al:M	Yield[c] (g)	Activity[d]	% Alkyl-toluenes[e]				
								A	**B**	**C**	**D**	**E**
1	**1**	10	1	30/43	250	10.72	1 072	13	60	7	12	8
2	**2**	10	1	30/38	250	8.71	871	36	58	4	2	-
3	**3**	10	1	30/37	250	2.80	280	53	47	-	-	-
4	**4**	10	1	30/39	250	4.67	467	83	15	1	-	1
5	**5**	10	1	30/41	250	10.84	1 084	8	67	11	10	4
6	**6**	10	1	30/38	250	3.39	339	89	7	2	-	2
7	**1**	10	0.5	30/40	250	4.90	980	16	62	6	9	7
8	**1**	10	2	30/42	250	15.93	798	8	56	12	18	6
9	**1**	10	1	30/41	200	6.42	642	13	55	8	14	10
10	**1**	10	1	30/41	300	12.51	1 251	7	57	7	16	13
11	**1**	10	1	30/42	350	10.27	1 027	6	54	9	20	11
12	**1**	5	1	30/38	250	4.73	473	14	57	10	13	6
13	**1**	20	1	30/43	250	17.43	1 743	17	59	7	10	7
14	**1**	30	1	30/45	250	24.62	2 462	15	63	8	9	5

[a]Reaction conditions: nNi = 10 µmol; solvent, toluene, 80 mL; temperature, 30 °C. [b]Initial temp was 30 °C, T_{min} and T_{max} = lowest and highest temperatures attained during the reaction period. [c]Determined by mass difference of 80 mL toluene (69.60 g) and mass of final solution. [d]Activity, kg product.mol.$^{-1}$catalyst.h^{-1}. [e]Determined by GC.

3.3.3.2. Ethylene oligomerization reactions in hexane and chlorobenzene solvents

The effect of solvent on the oligomerization of ethylene was investigated using complex **2** in hexane and chlorobenzene solvents and $EtAlCl_2$ (in hexane) as a co-catalyst (Table 3.3). All the reactions afforded C_4 and C_6 oligomers with greater selectivity towards C_6 oligomers. Both ^1H NMR spectra and GC-MS data supported the formation of these oligomers and the absence of alkylation reactions. Figure 3.9 is a typical ^1H NMR spectrum showing signals at about 5.00 ppm and 5.85 ppm corresponding to the olefinic protons. These results are in accord with those reported[14] for *N*-phosphino guanidine nickel(II) catalysts in the oligomerization of ethylene in dichloromethane and chlorobenzene solvents that give only butenes and hexenes, while reactions in benzene and toluene produce mainly Friedel-Crafts alkylated products.

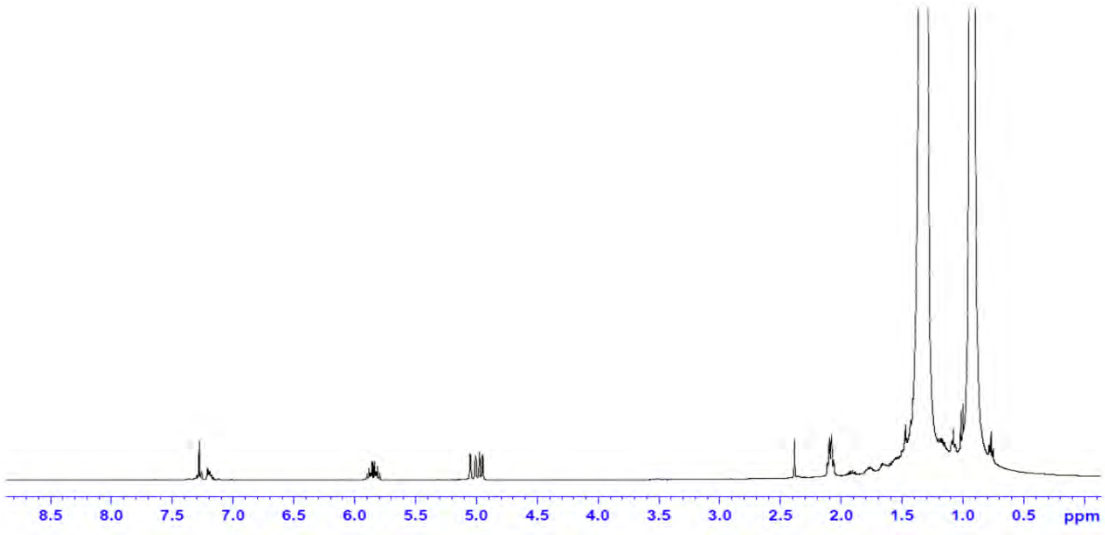

Figure 3.9: ^1H NMR spectrum of the products of catalyst **2** from the reaction at Al:Ni ratio of 250:1, temperature = 30 °C, pressure = 20 bar, time = 1 h, solvent = hexane. The presence of signals between 5-6 ppm indicates the presence of alkenes in the mixture.

Table 3.3: Effect of solvent on ethylene oligomerization reactions with **2**/$EtAlCl_2$.[a]

Entry	Solvent	Pressure (bar)	Time (h)	T_{min}/T_{max} (°C)	[b]Yield (g)	Activity[c]	%Oligomer Distribution[d]			
							C_4	**C_6**	**α-C_4**	**α-C_6**
1	Hexane	10	1	30/32	3.14	314	9	91	97	42
2	Hexane	10	0.5	30/32	1.39	278	10	90	94	34
3	Hexane	10	2	30/32	5.84	292	13	87	100	34
4	Hexane	20	1	30/34	3.51	351	18	82	100	39
5	Hexane	30	1	30/33	3.48	348	20	80	100	43
6	Chlorobenzene	10	1	30/52	6.91	691	15	85	94	50
7	Chlorobenzene	10	0.5	30/48	3.27	654	14	86	90	47
8	Chlorobenzene	20	1	30/57	8.65	865	7	93	100	48
9	Chlorobenzene	30	1	30/58	8.62	862	13	87	89	48

[a]Reaction conditions: complex **2**, nNi = 10 µmol; temperature, 30 °C. [b]Determined by mass difference of 80 mL hexane (52.72 g), 80 mL chlorobenzene (88.8 g) and mass of final solution. [c]Activity, kg oligomer.mol.$^{-1}$catalyst.h^{-1}. [d]Determined by GC.

The selectivity towards C_6 in comparison to C_4 by complex **2** mirrors the results obtained using nickel(II) complexes of pyrazolylamine ligands in chlorobenzene.[25] Analyses of the C_4 and C_6 fractions (Figure 3.10) showed higher selectivity towards α -C_4 (89-100%) compared to α -C_6 (42-50%). Thus isomerization of C_6 to produce 2-C_6 (*cis* and *trans*) was favored compared to isomerization of butenes. This observation points to possible chain running of the coordinated 1-hexene to produce internal C_6 oligomers as previously proposed by Brookhart and co-workers.[41] The absence of other C_6 isomers such as 4-methyl-2-pentene, 2-methyl-1-pentene, 2-methyl-2-pentene and 2,3-dimethyl-2-butene reveals lack of possible cleavage of C–C bonds of coordinated internal-C_6 olefins to give C_3 units which then undergo rapid recombination.[42-44]

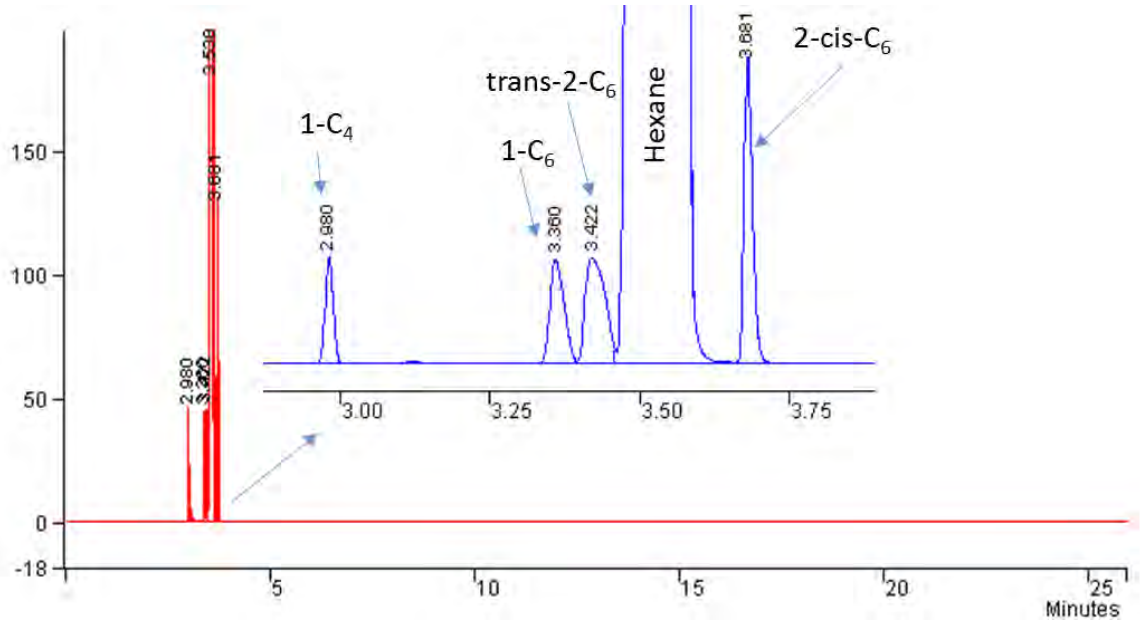

Figure 3.10: Gas chromatogram of product obtained using catalyst **2**, Al:Ni ratio of 250:1, temperature = 30 °C, pressure = 10 bar, time = 2 h, solvent = hexane showing isomerization of C_6 to internal olefins while only α-C_4 was obtained.

Our results are in tandem with those of Boudier *et al.*[39] where they recorded selectivity of 88-91% towards α-C_4 compared to 9-19% towards α-C_6 using imino-imidazole nickel(II) complexes. In contrast, Braunstein and co-workers observed very low selectivity towards α-

C_4 (10%) using pyridyl-triazole nickel(II) catalysts and $EtAlCl_2$ as a co-catalyst.[37] We also observed that reactions performed in chlorobenzene showed relatively higher compositions of C_4 than reactions in hexane. For example, under similar conditions, 15% and 9% of C_4 were recorded in chlorobenzene and hexane solvents, respectively (Table 3.3, entries, 1 and 6). This trend is supported by the higher catalytic activities observed in chlorobenzene (691 kg oligomer.mol.$^{-1}$catalyst.h^{-1}) compared to hexane experiments (314 kg oligomer.mol.$^{-1}$catalyst.h^{-1}). Higher catalytic activities are likely to promote chain termination over chain propagation hence lower oligomer fractions.[7, 45] Generally, higher catalytic activities were observed in toluene giving activities of up to 2 462 kg oligomer.mol.$^{-1}$catalyst.h^{-1} compared to the best activity of 862 kg oligomer.mol.$^{-1}$catalyst.h^{-1}obtained in chlorobenzene.

*3.3.3.3. Evaluation of **1-6** as ethylene oligomerization catalysts using MAO*

In order to further understand the influence of co-catalysts on the catalytic behavior of complexes **1-6**, we activated these pre-catalysts using MAO in toluene solvent. Table 3.4 shows a summary of the ethylene oligomerization data obtained for **1-6** using MAO as a co-catalyst. From the product distribution in Table 3.4, the role of the co-catalyst is quite discerning. Upon activation with MAO, all the complexes oligomerized ethylene to give C_4 as the major product (48-79%) and C_6, C_8 and double alkylated $(C_2)_2$-toluene as minor products (Scheme 3.4). Figure 3.11 shows detailed analyses of the C_4, C_6 and C_8 oligomer fractions obtained. This is in sharp contrast to the product distribution obtained using $EtAlCl_2$ in hexane as a co-catalyst where C_6 was the major product (80-91%). One conspicuous observation is the higher percentage composition of C_8 relative to C_6 using MAO as co-catalyst. It is thus conceivable that these oligomerization reactions do not follow the Schultz-Flory distribution.[46-48]

Table 3.4: Ethylene oligomerization data for **1-6** using MAO as co-catalyst in toluene.[a]

Entry	Cat	Pressure	Time	T_{min}/T_{max}	Al:M	Yield[c]	Activity[d]	% product distribution[e]						
		(bar)	(h)	(°C)[b]		(g)		**C_4**	**α-C_4**	**C_6**	**α-C_6**	**C_8**	**α-C_8**	**F**
1	**1**	10	1	30/32	1 000	7.37	737	61	64	5	68	19	13	15
2	**2**	10	1	30/33	1 000	6.81	681	64	74	10	65	13	25	13
3	**3**	10	1	30/31	1 000	2.75	272	64	68	8	49	14	26	14
4	**4**	10	1	30/32	1 000	3.59	359	75	58	2	100	13	22	10
5	**5**	10	1	30/33	1 000	8.23	823	45	39	9	41	21	51	25
6	**6**	10	1	30/32	1 000	3.18	318	54	61	16	50	15	27	15
7	**5**	10	1	30/31	1 500	8.38	838	69	31	10	66	11	55	10
8	**5**	10	1	30/33	2 000	6.97	697	76	30	3	66	13	45	8
9	**5**	20	1	30/33	1 000	10.66	1 066	59	84	1	100	19	41	21
10	**5**	30	1	30/33	1 000	12.04	1 204	79	25	4	62	11	30	6
11	**5**	10	0.5	30/32	1 000	3.88	776	51	67	5	53	22	44	22
12	**5**	10	2	30/32	1 000	8.04	804	48	84	10	76	24	30	18

[a]Reaction conditions: [M] = 10 μmol; solvent, toluene, 80 mL; temperature, 30 °C. [b]Initial temp was 30 °C, T_{min} and T_{max} = lowest and highest temperatures attained during the reaction period. [c]Determined by mass difference of 80 mL toluene (69.60 g) and mass of final solution. [d]Activity, kg product.mol.$^{-1}$catalyst.h^{-1}. [e]Determined by GC.

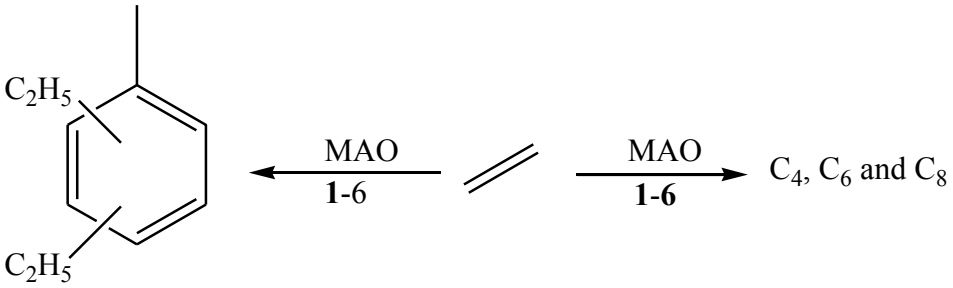

F

Scheme 3.4: Ethylene oligomerization accompanied by Friedel-Crafts alkylation of ethylene monomer to toluene with complexes **1-6**, and MAO as co-catalyst.

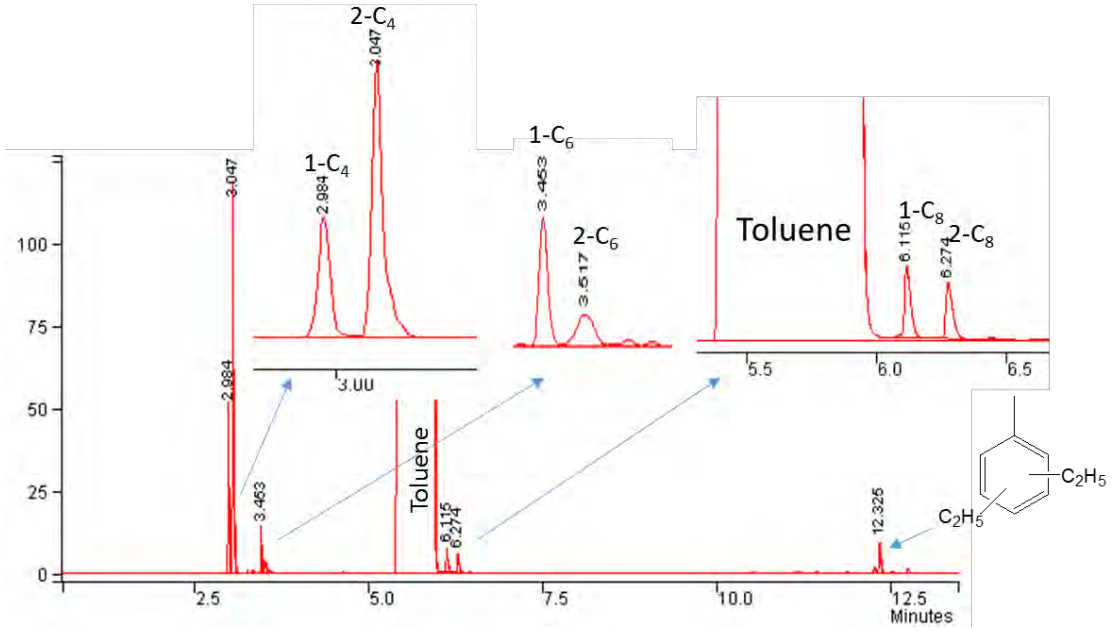

Figure 3.11: Gas chromatogram of products obtained using catalyst **5**, MAO:Ni ratio of 1 500:1, temperature = 30 °C, pressure = 10 bar, time = 1 h, solvent = toluene showing isomerization of C_4, C_6 and C_8 to internal olefins.

At this stage, we are unable to unambiguously account for this inconsistent chain propagation *vs* chain termination behavior. One can be tempted to argue that the double $(C_2)_2$-toluene is a C_4-toluene product. However, from the product distribution in the $EtAlCl_2$ reactions, minimal C_4-alkylation was observed for cobalt(II) and iron(II) catalysts **3** and **4**, respectively, while direct

alkylation of toluene by C_2 was the most favored. In addition, the absence of C_6- and C_8-alkyl toluenes further supports this assignment. GC-MS was once again very useful in product elucidation and Figures 3.12 and 3.13 show typical spectra of the oligomers obtained. For example, the GC-MS data gave molecular ions, M^+ = 56, 84 and 111 corresponding to C_4, C_6 and C_8, respectively. Indeed, each of these products was identified from their peaks which appeared at distinct retention times on the GC- mass spectrum resulting in unique fragmentation pattern in their mass spectra that matched well to each respective species. For example, in the butene spectrum (Figure 3.12) at a retention time of 0.97 min, loss of the CH_3 group results in the observed peak at m/z = 41, a propene molecule. Similarly, in the hexene spectrum (figure 3.13) at a retention time of 1.19-1.34 min, the loss of the initial CH_3 group results in the observed peak at m/z = 69. Subsequent losses of CH_2 groups results in the peaks at m/z = 55 and m/z= 41, attributed to a propene molecule. A similar trend was observed in the octene spectrum (Figure 3.14).

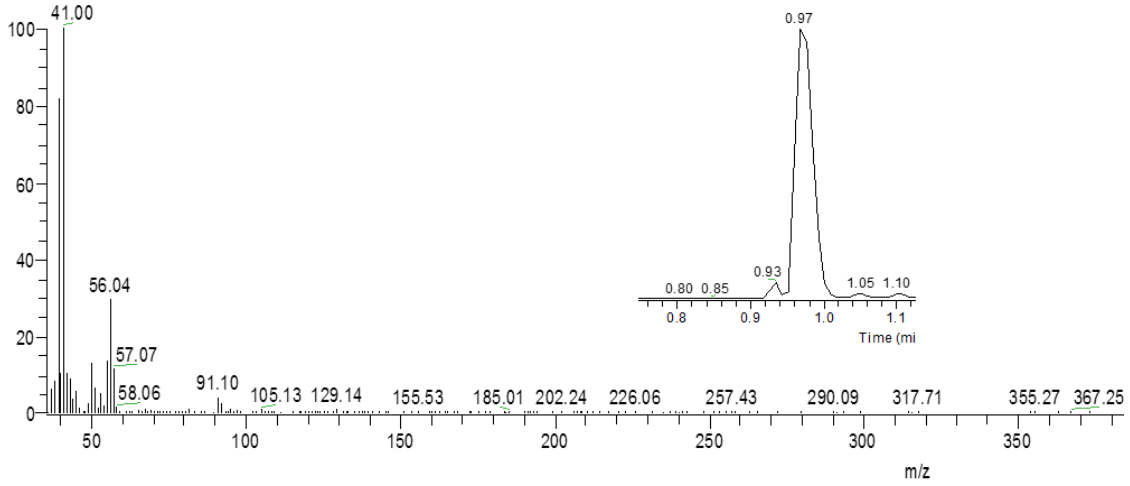

Figure 3.12: Mass spectrum of the butene product obtained from catalyst **1**, MAO:Ni ratio of 1 000:1, temperature = 30 °C, pressure = 10 bar, time = 1 h, solvent = toluene. M^+= 56.04 corresponds to the molecular ion mass of the butene at retention time of 0.97 min.

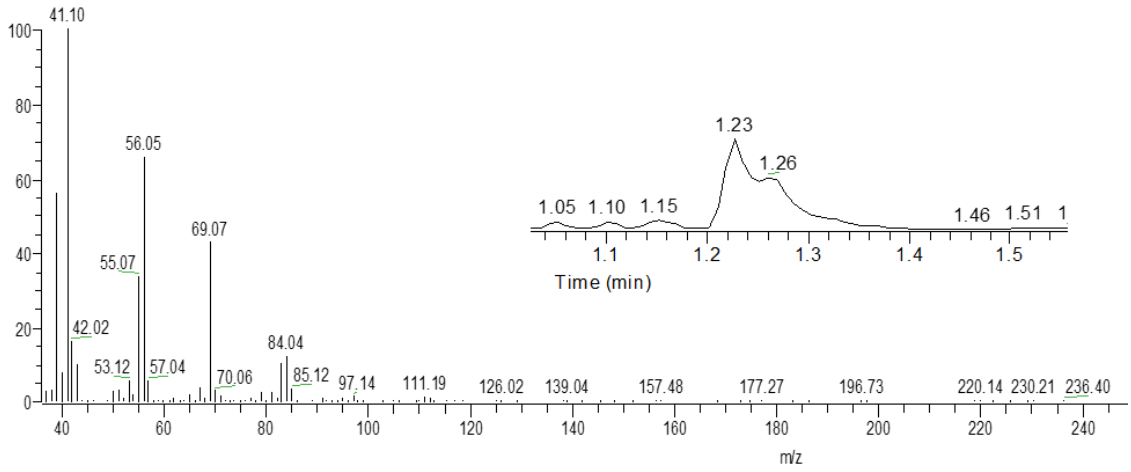

Figure 3.13: GC-mass spectrum of the hexene product obtained from catalyst **5**, MAO:Ni ratio of 1 500:1, temperature = 30 °C, pressure = 10 bar, time = 1 h, solvent = toluene. M^+= 84.04 corresponds to the molecular ion mass of the hexene at retention time of 1.19-1.34 min.

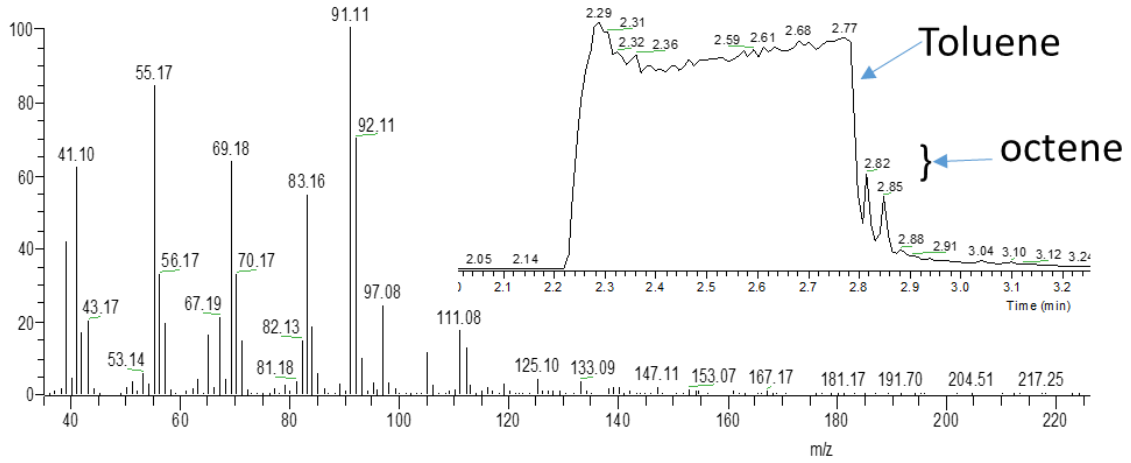

Figure 3.14: GC-mass spectrum of the octene product obtained from catalyst **5**, MAO:Ni ratio of 1 500:1, temperature = 30 °C, pressure = 10 bar, time = 1 h, solvent = toluene. M^+= 111.08 corresponds to the molecular ion mass of the octene at retention time of 2.82 min.

In a related work, Song *et al.*[22] using bis(phosphanyl)amine nickel(II) complexes observed the formation of C_4 and C_6 oligomers at 20 °C using MAO as co-catalyst, but at temperatures of 50 °C, they reported alkylation of toluene by the pre-formed oligomers. The selectivity towards α-

olefins when MAO was employed as an activator (Table 3.4) was generally lower compared to reactions using $EtAlCl_2$ co-catalyst (Table 3.2). Unlike in $EtAlCl_2$ reactions where we observed predominantly α-C_4 oligomers, activation by MAO gave lower selectivity of 35-84% towards α-C_4fractions (Table 3.4). A similar trend was observed in the compositions of α-C_6 (41-76%) using MAO compared to values of 80-92% for the nickel(II) complexes. A notable exception was observed with the iron(II) catalyst **4** which gave 100% α-C_6. The observed greater isomerization reactions of C_4 and C_6 oligomer fractions when MAO was used as an activator hints to a different catalytic species formed compared to activation using $EtAlCl_2$ co-catalyst.

3.3.3.4. Influence of catalyst structure on ethylene oligomerization reactions

In all the catalytic reactions investigated, we observed a significant effect of complex structure on both the catalytic activity and production distributions. Most notable was the role of the metal atom in regulating catalytic performance. Generally, the nickel(II) complexes **1**, **2** and **5** displayed higher catalytic activities compared to the cobalt(II) (**3**, **6**) and iron(II) (**4**) analogues (Tables 3.2 and 3.4). For example, in the $EtAlCl_2$ activation, the cobalt(II) and iron(II) complexes **3** and **4** exhibited marginal activities of 280 kg product.mol.$^{-1}$catalyst.h^{-1} and 467 kg product.mol.$^{-1}$catalyst.h^{-1}, respectively, compared to the activity of 1 072 kg product.mol.$^{-1}$catalyst.h^{-1} displayed by the analogue nickel complex **1**. The low catalytic activities of cobalt(II) and iron(II) complexes relative to nickel(II) analogues has been reported for nickel(II), cobalt(II) and iron(II) complexes of 2-(2-pyridyl)quinoxaline in ethylene oligomerization reactions[49] and was attributed to electronic factors.[50]

The ligand framework also influenced the catalytic activities of these complexes. In general, a change of pyrazolyl substituent from Me to Ph was followed by a slight increase in activity. For instance, in the MAO reactions, replacing the Me group (**2)** with a Ph group (**5**) resulted in an increase in activity from 681 to 823 kg product.mol.$^{-1}$catalyst.h^{-1}, respectively (Table 3.4, entries 2 and 5). One plausible reason for this trend could be the improved solubility of the complexes **5** and **6** bearing the bulkier phenyl groups.

The identity of the halides also conferred some effects on the catalytic behavior of the resultant catalysts. Complex **1** was found to be more active than the corresponding bromide analogue displaying activities of 1 072 and 871 kg product.mol.$^{-1}$catalyst.h^{-1}, respectively (Table 3.2, entries 1 and 2). This is consistent with observations in literature[24] and has been attributed to electronic factors and possible favorable activation process by the co-catalyst. However, the greater catalytic performance of the dichloride catalysts compared to their dibromide analogues contrasts with the results obtained using pyrazolyliminophosphorane[51] and 2-quinoxalinyl-6-iminopyridine[52] nickel(II) complexes where higher activities were reported for the dibromide catalysts. These findings were attributed to better solubility of the dibromide complexes in toluene than dichloride complexes.

We also observed the dependence of product distribution on catalyst structure. Most outstanding was the preferred direct alkylation of toluene by C_2 by cobalt(II) (**3**) and iron(II) (**4**) catalysts compared to the nickel(II) counterparts (Table 3.2, entries 1-4). As an illustration, the iron(II) complex **3** gave 83% of the C_2-toluene product indicating preference to Friedel-Crafts alkylation to initial oligomerization. This is not rather surprising considering that $FeCl_3$ is a better Friedel-

Crafts catalyst on its own.[53] Complex **5**, bearing Ph groups on the pyrazolyl motif, gave lower C_4 oligomers (45%) compared to the less sterically demanding complex **2** containing Me groups (64%) (Table 3.4, entries 2 and 5). This is in good agreement with increased chain propagation over chain termination with increase in steric hindrance around the metal center.[2, 7]

Another surprising result was the higher percentage composition of C_4 fraction of (64%) and (75%) obtained for the cobalt(II) and iron(II) complexes **3** and **4**, respectively (Table 3.4, entries 3-5). From the $EtAlCl_2$ activation reactions, we expected greater preference to the C_2-toluene alkylated product. This once again illustrates the role of MAO and $EtAlCl_2$ in controlling the product distribution. Our results agree with those of Alt and co-workers where iron(II) complexes of bis(arylimino)pyridine ligands favor dimerization of ethylene.[54]

3.3.3.5. Effect of reaction conditions on ethylene oligomerization reactions

The influence of reaction parameters such as Al/M ratio, time of the reaction and pressure on the catalytic behavior of these complexes were also investigated using complexes **1** and **5**. First, we varied the Al/Ni from 200 to 350 for the $EtAlCl_2$ reactions (Table 3.2, entries 1 and 9-11). An optimum Al/Ni ratio of 300/1 (Table 3.3, entry 10) was realized corresponding to activity of 1 251 kg product.mol.$^{-1}$catalyst.h^{-1}. Higher Al/Ni was required in the MAO reactions compared to experiments performed using $EtAlCl_2$. Using catalyst **5**, the Al/Ni was varied from 1 000 to 2 000 to record an optimum ratio of 1 500/1 (Table 3.4, entry 7). Higher Al/Ni ratios of 350:1 and 2000:1 in the $EtAlCl_2$ and MAO reactions, respectively, resulted in decreased catalytic activities possibly due to high accumulation of alkylaluminium impurities leading to catalyst deactivation.[55] Generally higher MAO/Ni ratios favored the formation of lower C_4 oligomers.

For example, percentage compositions of C_4 of 45% and 76% were observed at Al/Ni ratios of 1 000 and 2 000, respectively (Table 3.4, entries 5 and 8). This trend could be attributed to increased chain transfer to the co-catalyst or greater chain termination due to increased catalytic activities.[56]

The stability of the active species was probed using complexes **1** and **5** by varying reaction time from 0.5 h to 2 h (Table 3.2, entries 1 and 7-8 and Table 3.4, entries 1 and 11-12). Increasing the reaction time from 0.5 h to 1 h led to increased activity from 980 to 1 072 kg product.mol.$^{-1}$catalyst.h^{-1}, respectively (Table 3.2, entries 1 and 7). However, increasing reaction time to 2 h was marked by a decrease in activity to 798 kg product.mol.$^{-1}$catalyst.h^{-1} (Table 3.2, entry 8). This behavior of activity with time is consistent with an initiation stage between 0.5 h to 1 h and catalyst degradation between 1 h and 2 h.[45] A similar trend was observed for complex **5** using MAO as a co-catalyst (Table 3.4, entries 1 and 11-12). However, the general increase in quantitative yields of the products with time indicates appreciable stability of the active species.

It was also observed that reaction time had a profound influence on product distribution. From Table 2, it was evident that shorter reaction time gave higher amounts of ethyl-toluenes and butyl-toluenes while longer reaction times produced larger quantities of hexyl-toluenes and $(C_4)_2$-toluene. For example, increasing reaction time from 0.5 h to 2 h resulted in an increase of percentage composition of dibutyl-toluene from 9 to 18% (Table 3.2, entries 7 and 80. Similarly, the amount of ethyl-toluene reduced from 16 to 8%. This data is consistent with initial oligomerization of ethylene oligomers followed by Friedel-Crafts alkylation. Thus at shorter

reaction times, fewer amounts of butyl and hexyl-toluenes were present compared ethyl-toluenes.

The influence of ethylene concentration on the catalytic activities of the complexes was studied by varying ethylene pressure from 5 bar to 30 bar using catalysts **1** and **5** (Table 3.2, entries 11-14 and Table 3.4, entries 8-10). As expected, an increase in ethylene pressure from 5 bar to 30 bar resulted in marked increase in the activity of **1**/$EtAlCl_2$ system from 473 to 2,462 kg product.mol.$^{-1}$catalyst.h^{-1}, respectively (Table 3.2, entries 1, 12-14). Similarly, an increase in ethylene pressure from 10 to 30 bar led to increased catalytic activity of **5**/MAO system from 823 to 1,204 kg product.mol.$^{-1}$catalyst.h^{-1}, respectively (Table 3.4, entries 5, 9 and 10). We also observed that a change in ethylene concentration had a significant effect on the product distribution. For example, using $EtAlCl_2$ activator, increase in ethylene pressure favored the formation of butyl-toluenes indicating that more C_4 oligomers were produced (Table 3.2, entries 1, 12-14). The effect of ethylene pressure was more pronounced when MAO was used to activate the complexes. For instance, an increase in pressure from 10 bar to 30 bar was characterized by a remarkable increase in selectivity for C_4 fraction from 45 to 79%, respectively. Higher composition of lower fractions at higher pressures is consistent with increased catalytic activities leading to rapid chain termination.[41]

3.4. Summary and conclusions

A series of nickel(II), iron(II) and cobalt(II) complexes bearing unsymmetrical 2-(chloromethyl)-6-(pyrazol-1-ylmethyl)pyridine ligands were synthesized and structurally characterized. The complexes form active catalsyts in the oligomerization of ethylene upon activation with $EtAlCl_2$ and MAO co-catalysts. Both the catalytic activities of the complexes and products formed were largely controlled by the nature of the co-catalyst, solvent and

complex structure. Activation using $EtAlCl_2$ in toluene formed the most active systems giving predominantly Friedel-Crafts alkylation products of the preformed oligomers. On the other hand, use of $EtAlCl_2$ in hexane and chlorobenzene solvents displayed relatively lower catalytic activities to produce predominatly hexenes. The use of MAO as a co-catalyst led to the formation of mainly butenes with hexenes and octenes as minor products. Nickel(II) complexes were generally more active than the correspoindg iron(II) and cobalt(II) complexes. In addition, iron(II) and cobalt(II) complexes favored Friedel-Crafts alkyation reactions than nicke(II) complexes. In summary, we have demonstrated the role of solvent, co-catalyst and complex structure in regulating the behaviour of these transition metal complexes in ethylene oligomerization reactions.

3.5. References

1. Sun, W.; Zhang, S.; Jie, S.; Zhang, W. L., *J. Organomet. Chem* **2006**, *691*, 4196-4203.
2. Johnson, L. K.; Killian, C. M.; Brookhart, M., *J. Am. Chem. Soc.* **1995**, *117*, 6414-6415.
3. Johnson, L. K.; Mecking, S.; Brookhart, M., *J. Am. Chem. Soc.* **1996**, *118*, 267-268.
4. Mecking, S.; Johnson, L. K.; Wang, L.; Brookhart, M., *J. Am. Chem. Soc.* **1998**, *120*, 888-899.
5. Killian, C. M.; Tempel, D. J.; Johnson, L. K.; Brookhart, M., *J. Am. Chem. Soc.* **1996**, *118*, 11664-11665.
6. Feldman, J.; McLain, S. J.; Parthasarathy, A.; Marshall, W. J.; Calabrese, J. C.; Arthur, S. D., *Organometallics* **1997**, *16*, 1514-1516.
7. Ittel, S. D.; Johnson, L. K.; Brookhart, M., *Chem. Rev.* **2000**, *100*, 1169-1204.
8. Bianchini, C.; Giambastiani, G.; Rios, I. G.; Mantovani, G.; Meli, A.; Segarra, A. M., *Coord. Chem. Rev.* **2006**, *250*, 1391-1418.

9. Gao, R.; Sun, W.-H.; Redshaw, C., *Catal. Sci. Technol.* **2013**, *3*, 1172-1179.

10. Weng, Z.; Teo, S.; Koh, L. L.; Hor, T. A., *Chem. Commun.* **2006**, 1319-1321.

11. Hao, P.; Zhang, S.; Sun, W.-H.; Shi, Q.; Adewuyi, S.; Lu, X.; Li, P., *Organometallics* **2007**, *26*, 2439-2446.

12. Sun, W.-H.; Jie, S.; Zhang, S.; Zhang, W.; Song, Y.; Ma, H.; Chen, J.; Wedeking, K.; Fröhlich, R., *Organometallics* **2006**, *25*, 666-677.

13. Gao, R.; Zhang, M.; Liang, T.; Wang, F.; Sun, W.-H., *Organometallics* **2008**, *27*, 5641-5648.

14. Dyer, P. W.; Fawcett, J.; Hanton, M. J., *Organometallics* **2008**, *27*, 5082-5087.

15. Keim, W.; Kowaldt, F. H.; Goddard, R.; Krüger, C., *Angew. Chem. Int. Ed. Engl.* **1978**, *17*, 466-467.

16. Keim, W.; Behr, A.; Limbäcker, B.; Krüger, C., *Angew. Chem. Int. Ed. Engl.* **1983**, *22*, 503-503.

17. Skupinska, J., *Chem. Rev.* **1991**, *91*, 613-648.

18. Kermagoret, A.; Braunstein, P., *Dalton Trans.* **2008**, 585-587.

19. Kermagoret, A.; Braunstein, P., *Organometallics* **2007**, *27*, 88-99.

20. Chavez, P.; Rios, I. G.; Kermagoret, A.; Pattacini, R.; Meli, A.; Bianchini, C.; Giambastiani, G.; Braunstein, P., *Organometallics* **2009**, *28*, 1776-1784.

21. Kermagoret, A.; Tomicki, F.; Braunstein, P., *Dalton Trans.* **2008**, 2945-2955.

22. Song, K.; Gao, H.; Liu, F.; Pan, J.; Guo, L.; Zai, S.; Wu, Q., *Eur. J. Inorg. Chem.* **2009**, *2009*, 3016-3024.

23. Ojwach, S. O.; Guzei, I. A.; Benade, L. L.; Mapolie, S. F.; Darkwa, J., *Organometallics* **2009**, *28*, 2127-2133.

24. Budhai, A.; Omondi, B.; Ojwach, S. O.; Obuah, C.; Osei-Twum, E. Y.; Darkwa, J., *Catal. Sci. Technol.* **2013**, *3*, 3130-3135.

25. Obuah, C.; Omondi, B.; Nozaki, K.; Darkwa, J., *J. Mol. Catal. A: Chem.* **2014**, *382*, 31-40.

26. Baker, W.; Buggle, K. M.; McOmie, J. F. W.; Watkins, D. A. M., *J. Chem. Soc.* **1958**, 3594-3603.

27. Kitajima, N.; Fujisawa, K.; Fujimoto, C.; Morooka, Y.; Hashimoto, S.; Kitagawa, T.; Toriumi, K.; Tatsumi, K.; Nakamura, A., *J. Am. Chem. Soc.* **1992**, *114*, 1277-1291.

28. Bruker *APEX2, SAINT and SADABS, Bruker AXS Inc*, Madison, : Wisconsin, USA, 2012.

29. Sheldrick, G. M., *Acta Crystallogr.* **2007**, *64*, 112-122.

30. Farrugia, L. J., *J. Appl. Crystallogr.* **2012**, *45*, 849-854.

31. Watson, A. A.; House, D. A.; Steel, P. J., *Inorg. Chim. Acta* **1987**, *130*, 167-176.

32. Cotton, A. F.; Wilkinson, G.; Bochmann, M.; Murillo, C. A., Advanced Inorganic Chemistry, 6th ed.; John Wiley and Sons: New York, **1999**.

33. Dahlhoff, W. V.; Nelson, S. M., *J. Chem. Soc. A: Inorg., Phys. Theor.* **1971**, 2184-2190.

34. Bruno, I. J.; Cole, J. C.; Kessler, M.; Luo, J.; Motherwell, W. S.; Purkis, L. H.; Smith, B. R.; Taylor, R.; Cooper, R. I.; Harris, S. E., *J. Chem. Inf. Comput. Sci.* **2004**, *44*, 2133-2144.

35. Ainooson, M. K.; Ojwach, S. O.; Guzei, I. A.; Spencer, L. C.; Darkwa, J., *J. Organomet. Chem.* **2011**, *696*, 1528-1535.

36. Malgas-Enus, R.; Mapolie, S. F., *Inorg. Chim. Acta* **2014**, *409*, 96-105.

37. Schweinfurth, D.; Su, C.-Y.; Wei, S.-C.; Braunstein, P.; Sarkar, B., *Dalton Trans.* **2012**, *41*, 12984-12990.

38. He, F.; Xiang H.; Xiaoping C.; Carl R.; Wen-Hua S. *J. Organomet. Chem* **2012**, *712*, 46-51.

39. Boudier, A.; Breuil, P.-A. R.; Magna, L.; Olivier-Bourbigou, H.; Braunstein, P., *J. Organomet. Chem.* **2012**, *718*, 31-37.

40. Boudier, A.; Breuil, P.-A. R.; Magna, L.; Olivier-Bourbigou, H.; Braunstein, P., *Chem. Commun.* **2014**, *50*, 1398-1407.

41. Killian, C. M.; Johnson, L. K.; Brookhart, M., *Organometallics* **1997**, *16*, 2005-2007.

42. Jacobson, D.; Freiser, B., *Organometallics* **1984**, *3*, 513-519.

43. Jacobson, D.; Freiser, B., *J. Am. Chem. Soc.* **1983**, *105*, 736-742.

44. Jacobson, D.; Freiser, B., *J. Am. Chem. Soc.* **1983**, *105*, 5197-5206.

45. Doherty, M. D.; Trudeau, S.; White, P. S.; Morken, J. P.; Brookhart, M., *Organometallics* **2007**, *26*, 1261-1269.

46. Flory, P. J., *J. Am. Chem. Soc.* **1940**, *62*, 1561-1565.

47. Schultz, G., *Z. Phys. Chem.* **1939**, *43*, 25.

48. Svejda, S. A.; Brookhart, M., *Organometallics* **1999**, *18*, 65-74.

49. Shao, C.; Sun, W.-H.; Li, Z.; Hu, Y.; Han, L., *Catal. Commun.* **2002**, *3*, 405-410.

50. Laine, T. V.; Lappalainen, K.; Liimatta, J.; Aitola, E.; Löfgren, B.; Leskelä, M., *Macromol. Rapid Commun.* **1999**, *20*, 487-491.

51. Zhang, C.; Sun, W. H.; Wang, Z. X., *Eur. J. Inorg. Chem.* **2006**, *2006*, 4895-4902.

52. Adewuyi, S.; Li, G.; Zhang, S.; Wang, W.; Hao, P.; Sun, W.-H.; Tang, N.; Yi, J., *J. Organomet. Chem.* **2007**, *692*, 3532-3541.

53. Rueping, M.; Nachtsheim, B. J., *Beilstein J. Org. Chem.* **2010**, *6*, No. 6, 1-24.

54. Görl, C.; Beck, N.; Kleiber, K.; Alt, H. G., *J. Mol. Catal. A: Chem.* **2012**, *352*, 110-127.

55. Abbo, H. S.; Titinchi, S. J., *Molecules* **2013**, *18*, 4728-4738.

56. Chen, E. Y.-X.; Marks, T. J., *Chem. Rev.* **2000**, *100*, 1391-1434.

CHAPTER 4

(Pyrazolyl)-(phosphinoyl)pyridine iron(II), cobalt(II) and nickel(II) complexes: Synthesis, characterization and ethylene oligomerization studies

This chapter is adapted from the paper published in *J. Organometal. Chem.* ***2015***, *783, 64-72* and is based on the experimental work of the first author, George S. Nyamato. The contributions of the first author include syntheses of the ligands and complexes, ethylene catalysis and drafting of the manuscript.

4.1. Introduction

Olefins are the basic building blocks widely used in the production of lubricants, surfactants, plasticizers and polyolefins.[1, 2] Ethylene oligomerization is one of the most significant processes employing homogenous transition-metal catalysts[3] and is currently receiving great interest both in academia and industry. Since the discovery of Shell higher olefins process (SHOP) nickel(II) based catalysts,[4] significant amount of research efforts have been expedited on the design and development of alternative transition metal catalysts with improved catalytic performance with respect to activity, stability and selectivity.[5-9]

It has been extensively established that through careful manipulation of the catalyst structure, choice of co-catalyst and reaction conditions, the product selectivity can be greatly altered.[10] In this design, ligand structure has been shown to play a major role in regulating both the electronic and steric properties of the complexes[11, 12] *via* the incorporation of bulky groups, variation of the donor atom as well as electron withdrawing and donating groups.[13] In one such catalyst

design, He *et al.*[13, 14] showed that incorporation of P=O donor group in the ligand motif improves the catalytic activity and stability of transition metal complexes in ethylene polymerization reactions.

For the past decade, we have been involved in the design of pyrazolyl late transition metal complexes and their application in olefin oligomerization and polymerization reactions.[5, 7, 15-17] In 2009, we made an interesting observation that (pyrazolylmethyl)pyridine nickel(II) complexes upon activation with $EtAlCl_2$, catalyzed ethylene oligomerization reactions followed Friedel-Crafts alkylation of toluene solvent used by the pre-formed oligomers.[16] This finding was only preceded by another report by Dyer and co-workers, even though the extent of Friedel-Crafts alkylation was minimal in their system.[18] Following this discovery, we have extensively studied Friedel-Crafts alkylation reactions[5, 7, 15] to establish the role of the catalyst structure, solvent and nature of co-catalysts in controlling product distribution. From our accounts, in addition to literature reports, it is apparent that the pyrazolyl ligand plays a major role in promoting Friedel-Crafts alkylation of the pre-formed oligomers.[5, 7, 15] This hypothesis is further cemented by the lack of Friedel-Crafts alkylation products reported for a number of non-pyrazolyl transition metal catalysts.[19-22]

To gain in depth knowledge on the role of the pyrazolyl unit in these reactions, we are currently on the design of unsymmetrical (pyrazolyl)phosphine transition metal complexes containing a pyrazolyl unit and a secondary donor atom. It is noteworthy to mention the major differences in product distribution between the P^N^N systems (**II**) reported by Muller *et al.*[23] which exclusively produce polymers compared to our symmetrical pyrazolyl N^N^N[16] in which the

pre-formed oligomers undergo *in situ* Friedel-Crafts alkylation reactions (Chart 1). The P^N^N system is a hybrid of the SHOP (P^N)[4] model and the Brookhart (N^N) design,[24] and it is on this premise that we set to design a hybrid ligand system containing both the phosphine and pyrazolyl donor moieties (III). However, attempts to synthesize the phosphine ligand system **III** was hampered by *in situ* oxidation to the phosphinite ligand **IV** in very high yields. Thus in this contribution, we report the syntheses of a series of transition metal complexes of the N^N^O (pyrazolyl)-(phosphinoyl)pyridine ligands and their evaluation as catalysts in ethylene oligomerization reactions.

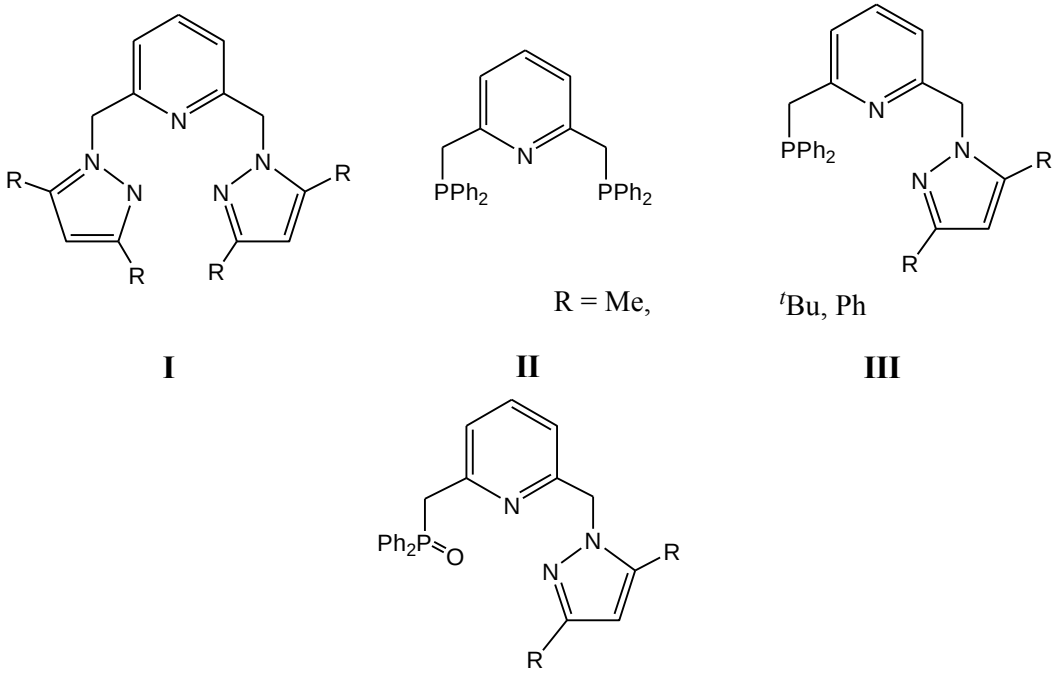

I **II** **III**

IV

Chart 4.1

4.2. Experimental Section

4.2.1. Materials and methods

All synthetic manipulations were performed using standard Schlenk techniques under a nitrogen atmosphere. All solvents were dried by distillation prior to use. Tetrabutylammonium bromide,

trimethylaluminium (TMA, 2M in toluene), $EtAlCl_2$ (1.0M in hexane), MAO (10 wt.% in toluene), 3,5-dimethylpyrazole, dibenzoylmethane, hydrazine hydrate, diphenylphosphine, *n*-butyllithium, thionyl chloride, 2,6-bis(hydroxymethyl)pyridine, and the metal salts were obtained from Sigma-Aldrich and used as received. Compounds 2-(chloromethyl)-6-((3,5-dimethyl-1H-pyrazol-1-yl)methyl)pyridine (**L1**) and 2-(chloromethyl)-6-((3,5-diphenyl-1H-pyrazol-1-yl)methyl)pyridine (**L2**)[15] and the starting materials 2,6-bis(chloromethyl)pyridine[25] and 3,5-diphenylpyrazole[26] were synthesized following the literature procedures. ^1H NMR and $^{13}C\{^1H\}$ NMR spectra were recorded on a Bruker 400 MHz spectrometer in $CDCl_3$ solution at room temperature using tetramethylsilane as an internal standard. Elemental analyses were performed on a Thermal Scientific Flash 2000 while ESI-mass spectra were recorded on an LC premier micro-mass spectrometer. Magnetic moments of the complexes were determined using Evans balance. GC analyses were performed using a Varian CP-3800 gas chromatograph equipped with a CP-Sil 5 CB (30 m × 0.2 mm × 0.25 μm) capillary column while GC–MS analyses were performed on a Shimadzu GC–MS-QP2010.

4.2.2. Synthesis of N^N^O (pyrazolyl)-(phosphinoyl)pyridine ligands

*4.2.2.1. 2-((3,5-dimethyl-1H-pyrazol-1-yl)methyl)-6-((diphenylphosphinoyl)methyl)pyridine (**L3**)*

n-Butyllithium (1.6 M in hexane, 3.0 mL, 4.75 mmol) was added drop-wise into a solution of diphenylphosphine (0.83 mL, 4.75 mmol) in tetrahydrofuran (15 mL) at 0 ºC. The bright red solution of lithium diphenylphosphide was stirred at this temperature for 1 h. The solution was then transferred *via* a cannula into a solution of 2-(chloromethyl)-6-((3,5-dimethyl-1H-pyrazol-1-yl)methyl)pyridine (**L1**) (1.12 g, 4.75 mmol) in THF (30 mL) at 0 ºC. The resulting solution

was stirred for 90 min at 0 ºC and then further at room temperature for 4 h. The solvent was then removed *in vacuo* and toluene (30 mL) was added. The organic layer was then washed twice with deoxygenated water (2 × 20 mL), dried over magnesium sulfate and filtered. Removal of the solvent *in vacuo* gave **L3** as a white solid. Yield: 1.68g (92%). ^{1}H NMR ($CDC1_3$): δ 2.07 (s, 3H, CH_3, pz); 2.16 (s, 3H, CH_3, pz); 3.92 (d, 2H, CH_2-P, $^{2}J_{PH}$ = 16. 0 Hz); 5.06 (s, 2H, CH_2-N); 5.77 (s, 1H, pz); 6.50 (d, 1H, 3-py, $^{3}J_{HH}$ = 8.0 Hz); 7.36 (d, 1H, 5-py, $^{3}J_{HH}$ = 8.0 Hz); 7.42 (dd, 4H, 3-ph, $^{3}J_{HH}$ = 8.0 Hz); 7.46 (dd, 2H, 4-ph, $^{3}J_{HH}$ = 8.0 Hz); 7.50 (d, 4H, 2-ph, $^{3}J_{HH}$ = 8.0 Hz); 7.74 (dd, 1H, 4-py, $^{3}J_{HH}$ = 8.0 Hz). ^{31}P{^{1}H} NMR: δ 29.70 ppm. ESI-MS: *m*/*z* (%) 384 (M^{+}−O), 53%). Anal. Calcd for $C_{24}H_{24}N_3OP$: C, 71.81; H, 6.03; N, 10.47. Found: C, 72.20; H, 5.97; N, 10.86.

*4.2.2.2. 2-((3,5-diphenyl-1H-pyrazol-1-yl)methyl)-6-((diphenylphosphinoyl)methyl)pyridine (**L4**)*

Ligand **L4** was prepared from *n*-butyllithium (1.6 M in hexane, 2.08 mL, 3.33 mmol), diphenylphosphine (0.58 mL, 3.33 mmol) and 2-(chloromethyl)-6-((3,5-diphenyl-1H-pyrazol-1-yl)methyl)pyridine (**L2**) (1.2g, 3.33 mmol) following the procedure described for **L3**. A white solid was obtained. Yield: 1.61g (95%). ^{1}H NMR ($CDC1_3$): δ 3.91 (d, 2H, CH_2-P, $^{2}J_{PH}$ = 16.0 Hz); 5.36 (s, 2H, CH_2-N); 6.71 (s, 1H, pz); 6.75 (d, 1H, 3-py, $^{3}J_{HH}$ = 7.6 Hz); 7.34-7.51 (m, 17H, Ar, $^{3}J_{HH}$ = 7.6 Hz); 7.71 (d, 4H, 2-Ph-P, $^{3}J_{HH}$ = 7.6 Hz); 7.86 (dd, 1H, 4-py $^{3}J_{HH}$ = 7.6 Hz) . ^{31}P{^{1}H} NMR: δ 29.83 ppm. ESI-MS: *m*/*z* (%) 509 (M^{+}−O), 100%). Anal. Calcd for $C_{34}H_{28}N_3OP$: C, 77.70; H, 5.37; N, 8.00. Found: C, 777.90; H, 4.97; N, 7.85.

4.2.3. Synthesis of metal complexes

*4.2.3.1. [{2-((3,5-dimethyl-1H-pyrazol-1-yl)methyl)-6-((diphenylphosphinoyl)methyl)-pyridine}$NiCl_2$] (**7**)*

Complex **7** was prepared by adding a solution of $NiCl_2$ (0.07g, 0.52 mmol) in dichloromethane (15 mL) to a solution of **L3** (0.20g, 0.52 mmol) in dichloromethane (15 mL). The resultant solution was stirred for 24 h. A green precipitate was formed and was isolated by filtration, washed with ethanol and diethyl ether and dried in vacuum, affording **7** as a green solid. Upon recrystallization from slow liquid diffusion of *n*-hexane into dichloromethane solution afforded green crystals suitable for single-crystal X-ray analysis. Yield: 0.18 g (67%). ESI-MS: *m*/*z* (%) 497 (M^+-Cl), 89%). Anal. Calcd for $C_{24}H_{24}N_3OPNiCl_2 \cdot CH_2Cl_2$: C, 48.75; H, 4.25; N, 6.82. Found: C, 48.92; H, 4.67; N, 6.88. μ_{eff} = 3.90 BM.

Complexes **8**-**12** were prepared following the procedure described for **7**.

*4.2.3.2. [{2-((3,5-dimethyl-1H-pyrazol-1-yl)methyl)-6-((diphenylphosphinoyl)methyl)-pyridine}$NiBr_2$] (**8**)*

[$NiBr_2$] (0.11g, 0.52 mmol) and **L3** (0.20g, 0.52 mmol). Brown solid. Yield: 0.25 g (79%). ESI-MS: *m*/*z* (%) 539 (M^+-Br, 32%). Anal. Calcd for $C_{24}H_{24}N_3OPNiBr_2 \cdot 2H_2O$: C, 43.94; H, 4.30; N, 6.41. Found: C, 43.71; H, 3.90; N, 6.25. μ_{eff} = 3.23 BM.

*4.2.3.3. [{2-((3,5-dimethyl-1H-pyrazol-1-yl)methyl)-6-((diphenylphosphinoyl)methyl)-pyridine}$CoCl_2$] (**9**)*

[$CoCl_2$] (0.07g, 0.52 mmol) and **L3** (0.20g, 0.52 mmol). Blue solid. Yield: 0.21 g (79%). ESI-MS: *m*/*z* (%) 495 (M^+−Cl, 22%). Anal. Calcd for $C_{24}H_{24}N_3OPCoCl_2 \cdot 0.5CH_2Cl_2$: C, 51.29; H, 4.39; N, 7.32. Found: C, 51.53; H, 4.50; N, 7.39. μ_{eff} = 4.36 BM.

*4.2.3.4. [{2-((3,5-dimethyl-1H-pyrazol-1-yl)methyl)-6-((diphenylphosphinoyl)methyl)-pyridine}$FeCl_2$] (**10**)*

[$FeCl_2.4H_2O$] (0.10g, 0.52 mmol) and **L3** (0.20g, 0.52 mmol). Yellow solid. Yield: 0.18 g (67 %). ESI-MS: *m*/*z* (%) 492 (M^+−Cl, 84%). Anal. Calcd for $C_{24}H_{24}N_3OPFeCl_2 \cdot 0.5CH_2Cl_2$: C, 48.97; H, 4.27; N, 6.85. Found: C, 49.35; H, 4.36; N, 6.32. μ_{eff} = 5.20 BM.

*4.2.3.5. [{2-((3,5-diphenyl-1H-pyrazol-1-yl)methyl)-6-((diphenylphosphinoyl)methyl)-pyridine}$NiBr_2$] (**11**)*

[$NiBr_2$] (0.04g, 0.20 mmol) and **L4** (0.10g, 0.20 mmol). Brown solid. Yield: 0.12 g (84%). ESI-MS: *m*/*z* (%) 664 (M^+−Br), 100%). Anal. Calcd for $C_{34}H_{28}N_3OPNiBr_2 \cdot CH_2Cl_2$: C, 50.71; H, 3.65; N, 5.07. Found: C, 50.72; H, 3.83; N, 4.77. μ_{eff} = 3.38 BM.

*4.2.3.6. [{2-((3,5-diphenyl-1H-pyrazol-1-yl)methyl)-6-((diphenylphosphinoyl)methyl)-pyridine}$CoCl_2$] (**12**)*

[$CoCl_2$] (0.03g, 0.20 mmol) and **L4** (0.10g, 0.20 mmol). Blue solid. Yield: 0.08 g (63 %). ESI-MS: *m*/*z* (%) 619 (M^+−Cl), 8%). Anal. Calcd for $C_{34}H_{28}N_3OPCoCl_2$: C, 62.31; H, 4.31; N, 6.41. Found: C, 62.28; H, 4.67; N, 6.47. μ_{eff} = 4.20 BM.

4.2.4. X-ray crystallography

The X-ray data were recorded on a Bruker Apex Duo equipped with an Oxford Instruments Cryojet operating at 100(2) K and an Incoatec microsource operating at 30 W power. Crystal and structure refinement data were collected with Mo Kα (λ = 0.71073 Å) radiation at a crystal-to-detector distance of 50 mm. The following conditions were used for the data collection: omega and phi scans with exposures taken at 30 W X-ray power and 0.50° frame widths using APEX2.[27] The data were reduced with the programme SAINT[27] using outlier rejection, scan speed scaling, as well as standard Lorentz and polarisation correction factors. A SADABS semi-empirical multi-scan absorption correction[27] was applied to the data. Direct methods, SHELXS-97[28] and WinGX[29] were used to solve all three structures. All non-hydrogen atoms were located in the difference density map and refined anisotropically with SHELXL-97.[28] All hydrogen atoms were included as idealised contributors in the least squares process. Their positions were calculated using a standard riding model with C-$H_{aromatic}$ distances of 0.93 Å and U_{iso} = 1.2 U_{eq} and C-$H_{methylene}$ distances of 0.99 Å and U_{iso} = 1.5 U_{eq}. The hydrogen atoms of the water molecule were located in the difference density map, and refined isotropically. Platon SQUEEZE[30] was used to remove disordered solvent from the lattice of (**7**) leaving solvent accessible voids of 171 $Å^3$.

4.2.5. General procedure for ethylene oligomerization reactions

Ethylene oligomerization reactions were carried out in a 400 mL stainless steel Parr reactor equipped with a mechanical stirrer, temperature controller and an internal cooling system. In a typical experiment, the reactor was preheated to 100 °C *in vacuo* and cooled to room temperature. The appropriate amount of the catalyst precursor (10.0 μmol) was transferred into

a dry Schlenk tube under nitrogen and toluene (20 mL) was added using a syringe. The required amount of co-catalyst ($EtAlCl_2$ or MAO) was then injected into the Schlenk tube containing the pre-catalyst to form the active catalytic system. The resultant solution was then transferred *via* cannula into the reactor. An additional 60 mL of toluene solvent was also transferred *via* cannula into the reactor giving a total volume of 80 mL. The reactor was then flushed three times with ethylene and the desired pressure and temperature was set and the reaction started. After the reaction time, the reactor was cooled to -15 °C using a bath of ice/liquid nitrogen and excess ethylene vented off. The contents were then transferred to a precooled flask and weighed. The reaction was then quenched by addition of 10% HCl (5 mL). A portion of the reaction mixture was sampled for GC and GC-MS analyses to determine the oligomer by comparison to the standard authentic samples. The amount of products formed was determined by mass difference of 80 mL toluene (69.60 g) and mass of final solution.

4.3. Results and discussion

4.3.1. Synthesis of the ligands and their metal complexes

The syntheses of the target unsymmetrical compounds **L1a** and **L2a** were performed by reactions of *n*-butyllithium with diphenylphosphine in tetrahydrofuran followed by addition of the appropriate compound 2-(chloromethyl)-6-((3,5-dimethyl-1H-pyrazol-1-yl)methyl)-pyridine (**L1**) or 2-(chloromethyl)-6-((3,5-diphenyl-1H-pyrazol-1-yl)methyl)pyridine (**L2**) (Scheme 1). However, isolation of compounds **L1a** and **L2a** in quantitative yields were unsuccessful due to *in situ* oxidation to form the corresponding phosphinite compounds 2-((3,5-dimethyl-1H-pyrazol-1-yl)methyl)-6-((diphenylphosphinoyl)methyl)pyridine (**L3**) and 2-((3,5-

diphenyl-1H-pyrazol-1-yl)methyl)-6-((diphenylphosphinoyl)methyl)-pyridine (**L4**) in 92% and 95% yields, respectively (Scheme 4.1).

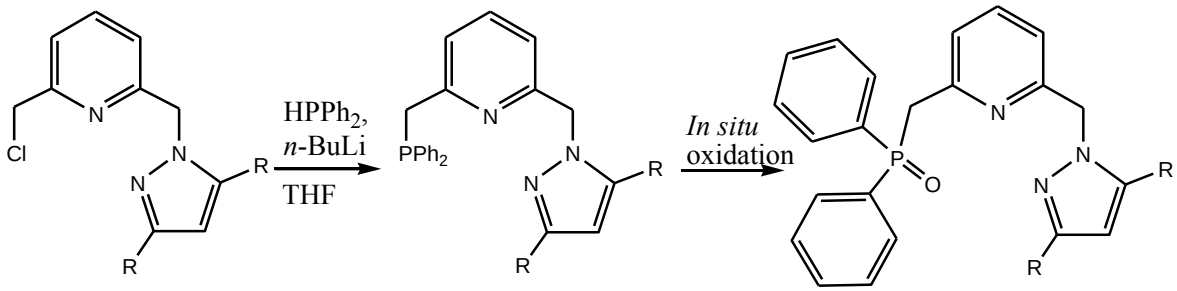

R = Me, **L1**
R = Ph, **L2**

R=Me, **L1a**
R=Ph, **L2a**

R=Me, **L3**
R = Ph, **L4**

Scheme 4.1: Synthesis of (pyrazolyl)-(phosphinoyl)pyridine ligands

This oxidation was unequivocally confirmed by $^{31}P\{^{1}H\}$ NMR studies (Figures 4.1, 4.2 and 4.3). In a typical experiment, a fresh sample from the reaction mixture was quickly transferred to an NMR tube containing deuterated chloroform ($CDCl_3$), sealed and the $^{31}P\{^{1}H\}$ NMR spectra acquired at intervals.

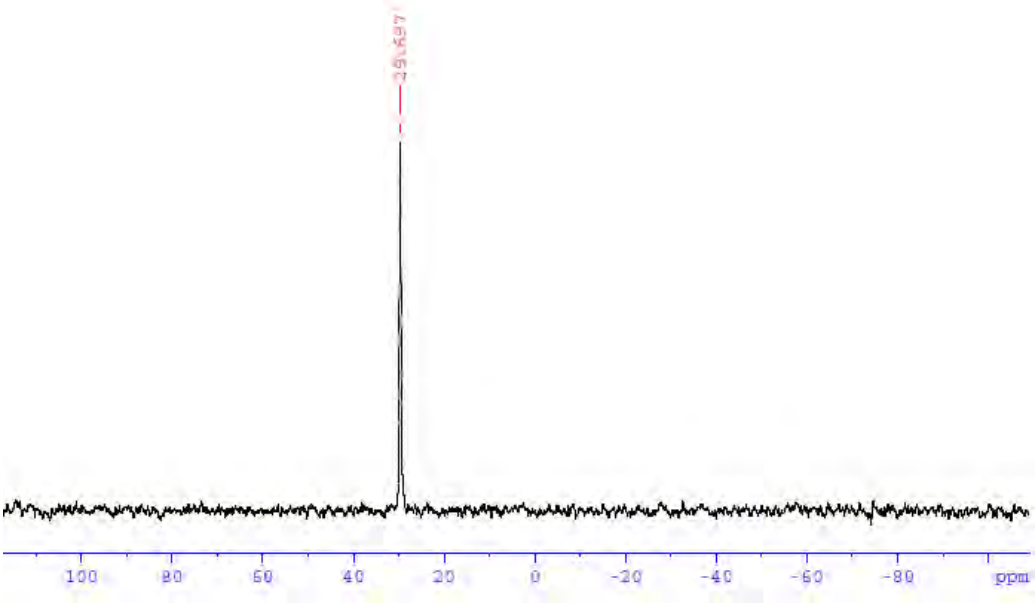

Figure 4.1: $^{31}P\{^{1}H\}$ NMR spectrum of **L3**

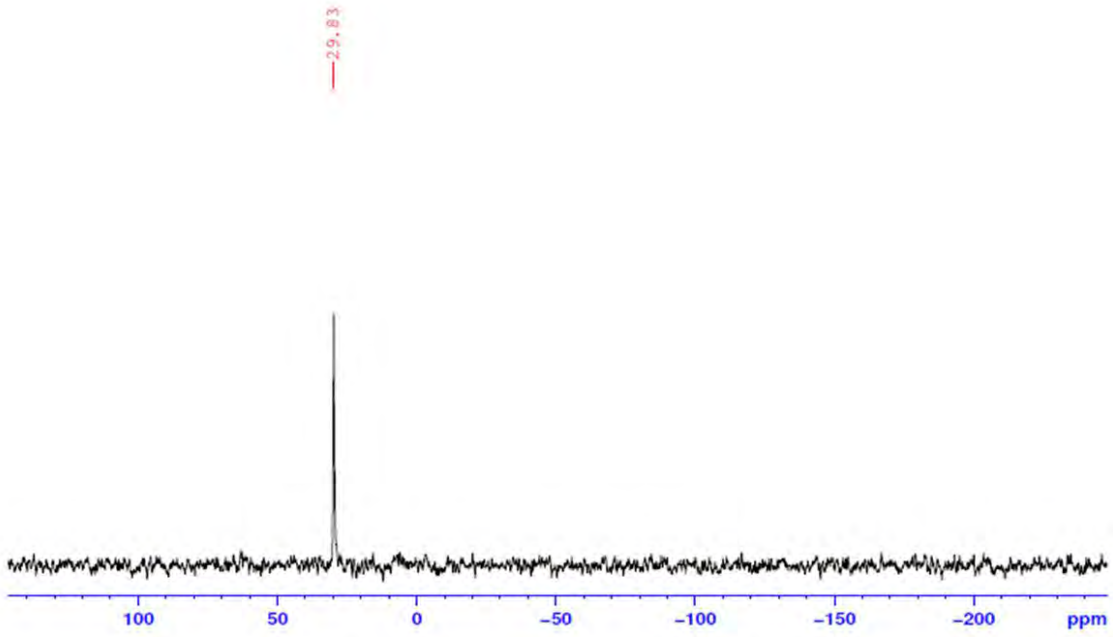

Figure 4.2: $^{31}P\{^{1}H\}$ NMR spectrum of **L4**

The $^{31}P\{^{1}H\}$ NMR spectrum showed sharp singlet signals at about δ -11 ppm as expected for the phosphine ligands **L1a** and **L2a**,[23, 31] and another singlet at around 29 ppm. The signal at 29 ppm was attributed to the oxidized phosphine in **L3** and **L4** consistent with literature findings for related compounds.[32] Further evidence of this oxidation was illustrated by the gradual increase of the signals at δ 29.70 ppm followed by concomitant decrease of the peak at δ -11 ppm (Figure 4.3). The ease of oxidation of **L1a** and **L2a** is consistent with the findings of Rapko *et al.*[31] regarding (phosphinomethyl)pyridine which they could not isolate and purify as a result of being air-sensitive. We can therefore infer that there was some source of oxygen that oxidized our desired products.

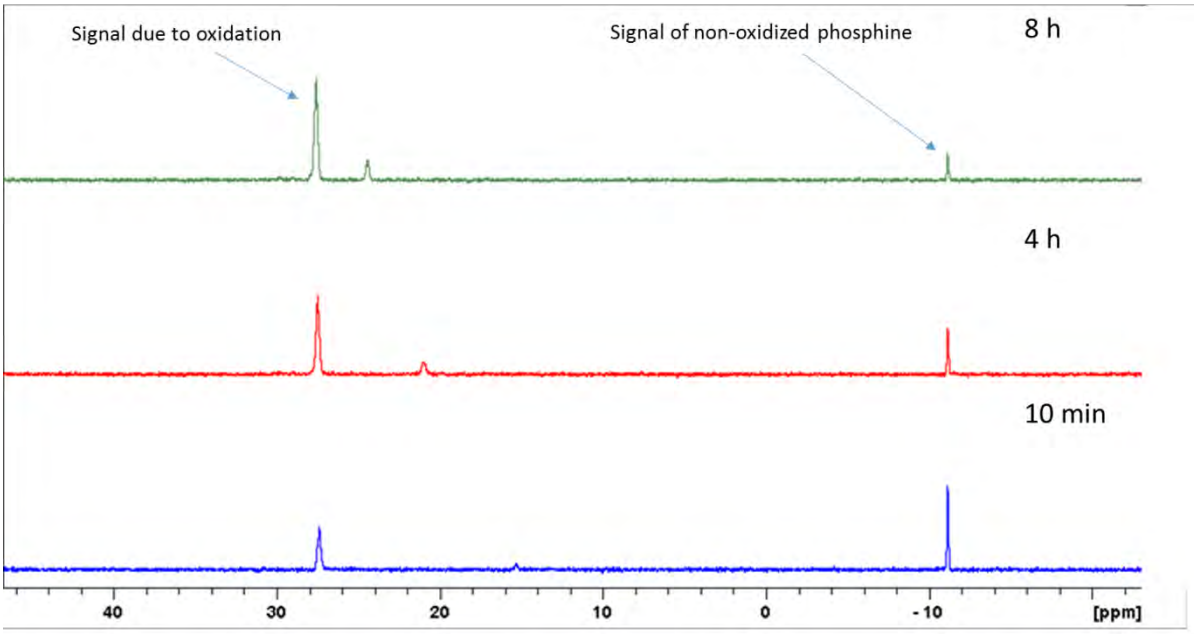

Figure 4.3: $^{31}P\{^{1}H\}$ NMR spectrum showing gradual oxidation of 2-(diphenylphosphinomethyl)-6-(pyrazol-1-ylmethyl)pyridine ligand **L1a**

Elemental analyses, ^{1}H, $^{13}C\{^{1}H\}$ NMR and mass spectral data were in agreement with the proposed structures for **L1a** and **L2a**. The signature peaks of the Cl-CH_2 linker protons at 4.64 ppm and 4.65 ppm of the starting compounds **L1** and **L2**, respectively, were diagnostic in the formation of **L3** and **L4**. On formation of **L3** and **L4**, these CH_2 linker protons shifted upfield and appeared as doublets at 3.92 ppm and 3.91 ppm (Figure 4.4 and 4.5), respectively, due to J_{PH} coupling constants of 16.0 Hz, in both cases, which confirmed the formation of pyrazolylpyridine phosphinoyl compounds **L3** and **L4**.[33] We thus made use of the phosphinoyl ligands to prepare their respective metal complexes towards olefin oligomerization and polymerization catalysts.

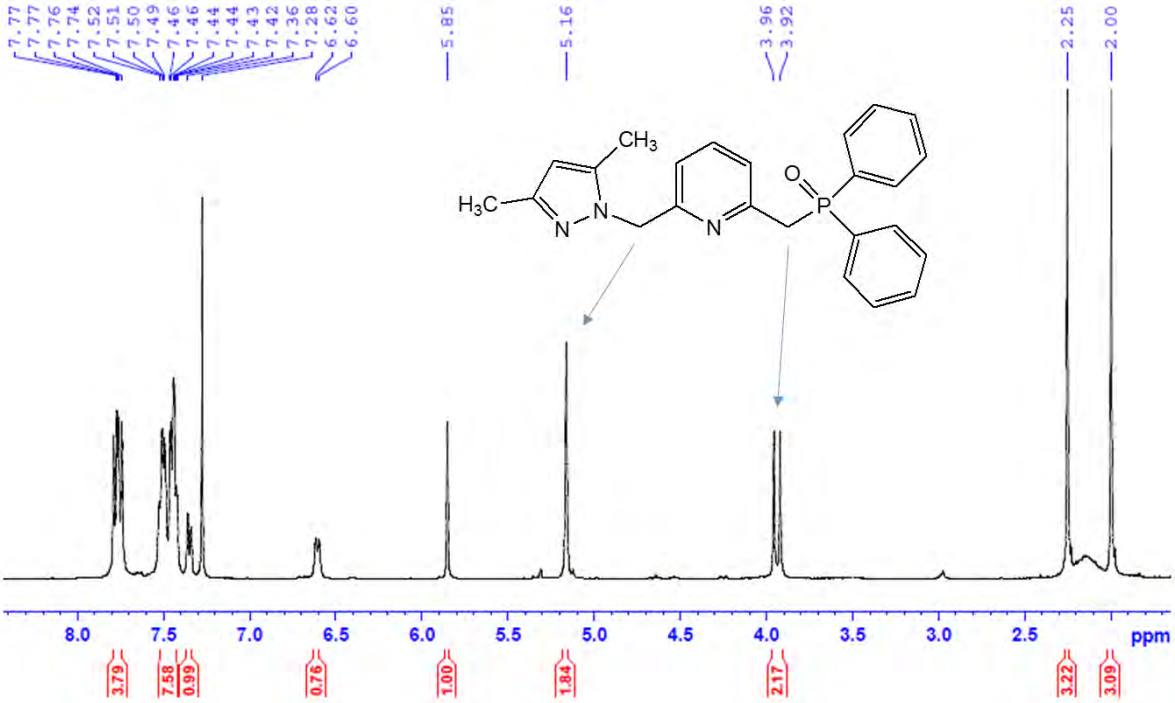

Figure 4.4: ^{1}H NMR spectrum of **L3**

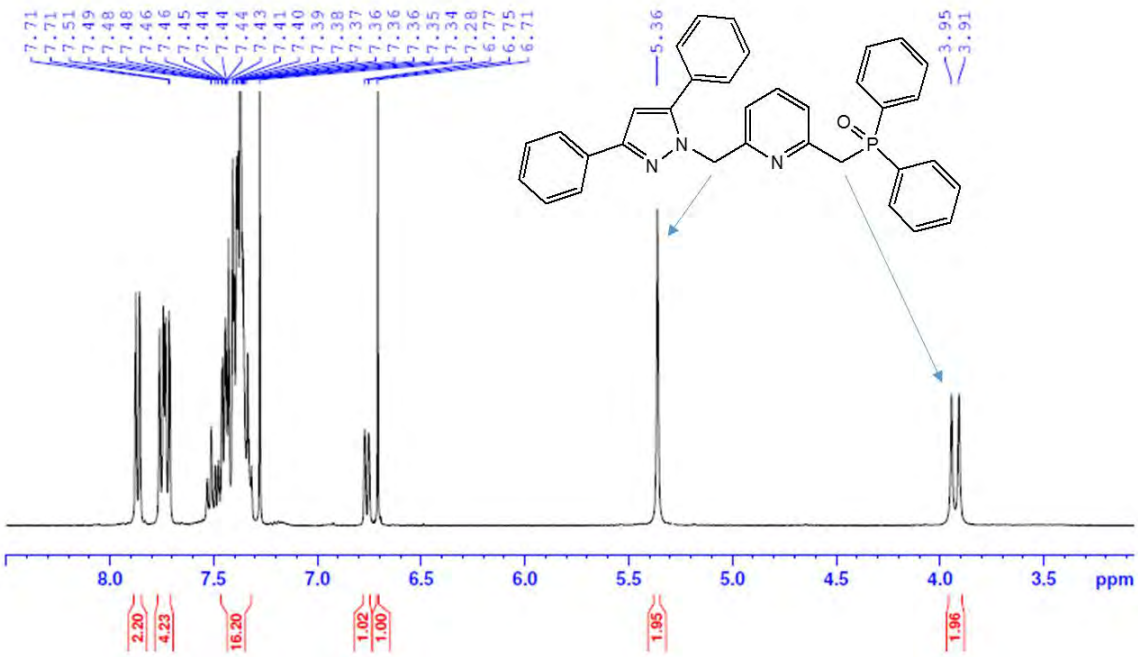

Figure 4.5: ^{1}H NMR spectrum of **L4**

Reactions of **L3** and **L4** with the appropriate metal salts in a 1:1 mole ratio in dichloromethane afforded the corresponding Ni, Fe and Co metal complexes **7-12** in moderate to high yields (Scheme 4.2).

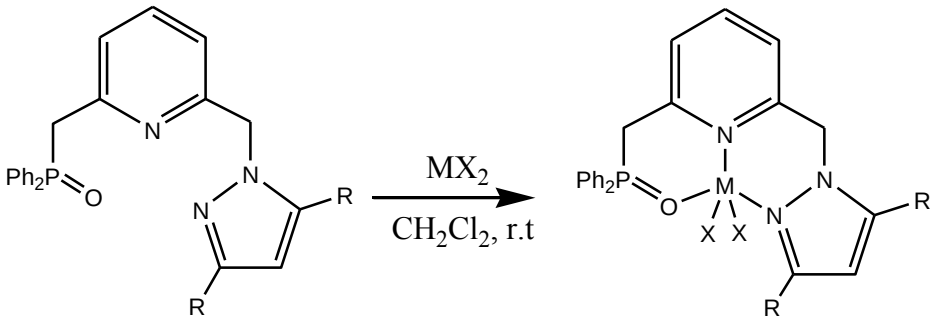

R = Me, M = Ni, X = Cl, (**7**) R = Me, M = Fe, X = Cl, (**10**)
R = Me, M = Ni, X = Br, (**8**) R = Ph, M = Ni, X = Br, (**11**)
R = Me, M = Co, X = Cl, (**9**) R = Ph, M = Co, X = Cl, (**12**)

Scheme 4.2: Synthesis of (pyrazolyl)-(phosphinoyl)pyridine nickel(II), cobalt(II) and iron(II) complexes

Due to the paramagnetic nature of these complexes, NMR spectroscopy was not useful in their structural elucidation. The complexes were therefore characterized by magnetic moment measurements, mass spectroscopy, elemental analyses, and single crystal X-ray crystallography for **7**, **11** and **12**. Mass spectrometry was very helpful in the elucidation of the molecular formulae of the complexes. For example, complex **11** (m/z = 744) showed a base peak at m/z = 664 which was due to fragmentation of one bromide ligand (Figure 4.6). Similar fragmentation pattern was observed for the other complexes; mainly characterized by halide abstraction.

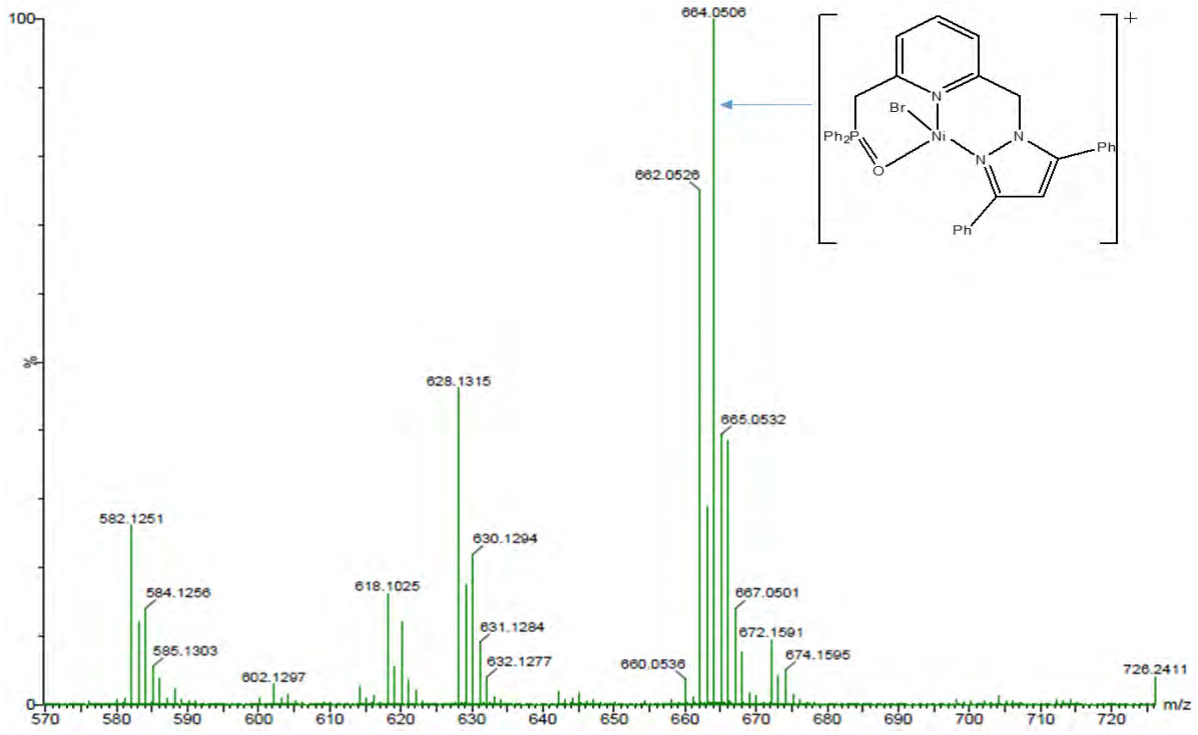

Figure 4.6: Mass spectrum of **11** showing the m/z = 664 (M^+-Br).

The magnetic moments of the nickel(II) complexes **7, 8** and **11** were found as 3.90 BM, 3.23 BM and 3.38 BM, respectively. These values were effectively higher than the expected spin only value of 2.83 BM for nickel(II) complexes, but fall within the expected range for high spin nickel(II) complexes of 2.9-4.2 BM.[34] Similarly, the magnetic moments for the cobalt(II) complexes **9** and **12** were determined to be 4.36 BM and 4.20 BM, respectively, while 5.20 BM was recorded for the iron(II) complex **10**. These values are within the expected range for spin-only values for high spin d^7 (Co^{2+}) and d^6 (Fe^{2+}) cations.[35] The elemental analyses data were consistent with one ligand motif and one metal center for complexes **7-12** and confirmed the purity and the empirical formulae of the complexes.

4.3.2. Molecular structures of complexes 7, 11 and 12

Single crystals, suitable for X-ray analysis for complexes **7**, **11** and **12** were grown from slow diffusion of *n*-hexane into dichloromethane solutions of the respective complexes at 4 °C. Compound **7** crystallized in the orthorhombic space group *Fddd* while **5** and **6** both crystallized in the triclinic space group *P*-1. The solid state structure of **7** is shown in Figure 4.7, while its crystal and structure refinement data are given in Table 4.1.

The asymmetric unit of **7** comprises a half molecule of the chelate, two chloride ions each with site occupancy of a half and a water molecule. The octahedral chelate has crystallographically imposed inversion symmetry with the nickel(II) ion located on an inversion center. Compound **7** displays a nominally octahedral geometry with two tridentate N^N^O ligands coordinated to the metal center. This is contrary to the proposed structure for which there is only one tridentate ligand unit and two chloride ions coordinated to the nickel(II) center. The elemental analysis data and mass spectrometry support the proposed 5-coordinate structure, implying that the solid-state structure is a minor product, formed during crystal growth. The bond parameters for compound **7** are summarized in Table 4.2.

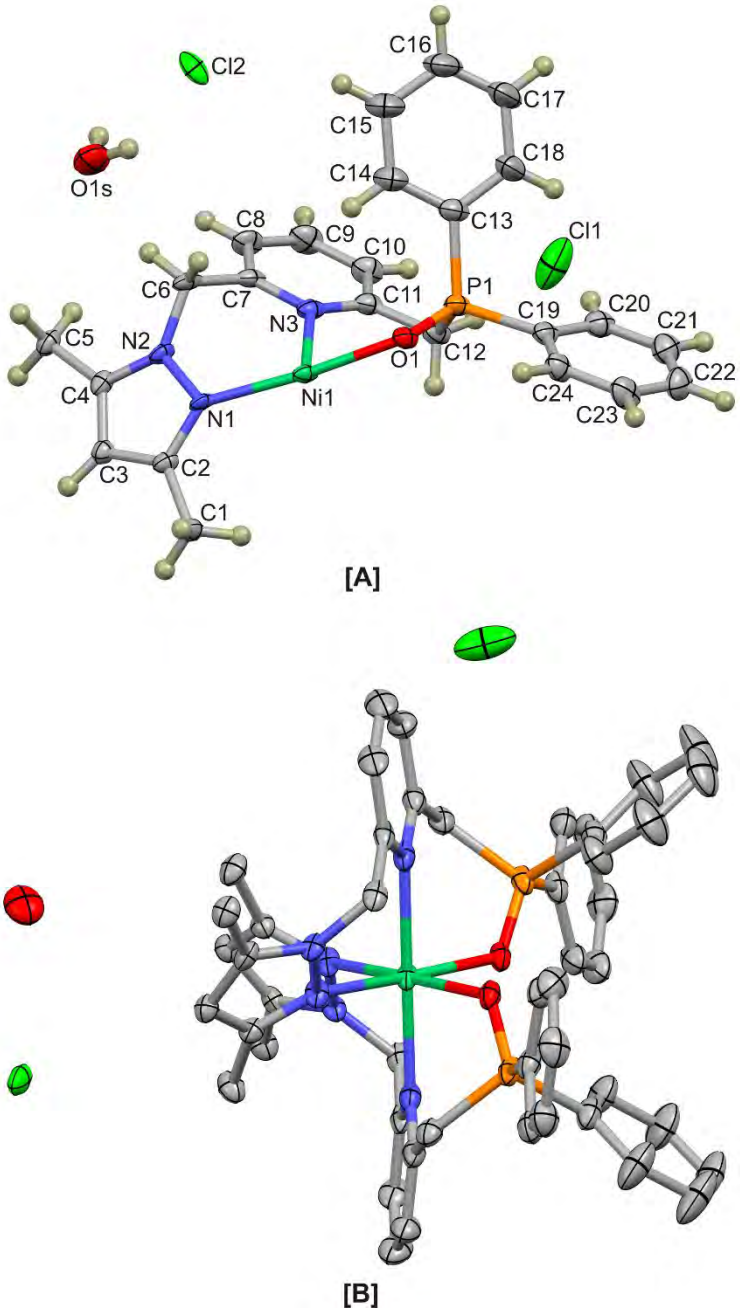

Figure 4.7: [A] Asymmetric unit of complex **7** showing the atom numbering scheme. Displacement ellipsoids are rendered at the 50% probability level; H atoms are depicted as spheres of common, arbitrary radius. The chloride ions each have a site occupancy of 0.5. [B] Displacement ellipsoid plot (50% probability) of the symmetry-completed, octahedral metal chelate. H atoms have been omitted for clarity.

Table 4.1: Crystal data and structure refinement details for complexes **7, 11 and 12.**

Parameter	**7**	**11**	**6**
Empirical formula	$C_{48}H_{48}Cl_3N_6NiO_2P_2 \cdot 2(Cl) \cdot 2(H_2O)$	$C_{34}\ H_{28}Br_2NiN_3OP.\ CH_2Cl_2$	$C_{34}\ H_{28}Cl_2CoN_3OP$
Formula weight	968.49	828.98	655.42
Temperature(K)	100(2)	296	100(2)
Wavelength (Å)	0.71073	0.71073	0.71073
Crystal system	orthorhombic	Triclinic	Triclinic
Space group	*Fddd*	P-1	P-1
a, b, c (Å)	22.159(5), 25.122(5), 37.667(6)	13.8629(14), 17.3500(15), 17.9969(17)	13.4042(15), 13.5617(18), 17.3858(19)
α, β, γ (°)	90, 90, 90	72.248(4), 89.748(5), 89.687(5)	92.215(5), 98.405(4), 102.936(5)
Volume($Å^3$)	20968(7)	4122.5(7)	3038.8(6)
Z	16	2	2
Density (calculated) (Mg/m^3)	1.272	1.336	1.427
Absorption coefficient (mm^{-1})	0.580	2.605	0.825
F(000)	8368.0	1664.0	1342.0
Theta range for data collection(°)	1.30 to 26.00	1.40 to 21.00	1.80 to 21.9
Reflections collected	24912	24539	18117
Completeness to θ (%)	98.5	80.10 (θ= 21.01%)	73.1(θ= 21.85%)
Goodness-of-fit on F^2	1.061	1.134	1.148
R indices (all data)	R_1 = 0.0797, wR_2 = 0.2008	R_1 = 0.1192, wR_2 = 0.2687	R_1 = 0.1328, wR_2 = 0.2193
Largest diff. peak and hole(e $Å^{-3}$)	2.27 and -0.80	2.07 and -0.98	0.94 and -0.74

A Mogul (version 1.6) structural search shows that the bond parameters are all within the range of those previously reported with the exception of the Ni-$N_{pyridine}$ bond. The Ni-$N_{pyridine}$ bond in this work measures 2.194(3) Å which is significantly longer than the mean of 2.062 Å for previously reported structures. This elongation is attributed to the ligand forming two six-membered chelation rings.

Complex **7** exhibits several intermolecular hydrogen bonds as well as intramolecular C–H···O interactions. The intermolecular interactions lead to a one-dimensional hydrogen-bonded supramolecular structure, co-linear with the *a*-axis. The intramolecular interactions are depicted in Figure 4.8 and the supramolecular hydrogen-bonded structure supported by the intermolecular interactions in Figure 4.9. Table 4.3 summarises the hydrogen bonding parameters of complex **7**.

Table 4.2: Selected bond lengths [Å] and angles [º] for complex **7**

Bond lengths [Å]		**Angles [º]**	
Ni1–N1	2.116(3)	N1–Ni1–N3	88.5(1)
Ni1–N3	2.194(3)	$N1^{i}$–Ni1-N3	91.7(1)
Ni1–O1	2.087(2)	N3–Ni–O1	88.9(1)
		N3–Ni1–$O1^{i}$	90.9(1)
		N1–Ni1–$O1^{i}$	94.1(1)
		N1–Ni1–$N1^{i}$	89.4(2)
		O1–Ni–$O1^{i}$	82.5(2)
		N3–Ni1–$N3^{i}$	179.7(2)

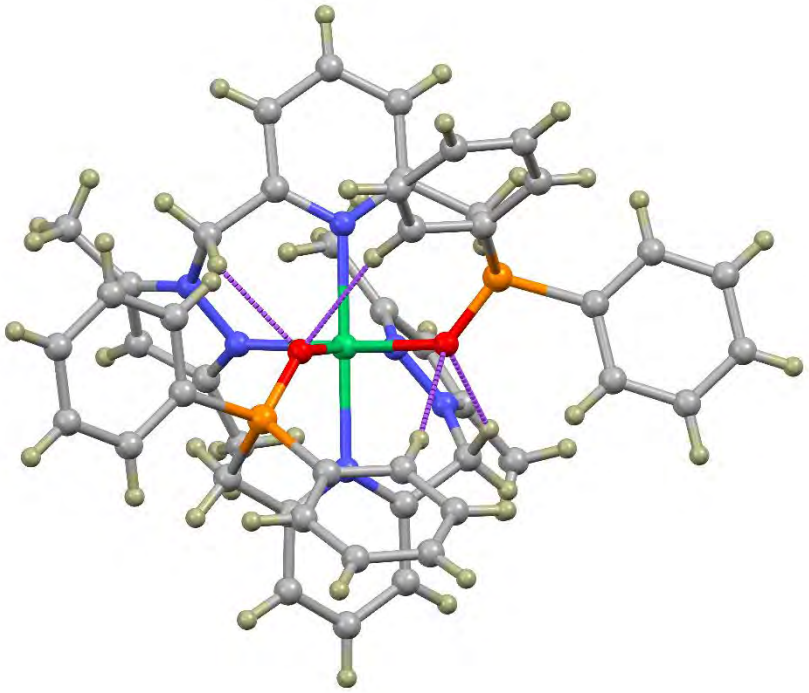

Figure 4.8: Intramolecular C–H···O interactions of complex **7**. The interaction distances are significantly shorter than the sum of the Van der Waals radii (refer to Table 4.3) of the interacting atoms; however, this gives little indication of the strength of the interaction as the bond lengths are largely determined by the geometry of the structure.

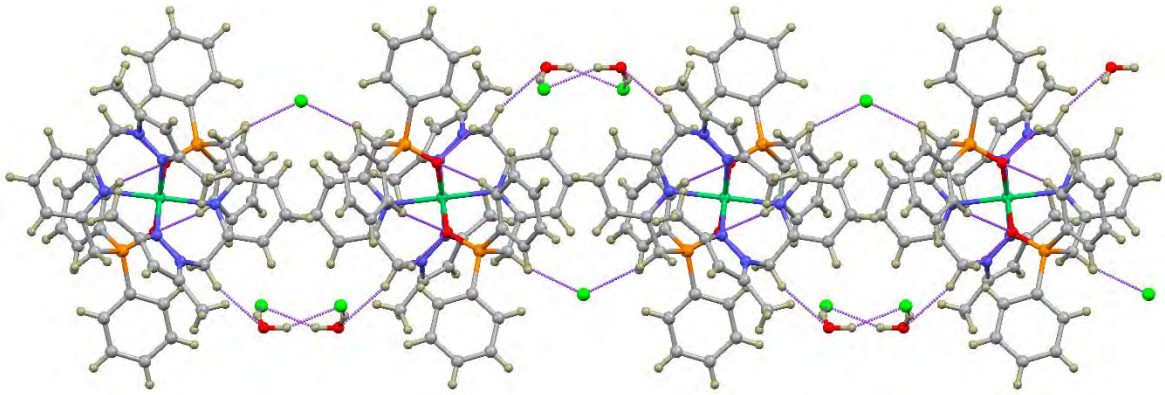

Figure 4.9: Supramolecular hydrogen-bonded structure of complex **7** viewed down the *c*-axis. The one-dimensional network runs co-linear with the *a*-axis. The network is supported by hydrogen bonds between the water solvate and chloride anions as well as weak C–H···O interactions between the water molecule and methylene hydrogen atoms.

Table 4.3: Intra and Intermolecular interaction parameters

Bond	D–H (Å)	H···A (Å)	D···A (Å)	D–H···A
Intramolecular				
C14–H14···O1	0.949	2.311	3.241(5)	166.5
C6–H6A···O1	0.989	2.225	3.012(4)	135.6
Intermolecular				
C6–H6B···O1S	0.991	2.452	3.399(5)	159.9
C12–H12A···Cl1	0.990	2.513	3.489(5)	168.5
O1S–H1S···Cl2	0.91(2)	2.28(5)	3.143(4)	158(8)
O1S–H2S···Cl2	0.90(5)	2.21(5)	3.014(4)	149(5)

The crystals of compounds **11** and **12** diffracted weakly and hence only low resolution structures could be elucidated (Figures 4.10 and 4.11). These low resolution structures illustrate the trigonal bipyramidal coordination geometry of the nickel(II) and cobalt(II) chelates.

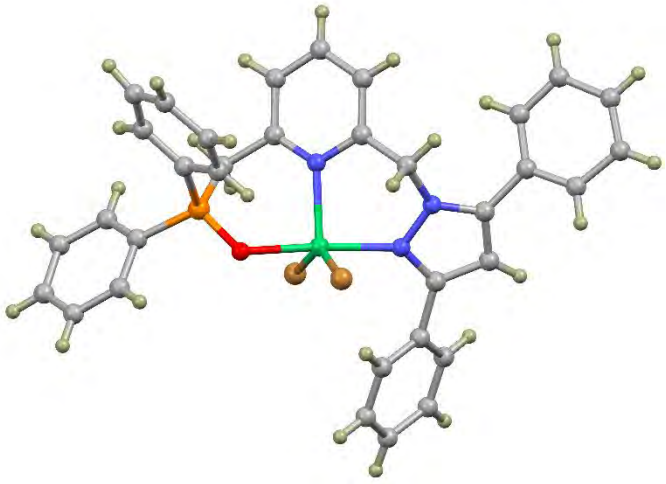

Figure 4.10: Low-resolution X-ray structure of compound **11**, illustrating the distorted trigonal bipyramidal coordination sphere of the nickel(II) ion. All atoms have been rendered as spheres of arbitrary radius.

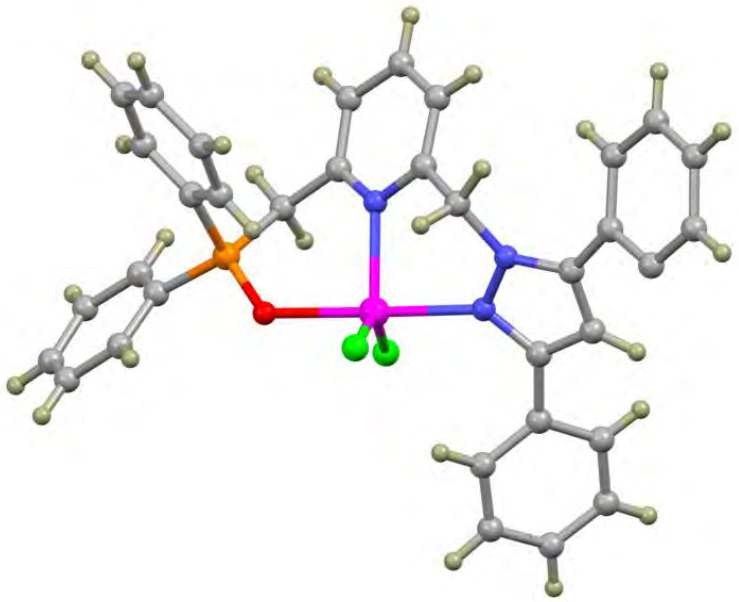

Figure 4.11: Low-resolution X-ray structure of compound **12**, illustrating the distorted trigonal bipyramidal coordination sphere of the cobalt(II) ion. All atoms have been rendered as spheres of arbitrary radius.

The low resolution X-ray structure of compound **11** (Figure 4.10) shows that the nickel(II) ion adopted a distorted trigonal bipyramidal coordination geometry. Two bromide ligands and the pyridine nitrogen atom of the tridentate N^N^O ligand occupy the equatorial positions. The pyrazole nitrogen atom and oxygen atom occupy the axial coordination sites. The molecular structure of **12** (Figure 4.11) displays a similar distorted trigonal bipyramidal geometry to that of compound **11** around the cobalt(II) ion with the tridentate N^N^O ligand and two chloride ligands forming the coordination sphere. The two chloride ligands and pyridine nitrogen atom occupy the equatorial plane; the pyrazole nitrogen atom and oxygen atom occupy the axial positions. This is the expected coordination geometry of the metal chelates, and is in agreement with the elemental analysis data.

4.3.3. Evaluation of complexes 7-12 as catalysts in ethylene oligomerization reactions

The catalytic activities of complexes **7-12** were evaluated in ethylene oligomerization using ethylaluminium dichloride ($EtAlCl_2$), methyl aluminoxane (MAO) or trimethylaluminium ($AlMe_3$) as co-catalysts in three different solvents; hexane, chlorobenzene and toluene. In all cases, the complexes showed appreciable catalytic activities of up to 540 kg oligomer.mol.$^{-1}$catalyst.h^{-1}. FID-GC and GC-MS analyses confirmed that the products were mainly of C_4 (butenes) oligomers. A notable observation was the dependence of catalytic activity, product distribution and selectivity on the nature of co-catalyst and solvent used. In the subsequent sections, we present detailed analyses of the products and discussion of our findings.

*4.3.3.1. Ethylene oligomerization reactions catalyzed by **7-12** using $EtAlCl_2$ as a co-catalyst*

We first investigated ethylene oligomerization reactions, catalyzed by complexes **7-12**, using $EtAlCl_2$ as a co-catalyst in hexane solvent. Table 4.4 shows a summary of the data obtained for pre-catalysts **7-12**. Initial studies carried out at 30 °C, 10 bar of ethylene using $EtAlCl_2$-to-precatalyst ratio of 250 indicated that these catalytic systems were quite active in ethylene oligomerization reactions to afford C_4 oligomer as the major product. It is evident from Table 4.4 that all the catalysts were highly selective resulting in the formation of predominantly C_4 (butene) and a small amounts of C_6 (hexene) oligomers. The identities of these oligomerization products were established by a combination of GC, ^{1}H NMR spectroscopy and GC-MS. For example, a typical ^{1}H NMR spectrum of the products obtained from catalyst **8** (Table 4.4, entry 2) showed peaks at around 5.4 ppm; characteristic peaks attributed to olefinic protons. Further analyses of the products by GC-MS confirmed the ethylene oligomerization products as C_4 and C_6 oligomers (Figures 4.12 and 4.13).

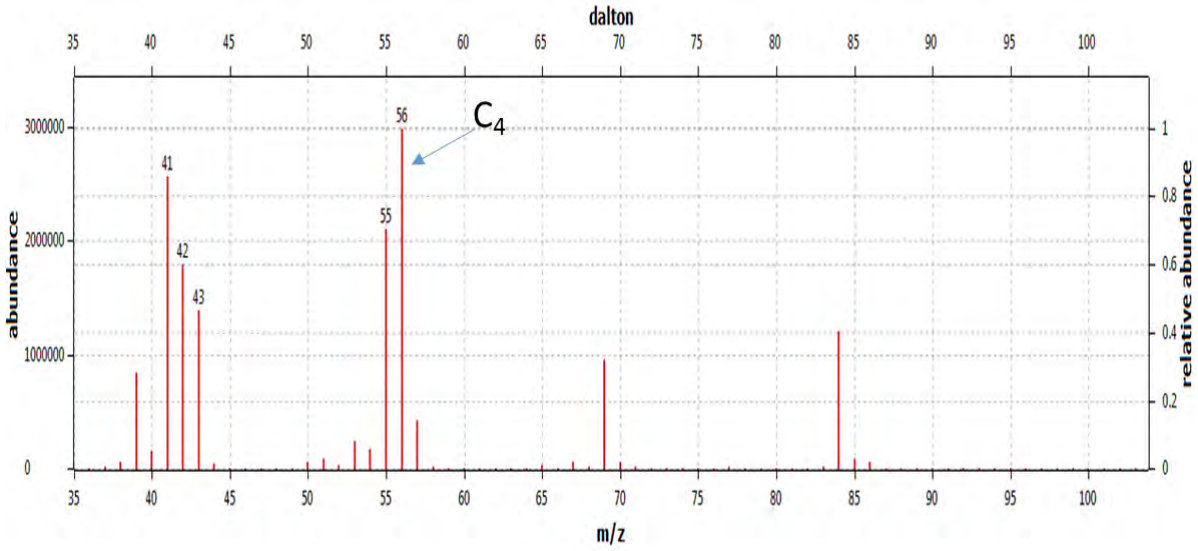

Figure 4.12: GC-mass spectrum of the product obtained from catalyst **7**, EtAlCl2:Ni ratio of 250:1, temperature = 30 °C, pressure = 10 bar, time = 1 h, solvent = hexane. M+= 56 corresponds to the molecular ion mass of the C4 oligomer.

Besides the predominance of the C_4 fraction compared to C_6 in the products, catalysts **7-12** also exhibited relatively higher selectivity for 1-butene (37-92%) compared to 1-hexene (5-19%). This therefore implies that isomerization of 1-hexene was favored compared to 1-butene. Ethylene oligomerization reactions resulting in the formation of lower oligomers, C_4 and C_6, have been previously reported.[36-39]

Table 4.4: Ethylene oligomerization studies with **7-12** in using $EtAlCl_2$ as co-catalyst in hexane.[a]

Entry	Catalyst	Pressure (bar)	Time (h)	T_{min}/T_{max} (°C)[b]	Al:M	Yield[c] (g)	Activity[d]	Product distribution and selectivity (%)[e]			
								C_4	**C_6**	**α-C_4**	**α-C_6**
1	**7**	10	1	30/34	250	3.07	310	97	3	63	17
2	**8**	10	1	30/34	250	3.64	360	94	6	65	8
3	**9**	10	1	30/32	250	1.98	200	93	7	37	12
4	**10**	10	1	30/32	250	1.07	110	94	6	60	6
5	**11**	10	1	30/34	250	2.73	270	98	2	79	11
6	**12**	10	1	30/33	250	1.59	160	99	1	52	12
7	**8**	20	1	30/34	250	3.92	390	96	4	74	16
8	**8**	30	1	30/34	250	4.31	430	95	5	77	19
9	**8**	10	0.25	30/33	250	1.14	460	91	9	72	15
10	**8**	10	0.5	30/34	250	2.35	470	94	6	67	11
11	**8**	10	2	30/33	250	3.88	190	97	3	61	5
12	**8**	10	1	30/33	100	2.02	200	98	2	92	9
13	**8**	10	1	30/34	200	2.78	280	96	4	71	14
14	**8**	10	1	30/38	350	2.77	280	96	4	65	13
[f]15	**8**	10	1	30/34	250	2.67	270	94	6	92	12

[a] Reaction conditions: nM = 10 μmol; solvent, toluene, 80 mL; temperature, 30 °C. [b]Initial temp was 30 °C, T_{min} and T_{max} = lowest and highest temperatures attained during the reaction period. [c]Determined by mass difference of 80 mL hexane (52.72 g) and mass of final solution. [d]Activity, kg oligomer.mol.$^{-1}$catalyst.h^{-1}. [e]Determined by GC. [f]Temperature, 50 °C.

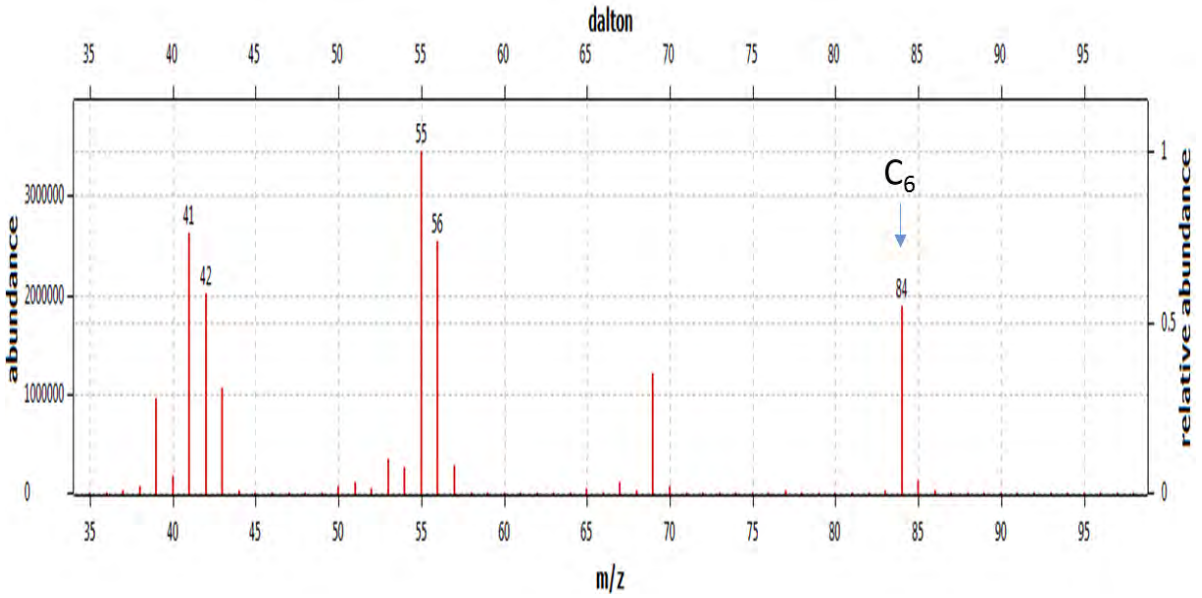

Figure 4.13: GC-mass spectrum of the product obtained from catalyst **7**, EtAlCl2:Ni ratio of 250:1, temperature = 30 °C, pressure = 10 bar, time = 1 h, solvent = hexane. M+= 84 corresponds to the molecular ion mass of the C6 oligomer.

4.3.3.2. Effect of solvent on product distribution and activity

Considering the role of solvents in determining the catalytic activity and product distribution in ethylene oligomerization reactions, the catalytic behaviour of complexes **7-12** was further investigated using chlorobenzene solvent. The oligomerization reactions in chlorobenzene solvent produced more exothermic reactions compared to the same reactions in hexane but with effective internal cooling, the reaction temperatures stabilized at 30 °C within 5-10 min (Table 4.5). This could be attributed to improved solubility of the pre-catalysts in chlorobenzene leading to higher catalytic activity.[40] The selectivity towards the formation of butene in chlorobenzene solvent reduced with enhanced formation of hexene compared to reactions in hexane. For example, in hexane solvent, the C_4 fraction was between 93-99% (Table 4.4, entries 1-6) compared to 83-87% in chlorobenzene (Table 4.5, entries 1-6). Consequently, the hexene

fraction increased from between 1-7% to 13-17% in hexane and chlorobenzene solvents, respectively.

The effect of the nature of solvent on catalytic activity in ethylene oligomerization reactions is apparent from Tables 4.4 and 4.5. For example, catalytic activities of complex **7** of 310 kg oligomer.mol.$^{-1}$catalyst.h^{-1} and 470 kg oligomer.mol.$^{-1}$catalyst.h^{-1} were reported in hexane and chlorobenzene, respectively.

Table 4.5: Ethylene oligomerization studies with **7-12** in using $EtAlCl_2$ as co-catalyst in chlorobenzene.[a]

Entry	Catalysts	T_{min}/T_{max} (°C)[b]	Yield[c] (g)	Activity[d]	Product distribution and selectivity (%)[e]			
					C_4	**C_6**	**α-C_4**	**α-C_6**
1	**7**	30/37	4.72	470	83	17	57	19
2	**8**	30/42	5.01	500	87	13	62	21
3	**9**	30/35	2.97	300	83	17	47	15
4	**10**	30/36	2.59	260	84	16	52	15
5	**11**	30/39	3.88	390	86	14	65	24
6	**12**	30/36	2.83	280	84	16	51	17

[a]Reaction conditions: nM = 10 µmol; time, 1h; pressure, 10 bar; temperature, 30 °C. Al:M ratio of 250:1; [b]initial temp was 30 °C, T_{min} and T_{max} = lowest and highest temperatures attained during the reaction period. [c]Determined by mass difference of 80 mL chlorobenzene (88.8 g) and mass of final solution. [d]Activity, kg oligomer.mol.$^{-1}$catalyst.h^{-1}. [e]Determined by GC.

This enhanced catalytic activity in chlorobenzene could be attributed to improved solubility of the pre-catalysts in chlorobenzene compared to in hexane, which is a less polar solvent. These results are consistent with improved catalytic activities in chlorobenzene for nickel(II)-catalyzed oligomerization of ethylene reported by Obuah *et al*.[40] In another related study, low catalytic activities in ethylene oligomerization reactions were reported for nickel metallodendritic catalysts in hexane solvent.[41] Similarly, ethylene oligomerization studies conducted in heptane catalyzed by nickel(II) complexes bearing N-((1-methyl-1H-imidazol-2-yl)methylene)-2-(methylthio)ethanamine resulted in the formation of mainly C_4 (79%) and hexene (21%) albeit with lower catalytic activity (1.63×10^6 $g_{C2H4}.mol.^{-1}Ni.h^{-1}$) compared to the same reaction conducted in toluene solvent (3.14×10^6 $g_{C2H4}.mol.^{-1}Ni.h^{-1}$).[19]

4.3.3.3. Effect of co-catalyst on catalytic activity and product distribution

Complexes **8-11** were activated by MAO, $AlMe_3$ or $EtAlCl_2$ in toluene solvent in order to probe the effect of changing the co-catalyst on these ethylene oligomerization reactions. Table 4.6 shows a summary of the ethylene oligomerization data obtained. From the results, it was clear that the type of aluminium co-catalysts had a significant effect on the catalytic activities of the pre-catalysts and product distribution. The nickel(II) complexes **8** and **11** showed moderate activities of up to 540 kg oligomer.mol.$^{-1}$catalyst.h^{-1} (Table 4.6, entry 1) while **9** and **10** exhibited low activity and the major oligomerization product was C_4 alkenes.

When activated with MAO, all the complexes oligomerized ethylene to afford C_4, C_6 and C_8 oligomers (Figure 4.14). A notable observation was the formation of the C_8 oligomer fractions in addition to the C_4 and C_4 fractions when MAO and toluene solvents were used. This contrasts

the formation of only C_4 and C_6 oligomers obtained using hexane solvent and $EtAlCl_2$ as a co-catalyst. The influence of the nature of co-catalyst on catalytic activity and product distribution is consistent with the observations made for cobalt(II) complex bearing N-(1-(6-(quinoxalin-2-yl)pyridine-2-yl)benzylamine ligand.[42] When this cobalt(II) complex was activated by Et_2AlCl, MMAO and MAO, the Et_2AlCl activated system produced exclusively C_4, while activation by MMAO and MAO generated more active catalysts that formed C_4, C_6, and traces of $C_{\geq 8}$.

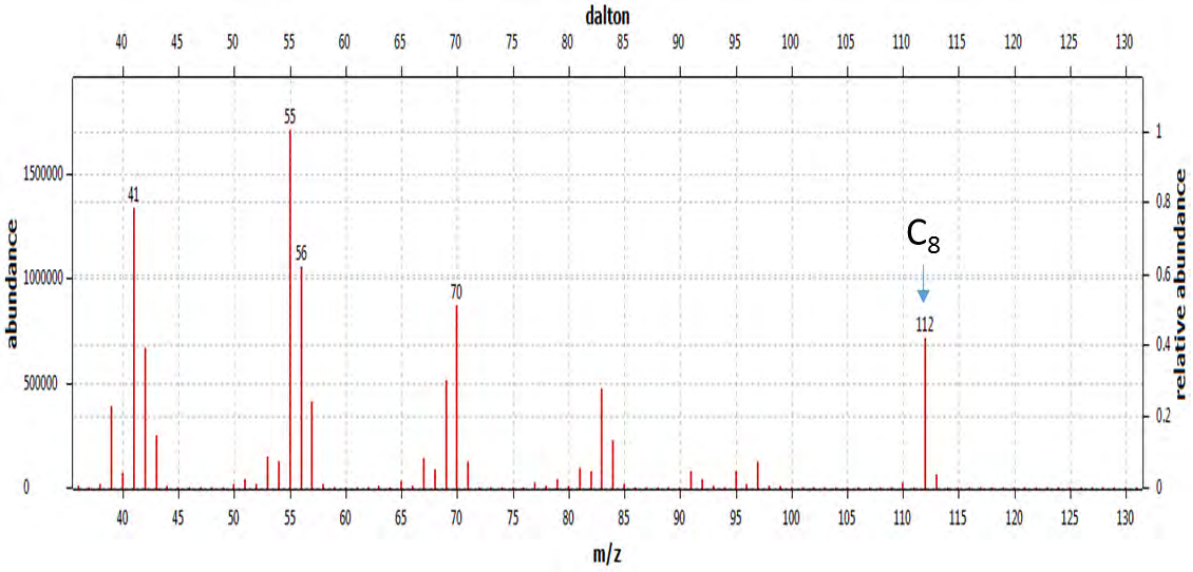

Figure 4.14: GC-mass spectrum of the product obtained from catalyst **8**, MAO:Ni ratio of 1 000:1, temperature = 30 °C, pressure = 10 bar, time = 1 h, solvent = toluene. M+= 112 corresponds to the molecular ion mass of the C8 oligomer.

Consistent with our recent studies,[15] attempts to activate the pre-catalysts using $EtAlCl_2$ in toluene solvent produced predominantly alkylated-toluenes of the pre-formed oligomers (Table 4.6, entry 5). Nonetheless, the $EtAlCl_2$ activated system in toluene generated the most active catalyst displaying activities of 790 kg oligomer.mol.$^{-1}$catalyst.h^{-1}.

Table 4.6: Ethylene oligomerization data for **8-11** in toluene using MAO, $EtAlCl_2$ or $AlMe_3$ as co-catalysts.[a]

Entry	Catalyst	Co-cat.	Al:M	T_{min}/T_{max} (°C)[b]	Yield[c] (g)	Activity[d]	Product distribution and selectivity (%)[f]					
							C_4	**C_6**	**C_8**	**α-C_4**	**α-C_6**	**α-C_8**
1	**8**	MAO	1 000	30/35	5.43	540	71	15	14	33	54	42
2	**9**	MAO	1 000	30/34	2.27	230	83	14	3	93	21	33
3	**10**	MAO	1 000	30/33	1.33	130	81	16	3	95	17	23
4	**11**	MAO	1 000	30/35	4.23	420	72	16	12	31	60	52
5	**8**[e]	$EtAlCl_2$	250	30/39	7.87	790	15	7	-	27	38	-
6	**8**	$AlMe_3$	250	30/39	1.17	120	100	-	-	88	-	-
7	**11**	$AlMe_3$	250	30/37	1.02	100	100	-	-	79	-	-

[a]Reaction conditions: nM = 10 μmol; solvent, toluene, 80 mL; pressure, 10 bar; time, 1 h; temperature, 30 °C. [b]Initial temp was 30 °C, T_{min} and T_{max} = lowest and highest temperatures attained during the reaction period. [c]Determined by mass difference of 80 mL toluene (69.60 g) and mass of final solution. [d]Activity, kg oligomer.mol.$^{-1}$catalyst.h^{-1}. [e]Alkyl toluene products observed (78%) indicating Friedel-Crafts alkylation of toluene solvent. [f]Determined by GC.

It is noteworthy to point out that while using $EtAlCl_2$ as a co-catalyst exhibited higher activity, the MAO activated system was highly selective for C_4 oligomers. Activation of the nickel(II) complexes **8** and **11** with a less Lewis acidic $AlMe_3$ generated very selective catalysts, producing exclusively C_4 oligomers (Table 4.6, entries 6 and 7) albeit with marginal activity. From these accounts, it is therefore conceivable that use of $EtAlCl_2$, MAO and $AlMe_3$ results in the generation of different active species

The significant role played by the nature of co-catalyst is further demonstrated by a report by Igarashi *et al*.[43] where (adamantylimido)vanadium(V) complexes containing (2-anilidomethyl)pyridine ligands produce mainly C_4 and small amounts of C_6 on activating using MAO as co-catalyst while the same complexes produce exclusively polyethylene when activated by Et_2AlCl. In another related work, Carlini *et al*.[44] showed that bis[(N-2,6-diisopropylphenyl)salicylaldiminate]nickel(II) complex forms exclusively octenes and butenes using $^{i}Bu_3Al$ and triethyl aluminium (Et_3Al) as co-catalysts, respectively.

4.3.3.4. Influence of catalyst structure on ethylene oligomerization reactions

The influence of catalyst structure on catalyst behaviour was also studied. From all the catalytic reactions investigated, we observed a significant influence of catalyst structure on both the catalytic activity and product distributions. It was apparent that nickel(II) complexes **7**, **8** and **11** displayed higher catalytic activities compared to the cobalt(II) (**9** and **12**) and iron(II) (**10**) analogues (Tables 4.4, 4.5 and 4.6). For example, in the $EtAlCl_2$ activation in hexane, the cobalt(II) and iron(II) complexes **9** and **10** exhibited lower activities of 200 kg oligomer.mol.$^{-1}$catalyst.h^{-1} and 110 kg oligomer.mol.$^{-1}$catalyst.h^{-1}, respectively, compared to the activity of 360

kg oligomer.mol.$^{-1}$catalyst.h^{-1} displayed by their nickel(II) analogue, complex **8**. A similar trend has also been reported for nickel(II), cobalt(II) and iron(II) complexes of 2-(2-pyridyl)quinoxaline in ethylene oligomerization reactions[45] and was attributed to electronic factors.[46] However, on comparing the catalytic performance of the cobalt(II) complex **9** and its iron(II) analogue **10**, the cobaltous catalyst **9** exhibited higher ethylene oligomerization activity than its ferrous counterpart **10**. Sun *et al.*[47] have also reported a similar trend in their investigations on ethylene oligomerization and polymerization reactions of ferrous and cobaltous 2-(ethylcarboxylato)-6-iminopyridyl complexes.

The impact of the nature of metal center in influencing product distribution was demonstrated by the high selectivity for 1-butene by cobalt(II) (93%) and iron(II) (95%) complexes **9** and **10**, respectively (Table 4.6), compared to selectivity of 33% for the nickel(II) complex **8**. This observation is in tandem with a report by Jie *et al.*[48] when studying iron(II), cobalt(II) and nickel(II) complexes bearing 2-arylimino-9-phenyl-1,10-phenanthroline ligands. Moreover, the predominant formation of linear α-olefins by cobalt(II) and iron(II) complexes has been reported earlier.[48]

We also noted that by varying the alkyl substituent on the pyrazolyl ring from methyl group to the bulkier phenyl group led to noticeable decrease in catalytic activities in all the catalytic systems. For example, replacing the methyl group in **8** with a phenyl group in **11** resulted in decreased activity from 540 kg oligomer.mol.$^{-1}$catalyst.h^{-1} to 420 kg oligomer.mol.$^{-1}$catalyst.h^{-1}, respectively, when using MAO as a co-catalyst (Table 4.6, entries 1 and 4). A similar observation has been reported for nickel(II) complexes for ethylene oligomerization based on

tridentate pyrazolyl ligands[49] and this may be attributed to bulkier ligands hindering coordination of ethylene to the active metal center.[50] From the results contained in Table 4.6, it is evident that there was no significant difference in the selectivity for 1-butene by **8** and **11**, suggesting that the introduction of steric hindrance on the pyrazolyl group by the bulkier phenyl substituent had little influence on product distribution. This concurs with recent observations for related nickel(II) complexes bearing pyrazolyl ligands.[50, 51]

The nature of the coordinated halide (X = Cl or Br) had a small influence on ethylene oligomerization based on complexes **7** and **8**. The nickel(II) bromide **8** showed slightly higher catalytic activity compared to its corresponding chloride analogue **7** (Table 4.4, entries 1 and 2), which may be attributed to better solubility of the bromide complex in both hexane and chlorobenzene compared to the chloride complex. The greater catalytic performance of the dibromide catalysts compared to their dichloride analogues is consistent with results obtained using 2-quinoxalinyl-6-iminopyridine,[36] 2-(benzimidazol-2-yl)-1, 10-phenanthroline[39] and pyrazolylimino-phosphorane[52] nickel(II) complexes.

Incorporation of the P=O donor group on the (pyrazolylmethyl)pyridine ligand framework changed the catalytic activities of these complexes in comparison to the 2-(chloromethyl)-6-((pyrazol-1-yl)methyl)pyridine and (pyrazolylmethyl)pyridine systems we recently reported.[15, 16] The current (pyrazolyl)-(phosphinoyl)pyridine complexes exhibited lower catalytic activities compared to the previous catalysts. This may be largely attributed to the sterically demanding bulky phenyl groups that could hinder accessibility of the ethylene monomer to the active metal

center. Despite the low catalytic activities of complexes **7-12**, they displayed considerable selectivity towards the C_4 oligomers of up to 99%.

4.3.3.5. Effect of reaction conditions on ethylene oligomerization reactions

Our study was extended to investigate the influence of reaction parameters such as Al/M ratio, time of the reaction and pressure on the catalytic behavior of complexes **7-12** using complex **8**. First, we varied the Al/Ni from 100:1 to 350:1 using $EtAlCl_2$ co-catalyst (Table 4.4, entries 2 and 12-14). The catalytic activity increased to a maximum of 360 kg oligomer.mol.$^{-1}$catalyst.h^{-1} at Al/M ratio of 250:1. Further increase in Al/Ni ratio to 350 was followed by a drop in the activity to 280 kg oligomer.mol.$^{-1}$catalyst.h^{-1}. This behavior has been largely associated with possible deactivation at higher $EtAlCl_2$ concentrations arising from higher amounts of impurities and ash/alumina content. Variation of Al/M ratio also had an effect on α-C_4 selectivity. Increasing the Al/M ratio from 100 to 350 resulted in a gradual decrease in α-C_4 selectivity from 92 to 65%, respectively.

The catalytic behaviour of **8** was monitored against time by varying reaction time from 0.25 h to 2 h (Table 4.4, entries 2 and 9-11). The results reveal that the catalysts remain active up to 0.5 h after which their productivity decreases gradually. Thus, the oligomerization activity increased from 0.25 h (460 kg oligomer.mol.$^{-1}$catalyst.h^{-1}) to 0.5 h (470 kg oligomer.mol.$^{-1}$catalyst.h^{-1}) and decreased substantially with prolonged reaction time up to 2 h (190 kg oligomer.mol.$^{-1}$catalyst.h^{-1}). This feature may be attributed to catalyst deactivation with time. We also observed that with increase in reaction time, selectivity towards C_4 fraction also increased. However, this was accompanied by a decrease in α-C_4 selectivity which may be attributed to increase in isomerization of the α-C_4 to form internal olefins.[39]

The effect of ethylene pressure on the catalytic activity of complex **8** was examined at different ethylene pressures at Al/M ratio of 250:1. As expected, increasing ethylene pressure from 10 bar to 30 bar (Table 4.6, entries 2, 7 and 8) resulted in an increase in activity from 360 kg oligomer.mol.$^{-1}$catalyst.h^{-1} to 430 kg oligomer.mol.$^{-1}$catalyst.h^{-1}, respectively.[15] In addition, the selectivity for α-C_4 also increased from 65 to 77%. Increased selectivity for α-C_4 with increase in ethylene concentration could be due to increased rate of dimerization, thus limiting parallel isomerization of 1-butene into 2-butenes.[53] We also observed that elevating the reaction temperature to 50 °C from 30 °C (Table 4.6, entry 15) resulted in reduction in catalytic activity which may result from thermal decomposition of the catalyst at high temperatures.[51]

4.4. Conclusions

Attempts to synthesize 2-(diphenylphosphinomethyl)-6-(pyrazol-1-ylmethyl)pyridine ligands resulted in the isolation of the oxidized-phosphine based compounds. A series of new nickel(II), iron(II) and cobalt(II) complexes bearing (pyrazolyl)-(phosphinoyl)pyridine ligands have been synthesized and structurally characterized. Solid state structure determination confirmed that the phosphinite ligands adopt an N^N^O tridentate coordination mode to the metal atoms. Activation of these complexes with $EtAlCl_2$, MAO or $AlMe_3$ resulted in the formation of active catalysts to afford 1-butene as the major product. Both the catalytic activity and product selectivity were largely dependent on the nature of the alkylaluminium co-catalyst, nature of solvent and complex structure. While the catalytic activities of these systems are minimal, their superiority lie in their high selectivity, a key component of catalyst design thus further demonstrating the difficulty in balancing catalyst activity and selectivity.

4.5. References

1. Chen, L.; Hou, J.; Sun, W.-H., *Appl. Catal. A: Gen.* **2003**, *246*, 11-16.
2. Vogt, D., Oligomerization of Ethylene to Higher Linear a-Olefins. In *Applied Homogeneous Catalysis with Organometallic Compounds*, Herrmann, B. C. a. W. A., Ed. Wiley-VCH: New York, 1996; Vol. 2, pp 240-252.
3. Keim, W., *Angew. Chem. Int. Ed.* **2013**, *52*, 12492-12496.
4. Keim, W.; Kowaldt, F. H.; Goddard, R.; Krüger, C., *Angew. Chem. Int. Ed. Engl.* **1978**, *17*, 466-467.
5. Ainooson, M. K.; Ojwach, S. O.; Guzei, I. A.; Spencer, L. C.; Darkwa, J., *J. Organomet. Chem.* **2011**, *696*, 1528-1535.
6. Boudier, A.; Breuil, P.-A. R.; Magna, L.; Olivier-Bourbigou, H.; Braunstein, P., *Chem. Commun.* **2014**, *50*, 1398-1407.
7. Budhai, A.; Omondi, B.; Ojwach, S. O.; Obuah, C.; Osei-Twum, E. Y.; Darkwa, J., *Catal. Sci. Technol.* **2013**, *3*, 3130-3135.
8. Gao, R.; Sun, W.-H.; Redshaw, C., *Catal. Sci. Technol.* **2013**, *3*, 1172-1179.
9. Wang, S.; Sun, W.-H.; Redshaw, C., *J. Organomet. Chem.* **2014**, *751*, 717-741.
10. Finiels, A.; Fajula, F.; Hulea, V., *Catal. Sci. Technol.* **2014**, *4*, 2412-2426.
11. Henrici-Olivé, G.; Olivé, S., *Angew. Chem. Int. Ed. Engl.* **1971**, *10*, 105-115.
12. Redshaw, C.; Tang, Y., *Chem. Soc. Rev.* **2012**, *41*, 4484-4510.
13. He, L. P.; Liu, J. Y.; Pan, L.; Li, Y. S., *J. Polym. Sci., Part A: Polym. Chem.* **2008**, *46*, 7062-7073.
14. He, L. P.; Mu, H. L.; Li, B. X.; Li, Y. S., *J. Polym. Sci., Part A: Polym. Chem.* **2010**, *48*, 311-319.

15. Nyamato, G. S.; Ojwach, S. O.; Akerman, M. P., *J. Mol. Catal. A: Chem.* **2014**, *394*, 274-282.

16. Ojwach, S. O.; Guzei, I. A.; Benade, L. L.; Mapolie, S. F.; Darkwa, J., *Organometallics* **2009**, *28*, 2127-2133.

17. Ojwach, S. O.; Tshivhase, M. G.; Guzei, I. A.; Darkwa, J.; Mapolie, S. F., *Can. J. Chem.* **2005**, *83*, 843-853.

18. Dyer, P. W.; Fawcett, J.; Hanton, M. J., *Organometallics* **2008**, *27*, 5082-5087.

19. Boudier, A.; Breuil, P.-A. R.; Magna, L.; Olivier-Bourbigou, H.; Braunstein, P., *J. Organomet. Chem.* **2012**, *718*, 31-37.

20. Chandran, D.; Lee, K. M.; Chang, H. C.; Song, G. Y.; Lee, J.-E.; Suh, H.; Kim, I., *J. Organomet. Chem.* **2012**, *718*, 8-13.

21. He, F.; Hao, X.; Cao, X.; Redshaw, C.; Sun, W.-H., *J. Organomet. Chem.* **2012**, *712*, 46-51.

22. Ma, J.; Feng, C.; Wang, S.; Zhao, K.-Q.; Sun, W.-H.; Redshaw, C.; Solan, G. A., *Inorg. Chem. Front.* **2014**, *1*, 14-34.

23. Müller, G.; Klinga, M.; Leskelä, M., *Z. Anorg. Allg. Chem.* **2002**, *628*, 2839-2846.

24. Johnson, L. K.; Killian, C. M.; Brookhart, M., *J. Am. Chem. Soc.* **1995**, *117*, 6414-6415.

25. Baker, W.; Buggle, K.; McOmie, J.; Watkins, D., *J. Chem. Soc.* **1958**, 3594-3603.

26. Kitajima, N.; Fujisawa, K.; Fujimoto, C.; Morooka, Y.; Hashimoto, S.; Kitagawa, T.; Toriumi, K.; Tatsumi, K.; Nakamura, A., *J. Am. Chem. Soc.* **1992**, *114*, 1277-1291.

27. Bruker *APEX2, SAINT and SADABS,*, Bruker AXS Inc: Madison, Wisconsin, USA, 2010.

28. Sheldrick, G. M., *Acta Crystallogr.* **2007**, *64*, 112-122.

29. Farrugia, L. J., *J. Appl. Crystallogr.* **1999**, *32*, 837-838.

30. Spek, A. L., *Acta Crystallogr. Sect. D: Biol. Crystallogr.* **2009**, *65*, 148-155.

31. Rapko, B.; Duesler, E.; Smith, P.; Paine, R.; Ryan, R., *Inorg. Chem.* **1993**, *32*, 2164-2174.

32. Ouizem, S.; Pailloux, S. L.; Ray, A. D.; Duesler, E. N.; Dickie, D. A.; Paine, R. T.; Hay, B. P., *Eur. J. Org. Chem.* **2014,** *2014*, 3132-3148.

33. Mitchell, T. N.; Costisella, B., *NMR—From Spectra to Structures: An Experimental Approach* **2007**, 164-207.

34. Cotton, F. A.; Wilkinson, G.; Murillo, C. A.; Bochmann, M.; Grimes, R., *Advanced Inorganic Chemistry*. Wiley New York: 1999; Vol. 5.

35. Dahlhoff, W.; Nelson, S., *J. Chem. Soc. A: Inorg., Phys., Theor.* **1971**, 2184-2190.

36. Adewuyi, S.; Li, G.; Zhang, S.; Wang, W.; Hao, P.; Sun, W.-H.; Tang, N.; Yi, J., *J. Organomet. Chem.* **2007**, *692*, 3532-3541.

37. Song, K.; Gao, H.; Liu, F.; Pan, J.; Guo, L.; Zai, S.; Wu, Q., *Eur. J. Inorg. Chem.* **2009**, *2009*, 3016-3024.

38. Sun, W.; Zhang, S.; Jie, S.; Zhang, W. L., *J. Organomet. Chem.* **2006**, *691*, 4196-4203.

39. Zhang, M.; Zhang, S.; Hao, P.; Jie, S.; Sun, W. H.; Li, P.; Lu, X., *Eur. J. Inorg. Chem.* **2007**, *2007*, 3816-3826.

40. Obuah, C.; Omondi, B.; Nozaki, K.; Darkwa, J., *J. Mol. Catal. A: Chem.* **2014**, *382*, 31-40.

41. Malgas-Enus, R.; Mapolie, S. F., *Inorg. Chim. Acta* **2014**, *409*, 96-105.

42. Sun, W.-H.; Hao, P.; Li, G.; Zhang, S.; Wang, W.; Yi, J.; Asma, M.; Tang, N., *J. Organomet. Chem.* **2007**, *692*, 4506-4518.

43. Igarashi, A.; Zhang, S.; Nomura, K., *Organometallics* **2012**, *31*, 3575-3581.

44. Carlini, C.; Isola, M.; Liuzzo, V.; Galletti, A. M. R.; Sbrana, G., *Appl. Catal. A: Gen.* **2002**, *231*, 307-320.

45. Shao, C.; Sun, W.-H.; Li, Z.; Hu, Y.; Han, L., *Catal. Commun.* **2002**, *3*, 405-410.

46. Laine, T. V.; Lappalainen, K.; Liimatta, J.; Aitola, E.; Löfgren, B.; Leskelä, M., *Macromol. Rapid Commun.* **1999**, *20*, 487-491.

47. Sun, W.-H.; Tang, X.; Gao, T.; Wu, B.; Zhang, W.; Ma, H., *Organometallics* **2004**, *23*, 5037-5047.

48. Jie, S.; Zhang, S.; Sun, W. H., *Eur. J. Inorg. Chem.* **2007**, *2007*, 5584-5598.

49. de Oliveira, L. L.; Campedelli, R. R.; Kuhn, M. C.; Carpentier, J.-F.; Casagrande, O. L., *J. Mol. Catal. A: Chem.* **2008**, *288*, 58-62.

50. Ulbrich, A. H.; Campedelli, R. R.; Milani, J. L. S.; dos Santos, J. H.; Casagrande, O. d. L., *Appl. Catal. A: Gen.* **2013**, *453*, 280-286.

51. Ajellal, N.; Kuhn, M. C.; Boff, A. D.; Hörner, M.; Thomas, C. M.; Carpentier, J.-F.; Casagrande, O. L., *Organometallics* **2006**, *25*, 1213-1216.

52. Zhang, C.; Sun, W. H.; Wang, Z. X., *Eur. J. Inorg. Chem.* **2006**, *2006*, 4895-4902.

53. Ulbrich, A. H.; Bergamo, A. L.; Casagrande, O. d. L., *Catal. Commun.* **2011**, *16*, 245-249.

CHAPTER 5

Potential hemi-labile (imino)pyridine palladium(II) complexes as selective ethylene dimerization catalysts: An experimental and theoretical approach

5.1. Introduction

Late transition metal complexes have been used as catalysts in a number of organic transformations, including ethylene oligomerization and polymerization reactions[1, 2] and still continue to receive considerable academic and industrial interest as catalysts for oligomerization of ethylene.[3] Particular attention has been directed towards nitrogen-donor late transition metal catalysts as olefin oligomerization and polymerization catalysts, almost two decades since the seminal work of Brookhart *et al*.[4] on the use of α-diimine ligands in the development of α-olefin oligomerization catalysts. These α-diimine and Schiff base ligands in general, are particularly attractive because of their ease of syntheses, ability to stabilize metals with varying oxidation states and ease of fine-tuning their electronic and steric properties.[5]

To date, several reviews have been published on late transition-metal α-olefin oligomerization and polymerization catalysis[6] and fundamental insight has been shed on the mechanism of ethylene oligomerization and polymerization reactions. Of particular significance is the discovery that catalyst activity and selectivity can be regulated through ligand modification as well as varying the identity of the metal center. For instance, the α-diimine palladium(II) and nickel(II) complexes by Brookhart *et al*.[7, 8] produce ethylene oligomers or polyethylenes depending on the steric properties of the ligand backbone. Bulky substituents adjacent to the metal site hinder chain transfer process which in turn favors polymerization resulting in the

formation of a high-molecular-weight polymer. However, less bulky groups generally favor oligomerization of olefins.[9] Hence, for effective ethylene oligomerization reactions, ligand design which promotes β-hydride transfer is essential.[10]

One strategy that has been adopted for the design of stable and more active catalysts for ethylene oligomerization and polymerization has been in the use of "hemi-labile ligands", pioneered by Jeffrey and Rauchfuss in 1979.[11] The hemi-labile ligand stabilizes the active metal center *via* chelate effect, but allows substrate coordination to the metal center.[10] In another report, hemilabile ligands based on bidentate P,O-ligands were found to influence both the selectivity and stability of transition metal catalysts.[12] In this design, the incoming monomer should be more strongly coordinating to the metal center than the hemilabile group. In our attempt to develop both active and stable ethylene oligomerization and polymerization catalysts, we herein report the syntheses of new palladium(II) complexes of (imino)pyridine ligands containing potential hemi-labile ether or amino pendant donor groups. The catalytic investigations of these complexes in ethylene oligomerization reactions, ^{1}H NMR and DFT studies have been systematically performed and are herein discussed.

5.2. Experimental section

5.2.1. Materials and methods

All synthetic manipulations were performed using standard Schlenk techniques under a nitrogen atmosphere. All solvents were dried by distillation prior to use. [$PdCl_2$(cod)] and [PdCl(Me)(cod)] were prepared by following literature procedures.[13] $PdCl_2$, 2-(methoxy)-ethylamine, 2-pyridinecarboxaldehyde, 2-acetylpyridine, 2-(methoxy)propylamine, *N,N*-

(diethyl)ethylenediamine and 6-bromopyridine-2-carboxaldehyde were obtained from Sigma-Aldrich and used as received. ^{1}H NMR and $^{13}C\{^{1}H\}$ NMR spectra were recorded on a Bruker 400 MHz spectrometer in $CDCl_3$ solution at room temperature using tetramethylsilane as an internal standard. Elemental analyses were performed on a Thermal Scientific Flash 2000 while ESI-mass spectra were recorded on an LC premier micro-mass spectrometer. The infrared spectra were recorded on a Perkin-Elmer spectrum 100 in the 4000-650 cm^{-1} range. Magnetic moments of the complexes were determined using Evans balance. GC analyses were performed using a Varian CP-3800 gas chromatograph equipped with a CP-Sil 5 CB (30 m × 0.2 mm × 0.25 μm) capillary column while GC‑MS analyses were performed on a Shimadzu GC‑MS-QP2010.

5.2.2. Synthesis of pyridyl ligands and their palladium(II) complexes

*5.2.2.1. 2-methoxy-N-(1-(pyridin-2-yl)ethylidene)ethanamine (**L5**)*

2-(methoxy)ethylamine (0.72 mL, 8.25 mmol) was added to a solution of 2-acetylpyridine (0.93 mL, 8.25 mmol) in toluene (70 mL) and para-toluene sulfonic acid (a small amount) was added. The mixture was refluxed for 2 h and the water formed was separated using Dean-Stark distillation. Refluxing was continued for 24 h and toluene was removed under reduced pressure. The resultant dark brown liquid was then re-dissolved in CH_2Cl_2 and washed once with 15 mL of deionised water. The organic layer was dried over anhydrous $MgSO_4$ and reduced under vacuum leaving behind **L5** as a brown liquid in 93% yield. ^{1}H NMR (400 MHz, $CDC1_3$): δ 2.24 (s, 3H, CH_3); 3.28 (s, 3H, CH_3-O); 3.55 (t, 2H, CH_2-O, $^{3}J_{HH}$ = 6.0 Hz); 3.63 (t, 2H, CH_2-N, $^{3}J_{HH}$ = 6.0 Hz); 7.08 (dd, 1H, 5-py, $^{3}J_{HH}$ = 7.6 Hz); 7.50 (dd, 1H, 4-py, $^{3}J_{HH}$ = 7.6 Hz); 7.96 (d, 1H, 3-py, $^{3}J_{HH}$ = 7.6 Hz); 8.42 (d, 1H, 6-py, $^{3}J_{HH}$ = 7.6 Hz). $^{13}C\{^{1}H\}$ NMR ($CDC1_3$): δ 25.74 (CH_3),

52.38 (CH_2-N), 58.71 (CH_3-O), 72.99 (CH_2-O), 121.05 (3-py-C), 124.10 (5-py-C), 136.25 (4-py-C), 148.21 (6-py-C), 155.65 (2-py-C), 168.00 (C=N). ESI-MS: m/z (%) 201 [$(M + Na)^+$, 100%]. FT-IR (cm^{-1}): $\upsilon_{(C=N)}$ = 1642. Anal. Calcd for $C_{10}H_{14}N_2O$: C, 67.39; H, 7.92; N, 15.72. Found: C, 66.98; H, 7.83; N, 15.91.

Compounds **L6**–**L9** were prepared following the same procedure as described for compound **L5**, using the appropriate reagents.

*5.2.2.2. 2-methoxy-N-((pyridin-2-yl)methylene)ethanamine (**L6**)*

2-(methoxy)ethylamine (0.81 mL, 9.34 mmol) was reacted with 2-pyridinecarboxaldehyde (0.89 mL, 9.34 mmol) and isolated as a light orange liquid in 95% yield. ^{1}H NMR (400 MHz, $CDC1_3$): δ 3.39 (s, 3H, CH_3-O); 3.72 (t, 2H, CH_2-N, $^3J_{HH}$ = 6.0 Hz); 3.86 (t, 2H, CH_2-O, $^3J_{HH}$ = 6.0 Hz); 7.31 (d, 1H, 3-py, $^3J_{HH}$ = 8.0 Hz); 7.72 (dd, 1H, 5-py, $^3J_{HH}$ = 8.0 Hz); 8.00 (dd, 1H, 4-py, $^3J_{HH}$ = 8.0 Hz); 8.42 (s, 1H, HC=N); 8.65 (d, 1H, 6-py, $^3J_{HH}$ = 8.0 Hz). $^{13}C\{^1H\}$ NMR ($CDC1_3$): δ 58.79 (CH_3-O), 60.73 (CH_2-N), 71.90 (CH_2-O), 121.44 (3-py), 124.72 (5-py), 136.50 (4-py), 149.34 (6-py), 154.32 (2-py), 163.45 (C=N). ESI-MS: m/z (%) 187 [$(M + Na)^+$, 100%]. FT-IR (cm^{-1}): $\upsilon_{(C=N)}$ = 1651. Anal. Calcd for $C_9H_{12}N_2O{\cdot}0.5CH_2Cl_2$: C, 55.21; H, 6.34; N, 13.55. Found: C, 55.60; H, 6.52; N, 14.01.

*5.2.2.3. 3-methoxy-N-((pyridin-2-yl)methylene)propan-1-amine (**L7**)*

2-methoxy)propylamine (0.95 mL, 9.34 mmol) was reacted with 2-pyridinecarboxaldehyde (0.89 mL, 9.34 mmol) and isolated as an orange liquid in 94% yield. ^{1}H NMR ($CDC1_3$): δ 2.00 (td, 2H, CH_2, $^3J_{HH}$ = 6.4 Hz); 3.37 (s, 3H, CH_3-O); 3.49 (t, 2H, CH_2-O, $^3J_{HH}$ = 6.4 Hz); 3.76 (t,

2H, CH_2-N, $^3J_{HH}$ = 6.4 Hz); 7.28 (dd, 1H, 5-py, $^3J_{HH}$ = 7.6 Hz); 7.74 (dd, 1H, 4-py, $^3J_{HH}$ = 7.6 Hz); 7.99 (d, 1H, 3-py, $^3J_{HH}$ = 7.6 Hz); 8.42 (s, 1H, HC=N); 8.66 (d, 1H, 6-py, $^3J_{HH}$ = 7.6 Hz). $^{13}C\{^1H\}$ NMR ($CDC1_3$): δ 30.56 (CH_2), 57.92 (CH_2-N), 58.49 (CH_3-O), 70.24 (CH_2-O), 121.20 (3-py), 124.60 (5-py), 136.47 (4-py), 149.33 (6-py), 154.50 (2-py), 162.16 (C=N). ESI-MS: m/z (%) 201 [$(M + Na)^+$, 100%]. FT-IR (cm^{-1}): $\upsilon_{(C=N)}$ = 1649. Anal. Calcd for $C_{10}H_{14}N_2O$: C, 67.39; H, 7.92; N, 15.72. Found: C, 67.27; H, 7.75; N, 15.60.

*5.2.2.4. N,N-diethyl-N-((pyridin-2-yl)methylene)ethane-1,2-diamine (**L8**)*

N,N-(diethyl)ethylenediamine (1 mL, 16.8 mmol) was reacted with 2-pyridinecarboxaldehyde (1.58 mL, 16.8 mmol) and isolated as a dark brown liquid in 92% yield. ^1H NMR (400 MHz, $CDC1_3$): δ 0.95 (t, 6H, CH_3-Et_2, $^3J_{HH}$ = 7.2 Hz); 2.50 (q, 4H, CH_2-Et_2, $^3J_{HH}$ = 7.2 Hz); 2.72 (t, 2H, CH_2-O, $^3J_{HH}$ = 7.2 Hz); 3.68 (t, 2H, CH_2-N, $^3J_{HH}$ = 7.2 Hz); 7.18 (dd, 1H, 5-py, $^3J_{HH}$ = 8.0 Hz); 7.61 (dd, 1H, 4-py, $^3J_{HH}$ = 8.0 Hz); 7.88 (d, 1H, 3-py, $^3J_{HH}$ = 8.0 Hz); 8.32 (s, 1H, HC=N); 8.54 (d, 1H, 6-py, $^3J_{HH}$ = 8.0 Hz). $^{13}C\{^1H\}$ NMR ($CDC1_3$): δ 11.81 (CH_3-Et_2), 47.42 (CH_2-Et_2), 53.17 (CH_2-O), 59.39 (CH_2-N), 121.17 (3-py), 124.57 (5-py), 136.45 (4-py), 149.31 (6-py), 154.49 (2-py), 162.57 (C=N). ESI-MS: m/z (%) 228 [$(M + Na)^+$, 100%]. FT-IR (cm^{-1}): $\upsilon_{(C=N)}$ = 1649. Anal. Calcd for $C_{12}H_{19}N_3$: C, 70.20; H, 9.33; N, 20.47. Found: C, 69.87; H, 8.83; N, 19.98.

*5.2.2.5. N-((6-bromopyridin-2-yl)methylene)-2-methoxyethanamine (**L9**)*

2-(methoxy)ethylamine (0.37 mL, 4.3 mmol) was reacted with 6-bromopyridine-2-carboxaldehyde (0.8 g, 4.3 mmol) and isolated as a dark brown liquid in 78% yield. ^1H NMR (400 MHz, $CDC1_3$): δ 3.39 (s, 3H, CH_3-O); 3.71 (t, 2H, CH_2-N, $^3J_{HH}$ = 5.6 Hz); 3.85 (t, 2H, CH_2-O, $^3J_{HH}$ = 5.6 Hz); 7.50 (d, 1H, 5-py, $^3J_{HH}$ = 8.0 Hz); 7.58 (dd, 1H, 4-py, $^3J_{HH}$ = 8.0 Hz);

8.00 (d, 1H, 3-py, $^{3}J_{HH}$ = 8.0 Hz); 8.36 (s, 1H, HC=N). $^{13}C\{^{1}H\}$ NMR ($CDC1_3$): δ 58.76 (CH_3-O), 60.54 (CH_2-N), 71.88 (CH_2-O), 121.43 (3-py), 124.67 (5-py), 139.52 (4-py), 140.34 (6-py), 153.41 (2-py), 163.84 (C=N). ESI-MS: m/z (%) 265 [$(M + Na)^+$, 65%]. FT-IR (cm^{-1}): $\upsilon_{(C=N)}$ = 1651. Anal. Calcd for $C_9H_{11}BrN_2O$: C, 44.47; H, 4.56; N, 11.52. Found: C, 44.75; H, 4.49; N, 11.89.

*5.2.2.6. 2-((pyridin-2-yl)methyleneamino)ethanol (**L10**)*

Ethanolamine (0.57g, 9.33 mmol) was added to a solution of 2-pyridinecarboxaldehyde (1.0g, 9.33 mmol) in ethanol (40 mL) and *para*-toluene sulfonic acid (a small amount) was added. And the mixture stirred at 45 ^{o}C for 24 h. The solvent was then evaporated and the resultant light brown liquid was re-dissolved in CH_2Cl_2 and washed once with 10 mL of deionised water. The organic layer was dried over anhydrous $MgSO_4$ and reduced under vacuum leaving behind **L10** as a light brown liquid in 85% yield. ^{1}H NMR (400 MHz, $CDC1_3$): δ 3.69 (t, 2H, CH_2-N, $^{3}J_{HH}$ = 5.6 Hz); 3.83 (t, 2H, CH_2-O, $^{3}J_{HH}$ = 5.6 Hz); 7.18 (dd, 1H, 5-py, $^{3}J_{HH}$ = 8.0 Hz); 7.58 (dd, 1H, 4-py, $^{3}J_{HH}$ = 8.0 Hz); 7.78 (d, 1H, 3-py, $^{3}J_{HH}$ = 8.0 Hz); 8.29 (s, 1H, HC=N); 8.48 (d, 1H, 6-py, $^{3}J_{HH}$ = 8.0 Hz). $^{13}C\{^{1}H\}$ NMR ($CDC1_3$): δ 51.71 (CH_2-N), 60.68 (CH_2-O), 121.01 (3-py), 124.56 (5-py), 136.41 (4-py), 149.30 (6-py), 154.23 (2-py), 158.34 (C=N). FT-IR (cm^{-1}): 1650 $\upsilon_{(C=N)}$. Anal. Calcd for $C_8H_{10}N_2O$: C, 63.98; H, 6.71; N, 18.65. Found: C, 63.53; H, 6.24; N, 18.81.

*5.2.2.7. PdMeCl {2-methoxy-N-(1-(pyridin-2-yl)ethylidene)ethanamine} (**13**)*

Ligand **L5** (0.14g, 0.75 mmol) was dissolved in 15 mL of diethyl ether and to this solution was added [PdCl(Me)(cod)] (0.20 g, 0.75 mmol), forming a yellow solution. The reaction mixture was then stirred for 24 h at room temperature after which a yellow precipitate was isolated by

filtration, washed with hexane (10 mL) and dried under vacuum to afford complex **13** as a yellow powder. Recrystallization from MeOH afforded yellow crystals suitable for single-crystal X-ray analysis. Yield: 0.17 g (68%). ^{1}H NMR ($CDC1_3$): δ 0.85 (s, 3H, Pd-CH_3); 1.00 (s, 3H_{iso}, Pd-CH_3); 2.43 (s, 3H, CH_3); 2.52 (s, 3H_{iso}, CH_3); 3.30 (s, 3H, CH_3-O); 3.32 (s, 3H_{iso}, CH_3-O); 3.75 (t, 2H, CH_2-O, $^{3}J_{HH}$ = 4.8 Hz); 3.88 (t, 2H_{iso}, CH_2-O, $^{3}J_{HH}$ = 4.8 Hz); 4.06 (t, 2H, CH_2-N, $^{3}J_{HH}$ = 4.8 Hz); 4.24 (t, 2H_{iso}, CH_2-N, $^{3}J_{HH}$ = 4.8 Hz); 7.57 (dd, 1H, 5-py, $^{3}J_{HH}$ = 6.4 Hz); 7.60 (dd, 1H_{iso}, 5-py, $^{3}J_{HH}$ = 6.4 Hz); 7.62 (dd, 4-py, 1H, $^{3}J_{HH}$ = 7.6 Hz); 7.79 (dd, 1H_{iso}, 4-py, $^{3}J_{HH}$ = 7.6 Hz); 7.97 (d, 1H, 3-py, $^{3}J_{HH}$ = 7.6 Hz); 8.12 (d, 1H_{iso}, 3-py, $^{3}J_{HH}$ = 7.6 Hz); 8.68 (d, 1H, 6-py, $^{3}J_{HH}$ = 5.2 Hz); 9.23 (d, 1H_{iso}, 6-py, $^{3}J_{HH}$ = 5.2 Hz). $^{13}C\{^{1}H\}$ NMR ($CDC1_3$): δ -2.93 (CH_3-Pd), 0.14$_{iso}$ (CH_3-Pd), 25.87 (CH_3), 26.02$_{iso}$ (CH_3), 52.17(CH_2-N), 52.69$_{iso}$ (CH_2-N), 57.81 (CH_3-O), 58.10$_{iso}$ (CH_3-O), 70.51 (CH_2-O), 71.48$_{iso}$ (CH_2-O), 124.74 (3-py-C), 126.72$_{iso}$ (3-py-C), 127.80 (5-py-C), 127.87$_{iso}$ (5-py-C), 138.45 (4-py-C), 138.72$_{iso}$ (4-py-C), 148.15 (6-py-C), 149.22$_{iso}$ (6-py-C), 151.81 (2-py-C), 155.53$_{iso}$ (2-py-C), 166.11(C=N), 168.79$_{iso}$ (C=N). ESI-MS: m/z (%) 299 [M^{+}-Cl, 53%], 285 [M^{+}-ClMe, 93%]. FT-IR (cm^{-1}): $\upsilon_{(C=N)}$ =1595. FT-IR (cm^{-1}): ν(C=N) =1587. Anal. Calcd for $C_{13}H_{22}ClN_3Pd$: C, 39.42; H, 5.11; N, 8.36. Found: C, 39.01; H, 5.04; N, 8.26.

Complexes **14** - **17** were prepared following the same procedure described for **13**.

*5.2.2.8. PdMeCl{2-methoxy-N-((pyridin-2-yl)methylene)ethanamine} (**14**)*

[PdCl(Me)(cod)] (0.20 g, 0.75 mmol) and **L6** (0.12 g, 0.75 mmol). Yellow solid. Recrystallization from MeOH afforded yellow crystals suitable for single-crystal X-ray analysis. Yield: 0.18 g (76%). ^{1}H NMR ($CDC1_3$): δ 0.94 (s, 3H, Pd-CH_3); 1.09 (s, 3H_{iso}, Pd-CH_3); 3.35

(s, 3H, CH_3-O); 3.68 (t, 2H, CH_2-N, $^3J_{HH}$ = 4.8 Hz); 3.85 (t, 2H_{iso}, CH_2-N, $^3J_{HH}$ = 4.8 Hz); 3.93 (t, 2H, CH_2-O, $^3J_{HH}$ = 4.8 Hz); 4.06 (t, 2H_{iso}, CH_2-O, $^3J_{HH}$ = 4.8 Hz); 7.60 (dd, 1H, 5-py, $^3J_{HH}$ = 7.2 Hz); 7.64 (dd, 1H_{iso}, 5-py, $^3J_{HH}$ = 7.2 Hz); 7.70 (dd, 1H, 4-py, $^3J_{HH}$ = 7.2 Hz); 7.85 (dd, 1H_{iso}, 4-py, $^3J_{HH}$ = 7.2 Hz); 7.97 (d, 1H, 3-py, $^3J_{HH}$ = 7.2 Hz); 8.14 (d, 1H_{iso}, 3-py, $^3J_{HH}$ = 7.2 Hz); 8.27 (s, 1H, HC=N); 8.34 (s, 1H_{iso}, HC=N); 8.66 (d, 1H, 6-py, $^3J_{HH}$ = 7.2 Hz); 9.07 (d, 1H_{iso}, 6-py, $^3J_{HH}$ = 7.2 Hz). $^{13}C\{^1H\}$ NMR ($CDC1_3$): δ -3.03 (Pd-CH_3), 0.12$_{iso}$ (Pd-CH_3), 58.22 (CH_3-O), 58.80$_{iso}$ (CH_3-O), 58.97(CH_2-N), 59.23$_{iso}$ (CH_2-N), 69.53 (CH_2-O), 70.06$_{iso}$ (CH_2-O), 125.84 (3-py-C), 127.06$_{iso}$ (3-py-C), 127.70 (5-py-C), 127.99$_{iso}$ (5-py-C), 138.59 (4-py-C), 138.66$_{iso}$ (4-py-C), 148.75 (6-py-C), 149.38$_{iso}$ (6-py-C), 151.65 (2-py-C), 155.82$_{iso}$ (2-py-C), 162.53 (C=N), 167.99$_{iso}$ (C=N). ESI-MS: m/z (%) 285 [M^+-Cl, (^{35}Cl) 14%], 287 [M^+-Cl, (^{37}Cl) 12%], 269 [M^+-ClMe, (^{35}Cl) 100%], 271 [M^+-ClMe, (^{37}Cl) 91%]. FT-IR (cm^{-1}): $\upsilon_{(C=N)}$ =1587. FT-IR (cm^{-1}): ν(C=N) =1590. Anal. Calcd for $C_{13}H_{22}ClN_3Pd$: C, 37.40; H, 4.71; N, 8.72. Found: C, 37.41; H, 4.72; N, 8.59.

*5.2.2.9. PdMeCl{3-methoxy-N-((pyridin-2-yl)methylene)propan-1-amine} (**15**)*

[PdCl(Me)(cod)] (0.20 g, 0.75 mmol) and **L7** (0.13 g, 0.75 mmol). Yellow solid. Yield: 0.19 g (75%). ^1H NMR ($CDC1_3$): δ 1.04 (s, 3H, Pd-CH_3); 1.08 (s, 3H_{iso}, Pd-CH_3); 2.04 (td, 2H, CH_2, $^3J_{HH}$ = 6.8 Hz); 2.23 (td, 2H_{iso}, CH_2, $^3J_{HH}$ = 6.8 Hz); 3.34 (s, 3H, CH_3-O); 3.41 (t, 2H, CH_2-O, $^3J_{HH}$ = 6.8 Hz); 3.45 (t, 2H_{iso}, CH_2-O, $^3J_{HH}$ = 6.8 Hz); 3.93 (t, 2H, CH_2-N, $^3J_{HH}$ = 6.8 Hz); 4.02 (t, 2H_{iso}, CH_2-N, $^3J_{HH}$ = 6.8 Hz); 7.61 (d, 1H, 3-py, $^3J_{HH}$ = 8.0 Hz); 7.64 (d, 1H_{iso}, 3-py, $^3J_{HH}$ = 8.0 Hz); 7.67 (dd, 1H, 5-py, $^3J_{HH}$ = 8.0 Hz); 7.70 (dd, 1H_{iso}, 5-py, $^3J_{HH}$ = 8.0 Hz); 7.97 (dd, 1H, 4-py, $^3J_{HH}$ = 8.60 Hz); 8.08 (dd, 1H_{iso}, 4-py, $^3J_{HH}$ = 8.0 Hz); 8.27 (s, 1H, HC=N); 8.38 (s, 1H_{iso}, HC=N); 8.64 (d, 1H, 6-py, $^3J_{HH}$ = 8.0 Hz); 9.11 (d, 1H_{iso}, 6-py, $^3J_{HH}$ = 8.0 Hz). $^{13}C\{^1H\}$ NMR

($CDC1_3$): δ -3.01 (Pd-CH_3), 0.09$_{iso}$ (Pd-CH_3), 30.15 (CH_2), 30.89$_{iso}$ (CH_2), 57.21 (CH_2-N), 58.02$_{iso}$ (CH_2-N), 58.47 (CH_3-O), 58.93$_{iso}$ (CH_3-O), 70.01(CH_2-O), 70.55$_{iso}$ (CH_2-O), 124.44 (3-py-C), 126.61$_{iso}$ (3-py-C), 127.15 (5-py-C), 127.92$_{iso}$ (5-py-C), 138.11 (4-py-C), 138.77$_{iso}$ (4-py-C), 148.85 (6-py-C), 149.35$_{iso}$ (6-py-C), 150.95 (2-py-C), 154.99$_{iso}$ (2-py-C), 162.55 (C=N), 165.91$_{iso}$ (C=N). ESI-MS: m/z (%) 301 [M^+-Cl, (^{35}Cl) 87%], 303 [M^+-Cl, (^{37}Cl) 38%]. FT-IR (cm^{-1}): $\upsilon_{(C=N)}$ =1595. Anal. Calcd for $C_{13}H_{22}ClN_3Pd$: C, 39.42; H, 5.11; N, 8.36. Found: C, 39.23; H, 4.93; N, 8.15.

*5.2.2.10. PdMeCl{N,N-diethyl-N-((pyridin-2-yl)methylene)ethane-1,2-diamine} (**16**)*

[PdCl(Me)(cod)] (0.20 g, 0.75 mmol) and **L8** (0.15 g, 0.75 mmol). Dirty yellow solid. Yield: 0.22 g (82%). ^{1}H NMR (400 MHz, $CDC1_3$): δ 0.97 (t, 6H, CH_3-Et_2, $^3J_{HH}$ = 7.2 Hz); 0.98 (t, 6H$_{iso}$, CH_3-Et_2, $^3J_{HH}$ = 7.2 Hz); 1.12 (s, 3H, Pd-CH_3); 1.14 (s, 3H$_{iso}$, Pd-CH_3); 2.48 (q, 4H, CH_2-Et_2, $^3J_{HH}$ = 7.2 Hz); 2.56 (q, 4H$_{iso}$, CH_2-Et_2, $^3J_{HH}$ = 7.2 Hz); 2.77 (t, 2H, CH_2-O, $^3J_{HH}$ = 7.2 Hz); 3.18 (t, 2H$_{iso}$, CH_2-O, $^3J_{HH}$ = 7.2 Hz); 3.74 (t, 2H, CH_2-N, $^3J_{HH}$ = 7.2 Hz); 4.07 (t, 2H$_{iso}$, CH_2-N, $^3J_{HH}$ = 7.2 Hz); 7.60 (dd, 1H, 5-py, $^3J_{HH}$ = 8.0 Hz); 7.64 (dd, 1H$_{iso}$, 5-py, $^3J_{HH}$ = 8.0 Hz); 7.67 (dd, 1H, 4-py, $^3J_{HH}$ = 8.0 Hz); 7.75 (dd, 1H$_{iso}$, 4-py, $^3J_{HH}$ = 8.0 Hz); 7.96 (d, 1H, 3-py, $^3J_{HH}$ = 8.0 Hz); 7.98 (d, 1H$_{iso}$, 3-py, $^3J_{HH}$ = 8.0 Hz); 8.06 (s, 1H, HC=N); 8.25(s, 1H$_{iso}$, HC=N) 8.62 (d, 1H, 6-py, $^3J_{HH}$ = 8.0 Hz); 9.08 (d, 1H$_{iso}$, 6-py, $^3J_{HH}$ = 8.0 Hz). ^{13}C{^{1}H} NMR ($CDC1_3$): δ -2.96 (Pd-CH_3), 0.12$_{iso}$ (Pd-CH_3), 12.03 (CH_3-Et_2), 12.39$_{iso}$ (CH_3-Et_2), 47.43 (CH_2-Et_2), 47.52$_{iso}$ (CH_2-Et_2), 52.65 (CH_2-O), 58.13 (CH_2-N), 125.38 (3-py-C), 126.87$_{iso}$ (3-py-C), 127.52 (5-py-C), 127.68$_{iso}$ (5-py-C), 138.55 (4-py-C), 138.67$_{iso}$ (4-py-C), 148.71 (6-py-C), 149.35$_{iso}$ (6-py-C), 151.86 (2-py-C), 152.46 (2-py-C), 164.49 (C=N), 166.79 (C=N). ESI-MS: m/z (%) 326 [M^+-Cl, (^{35}Cl)

100%], 328 [M^+-Cl, (^{37}Cl) 92%]. FT-IR (cm^{-1}): $\upsilon_{(C=N)}$ =1597. Anal. Calcd for $C_{13}H_{22}ClN_3Pd$: C, 43.11; H, 6.12; N, 11.60. Found: C, 43.57; H, 5.75; N, 11.53.

*5.2.2.11. PdMeCl{N-((6-bromopyridin-2-yl)methylene)-2-methoxyethanamine} (**17**)*

[PdCl(Me)(cod)] (0.20 g, 0.75 mmol) and **L9** (0.18 g, 0.75 mmol). Brick red solid. Yield: 0.24 g (79%). ^{1}H NMR (400 MHz, CDC1$_3$): δ 0.87 (s, 3H, Pd-CH_3); 1.30 (s, 3H$_{iso}$, Pd-CH_3); 3.28 (s, 3H, CH_3-O); 3.36 (s, 3H$_{iso}$, CH_3-O); 3.42 (t, 2H, CH_2-N, $^3J_{HH}$ = 5.6 Hz); 3.67 (t, 2H$_{iso}$, CH_2-N, $^3J_{HH}$ = 5.6 Hz); 3.78 (t, 2H, CH_2-O, $^3J_{HH}$ = 5.6 Hz); 3.88 (t, 2H$_{iso}$, CH_2-O, $^3J_{HH}$ = 5.6 Hz); 7.45 (d, 1H, 5-py, $^3J_{HH}$ = 8.0 Hz); 7.60 (d, 1H$_{iso}$, 5-py, $^3J_{HH}$ = 8.0 Hz); 7.74 (dd, 1H, 4-py, $^3J_{HH}$ = 8.0 Hz); 7.78 (dd, 1H$_{iso}$, 4-py, $^3J_{HH}$ = 8.0 Hz); 7.81 (d, 1H, 3-py, $^3J_{HH}$ = 8.0 Hz); 7.92 (d, 1H$_{iso}$, 3-py, $^3J_{HH}$ = 8.0 Hz); 8.08 (s, 1H, HC=N); 8.35 (s, 1H, HC=N). ^{13}C{^{1}H} NMR (CDC1$_3$): δ -2.08 (Pd-CH_3), 0.15$_{iso}$ (Pd-CH_3), 58.22 (CH_3-O), 58.92$_{iso}$ (CH_3-O), 58.95(CH_2-N), 59.70$_{iso}$ (CH_2-N), 69.97 (CH_2-O), 71.25$_{iso}$ (CH_2-O), 125.99 (3-py-C), 127.18$_{iso}$ (3-py-C), 127.47 (5-py-C), 127.82$_{iso}$ (5-py-C), 138.67 (4-py-C), 138.89$_{iso}$ (4-py-C), 142.71 (6-py-C), 143.01$_{iso}$ (6-py-C), 151.05 (2-py-C), 154.93$_{iso}$ (2-py-C), 162.86 (C=N), 167.51$_{iso}$ (C=N). ESI-MS: m/z (%) 364 [M^+-Cl, (^{35}Cl) 23%], 366 [M^+-Cl, (^{37}Cl) 17%], 348 [M^+-ClMe, (^{35}Cl) 100%], 250 [M^+-ClMe, (^{37}Cl) 69%]. FT-IR (cm^{-1}): $\upsilon_{(C=N)}$ =1593. Anal. Calcd for $C_{13}H_{22}ClN_3Pd$: C, 30.03; H, 3.53; N, 7.00. Found: C, 30.48; H, 3.55; N, 7.07.

*5.2.2.12. [PdMe{2-methoxy-N-(1-(pyridin-2-yl)ethylidene)ethanamine}]$^+$[BAr'$_4$]$^-$ (**13a**)*

Complex **13** (0.06g, 0.18 mmol) was dissolved in 15 mL of CH_2Cl_2 and to this solution was added NaBAr'$_4$ (0.16 g, 0.18 mmol). The reaction mixture was then stirred for 1 h at room temperature, filtered through a plug of celite and the filtrate evaporated *in vacuo* to afford an

oily compound. The oily compound was then dried under vacuum overnight. Yield: 0.15 g (72%). ^{1}H NMR ($CDC1_3$): δ 0.97 (s, 3H, Pd-CH_3); 2.45 (s, 3H, CH_3); 3.18 (s, 3H, CH_3-O); 3.35 (t, 2H, CH_2-O, $^{3}J_{HH}$ = 4.8 Hz); 3.78 (t, 2H, CH_2-N, $^{3}J_{HH}$ = 4.8 Hz); 7.48 (dd, 1H, 5-py $^{3}J_{HH}$ = 7.6 Hz); 7.51 (s, 4H, BAr'$_4$); 7.69 (s, 8H, BAr'$_4$); 7.74 (dd, 1H, 4-py, $^{3}J_{HH}$ = 7.6 Hz); 7.89 (d, 1H, 3-py $^{3}J_{HH}$ = 7.6 Hz); 8.01 (d, 1H, 6-py, $^{3}J_{HH}$ = 7.6 Hz). Positive ion ESI-MS: m/z (%) 299 [M^+, 53%]. Negative ion ESI-MS: m/z (%) 863 [M^-, 100%].

Complexes **14a** – **17a** were prepared following the same procedure described for **13a**.

*5.2.2.13. [PdMe{2-methoxy-N-((pyridin-2-yl)methylene)ethanamine }]$^+$[BAr'$_4$]$^-$ (**14a**)*

Complex **14** (0.06 g, 0.18 mmol) and NaBAr'$_4$ (0.16 g, 0.18 mmol). Yield: 0.13 g (65%). ^{1}H NMR ($CDC1_3$): δ 1.07 (s, 3H, Pd-CH_3); 3.35 (s, 3H, CH_3-O); 3.55 (t, 2H, CH_2-N, $^{3}J_{HH}$ = 4.8 Hz); 3.79 (t, 2H, CH_2-O, $^{3}J_{HH}$ = 4.8 Hz); 7.55 (dd, 1H, 5-py, $^{3}J_{HH}$ = 7.6 Hz); 7.50 (s, 4H, BAr'$_4$); 7.71 (s, 8H, BAr'$_4$); 7.73 (dd, 1H, 4-py, $^{3}J_{HH}$ = 7.6 Hz); 7.85 (d, 1H, 3-py, $^{3}J_{HH}$ = 7.6 Hz); 8.01 (s, 1H, HC=N); 8.33 (d, 1H, 6-py, $^{3}J_{HH}$ = 7.6 Hz). Positive ion ESI-MS: m/z (%) 268 [M^+-Me, 70%]. Negative ion ESI-MS: m/z (%) 863 [M^-, 100%].

*5.2.2.14. [PdMe{3-methoxy-N-((pyridin-2-yl)methylene)propan-1-amine }]$^+$[BAr'$_4$]$^-$ (**15a**)*

Complex **15** (0.07 g, 0.18 mmol) and NaBAr'$_4$ (0.16 g, 0.18 mmol). Yield: 0.16 g (75%). ^{1}H NMR ($CDC1_3$): δ 1.02 (s, 3H, Pd-CH_3); 2.15 (td, 2H, CH_2, $^{3}J_{HH}$ = 6.8 Hz); 3.25 (s, 3H, CH_3-O); 3.45 (t, 2H, CH_2-O, $^{3}J_{HH}$ = 6.8 Hz); 3.71 (t, 2H, CH_2-N, $^{3}J_{HH}$ = 6.8 Hz); 7.68 (dd, 1H, 5-py, $^{3}J_{HH}$ = 7.6 Hz); 7.49 (s, 4H, BAr'$_4$); 7.69 (s, 8H, BAr'$_4$); 7.72 (dd, 1H, 4-py, $^{3}J_{HH}$ = 7.6 Hz); 7.85

(d, 1H, 3-py, $^3J_{HH}$ = 7.6 Hz); 8.10 (s, 1H, HC=N); 8.35 (d, 1H, 6-py, $^3J_{HH}$ = 7.6 Hz). Positive ion ESI-MS: m/z (%) 268 [M^+-Me, 70%]. Negative ion ESI-MS: m/z (%) 863 [M^-, 100%].

*5.2.2.15. [PdMe{N,N-diethyl-N-((pyridin-2-yl)methylene)ethane-1,2-diamine}]$^+$[BAr'$_4$]$^-$ (**16a**)*

Complex **16** (0.06 g, 0.18 mmol) and NaBAr'$_4$ (0.16 g, 0.18 mmol). Yield: 0.16 g (78%). ^{1}H NMR (CDC1$_3$): δ 0.89 (t, 6H, CH_3-Et_2, $^3J_{HH}$ = 7.2 Hz); 1.11 (s, 3H, Pd-CH_3); 2.55 (q, 4H, CH_2-Et_2, $^3J_{HH}$ = 7.2 Hz); 2.95 (t, 2H, CH_2-O, $^3J_{HH}$ = 7.2 Hz); 3.88 (t, 2H, CH_2-N, $^3J_{HH}$ = 7.2 Hz); 7.51 (dd, 1H, 5-py, $^3J_{HH}$ = 8.0 Hz); 7.50 (s, 4H, BAr'$_4$); 7.79 (s, 8H, BAr'$_4$); 7.72 (dd, 1H, 4-py, $^3J_{HH}$ = 8.0 Hz); 7.97 (d, 1H, 3-py, $^3J_{HH}$ = 8.0 Hz); 8.03 (s, 1H, HC=N); 8.60 (d, 1H, 6-py, $^3J_{HH}$ = 8.0 Hz). Positive ion ESI-MS: m/z (%) 326 [M^+, 37%]. Negative ion ESI-MS: m/z (%) 863 [M^-, 100%].

*5.2.2.16. [PdMe{N-((6-bromopyridin-2-yl)methylene)-2-methoxyethanamine}]$^+$[BAr'$_4$]$^-$ (**17a**)*

Complex **17** (0.07 g, 0.18 mmol) and NaBAr'$_4$ (0.16 g, 0.18 mmol). Yield: 0.15 g (68%). ^{1}H NMR (CDC1$_3$): δ 0.85 (s, 3H, Pd-CH_3); 3.75 (s, 3H, CH_3-O); 3.50 (t, 2H, CH_2-N, $^3J_{HH}$ = 5.6 Hz); 3.97 (t, 2H, CH_2-O, $^3J_{HH}$ = 5.6 Hz); 7.41 (d, 1H, 5-py, $^3J_{HH}$ = 8.0 Hz); 7.48 (s, 4H, BAr'$_4$); 7.62 (dd, 1H, 4-py, $^3J_{HH}$ = 8.0 Hz); 7.73 (s, 8H, BAr'$_4$); 7.73 (d, 1H, 3-py, $^3J_{HH}$ = 8.0 Hz); 8.17 (s, 1H, HC=N). Positive ion ESI-MS: m/z (%) 364 [M^+-Me, 53%]. Negative ion ESI-MS: m/z (%) 863 [M^-, 100%].

5.2.3. X-ray crystallography

The X-ray data were recorded on a Bruker Apex Duo equipped with an Oxford Instruments Cryojet operating at 100(2) K and an Incoatec microsource operating at 30 W power. Crystal

and structure refinement data are given in Table 5.1. The data were collected with Mo Kα (λ = 0.71073 Å) radiation at a crystal-to-detector distance of 50 mm. The following conditions were used for the data collection: omega and phi scans with exposures taken at 30 W X-ray power and 0.50° frame widths using APEX2.[14] The data were reduced with the programme SAINT[14] using outlier rejection, scan speed scaling, as well as standard Lorentz and polarisation correction factors. A SADABS semi-empirical multi-scan absorption correction[14] was applied to the data. Direct methods, SHELX-2014[15] and WinGX[16] were used to solve both structures. All non-hydrogen atoms were located in the difference density map and refined anisotropically with SHELX-2014.[15] All hydrogen atoms were included as idealised contributors in the least squares process. Their positions were calculated using a standard riding model with C-$H_{aromatic}$ distances of 0.93 Å and U_{iso} = 1.2 Ueq, C-$H_{methylene}$ distances of 0.99 Å and U_{iso} = 1.2 Ueq and C–H_{methyl} distances of 0.98 Å and U_{iso} = 1.5 Ueq.

5.2.4. General procedure for ethylene oligomerization reactions

Ethylene oligomerization reactions were carried out in a 400 mL stainless steel Parr reactor equipped with a mechanical stirrer, temperature controller and an internal cooling system. In a typical experiment, the cationic catalyst precursors were generated *in situ* by charging the reactor with equimolar amounts of the neutral complex (**13**-**17**) and $NaBAr_4$ {Ar = B[3,5-$(CF_3)_2(C_6H_3)]_4$}. The reactor was then sealed, evacuated, and charged *via* cannula with toluene (80.0 mL). The reactor was then flushed three times with ethylene and once the reaction temperature had been reached, the ethylene pressure was adjusted to the desired pressure and held by continuous feeding of the reactor with ethylene and ethylene consumption monitored during the catalytic reactions. After the reaction time, the reactor was cooled to -15 °C using a

bath of ice/liquid nitrogen and excess ethylene vented off. The reaction was then quenched by addition of 10% HCl (5 mL). A portion of the reaction mixture was sampled for GC and GC-MS analyses and the solvent from the remaining portion was then removed *in vacuo*.

5.2.5. Density functional theoretical (DFT) studies

DFT calculations were performed in gas phase to identify the energy-minimized structures based on B3LYP/LANL2DZ.[17-19] The Gaussian 09, revision A.1 suite of programs was used for all the computations.[20] The geometries and energies of the complexes were optimized using a split basis set; LANL2DZ for Pd and 6-311G for all other atoms. The structures of the complexes were optimized without symmetry constraints.

5.3. Results and discussion

5.3.1. Syntheses of (imino)pyridine ligands and their palladium(II) complexes

(Imino)pyridine ligands **L5-L10** were obtained in excellent yields (>90%) by condensation reactions between the appropriate aldehydes and the corresponding amines (Scheme 5.1).

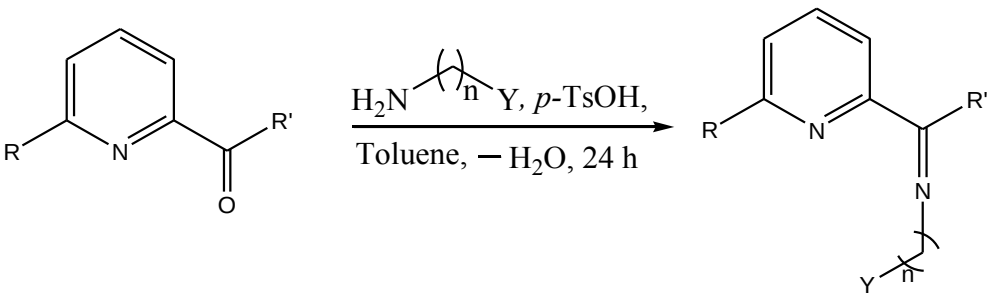

R = H, R' = Me, n = 2, Y= OMe (**L5**) R = H, R' = H, n = 2, Y= NEt_2 (**L8**)
R = H, R' = H, n = 2, Y= OMe (**L6**) R = Br, R' = H, n = 2, Y= OMe (**L9**)
R = H, R' = H, n = 3, Y= OMe (**L7**) R = H, R' = H, n = 2, Y= OH (**L10**)

Scheme 5.1: Synthesis of (imino)pyridine ligands

All the ligands were obtained without further purifications and displayed good solubility in most organic solvents. The identity of the ligands was established using FT-IR, ^{1}H NMR, ^{13}C{^{1}H}, mass spectrometry and elemental analyses. As an illustration, the NMR spectrum of **L5** (Figure 5.1), showed four peaks within the 7.22-8.55 ppm range which were attributed to the four pyridyl aromatic protons.

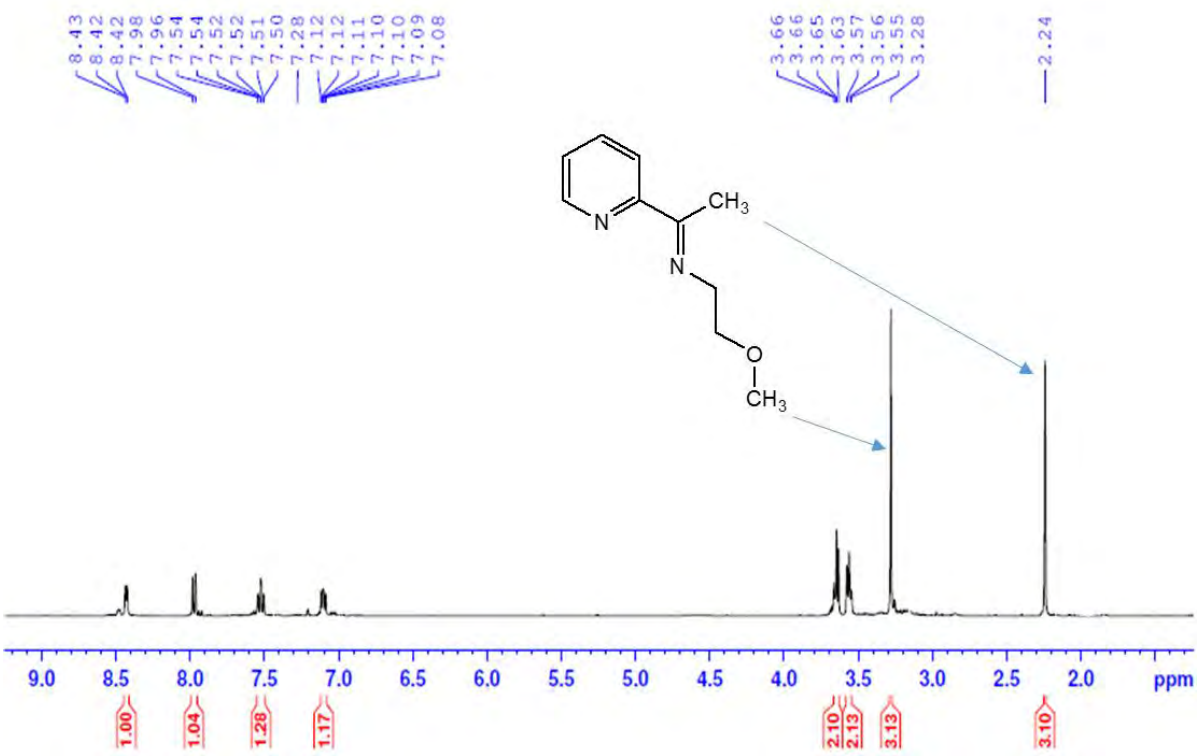

Figure 5.1: ^{1}H NMR spectrum showing the signature peaks of **L5**

The two protons of the carbon adjacent to the imino nitrogen were observed as a triplet at 3.67 ppm while the signal of the two protons of the carbon adjacent to oxygen were shifted down-field to 3.75 ppm due to the effect of the more electron-withdrawing oxygen compared to nitrogen. The three protons of the methoxy group appeared down-field as a singlet at 3.41 ppm relative to the singlet of the three protons of the imine methyl group which was observed at 2.36 ppm. The ^{1}H NMR spectra of the other ligands **L6-L10** were also consistent with the expected

structures. Changing the aldehyde to pyridinecarboxaldehyde resulted in the appearance of five peaks in the aromatic region due to the additional peak of the imine proton (Figure 5.2).

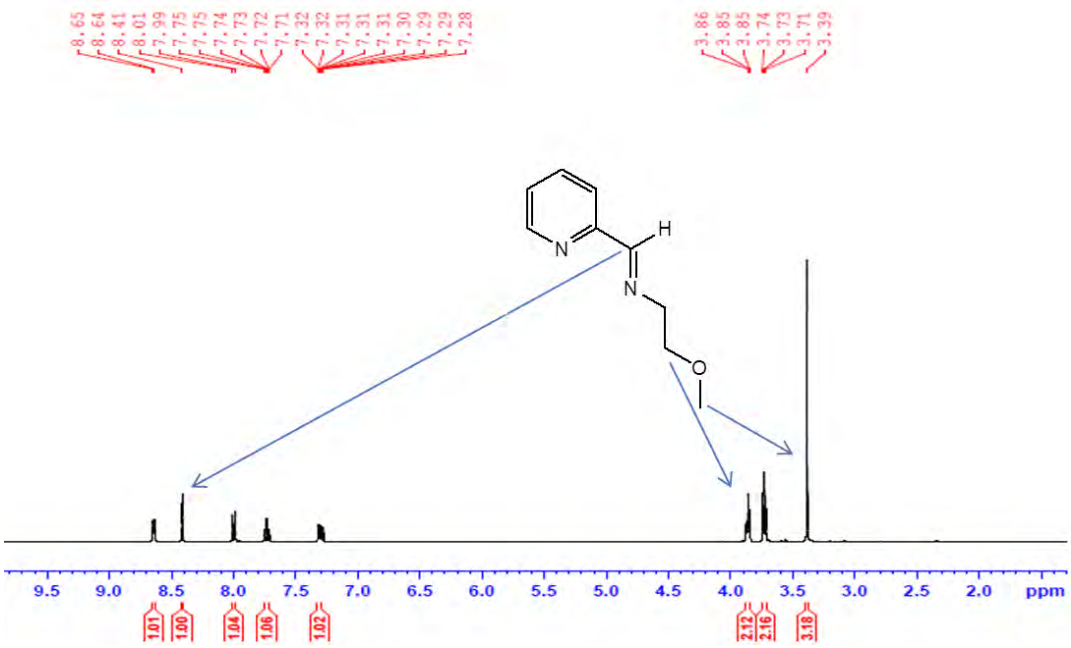

Figure 5.2: ^{1}H NMR spectrum of **L6** showing the characteristic signal of the imine proton.

$^{13}C\{^{1}H\}$ NMR spectroscopy was equally significant in the structural elucidation of these ligands. For example, the imine carbon of **L5** was observed at 168.00 ppm and showed a down-field shift compared to the corresponding peaks of **L6-L9**, with that of **L6**, for example being observed at 163.45 ppm (Figure 5.3). The down-field shift of **L5** may be attributed to the electron donating methyl group at the imine carbon.

Mass spectrometry data of ligands **L5-L10** (Figure 5.4) showed base peaks that corresponded to sodium-coordinated molecular ions which were very much in good correlation with the proposed structures. The IR spectra of compounds **L5-L10** showed strong absorption bands in the 1639–1651 cm^{-1} range (C=N stretching) consistent with the presence of the imine groups.[6, 21] These

C=N stretching vibrations in the FT-IR spectra were in agreement with those reported for imino-imidazole ligands bearing similar pendant groups.[22]

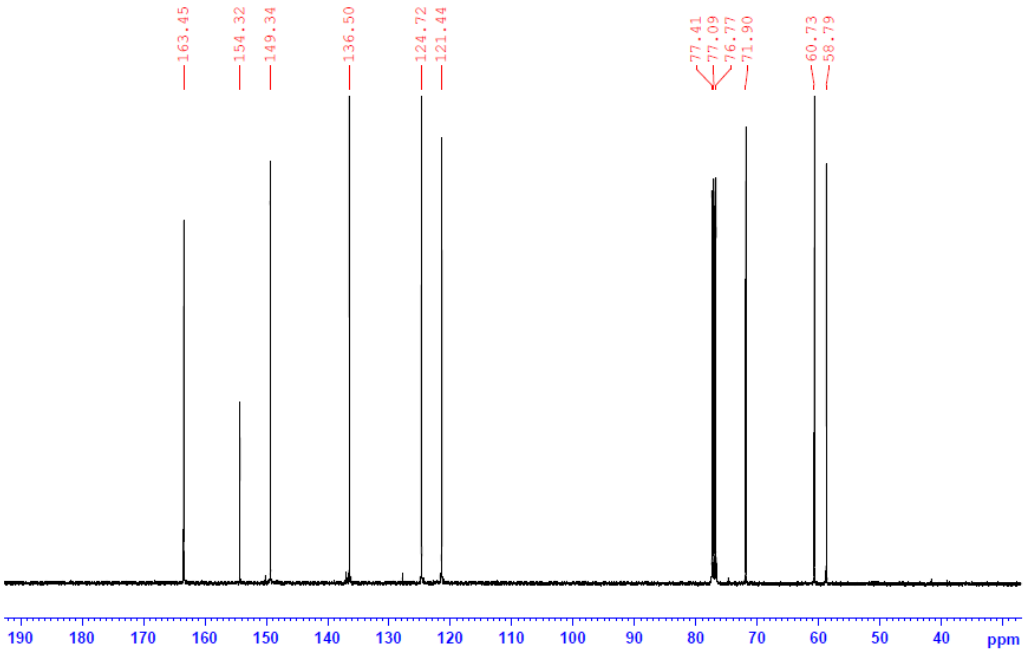

Figure 5.3: $^{13}C\{^{1}H\}$ NMR spectrum of **L6**

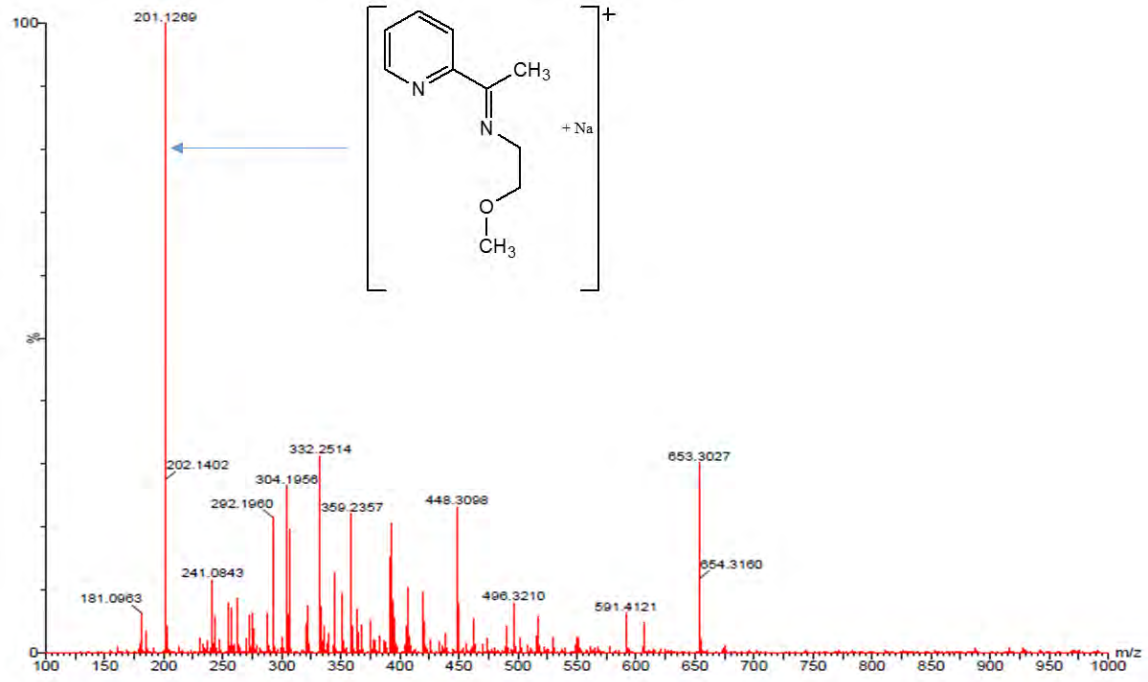

Figure 5.4: Mass spectrum of ligand **L5** showing base peak corresponding to sodium-coordinated molecular ion

Reactions of compounds **L1-L5** with [PdCl(Me)(cod)] afforded the corresponding neutral palladium(II) complexes **13-17** in good yields (Scheme 5.2). The complexes were also characterized by FT-IR spectroscopy, ^{1}H NMR spectroscopy, mass spectrometry and single-crystal X-ray crystallography for **13** and **14**. Treatment of the neutral complexes **13-17** with one equivalent of $NaBAr'_4$ in CH_2Cl_2 solvent afforded the respective cationic complexes **13a-17a** in moderate yields.

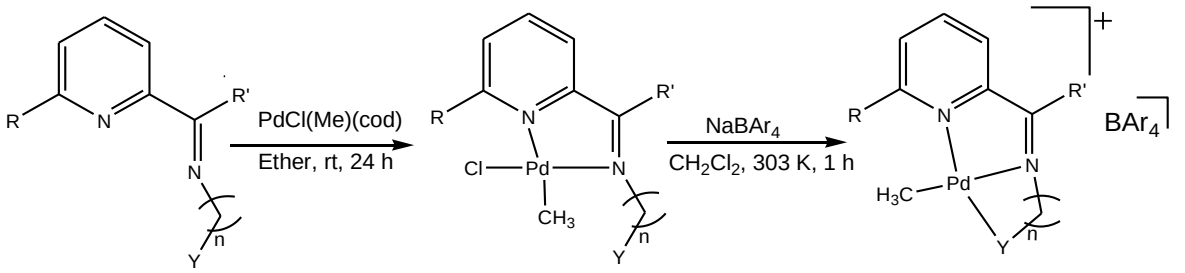

R = H, R' = Me, n = 2, Y= OMe (**13**)
R = H, R' = H, n = 2, Y= OMe (**14**)
R = H, R' = H, n = 3, Y= OMe (**15**)
R = H, R' = H, n = 2, Y= NEt_2 (**16**)
R = Br, R' = H, n = 2, Y= OMe (**17**)

R = H, R' = Me, n = 2, Y = OMe (**13a**)
R = H, R' = H, n = 2, Y = OMe (**14a**)
R = H, R' = H, n = 3, Y = OMe (**15a**)
R = H, R' = H, n = 2, Y = NEt_2 (**16a**)
R = Br, R' = H, n = 2, Y = OMe (**17a**)

Scheme 5.2: Syntheses of (imino)pyridine palladium(II) complexes

Comparison of ^{1}H and ^{13}C{^{1}H} NMR spectra of ligands **L5-L9** to the spectra of their corresponding palladium(II) complexes **13-17** provided valuable tool in structural elucidation of the complexes. Interestingly, two sets of signals were observed in the spectra of all the complexes in comparison to one set reported in the respective ligand spectra. For example, the ^{1}H NMR spectrum of complex **13** (Figure 5.5b) showed two set of peaks for each proton in 1:1 ratio. These sets of signals may be attributed to the presence of two isomers in which the methyl ligand is either *trans* or *cis* to the imino nitrogen atom.

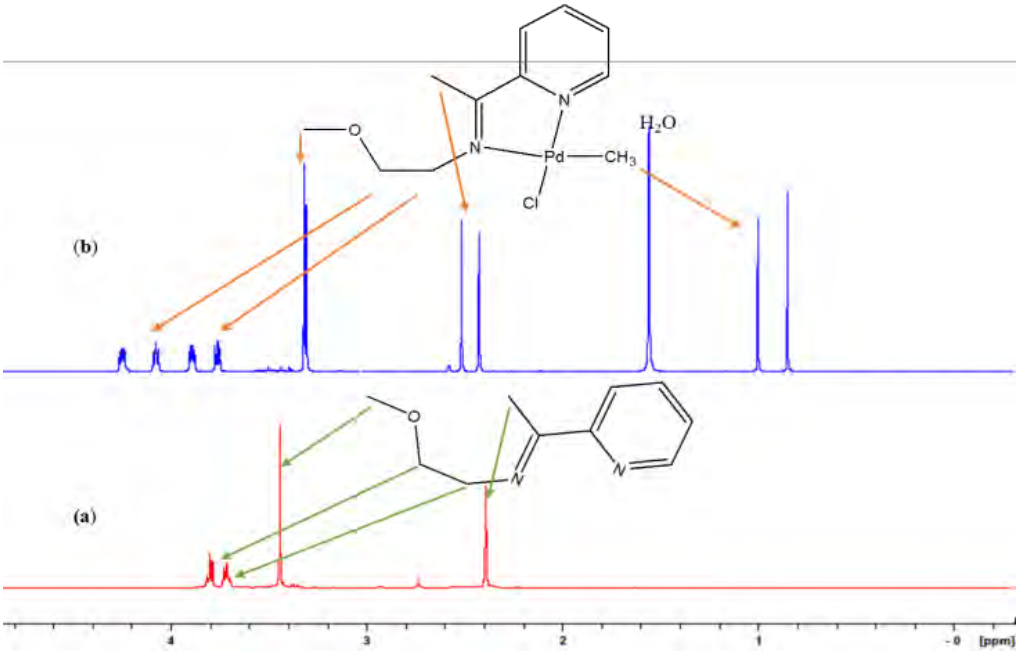

Figure 5.5: ^{1}H NMR spectra of ligand **L5** showing signature peaks of the protons on the pendant group of the pyridyl ligand (a), and complex **13**, (b), showing two sets of signals for each corresponding peak on the ligand (NMR solvent; $CDCl_3$).

The possibility of *trans-cis* isomerization was further deduced from the ^{1}H-^{1}H NOESY NMR of complex **14** (Figure 5.6). From the ^{1}H-^{1}H NOESY spectrum of complex **14**, the observation of a chemical exchange process between the methyl ligand protons (Pd-Me; 1.06 ppm) and the H_6 pyridine proton (8.66 ppm) established the formation of the isomer in which the methyl ligand is *trans* to the imino nitrogen. On the other hand, the observed correlation between the methyl ligand protons (0.94 ppm) and the methoxy protons (3.35 ppm) confirmed the occurrence of the isomer in which the methyl ligand is *cis* to the imino nitrogen, consistent with the solid state structure of **14** (vide infra).

On the other hand, ^{1}H NMR spectra of the cationic complexes **13a-17a**, showed only one set of signals for each proton. This could be due to loss of isomerism upon chloride abstraction. A typical ^{1}H NMR spectrum depicting the absence of two sets of signals is given for complex **14a** in Figure 5.7. An up-field shift of the CH_2CH_2 protons was observed which points to possible stabilization of the complex by the hemi-labile arm, as proposed in Scheme 5.2.

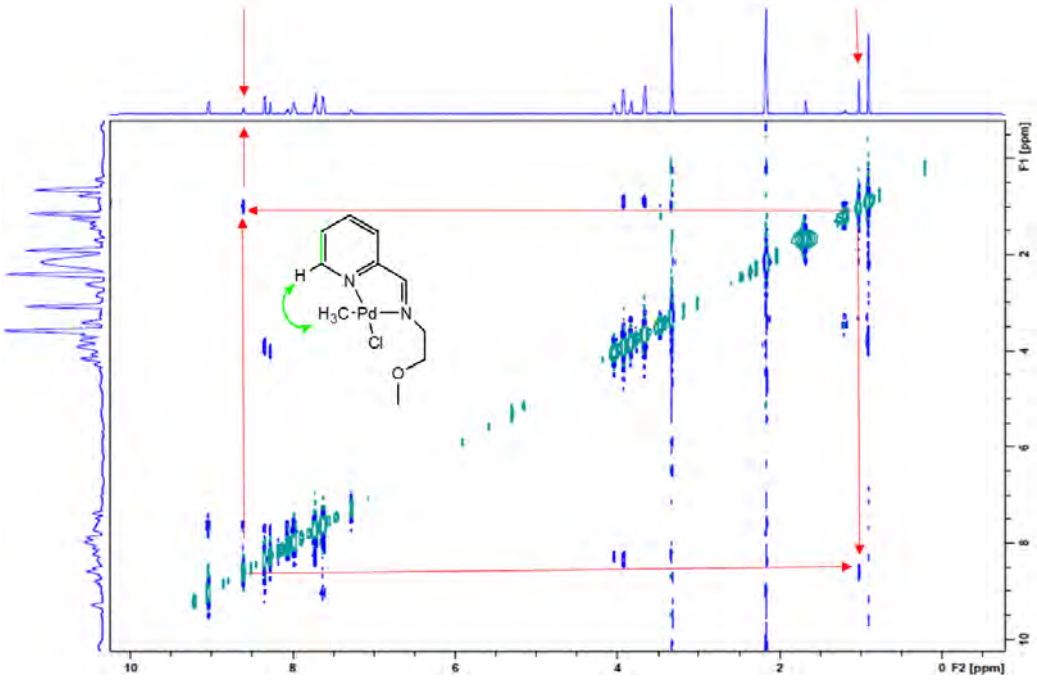

Figure 5.6: ^{1}H-^{1}H NOESY NMR spectrum of complex **14** showing correlation between protons py, H-6 (8.66 ppm) and Pd-Me (1.06 ppm) attributable to the *trans* isomer.

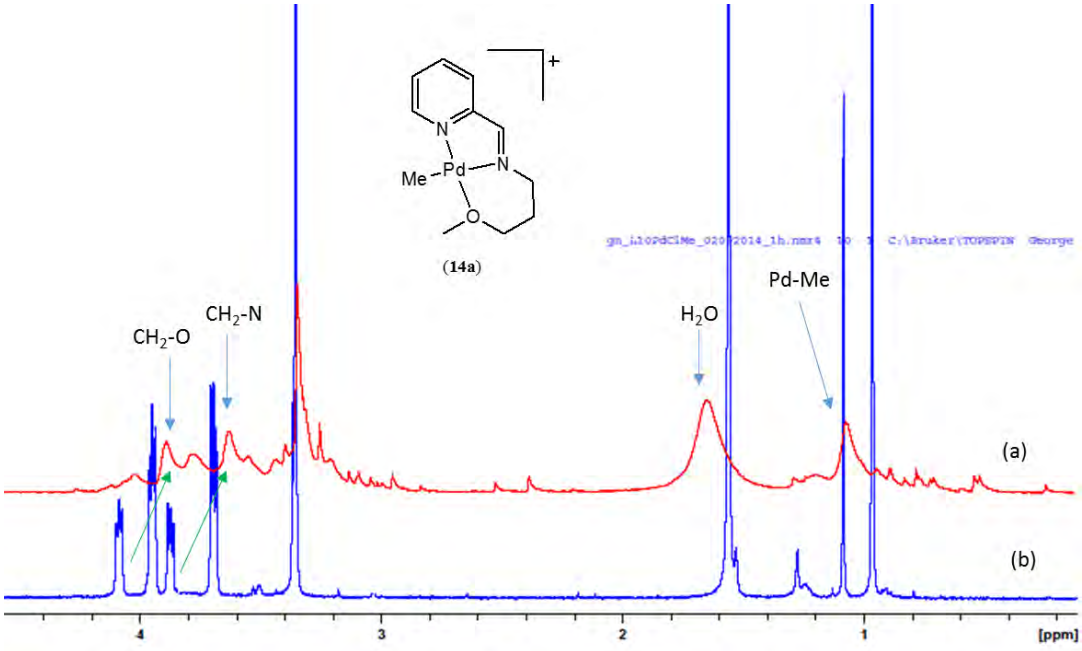

Figure 5.7: ^{1}H NMR spectra of complexes **14a** (a) showing single signals, in contrast to two sets of signals observed for complex **14** (b) (NMR solvent; $CDCl_3$).

In order to further understand the occurrence of the two sets of signals in the ^{1}H NMR spectra, variable temperature ^{1}H NMR studies were done between 30 to 90 °C for complex **14** (Figure 5.8). Indeed, no change in the appearance of the ^{1}H NMR spectrum was observed, even at 90 °C. This further confirms the existence of the thermodynamically stable *cis* and *trans* isomers, and rules out possible kinetic interconversion around the alkyl linkers to form chair and boat conformations.

This phenomenon of *trans-cis* isomerization in palladium(II) complexes has been reported in literature.[23-26] For example, in a report by Kress *et al*.[23] on the cationic complex [(Py-2-CMe=NAr)PdMe(MeCN)]$^{+}$BAf$_4^{-}$, the ^{1}H NMR spectrum exhibited two sets of resonances in an approximate ratio of 2:1 and was attributed to the presence of two geometrical isomers.

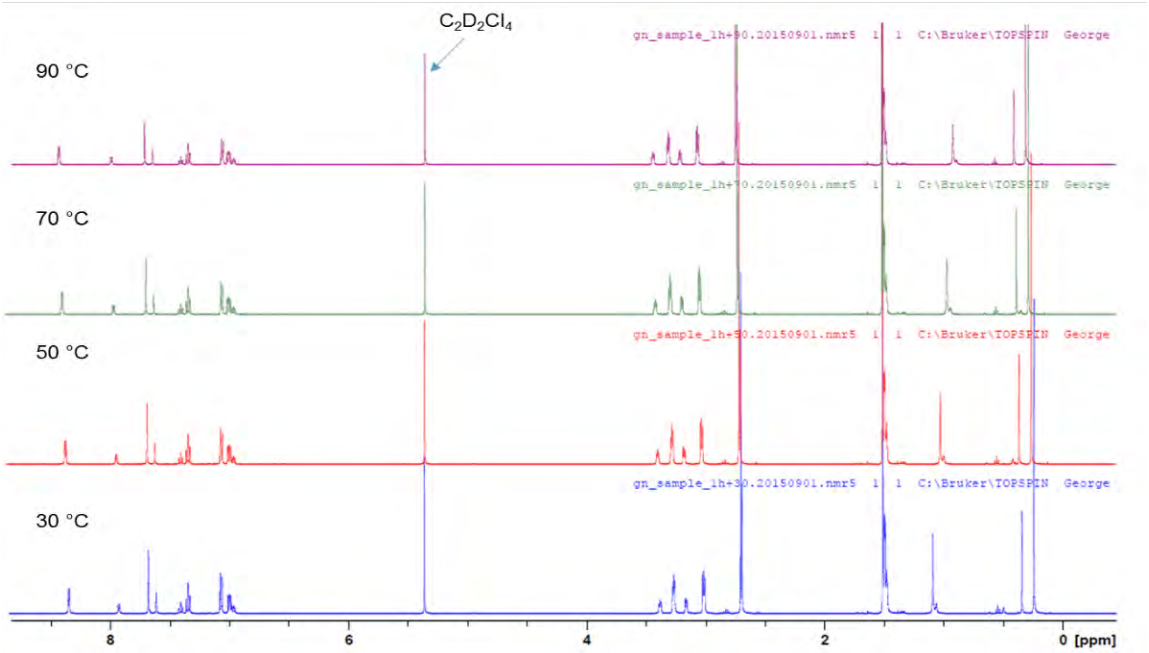

Figure 5.8: Variable temperature (30-90 °C) ^{1}H NMR spectrum of complex **14** showing two sets of signals for each corresponding peak of the ligand (NMR solvent; $C_2D_2Cl_4$). The independence of the spectrum of temperature confirms formation of *cis* and *trans* isomers and rules out kinetic interconversions between the chair and boat conformations.

Furthermore, DFT studies were also performed using two geometric isomers of complex **14** (**14-I** and **14-II**) using a split basis set LANL2DZ for palladium(II) and 6311G(dp) for the remaining atoms (Figure 5.9). From DFT calculations, the formation of both isomers **14-I** and **14-II** was thermodynamically feasible with a small energy difference of $\Delta E = 0.731$ kJ mol^{-1} between the *cis* and *trans* isomers. This corroborates well with the *trans-cis* labilisation theory as inferred from the ^{1}H and NOESY NMR spectroscopy data. Indeed, a more negative enthalpy value was obtained for isomer **14-I** in which the methyl group is *trans* to the pyridine consistent with the solid state structure of **14** (vide infra).

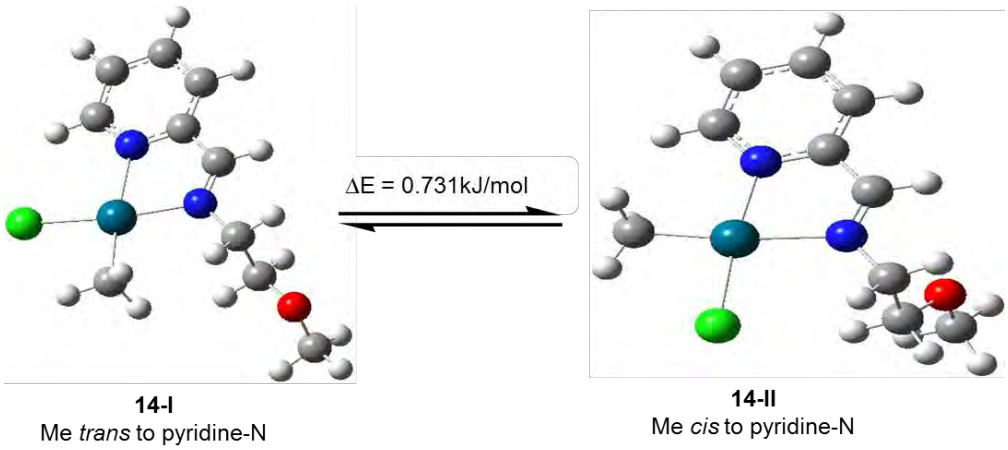

Figure 5.9: Optimized geometries of complex **14** computed using a split basis set LANL2DZ for palladium(II) and 6311G(dp) for the remaining atoms.

Complexes **13-17** were further characterized by mass spectrometry. The ESI mass spectra of complexes **13-16** showed various fragments attributed to the individual complexes. For example, the molecular ion of complex **16** showed a base peak at 326 (Figure 5.10) corresponding to the loss of a Cl-ligand. In addition, positive and negative ion mass spectral data were also collected for the cationic complexes **13a-17a** and confirmed the presence of both the cationic species, and the counter-anion, $[Bar'_4]^-$, as shown in Figure 5.11. Furthermore, FT-IR spectra of the complexes exhibited a shift of the absorption band of the imino group (C=N) from 1639–1651 cm^{-1} range in the free ligands to lower wavenumbers (1587-1595 cm^{-1}) in the complexes and further confirmed formation of complexes **13-17**.

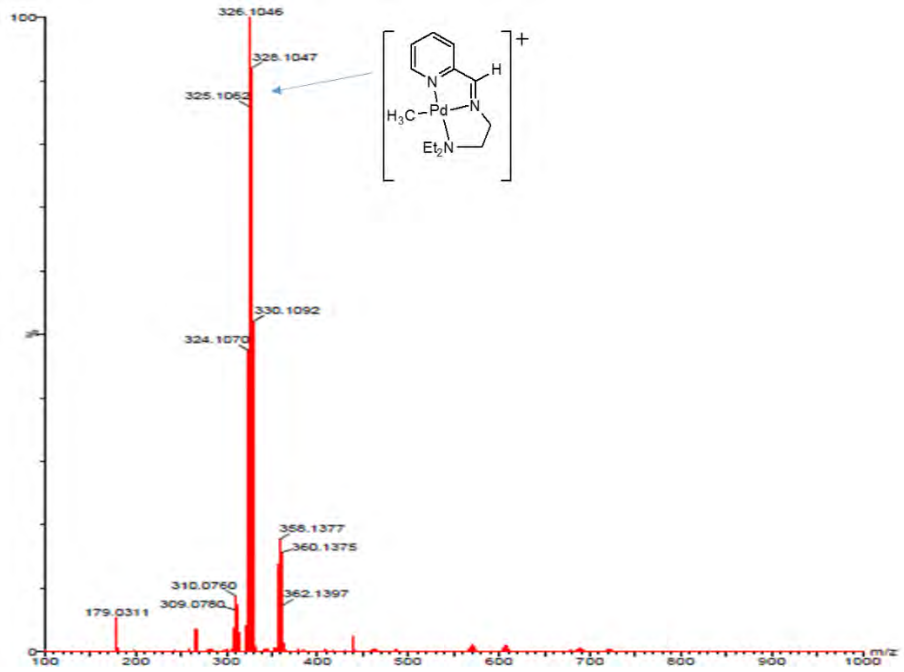

Figure 5.10: Mass spectrum of **16** showing the m/z = 326 (M^+-Cl).

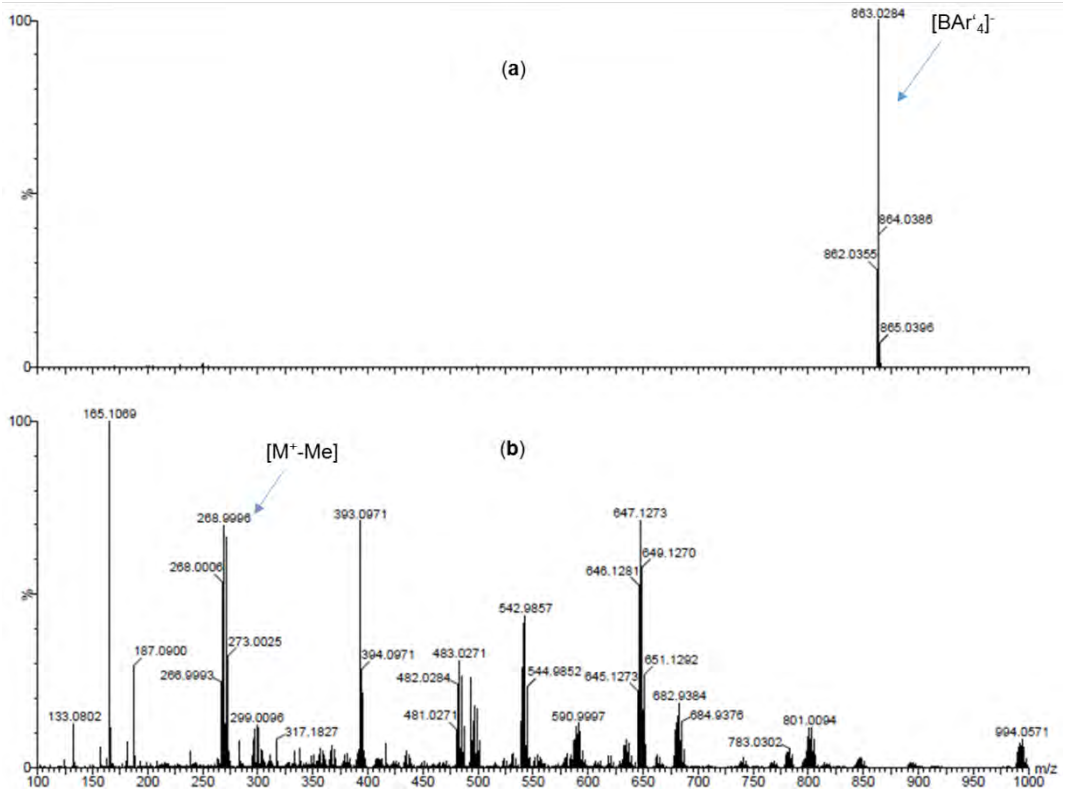

Figure 5.11: Positive and negative mass spectra of **14a** confirming the presence of both the counter-anion (a) and the cationic species (b).

5.3.2 Molecular structures of complexes 13 and 14

Single crystals of complexes **13** and **14** suitable for single crystal X-ray diffraction analyses were grown by slow evaporation of a methanolic solution of the respective complexes. The chloride and methyl groups of compound **13** (Figure 5.12) exhibit positional disorder.

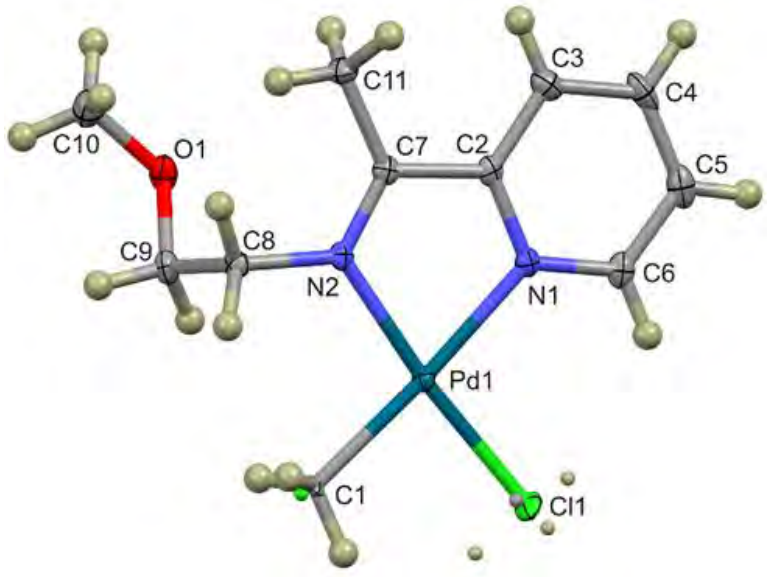

Figure 5.12: Thermal ellipsoid plot of **13** showing 50% probability surfaces. Hydrogen atoms and the atoms of the minor conformer have been rendered as spheres of arbitrary radius. Selected bond lengths [Å] and angles [°]: Pd(1)-N(2), 2.054(3); Pd(1)-C(1), 2.07(1); Pd(1)-N(1), 2.108(3); Pd(1)-Cl(1), 2.309(2); N(2)-Pd(1)-C(1), 96.9(3); N(2)-Pd(1)-N(1), 78.7(1); C(1)-Pd(1)-Cl(1), 88.7(3); N(3)-Pd(1)-Cl(1), 95.59(8). The reported bond lengths are those of the major conformer.

The dominant form comprises the chloride ligand *trans* to the imino N atom with a site occupancy of 87%. The conformation with the chloride ligand *cis* to the imino N atom is a minor component with 13% site occupancy. Compound **14** exhibits only a single conformer with the chloride ligand *trans* to the imino N atom. In complex **13**, the bidentate *N,N*' donor ligand coordinated the palladium(II) centre through the pyridyl and imino nitrogen atoms yielding a

five-membered chelation ring. The third and fourth coordination sites are occupied by methyl and chloride ligands. This yields a nominally square planar coordination geometry; expected for the d^8 metal ion.

The *cis* bond angles describing the coordination sphere range from 78.7(1)° to 96.9(3)°. The N–Pd–N bond angle is the most acute, as it is limited by the bite of the bidentate ligand. The N_{imine}–Pd–C_{methyl} bond angle is the most obtuse, this relatively large bond angle minimises non-bonded repulsion between the methyl ligand and the methylene hydrogen atoms. The Pd–Cl and Pd–C bond lengths measure 2.309(2) and 2.07(1) Å, respectively. The imine bond (C7–N2) measures 1.292(4) Å, highlighting the double bond character. The reported geometric parameters are those of the major conformer of complex **13**.

Complex **14** (Figure 5.13) has the same coordination geometry as complex **13**, i.e. square planar with the chloride ligand *trans* to the imino N atom. The *cis* bond angles describing the coordination sphere of complex **14** range from 78.8(1)° to 97.4(1)°. As with complex **13**, the N–Pd–N and N_{imine}–Pd–C_{methyl} bond angles are the most acute and obtuse angles, respectively. The Pd–Cl and Pd–C bond lengths measure 2.302(1) and 2.068(12) Å, respectively. These bond parameters are comparable to those of related palladium(II) compounds.[27] Crystallographic data and structural refinement parameters for **13** and **14** are given in Table 5.1.

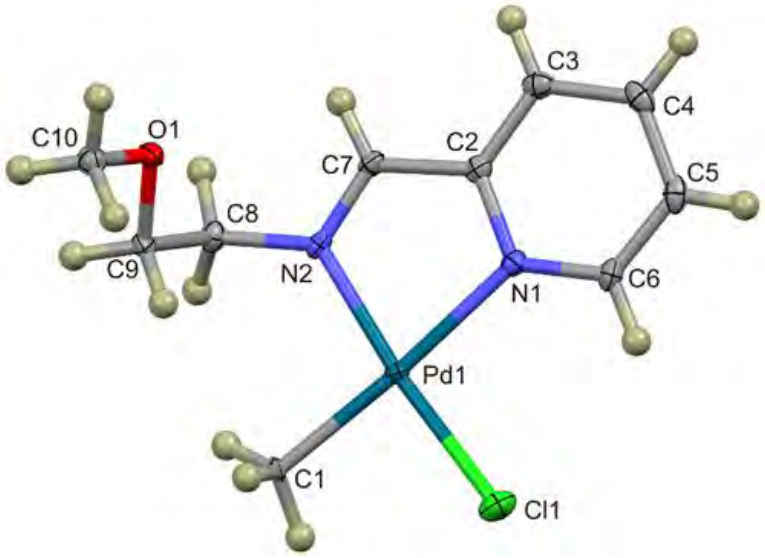

Figure 5.13: Thermal ellipsoid plot of **14** showing 50% probability surfaces. Hydrogen atoms and the atoms of the minor conformer have been rendered as spheres of arbitrary radius. Selected bond lengths [Å] and angles [°]:Pd(1)-N(2), 2.054(2); Pd(1)-C(1), 2.068(2); Pd(1)-N(1), 2.129(3); Pd(1)-Cl(1), 2.302(1); N(2)-Pd(1)-C(1), 97.4(1); N(2)-Pd(1)-N(1), 78.8(1); C(1)-Pd(1)-Cl(1), 88.36(8); N(3)-Pd(1)-Cl(1), 95.46(7).

Table 5.1: Crystal data and structure refinement details for complexes **13** and **14**.

Crystal data	**13**	**14**
Chemical formula	$C_{11}H_{17}ClN_2OPd$	$C_{10}H_{15}ClN_2OPd$
Molar mass (g mol^{-1})	335.11	321.09
Crystal system, space group	Monoclinic, $P2_1/c$	Triclinic, $P\bar{1}$
Temperature (K)	100(2)	100(2)
a, b, c (Å)	8.599(2), 20.087(4), 7.461(2)	8.535(2), 9.051(3), 9.068(2)
α, β, γ(°)	90, 105.232(4), 90	65.93(1), 66.01(2), 73.24(2)
V (Å)	1243.5(5)	578.0(3)
Z	4	2
Radiation type	Mo Kα	Mo Kα
μ (mm^{-1})	1.69	1.81
Crystal size (mm)	0.19 × 13 × 0.07	0.19 × 0.10 × 0.04
Data collection		
Diffractometer	Bruker APEXII CCD diffractometer	
Absorption correction	Multi-scan, *SADABS*, Bruker 2012	
T_{min}, T_{max}	0.740, 0.891	0.725, 0.931
No. of measured, independent and observed [$I > 2\sigma(I)$] reflections	7028, 2440, 2332	9372, 2259, 2156
R_{int}	0.026	0.025
Refinement		
$R[F^2 > 2\sigma(F^2)]$, $wR(F^2)$, S	0.027, 0.06, 1.16	0.021, 0.055, 1.10
No. of parameters	157	138
H-atom treatment	H atom parameters constrained	
$\Delta\rho_{max}$, $\Delta\rho_{min}$ (e Å^{-3})	0.60, −0.55	0.62, −0.49

5.3.3 Ethylene oligomerization reactions

The palladium(II) complexes **13**–**17** were evaluated as catalyst precursors in the oligomerization of ethylene using $NaBAr_4$ (Ar = 3,5-$(CF_3)_2C_6H_3$) and MAO as activators. In a typical experiment, approximately 10 μmol of the respective complex was reacted with either stoichiometric equivalent of $NaBAr_4$ in CH_2Cl_2 or 1 000-fold excess of MAO in toluene. In both cases, moderate activities were obtained to afford mainly butenes.

*5.3.3.1. Ethylene oligomerization reactions of complexes **13**–**17** using MAO activator*

The catalytic performance of the neutral palladium(II) catalyst precursors **13-17** in ethylene oligomerization was evaluated using MAO as a cocatalyst. The studies were carried out at 30 °C under 20 bar of ethylene pressure with Al/Pd ratios of 1 000 in toluene. The ethylene oligomerization results are summarized in Table 5.2. All the complexes showed modest catalytic activities in ethylene oligomerization displaying TOF of between 6 500 mol.ethylene.mol.$^{-1}$Pd.h^{-1} to 9 860 mol.ethylene.mol.$^{-1}$Pd.h^{-1}. More significantly, catalysts **13-17** displayed considerable selectivity towards butenes (84-91%) and small amounts of C_6 and C_8. The formation of these products was established and confirmed by GC and GC-MS. The greater selectivity towards C_4 oligomers reported for complexes **13-17**, may originate from lack of steric crowding/protection around the palladium atom.[28, 29] Thus chain propagation is not favored due to the reduced stability of the ethylene complex, which is the catalyst resting state.[29] It is therefore not surprising that all the catalysts (**13-17**) produced comparable amounts of C_4, (83-91%) due to their similar steric properties.

Few reports exist in literature in which palladium(II) catalysts produce exclusively butene oligomers in ethylene oligomerization reactions.[30-33] An example is the use of binuclear bis-α-diimine palladium(II) complexes and MAO as a co-catalyst[30] in which moderate selectivity towards butenes (75%) was observed. It is however important to note that in this particular report, appreciable amounts of C_6, C_8 and even trace amounts of higher olefins were obtained. The structure of the palladium(II) complexes was also observed to influence their catalytic activities. In particular, the substituents on the imine carbon played a significant role in controlling the catalytic activities of the resultant catalysts. For instance, complex **13** bearing a methyl substituent exhibited marginally lower activity of 7 060 mol.ethylene.mol.$^{-1}$Pd.h^{-1} than the unsubstituted complex **14** whose activity was 7 610 mol.ethylene.mol.$^{-1}$Pd.h^{-1} (Table 5.2, entries 1 and 2). In addition, increasing the length of the alkyl linker from ethylene (**14)** to a propyl (**15**) resulted in a decrease in TOF from 7 610 to 6 500 mol. ethylene/mol. Pd. h, respectively.

The enhanced catalytic activities of **14** relative to complexes **13** and **15** could be attributed to greater electrophilicity of palladium(II) center in **14** compared to **13** and **15**. The electron donating ability of the methyl and propyl groups in **13** and **15** are likely to decrease the positive charge on the metal atom, thus limit ethylene coordination.[31, 34, 35] Thus it is not surprising that the most active complex **5** (TOF = 9 860 mol. ethylene/mol. Pd. h), bears the more electron-withdrawing bromine substituent on the pyridine ring.[36]

Table 5.2: Ethylene oligomerization of neutral palladium(II) complexes **13-17** with MAO.[a]

Entry	Complex	Pressure (bar)	Time (h)	Al:M	TOF[b]	Product distribution and selectivity (%)[c]			
						C_4	**C_6**	**C_8**	**1-C_4**
1	**13**	20	1	1 000	7 060	87	11	2	94
2	**14**	20	1	1 000	7 610	84	13	3	96
3	**15**	20	1	1 000	6 500	86	13	1	95
4	**16**	20	1	1 000	6 630	91	8	1	97
5	**17**	20	1	1 000	9 860	86	12	2	96
6	**14**	5	1	1 000	1 030	78	16	6	95
7	**14**	10	1	1 000	4 180	81	14	5	96
8	**14**	30	1	1 000	9 770	89	9	2	96
9	**14**	20	0.5	1 000	6 340	84	15	1	97
10	**14**	20	2	1 000	4 820	81	16	3	93
11	**14**	20	4	1 000	2 760	81	15	4	89
12	**17**	20	0.5	1 000	7350	83	16	1	96
13	**17**	20	2	1 000	3890	80	18	2	92
14	**17**	20	4	1 000	1970	77	19	4	91
15	**14**	20	1	500	5 750	82	15	3	94
16	**14**	20	1	1 500	7 210	80	17	3	96

[a]Reaction conditions: nM = 10 μmol; solvent, toluene, 80 mL; temperature, 30 °C. [b]In units of (mol of ethylene)/((mol of Pd) h). [c]Determined by GC.

The nature of the pendant/hemi-labile arm was also noted to influence the activities of the resultant catalysts. For instance, substitution of a methoxy group in **14** by an amino group (**16**) led to a reduction in catalytic activity from 7 610 to 6 630 mol. ethylene/mol. Pd. h, respectively. This is likely to result from stronger coordination of the N to Pd (hard-soft acid base theory) thus hindering ethylene coordination. In hemi-labile ligand design, it is important for the labile donor atom to be weakly coordinating to allow substrate coordination.

A similar observation was made by Shi *et al*.[37] in ethylene oligomerization studies using palladium(II) complexes of hemi-labile P^N^O ligands. In their work, catalysts bearing an O–H group exhibited no catalytic activity due to the non-labile phenolate group that hindered ethylene coordination to the palladium(II). In another study, poor catalytic activities were reported for hemi-labile pyridyl-imine palladium(II) complexes bearing thiophene or furan groups; due to the inability of ethylene to displace the coordinated furan or thiophene groups.[6] It can therefore be concluded that the pendant arms in complexes **13**-**17** are weakly coordinating, enough to be displaced by the incoming ethylene monomer due to their observed catalytic activities.

*5.3.3.2 Effect of reaction conditions on ethylene oligomerization using complex **14***

Upon establishing that complexes **13**-**17** produce active catalysts in ethylene oligomerization, we used complex **14** to investigate the effect of reaction conditions on ethylene oligomerization reactions. First we varied the effect of ethylene pressure from 5 to 30 bar and observed an increase in catalytic activity from 1 030 to 9 770 mol. ethylene/mol. Pd. h, respectively. This could be attributed to higher monomer concentration favoring ethylene coordination to the

palladium(II) metal center.[32] More interesting was the greater selectivity towards C_4 oligomers at higher ethylene pressures. For examples, C_4 compositions of 78% and 89% were obtained at 5 and 30 bar, respectively; a phenomenon we attribute to increased chain termination at high pressures (Table 5.2, entries 2, 6, 7 and 8).

The effect of reaction time was probed by varying reaction period from 0.5 h to 2 h to shed more light on the stability of complex **14** (Table 5.2, entries 2, 9, 10 and 11). A two phase profile was observed. Thus, increasing the reaction time from 0.5 h to 1 h led to an increase in TOF from 6 340 mol.ethylene.mol.$^{-1}$Pd.h^{-1} to 7 610 mol.ethylene.mol.$^{-1}$Pd.h^{-1} (Table 5.2, entries 2 and 9). However, further increase of reaction time to 2 h and 4 h was marked by drastic decrease of TOF to 4 820 and 2 760 mol. ethylene/mol. Pd. h, respectively (Table 5.2, entries 10 and 11). This profile depicts an initiation/activation stage (between 0.5 h-1 h) and deactivation process after 1 h. Thus complex **14** can be said to be stable within 1 h of reaction time, after which it suffers from decomposition.[32, 38, 39]

Complex **17**, which was the most active, recorded a more drastic loss in TOF after longer reaction times. For example, TOFs of 9 860 mol.ethylene.mol.$^{-1}$Pd.h^{-1} and 970 mol.ethylene.mol.$^{-1}$Pd.h^{-1} were obtained within 1 and 4 h, respectively. These results are a clear illustration of the delicate balance between catalyst activity and stability. While complex **17** was more active than **14**, it was found to be far much less stable compared to **14**. We did not observe any significant influence on reaction time on product composition and selectivity of both catalysts **14** and **17**.

The effect of MAO concentration was also investigated by varying the Al/Pd ratio form 500 to 1 500. Increasing the co-catalyst to catalyst ratio (Al/Pd) from 500 to 1 000 resulted in an increase in catalytic activity from 5 750 mol.ethylene.mol.$^{-1}$Pd.h^{-1}to 7 610 mol. ethylene/mol. Pd. h, respectively. However, a further increase of the Al/Pd ratio to 1 500 was followed by a decrease in activity to 7 210 mol.ethylene.mol.$^{-1}$Pd.h^{-1} (Table 5.2, entries 2, 15 and 16). Thus a threshold Al/Pd ratio of 1 000 is required, beyond which catalyst deactivation occurs possibly due to buildup of trimethylaluminium impurities.[40, 41]

*5.3.3.3. Ethylene oligomerization reactions of complexes **13–17** using $NaBAr_4$ as activator*

In order to circumvent the limitations associated with MAO,[42] catalytically active cationic species were generated by reacting complexes **13-17** with NABAr'$_4$, *in situ*, in the presence of ethylene (Scheme 5.3) to afford the cationic complexes **13a**−**17a** following literature procedure.[39]

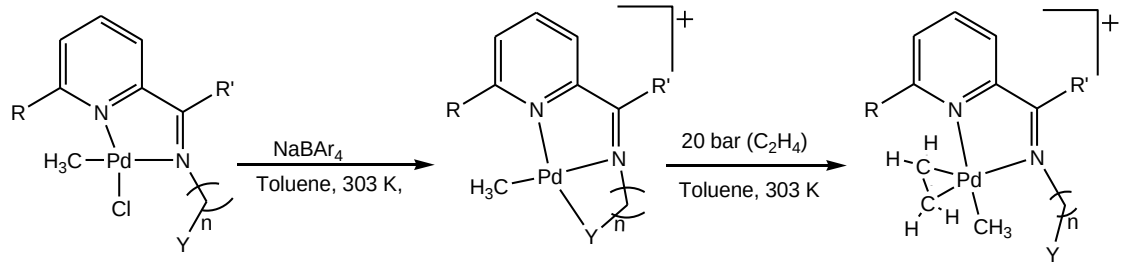

R = H, R' = Me, n = 2, Y= OMe (**13**)
R = H, R' = H, n = 2, Y= OMe (**14**)
R = H, R' = H, n = 3, Y= OMe (**15**)
R = H, R' = H, n = 2, Y= NEt_2 (**16**)
R = Br, R' = H, n = 2, Y= OMe (**17**)

R = H, R' = Me, n = 2, Y = OMe (**13a**)
R = H, R' = H, n = 2, Y = OMe (**14a**)
R = H, R' = H, n = 3, Y = OMe (**15a**)
R = H, R' = H, n = 2, Y = NEt_2 (**16a**)
R = Br, R' = H, n = 2, Y = OMe (**17a**)

R = H, R' = Me, n = 2, Y = OMe (**13b**)
R = H, R' = H, n = 2, Y = OMe (**14b**)
R = H, R' = H, n = 3, Y = OMe (**15b**)
R = H, R' = H, n = 2, Y = NEt_2 (**16b**)
R = Br, R' = H, n = 2, Y = OMe (**17b**)

Scheme 5.3: Generation of cationic palladium(II) and reactions with ethylene

The hemi-labile behaviour of these cationic complexes as depicted in Scheme 5.3 is not new. Shi *et al*.[37] investigated a similar phenomenon for palladium(II) complexes containing P^N^O donor ligands where the hemi-labile nature of the ether donor atom facilitated oligomerization

of ethylene. Table 5.3 shows the ethylene to oligomerization data obtained using cationic compounds **13a-17a** as catalysts.

The cationic catalysts **13a-17a** exhibited appreciable activities with TOFs between 4 840 mol.ethylene.mol.$^{-1}$Pd.h^{-1} to 7 310 mol.ethylene.mol.$^{-1}$Pd.h^{-1}. Generally, the activities of these cationic catalysts were lower compared to those of their respective neutral catalysts. For example, activities of 7 310 mol.ethylene.mol.$^{-1}$Pd.h^{-1} and 9 860 mol.ethylene.mol.$^{-1}$Pd.h^{-1} were obtained for catalysts **17a** and **5**/MAO, respectively. This trend could largely be attributed to the more Lewis acid MAO co-catalyst, which has the potential to afford more electrophilic palladium(II) metal centers in the active species.[43]

Table 5.3: Ethylene dimerization data of cationic palladium(II) complexes **13a-17a**.[a]

Entry	Catalyst	TOF[b]	% Product distribution[c]	
			C_4	**(α-C_4)**
1	**13a**	5580	>99	49
2	**14a**	6560	>99	61
3	**15a**	4840	>99	55
4	**16a**	5270	>99	59
5	**17a**	7310	>99	47

[a]Reaction conditions: [M] = 10 μmol; Time 2 h; Pressure, 20 bar; solvent, CH_2Cl_2, 80 mL; temperature, 30 °C; [b]mol. ethylene/mol. Pd. h. [c]Determined by GC.

In terms of product distribution, there was a significant shift of selectivity towards C_4 oligomers using cationic catalysts **13a-17a**. The product composition was mainly C_4 (>97%) in comparison to compositions of 83-91% obtained using the **13-17**/MAO systems. Thus, the use of MAO as a co-catalyst could be responsible for the lower selectivities reported for complexes **13-17**. Selective dimerization of ethylene using palladium(II) catalysts is rare, though few systems have

been reported in literature.[31-33] For example, palladium(II) complexes bearing phosphine-sulfonamide ligands[32] oligomerized ethylene to mainly butenes.

It is however, important to note that in these systems, as in the results of Kamer *et al*.,[44] few amounts of C_6, C_8 and even higher oligomers were reported further highlighting the unusual ease of chain termination steps using catalysts **13a-17a**. Another interesting observation was the lower fractions of α–C_4 using **13a-17a** (47-61%) compared to reactions using **13-17**/MAO catalytic system (94-97%). This was indicative of enhanced chain walking leading to isomerization reactions for catalysts **13a-17a**. A possible explanation to this trend could be reduced ethylene insertion into the Pd-H/Me bonds resulting from a more stable Pd-ethylene complex as the resting state. From these accounts, it is therefore conceivable that use of MAO and $NaBAr_4$ results in the formation of different active species.

5.3.3.4. DFT investigations of the activation and ethylene insertion barriers of the palladium(II) complexes.

In order to gain insight into the observed catalytic behaviour of palladium(II) complexes **13a-17a** and the role of the ligand structure, density functional theory (DFT) calculations were performed on the ground-state electronic structures of complexes **13a-17a** (Scheme 5.3). The computations were performed using a split basis set LANL2DZ for palladium(II) and 6311G(dp) for the remaining atoms. Table 5.4 shows the ethylene co-ordination thermodynamic data obtained for **13a-17a**.

Table 5.4: DFT calculated parameters of complexes **13a-17a**

Complex	**13a**	**14a**	**15a**	**16a**	**17a**
NBO charge, Pd	0.547	0.555	0.524	0.487	0.570
NBO charge, Pd[a]	0.463	0.456	0.443	0.452	0.453
$\Delta H_{Coordination}$ (Kcal/mol)	-11.89	-14.93	+2.02	-3.30	-18.90
$\Delta G_{Coordination}$ (Kcal/mol)	-2.25	-5.43	+9.55	+4.50	-9.25
Pd-Y (Å)	2.210	2.229	2.163	2.187	2.231
TOF[b]	5 580	6 560	4 840	5 270	7 310

[a]NBO charge (Pd) of ethylene-coordinated complexes, **13b-17b**. [b]mol. ethylene/mol. Pd. h.

A linear relationship between ethylene binding energy and catalytic activity was obtained (Figure 5.14). Thus it is clear that ethylene binding to the palladium(II) center greatly influenced the catalytic activities of the complexes. For example, while the most active catalyst **17a** (TOF = 7 310 mol. ethylene/mol. Pd. h) displayed negative/favorable binding energy (- ΔG = -9.25 Kcal/mol and ΔH = -18.90 Kcal/mol), the least active catalyst **15a** (TOF = 4 840 mol. ethylene/mol. Pd. h) exhibited higher binding energy of ΔG = + 4.50 Kcal/mol and ΔH = + 2.02 Kcal/mol.

The favorable binding energy in **17a** could be attributed to greater electrophilicity of the metal center in **17a** due to the electron-withdrawing ability of the bromide substituent. In comparison to literature values, ethylene binding energies of catalysts **13a-17a** are relatively higher than typical values of between -30 to -60 Kcal/mol.[45] In a study by Morokuma *et al.*,[46] ethylene binding energy for the Brookhart type α-diimine palladium(II) complexes of ΔG = -18.4 and ΔH = -29.4 kcal/mol were reported. This is consistent with the lower catalytic activities of **13a-**

17a compared to the Brookhart systems and might result from lower electrophilicity of the palladium(II) metal centers.

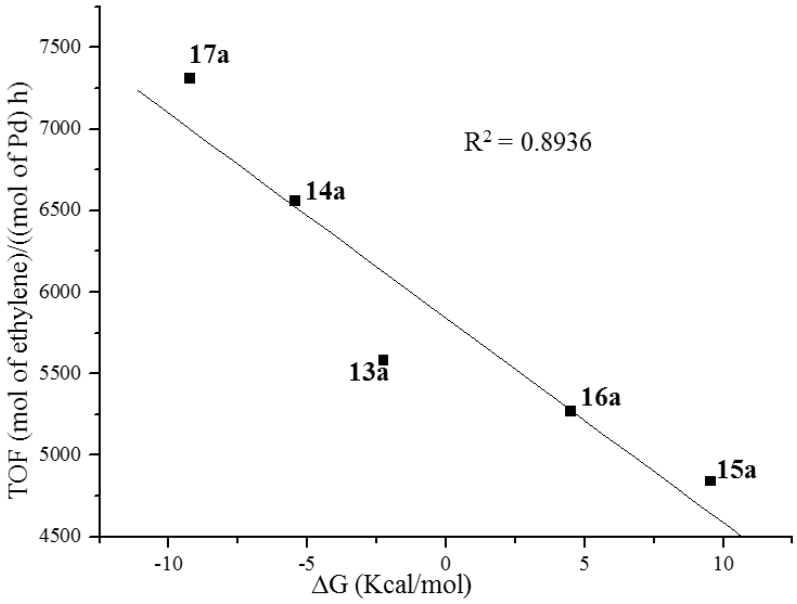

Figure 5.14: Plot of TOF in mol.ethylene.mol.$^{-1}$Pd.h^{-1} against ΔG (Kcal/mol) showing the dependence of catalytic performance on enthalpy of coordination.

The effect of NBO charges of the palladium(II) metal center and role of ligand motif on the catalytic activities of **13a**-**17a** is appreciated by a closer examination of the trend of turnover frequency versus NBO charges (Figure 5.15). Generally, higher catalytic activities were obtained with increase in the positive charge of the metal atom with exceptions of complex **16a** (different electron contribution of N donor atom compared to O atoms in complexes **13a**, **14a**, **15a** and **17a**). This trend may be due to enhanced rate of ethylene coordination to the palladium(II) center, the turnover-limiting step.[36]

From ligand design perspective, introduction of electron-donating methyl and propyl groups in **13a** and **15a**, respectively, might have led to more electron rich palladium(II) centers and consequently reduced catalytic activities. However, there is significant deviation from linearity which indicates that other factors, other than the net positive charge of metal center, influenced the catalytic behavior of these palladium(II) complexes.

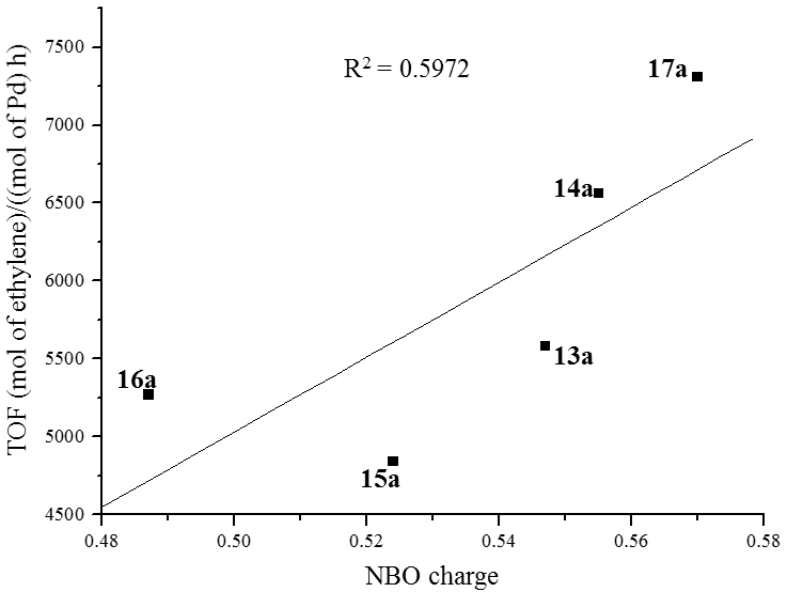

Figure 5.15: Plot of TOF (mol.ethylene.mol.$^{-1}$Pd.h^{-1}) against NBO charge illustrating the influence of NBO charge on catalytic activity.

Indeed complex **17a**, bearing electron-withdrawing group**,** exhibited the greatest NBO charge of 0.570 and concomitant highest catalytic activity of 7 310 mol. ethylene/mol. Pd. h. Consistent with literature reports,[47] coordination of ethylene to the palladium(II) metal centers lowered the net positive charges of the palladium(II). For example, while the net positive palladium(II) charge of **13a** and **17a** were recorded as 0.547 and 0.570, their corresponding ethylene-complexes were obtained as 0.463 and 0.453, respectively. It is therefore reasonable to argue that reduced electrophilicity of palladium(II) center upon ethylene coordination could have

promoted β-hydride elimination over chain propagation (subsequent ethylene coordination and insertion) thus accounting for the formation of mainly butenes.

One key component of hemi-labile ligands is the strength of the metal-ligand bond relative to the incoming monomer. We thus investigated the relationship between the Pd-Y bond length (Y= hemi-labile donor atom) and resultant catalytic activities of the complexes. From the DFT results, a general increase in Pd-Y bond length was followed by an increase in catalytic activity (Table 5.4 and Figure 5.16). For example, increase in Pd-Y bond length from 2.229 Å (**14a**) to 2.231 Å (**17a**) resulted in an increase in the catalytic activity from 6 560 to 7 310 mol. ethylene/mol. Pd. h. This trend could be largely attributed to increased possibility of displacement of the hemi-labile donor atom in **17a** compared to **14a** by the incoming ethylene monomer. This, thus, facilitates ethylene coordination to the palladium(II) metal center leading to enhanced catalytic activity observed in **17a** compared to **14a**.

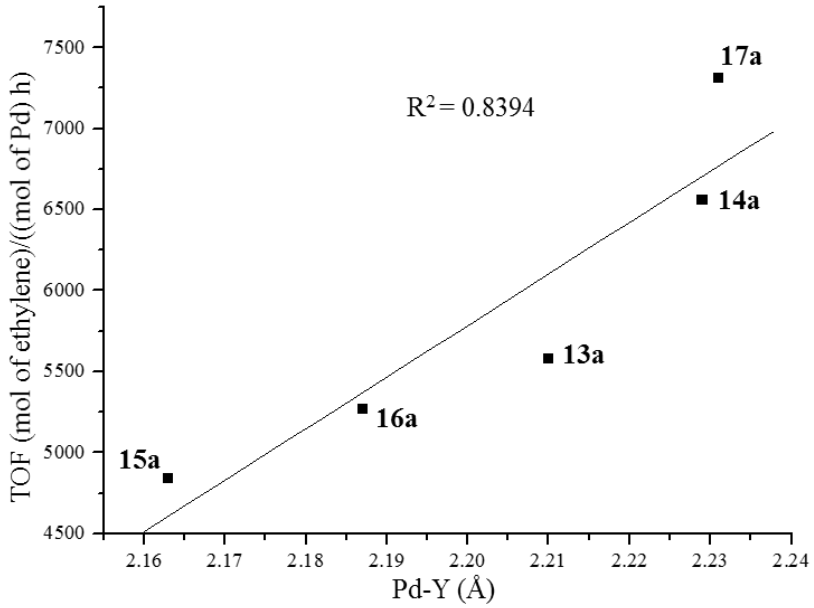

Figure 5.16: Plot of TOF in mol.ethylene.mol.$^{-1}$Pd.h^{-1} against Pd-Y (Å) depicting clear dependence of catalytic activity on the Pd-Y bond length.

5.3.3.5. Relative stabilities of cationic species ***13a-17a***

In an attempt to gain further insight into the observed catalytic behaviour of the cationic palladium(II) complexes **13a-17a**, the stability of these complexes was investigated in $CDCl_3$ at room temperature using ^1H NMR spectroscopy. This was done to establish the relationship between their stability and observed catalytic activities. In a typical experiment, half-lives of cationic complexes were determined by reacting equimolar amounts of **13-17** with $NaBAr_4$ in an NMR tube in $CDCl_3$ solution. The half-lives were established by monitoring the disappearance of the Pd-CH_3 peak using proton peaks of the BAr_4^- counter ion as an internal standard (Figure 5.17). Table 5.5 shows the relative half-lives and corresponding TOFs data for **13a-17a**.

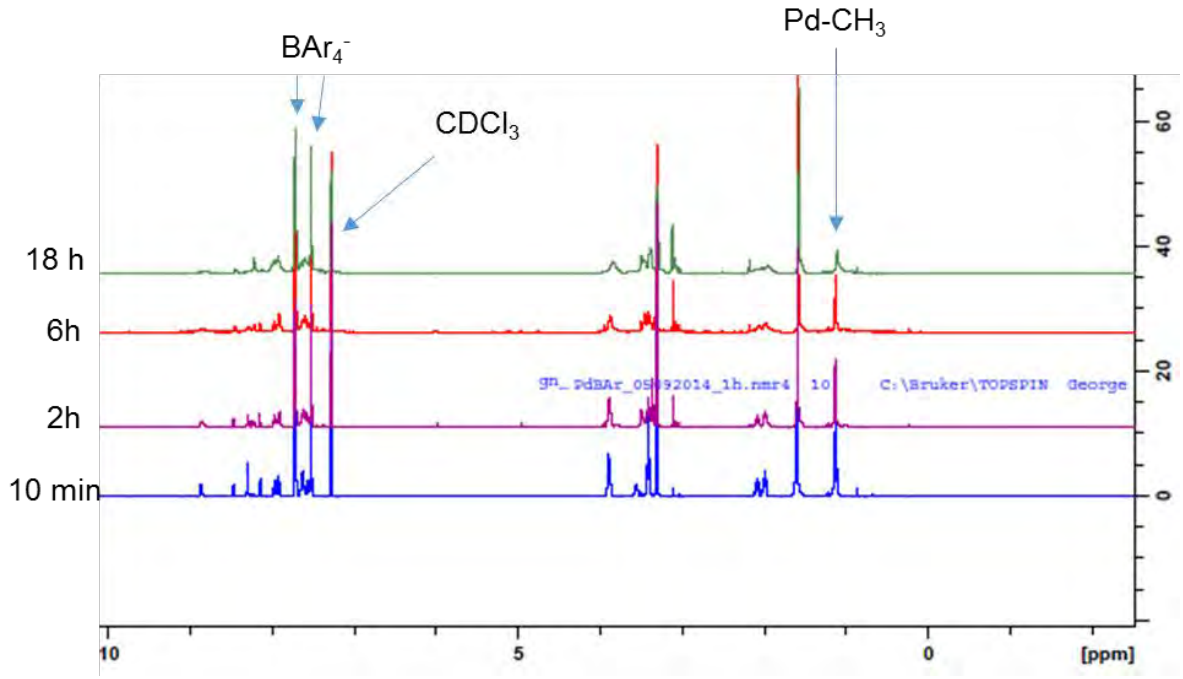

Figure 5.17: ^{1}NMR spectrum showing gradual decomposition of cationic species of **17a**

From Table 5.5, complex **17a** was found to be the least stable while complex **16a** was the most stable. Consistent with DFT studies, the lower stability of **17a** could arise from the higher

electrophilicity of the palladium(II) metal center due to the electron withdrawing bromide group. On the other hand, the greater donor abilities of the ligand systems in **13a**, **15a** and **16a** could be responsible for their observed longer half-lives and enhanced stabilities. What is more discerning from the results in Table 5.5 is the drastic decline in TOF of **17a** within 4 h in comparison to catalyst **14a**. For example, using **17a**, TOFs of 7 310 mol.ethylene.mol.$^{-1}$Pd.h^{-1} and 970 mol.ethylene.mol.$^{-1}$Pd.h^{-1} were obtained after 0.5 h and 4 h, respectively; translating to a drop in catalytic activity of 87%.

Table 5.5: Relative half-lives and catalytic activities of cationic species **13a**-**17a**[a]

Complex	$t_{½}$ ($CDCl_3$)	NBO charge	TOF[b] (0.5 h)	TOF[b] (4 h)
13a	17 h	0.547	5 580	3 130
14a	11 h	0.555	6 560	2 760
15a	16 h	0.524	4 840	2810
16a	27 h	0.487	5 270	2 970
17a	6 h	0.570	7 310	970

[a]Half-lives determined in $CDCl_3$ solvents by ^{1}H NMR spectroscopy using BAr'$_4$ protons as reference standard. Oligomerization conditions: pressure, 20 bar; nPd = nNaBAr$_4$ = 10 µmol; solvent, CH_2Cl_2; [b]In units of mol. ethylene/mol. Pd. h.

On the other hand, TOFs of 6 560 mol.ethylene.mol.$^{-1}$Pd.h^{-1} and 2 760 mol.ethylene.mol.$^{-1}$Pd.h^{-1} were recorded after 0.5 and 4 h, respectively, for **14a**; corresponding to a drop in activity of 58%. Notably, the catalytic activities of complexes **13a**-**17a** followed the trend, **15a<16a<13a<14a<17a** which was inversely proportional to the trend observed for their respective stabilities, **17a<14a<13a≈16a<15a**. Thus, the more active and electron deficient system (**17a**) exhibited the lowest stability over longer reaction times, consistent with the shorter half-life (6 h) observed.

5.4. Conclusions

Neutral and cationic palladium(II) complexes anchored on potential hemi-labile (imino)pyridine ligands have been synthesized and evaluated as catalyst precursors in ethylene oligomerization reactions. Activation of these palladium(II) complexes with either MAO or $NaBAr_4$ produced active catalysts for selective ethylene dimerization to mainly butenes. The catalytic activities of the complexes were largely controlled by the ligand architecture and the pedant arms in the complexes allowed for coordination of the incoming ethylene monomer. From DFT calculations, high ethylene binding energies point to possible competition for coordination to the palladium(II) metal center between the ethylene monomer and the pendant moieties in the ligand framework. The results in this work further demonstrate the delicate balance between catalyst activity and stability and provide valuable experimental and theoretical insight in rational ligand design.

5.5. References

1. Malinoski, J. M.; Brookhart, M., *Organometallics* **2003**, *22*, 5324-5335.
2. Chen, Q.; Yu, J.; Huang, J., *Organometallics* **2007**, *26*, 617-625.
3. Obuah, C.; Omondi, B.; Nozaki, K.; Darkwa, J., *J. Mol. Catal. A: Chem.* **2014**, *382*, 31-40.
4. Johnson, L. K.; Killian, C. M.; Brookhart, M., *J. Am. Chem. Soc.* **1995**, *117*, 6414-6415.
5. McGarrigle, E. M.; Gilheany, D. G., *Chem. Rev.* **2005**, *105*, 1563-1602.
6. Motswainyana, W. M.; Ojwach, S. O.; Onani, M. O.; Iwuoha, E. I.; Darkwa, J., *Polyhedron* **2011**, *30*, 2574-2580.
7. Ittel, S. D.; Johnson, L. K.; Brookhart, M., *Chem. Rev.* **2000**, *100*, 1169-1204.

8. Killian, C. M.; Tempel, D. J.; Johnson, L. K.; Brookhart, M., *J. Am. Chem. Soc.* **1996**, *118*, 11664-11665.
9. Carlini, C.; Marchionna, M.; Galletti, A. M. R.; Sbrana, G., *J. Mol. Catal. A: Chem.* **2001**, *169*, 79-88.
10. Deckers, P. J.; Hessen, B.; Teuben, J. H., *Angew. Chem. Int. Ed.* **2001**, *40*, 2516-2519.
11. Jeffrey, J. C.; Rauchfuss, T. B., *Inorg. Chem.* **1979**, *18*, 2658-2666.
12. Mecking, S.; Keim, W., *Organometallics* **1996**, *15*, 2650-2656.
13. Rülke, R.; Ernsting, J.; Spek, A.; Elsevier, C.; van Leeuwen, P. W.; Vrieze, K., *Inorg. Chem.* **1993**, *32*, 5769-5778.
14. Bruker *APEX2, SAINT and SADABS, Bruker AXS Inc*, Madison, : Wisconsin, USA, 2012.
15. Sheldrick, G. M., *Acta Crystallogr. Sect. A: Found. Crystallogr.* **2007**, *64*, 112-122.
16. Farrugia, L. J., *Appl. Crystallogr.* **2012**, *45*, 849-854.
17. Hay, P. J.; Wadt, W. R., *J. Chem. Phys.* **1985**, *82*, 270-283.
18. Becke, A. D., *J. Chem. Phys.* **1993**, *98*, 5648-5652.
19. Lee, C.; Yang, W.; Parr, R. G., *Phys. Rev. B* **1988**, *37*, 785-789.
20. Frisch, M. J. T., G. W.; Schlegel, H. B.; Scuseria, G. E.; Robb, M. A.; Cheeseman, J. R.; Scalmani, G.; Barone, V.; Mennucci, B.; Petersson, G. A.; Nakatsuji, H.; Caricato, M.; Li, X.; Hratchian, H. P.; Izmaylov, A. F.; Bloino, J.; Zheng, G.; Sonnenberg, J. L.; Hada, M.; Ehara, M.; Toyota, K.; Fukuda, R.; Hasegawa, J.; Ishida, M.; Nakajima, T.; Honda, Y.; Kitao, O.; Nakai, H.; Vreven, T.; Montgomery Jr., J. A.; Peralta, J. E.; Ogliaro, F.; Bearpark, M.; Heyd, J. J.; Brothers, E.; Kudin, K. N.; Staroverov, V. N.; Kobayashi, R.; Normand, J.; Raghavachari, K.; Rendell, A.; Burant, J. C.; Iyengar, S. S.; Tomasi, J.; Cossi, M.; Rega, N.; Millam, J. M.; Klene, M.; Knox, J. E.; Cross, J. B.; Bakken, V.; Adamo, C.; Jaramillo, J.;

Gomperts, R.; Stratmann, R. E.; Yazyev, O.; Austin, A. J.; Cammi, R.; Pomelli, C.; Ochterski, J. W.; Martin, R. L.; Morokuma, K.; Zakrzewski, V. G.; Voth, G. A.; Salvador, P.; Dannenberg, J. J.; Dapprich, S.; Daniels, A. D.; Farkas, O.; Foresman, J. B.; Ortiz, J. V.; Cioslowski, J.; Fox, D. J., Gaussian, Inc., Wallingford, CT. In *Gaussian*, 2010.

21. Singh, P.; Das, S.; Dhakarey, R., *J. Chem.* **2009**, *6*, 99-105.
22. Boudier, A.; Breuil, P.-A. R.; Magna, L.; Olivier-Bourbigou, H.; Braunstein, P., *J. Organomet. Chem.* **2012**, *718*, 31-37.
23. Meneghetti, S. P.; Lutz, P. J.; Kress, J., *Organometallics* **1999**, *18*, 2734-2737.
24. Obuah, C.; Ainooson, M. K.; Boltina, S.; Guzei, I. A.; Nozaki, K.; Darkwa, J., *Organometallics* **2013**, *32*, 980-988.
25. Ojwach, S. O.; Guzei, I. A.; Darkwa, J., *J. Organomet. Chem.* **2009**, *694*, 1393-1399.
26. Carfagna, C.; Gatti, G.; Paoli, P.; Binotti, B.; Fini, F.; Passeri, A.; Rossi, P.; Gabriele, B., *Organometallics* **2013**, *33*, 129-144.
27. Owen, G. R.; Burkill, H. A.; Vilar, R.; White, A. J.; Williams, D. J., *J. Organomet. Chem.* **2005**, *690*, 5113-5124.
28. Britovsek, G. J.; Gibson, V. C.; McTavish, S. J.; Solan, G. A.; White, A. J.; Williams, D. J.; Kimberley, B. S.; Maddox, P. J., *Chem. Commun.* **1998**, 849-850.
29. Britovsek, G. J.; Mastroianni, S.; Solan, G. A.; Baugh, S. P.; Redshaw, C.; Gibson, V. C.; White, A. J.; Williams, D. J.; Elsegood, M. R., *Chem. Eur. J.* **2000**, *6*, 2221-2231.
30. Netalkar, S. P.; Budagumpi, S.; Abdallah, H. H.; Netalkar, P. P.; Revankar, V. K., *J. Mol. Struct.* **2014**, *1075*, 559-565.
31. Swarts, A. J.; Zheng, F.; Smith, V. J.; Nordlander, E.; Mapolie, S. F., *Organometallics* **2014**, *33*, 2247-2256.

32. Zhang, Y.; Cao, Y.; Leng, X.; Chen, C.; Huang, Z., *Organometallics* **2014**, *33*, 3738-3745.

33. Mogorosi, M. M.; Mahamo, T.; Moss, J. R.; Mapolie, S. F.; Slootweg, J. C.; Lammertsma, K.; Smith, G. S., *J. Organomet. Chem.* **2011**, *696*, 3585-3592.

34. Milani, B.; Marson, A.; Scarel, A.; Mestroni, G.; Ernsting, J. M.; Elsevier, C. J., *Organometallics* **2004**, *23*, 1974-1977.

35. Ohno, K.; Nagasawa, A.; Fujihara, T., *Dalton Trans.* **2015**, *44*, 368-376.

36. Wang, S.; Sun, W.-H.; Redshaw, C., *J. Organomet. Chem.* **2014**, *751*, 717-741.

37. Shi, P.-Y.; Liu, Y.-H.; Peng, S.-M.; Liu, S.-T., *Organometallics* **2002**, *21*, 3203-3207.

38. Li, K.; Darkwa, J.; Guzei, I. A.; Mapolie, S. F., *J. Organomet. Chem.* **2002**, *660*, 108-115.

39. Oberhauser, W.; Manca, G.; Ienco, A.; Strabler, C.; Prock, J.; Weninger, A.; Gutmann, R.; Brüggller, P., *Organometallics* **2014**, *33*, 4067-4075.

40. Abbo, H. S.; Titinchi, S. J., *Molecules* **2013**, *18*, 4728-4738.

41. Adewuyi, S.; Li, G.; Zhang, S.; Wang, W.; Hao, P.; Sun, W.-H.; Tang, N.; Yi, J., *J. Organomet. Chem.* **2007**, *692*, 3532-3541.

42. Estenoz, D. A.; Chiovetta, M. G., *J. Appl. Polym. Sci.* **2001**, *81*, 285-311.

43. Zurek, E.; Ziegler, T., *Prog. Polym. Sci.* **2004**, *29*, 107-148.

44. Flapper, J.; Kooijman, H.; Lutz, M.; Spek, A. L.; van Leeuwen, P. W.; Elsevier, C. J.; Kamer, P. C., *Organometallics* **2009**, *28*, 1180-1192.

45. Deng, L.; Margl, P.; Ziegler, T., *J. Am. Chem. Soc.* **1997**, *119*, 1094-1100.

46. Musaev, D. G.; Svensson, M.; Morokuma, K.; Strömberg, S.; Zetterberg, K.; Siegbahn, P. E., *Organometallics* **1997**, *16*, 1933-1945.

47. Chang, M., *Bull. Korean Chem. Soc.* **1999**, *20*, 1269-1276.

CHAPTER 6

Ethylene oligomerization studies by nickel(II) complexes chelated by (amino)pyridine ligands: Experimental and density functional theory studies

6.1. Introduction

Oligomerization of ethylene currently constitutes one of the predominant industrial processes for the production of linear α-olefins (LAO), which are extensively used in the manufacture of a wide range of products such as oxo-alcohols used in detergents and plasticizers, poly-α-olefins for the synthetic lubricant pool, oil field chemicals and as comonomers for the production of linear low-density polyethylene (LLDPE).[1] The global LAO supply is dominated by the ''*full-range processes*'' of Chevron Phillips Chemical (CPChem), INEOS and Shell.[2] In recent years, significant progress has been made in selective oligomerization of ethylene, targeting a narrow product distribution. The quest for selective oligomerization of ethylene has been driven by the souring demand for C_4-C_{10} olefins for the production of linear low-density polyethylene resins (LLDPE).[3]

Originally, LAOs were manufactured by the Ziegler (Alfen) process[4] while the current industrial processes utilize catalysts that include either alkylaluminium compounds or a combination of alkylaluminium compounds with early transition metal compounds or the nickel(II) complex containing P-O chelate developed by Keim *et al*., the Shell higher olefin process (SHOP).[5, 6] In the past decade, transition-metal catalyzed oligomerization of ethylene to short chain α-olefins has attracted great attention in both academic and industrial research.[7, 8] When compared to

conventional catalysts, late-transition metal catalysts have the advantage of being less electrophilic and better tolerant to polar monomers.[9]

Since the discovery of the ‘‘nickel effect’’ in the 1960s by Wilke,[10] nickel is still playing a pivotal role in late transition metal catalysis for olefin oligomerization and polymerization, and continues to be one of the most studied metals in this field.[11] The commercialization of SHOP[5, 12] together with the discovery of α-diimine-type nickel(II) dichloride complexes[13-15] as highly active pre-catalysts for ethylene oligomerization and polymerization, revitalized research into nickel(II) systems for ethylene reactivity. The focus has fundamentally been on ligand design. The insights gained so far indicate that the ability to control the catalytic behavior of any new catalyst lies in the coordination environment which can be systematically varied by changing the substituents in the ligand.[16] Unfortunately, despite the extensive research, this influence of ligand environment on catalytic properties of a transition metal complex still remains a major challenge to predict.[17]

In Chapter 5, we reported a new family of palladium(II) complexes bearing a series of (imino)pyridine ligands which were found to dimerize ethylene with moderate activity upon activation with methylaluminoxane (MAO). In this Chapter, we have extended the use of these ligands to make nickel(II) complexes as potential catalysts in olefin oligomerization reactions. Despite the advantages offered by Schiff base ligands such as the ease of synthesis, the ability to stabilize metals in different oxidation states and the ability to fine-tune both the electronic and steric properties of the ligands, our attempts to synthesize (imino)pyridine nickel(II) complexes were not successful due to possible hydrolysis of the imine group in the ligands. Analyses of the

products by ^{1}H NMR spectroscopy confirmed ligand hydrolysis due to the signal observed at 9.00 ppm, associated with the aldehyde proton. Similar observations of metal mediated hydrolysis have been reported in literature.[18, 19] To circumvent this drawback, the imine ligands (**L5-L10**) were reduced to their analogous amines and subsequently used to prepare new (amino)pyridine nickel(II) complexes. Thus in this Chapter, we report the syntheses and characterization of these (amino)pyridine nickel(II) complexes and their behavior as ethylene oligomerization catalysts.

6.2. Experimental section

6.2.1. Materials and methods

All synthetic manipulations were performed using standard Schlenk techniques under a nitrogen atmosphere. All solvents were dried by distillation prior to use. Nickel(II) bromide-1,2-dimethoxyethane complex [$NiBr_2$(DME)], sodium borohydride ($NaBH_4$), 2-(methoxy)-ethyl-amine, 2-pyridinecarboxaldehyde, 2-acetylpyridine, N,N-(diethyl)ethylenediamine and ethanolamine were obtained from Sigma-Aldrich and used as received. ^{1}H NMR and $^{13}C\{^{1}H\}$ NMR spectra were recorded on a Bruker 400 MHz spectrometer in $CDCl_3$ solution at room temperature using tetramethylsilane as an internal standard. Elemental analyses were performed on a Thermal Scientific Flash 2000 while ESI-mass spectra were recorded on an LC premier micro-mass spectrometer. The infrared spectra were recorded on a Perkin-Elmer spectrum 100 in the 4000-650 cm^{-1} range. Magnetic moments of the complexes were determined using Evans balance. GC analyses were performed using a Varian CP-3800 gas chromatograph equipped with a CP-Sil 5 CB (30 m × 0.2 mm × 0.25 μm) capillary column while GC‑MS analyses were performed on a Shimadzu GC‑MS-QP2010.

6.2.2. Syntheses of (amino)pyridine ligands and their nickel(II) metal complexes

*6.2.2.1. N-(2-methoxyethyl)-1-(pyridin-2-yl)ethanamine (**L5a**)*

To a methanol solution of 2-methoxy-N-(1-(pyridin-2-yl)ethylidene)ethanamine (0.5 g, 2.80 mmol) was added $NaBH_4$ (0.53 g, 14.03 mmol) and stirred at 25 °C for 4 h. The brown solution of 2-methoxy-N-(1-(pyridin-2-yl)ethylidene)ethanamine changed to light orange during this period. The solvent was evaporated and the resulting liquid was then re-dissolved in $CHCl_3$ and washed once with 20 mL of deionised water. The organic layer was dried over anhydrous $MgSO_4$ and reduced under vacuum to afford **L5a** as light orange oil. Yield = 0.42 g (83%). ^1H NMR (400 MHz, $CDC1_3$): δ 1.39 (d, 3H, $^3J_{HH}$ = 6.8 Hz, CH_3); 2.59 (t, 1H, $^3J_{HH}$ = 6.0 Hz, CH_2-NH); 2.69 (t, 1H, $^3J_{HH}$ = 6.0 Hz, CH_2-NH); 3.34 (s, 3H, CH_3-O); 3.45 (t, 1H, $^3J_{HH}$ = 6.0 Hz, CH_2-O); 3.60 (t, 1H, $^3J_{HH}$ = 6.0 Hz, CH_2-O); 3.87 (q, 1H, $^3J_{HH}$ = 6.8 Hz, CH-NH); 7.33 (d, 1H, $^3J_{HH}$ = 7.6 Hz, 3-py-H); 7.62 (m, 2H, $^3J_{HH}$ = 7.6 Hz, 4,5-py-H); 8.54 (d, 1H, $^3J_{HH}$ = 7.6 Hz, 6-py-H). $^{13}C\{^1H\}$ NMR ($CDC1_3$): δ 17.18 (CH_3-C), 46.57 (CH_2-N), 58.65 (CH_3-O), 60.28 (CH-N), 71.79 (CH_2-N), 121.51 (3-py), 124.34 (5-py), 136.68 (4-py), 149.19 (6-py), 163.32 (2-py). FT-IR (cm^{-1}): 3313 υ(NH). Anal. Calcd for $C_{10}H_{16}N_2O{\cdot}0.25CHCl_3$: C, 58.60; H, 7.80; N, 13.33. Found: C, 58.78; H, 7.71; N, 13.41.

Compounds **L6a, L8a** and **L10a** were prepared following the same procedure as described for compound **L5a**, using the appropriate reagents.

*6.2.2.2. 2-methoxy-N-((pyridin-2-yl)methyl)ethanamine (**L6a**)*

2-methoxy-N-((pyridin-2-yl)methylene)ethanamine (0.50 g, 3.05 mmol) was reacted with $NaBH_4$ (0.58 g, 15.24 mmol) to give a light orange oil. Yield = 0.44 g (87%). ^1H NMR (400

MHz, $CDC1_3$): δ 2.82 (t, 2H, $^3J_{HH}$ = 5.6 Hz, CH_2-NH); 3.34 (s, 3H, CH_3-O); 3.51 (t, 2H, $^3J_{HH}$ = 5.6 Hz, CH_2-O); 3.93 (s, 2H, CH_2-py); 7.12 (dd, 1H, $^3J_{HH}$ = 8.0 Hz, 4-py-H); 7.30 (d, 1H, $^3J_{HH}$ = 8.0 Hz, 6-py-H); 7.60 (dd, 1H, $^3J_{HH}$ = 8.0 Hz, 5-py-H); 8.53 (d, 1H, $^3J_{HH}$ = 8.0 Hz, 3-py-H). $^{13}C\{^1H\}$ NMR ($CDC1_3$): δ 48.68 (CH_2-N), 54.67 (CH_2-py), 58.79 (CH_3-O), 71.54 (CH_2-O), 121.11 (5-py), 122.33 (3-py), 136.57 (4-py), 149.27 (6-py), 158.73 (2-py). FT-IR (cm^{-1}): 3366 υ(NH). ESI-MS: m/z (%) 167 [M^+, 100%]; 189 [$(M + Na)^+$, 55%]. Anal. Calcd for $C_9H_{14}N_2O$: C, 65.03; H, 8.49; N, 16.85. Found: C, 65.46; H, 8.06; N, 16.52.

*6.2.2.3. N,N-diethyl-N-((pyridin-2-yl)methyl)ethane-1,2-diamine (**L8a**)*

N,N-diethyl-N-((pyridin-2-yl)methylene)ethane-1,2-diamine (0.50 g, 2.44 mmol) was reacted with $NaBH_4$ (0.46 g, 12.18 mmol) to give a light orange oil. Yield = 0.47 g (94%).^{1}H NMR (400 MHz, $CDC1_3$): δ 0.98 (t, 6H, $^3J_{HH}$ = 7.2 Hz, CH_3-Et_2); 2.48 (q, 4H, $^3J_{HH}$ = 7.2 Hz, CH_2-Et_2); 2.57 (t, 2H, $^3J_{HH}$ = 6.4 Hz, CH_2-NH); 2.69 (t, 2H, $^3J_{HH}$ = 6.4 Hz, CH_2-N); 3.92 (s, 2H, CH_2-py); 6.20 (d, 1H, $^3J_{HH}$ = 8.0 Hz, 6-py-H); 7.30 (d, 1H, $^3J_{HH}$ = 8.0 Hz, 3-py-H); 7.60 (dd, 1H, $^3J_{HH}$ = 8.0 Hz, 4-py-H); 8.53 (dd, 1H, $^3J_{HH}$ = 8.0 Hz, 5-py-H). $^{13}C\{^1H\}$ NMR ($CDC1_3$): δ 11.58 (CH_3-Et_2), 46.13 (CH_2-NH), 47.05 (CH_2-Et_2), 52.56 (CH_2-N), 55.16 (CH_2-py), 121.86 (3-py), 122.17 (5-py), 136.39 (4-py), 149.22 (6-py), 159.76 (2-py). FT-IR (cm^{-1}): 3304. υ(NH). ESI-MS: m/z (%) 208 [M^+, 100%]; 230 [$(M + Na)^+$, 81%]. Anal. Calcd for $C_{12}H_{21}N_3 \cdot 0.5CHCl_3$: C, 56.23; H, 8.12; N, 15.74. Found: C, 55.96; H, 7.66; N, 15.27.

*6.2.2.4. 2-((pyridin-2-yl)methylamino)ethanol (**L10a**)*

2-((pyridin-2-yl)methyleneamino)ethanol (0.50 g, 3.33 mmol) was reacted with $NaBH_4$ (0.63 g, 16.65 mmol) to give a light brown oil. Yield = 0.44 g (87%). ^{1}H NMR (400 MHz, $CDC1_3$): δ

2.76 (t, 2H, $^{3}J_{HH}$ = 5.4 Hz, CH_2-NH); 3.62 (t, 2H, $^{3}J_{HH}$ = 5.4 Hz, CH_2-O); 3.88 (s, 2H, CH_2-py); 7.11 (dd, 1H, $^{3}J_{HH}$ = 7.6 Hz, 4-py-H); 7.24 (d, 1H, $^{3}J_{HH}$ = 7.6 Hz, 6-py-H); 7.59 (dd, 1H, $^{3}J_{HH}$ = 7.6 Hz, 5-py-H); 8.48 (d, 1H, $^{3}J_{HH}$ = 7.6 Hz, 3-py-H). $^{13}C\{^{1}H\}$ NMR ($CDC1_3$): δ 51.07 (CH_2-NH), 54.35 (CH_2-py), 60.73 (CH_2-O), 122.11 (5-py), 122.48 (3-py), 136.72 (4-py), 149.05 (6-py), 159.30 (2-py). FT-IR (cm^{-1}): 3278. υ(NH) ESI-MS: m/z (%) 153 [M^+, 100%]; 175 [$(M + Na)^+$, 27%]. Anal. Calcd for $C_8H_{12}N_2O$: C, 63.13; H, 7.95; N, 18.41. Found: C, 62.88; H, 7.49; N, 18.07.

6.2.2.5. Bis{2-methoxyethyl-1-(pyridin-2-yl)ethanamine}1NiBr₂ ***(18)***

A THF solution (5 mL) of **L5a** (0.10 g, 0.55 mmol) was added to a THF solution (5 mL) of [$NiBr_2$DME] (0.17 g, 0.55 mmol). The reaction mixture turned dark brown immediately and was allowed to stir for 24 h. The resultant precipitate was then isolated by filtration, washed with diethyl ether to afford complex **18** as a brown solid. Yield = 0.17 g (76%). FT-IR (cm^{-1}): 3402 υ(NH). ESI-MS: m/z (%) 317 [$(M-Br)^+$, 100%]. μ_{eff} = 3.72 BM. Calcd for $C_{20}H_{32}Br_2N_4NiO_2 \cdot 4H_2O$: C, 36.90; H, 6.19; N, 8.61. Found: C, 37.01; H, 5.92; N, 8.64.

Complexes **19-21** were prepared following the procedure described for complex **18**.

6.2.2.6. Bis{2-methoxy-N-((pyridin-2-yl)methyl)ethanamine}NiBr₂] ***(19)***

[$NiBr_2$DME] (0.19 g, 0.60 mmol) and **L6a** (0.10 g, 0.60 mmol). Green solid was formed which on recrystallization from $CHCl_3$ solution afforded green crystals suitable for single-crystal X-ray analysis Yield: 0.17 g (75%). FT-IR (cm^{-1}): 3238. υ(NH). ESI-MS: m/z (%) 304 [$(M-Br)^+$,

100%]. μ_{eff} = 3.77 BM. Calcd for $C_{18}H_{28}Br_2N_4NiO_2$: C, 39.24; H, 5.12; N, 10.17. Found: C, 39.57; H, 5.65; N, 10.53.

*6.2.2.7. Bis{N,N-diethyl-N-((pyridin-2-yl)methyl)ethane-1,2-diamine}$NiBr_2$ (**20**)*

[$NiBr_2$DME] (0.15 g, 0.48 mmol) and **L8a** (0.10 g, 0.48 mmol). Green solid. Yield: 0.16 g (79%). FT-IR (cm^{-1}): 3393. υ(NH). ESI-MS: m/z (%) 346 [$(M-Br)^+$, 25%]; 264 [$(M-Br_2)^+$, 100%]. μ_{eff} = 3.70 BM. Calcd for $C_{24}H_{42}Br_2N_6Ni$: C, 42.82; H, 5.75; N, 12.48. Found: C, 43.13; H, 6.22; N, 12.86.

*6.2.2.8. Bis{2-((pyridin-2-yl)methylamino)ethanol}$NiBr_2$ (**21**)*

[$NiBr_2$DME] (0.20 g, 0.66 mmol) and **L10a** (0.10 g, 0.66 mmol). Violet solid was formed which on recrystallization from $CHCl_3$ solution afforded violet crystals suitable for single-crystal X-ray analysis. Yield: 0.20 g (83%). FT-IR (cm^{-1}): 3069. υ(NH). ESI-MS: m/z (%) 290 [$(M-Br)^+$, 49%]; 209 [$(M-Br_2)^+$, 27%]. μ_{eff} = 3.75 BM. Calcd for $C_{16}H_{24}Br_2N_4NiO_2 \cdot 2H_2O$: C, 34.38; H, 5.05; N, 10.02. Found: C, 34.41; H, 4.58; N, 10.02.

6.2.3. X-ray crystallography

X-ray data collection for compounds **19** and **21** were recorded on a Bruker Apex Duo diffractometer equipped with an Oxford Instruments Cryojet operating at 100(2) K and an Incoatec microsource operating at 30 W power. Crystal and structure refinement data are given in Table 6.1. For both structures the data were collected with Mo Kα (λ = 0.71073 Å) radiation at a crystal-to-detector distance of 50 mm. The data collections were performed using omega and phi scans with exposures taken at 30 W X-ray power and 0.50° frame widths using

APEX2.[20] The data were reduced with the programme SAINT[20] using outlier rejection, scan speed scaling, as well as standard Lorentz and polarisation correction factors. A SADABS semi-empirical multi-scan absorption correction[20] was applied to the data. Direct methods, SHELXS-97[21] and WinGX[22] were used to solve both structures. All non-hydrogen atoms were located in the difference density map and refined anisotropically with SHELXL-97.[21] All hydrogen atoms were included as idealized contributors in the least squares process. Their positions were calculated using a standard riding model with C–$H_{aromatic}$ distances of 0.95 Å and U_{iso} = 1.2 U_{eq}, C–$H_{methylene}$ distances of 0.99 Å and U_{iso} = 1.2 Ueq and C–H_{methyl} distances of 0.98 Å and U_{iso} = 1.5 Ueq. The amine N-H and hydroxyl O–H and water hydrogen atoms were located in the difference density map and refined isotropically.

6.2.4. General procedure for ethylene oligomerization reactions

Ethylene oligomerization reactions were carried out in a 400 mL stainless steel Parr reactor equipped with a mechanical stirrer, temperature controller and an internal cooling system. In a typical experiment, the reactor was preheated to 100 °C in *vacuo* and cooled to room temperature. An appropriate amount of the catalyst precursor (10.0 μmol) was transferred into a dry Schlenk tube under nitrogen and toluene (20 mL) was added using a syringe. The required amount of co-catalyst ($EtAlCl_2$ or MAO) was then injected into the Schlenk tube containing the pre-catalyst, and the resultant solution was transferred *via* cannula into the reactor. An additional 60 mL of toluene solvent was also transferred *via* cannula into the reactor giving a total volume of 80 mL. The reactor was then flushed three times with ethylene and the desired pressure and temperature was set and the reaction started. After the reaction time, the reaction was stopped by cooling the reactor to -20 °C and excess ethylene vented off. An exact amount of heptane

(0.1 mL) was added as an internal standard and the mixture was analyzed quantitatively by GC. Using the internal standard method equation, the response factors of hexene and octene were as shown in Eq. 6.1.

$$\text{Response Factor (RF)} = (A_x \times A_{is})/(m_x \times m_{is}) \ldots\ldots\ldots\ldots \text{Eq. 6.1}$$

Where A_x = peak area of the analyte

A_{is} = peak area of the internal standard

m_x = mass (or concentration, C_x) of analyte, and

m_{is} = mass (or concentration, C_{is}) of the internal standard

Typically, a solution containing equimolar amounts of hexene (or octene) and heptane (internal standard, 0.1 mL) was prepared and injected into the GC. The percent area ratio of hexene (or octene) with respect to that of heptane was determined and the response factor was calculated as an average of two independent runs. Plots of response factor against alkene (pentene, hexene, heptane, octene, nonene and decene) molecular weight were done and the response factor of butene, not directly measured, was extrapolated from the plot.

6.2.5. Density functional theoretical (DFT) studies

DFT calculations were performed in gas phase to identify the energy-minimized structures based on B3LYP/LANL2DZ.[23-25] The Gaussian09 suite of programs was used for all the computations.[26] The geometries and energies of the complexes were optimized using a split basis set; LANL2DZ for Pd and 6-311G for all other atoms. The structures of the complexes were optimized without symmetry constraints.

6.3. Results and discussion

6.3.1. Syntheses of ligands and complexes

Treatment of the (imino)pyridine ligands **L5, L6, L8** and **L10** (synthesized in Chapter 5) with 5 equivalents of $NaBH_4$ produced the respective (amino)pyridine ligands **L5a**, **L6a**, **L8a** and **L10a** in quantitative yields (Scheme 1).

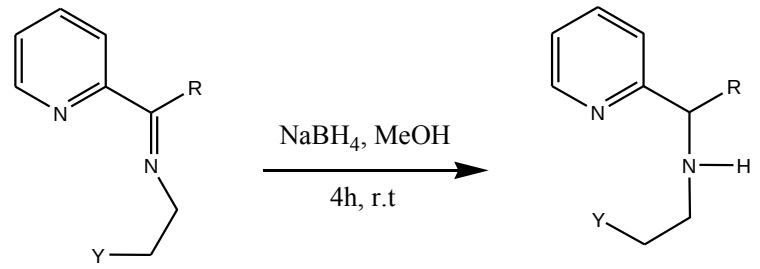

R = Me, Y= OMe, (**L5**)
R = H, Y= OMe, (**L6**)
R = H, Y= NEt_2, (**L8**)
R = H, Y= OH, (**L10**)

R = Me, Y= OMe, (**L5a**)
R = H, Y= OMe, (**L6a**)
R = H, Y= NEt_2, (**L8a**)
R = H, Y= OH, (**L10a**)

Scheme 6.1: Synthesis of (amino)pyridine ligands via reduction of respective imine ligands

The ligands were fully characterized by ^1H NMR, $^{13}C\{^1H\}$ NMR and FT-IR spectroscopy, mass spectrometry and elemental analyses. ^1H NMR spectroscopy was particularly instrumental in the structural elucidation of these amine ligands, and their spectra showed all the signature peaks expected of these reduced compounds. For example, the absence of the imine peak at between 8.31-8.45 ppm and the emergence of new singlets attributed to CH_2 protons at between 3.88-3.93 ppm in the ^1H NMR spectra confirmed successful reduction of the imine ligands to their corresponding amine compounds (Figure 6.1).

The (amino)pyridine ligands **L5a**, **L6a**, **L8a** and **L10a** were also characterized by $^{13}C\{^1H\}$ NMR and all the expected carbon peaks were observed. For example, upon reduction of the imine bond, the signature carbon peak of the $–CH_2-$ group in **L6a** shifted significantly up-field to 54.67

cm^{-1} compared to its corresponding peak of the imine carbon of **L6** (Figure 6.2) which was observed at 163.45 cm^{-1}.

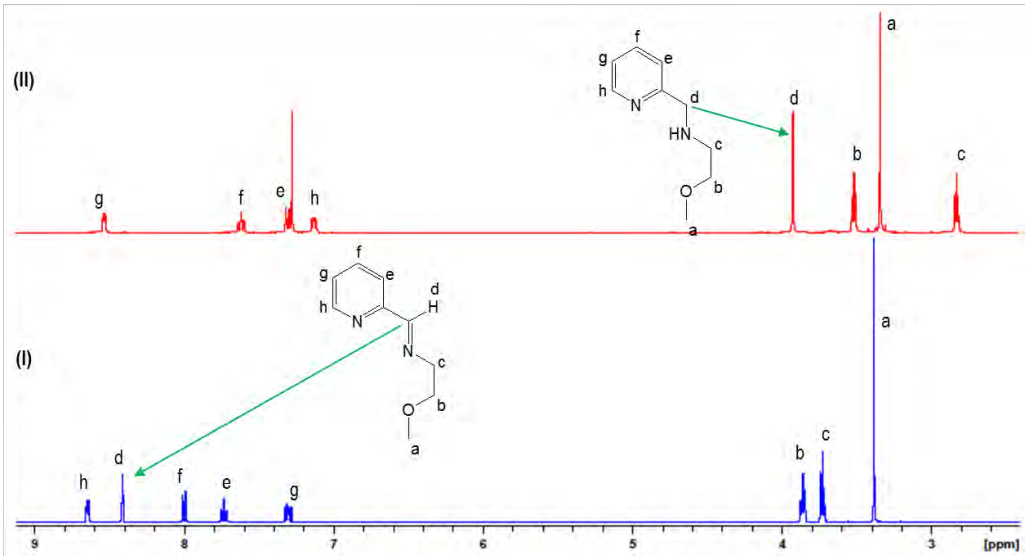

Figure 6.1: ^{1}H NMR spectrum of **L6** (I) and **L6a** (II) showing the shift of signature peaks upon reduction of ligand **L6** to **L6a**.

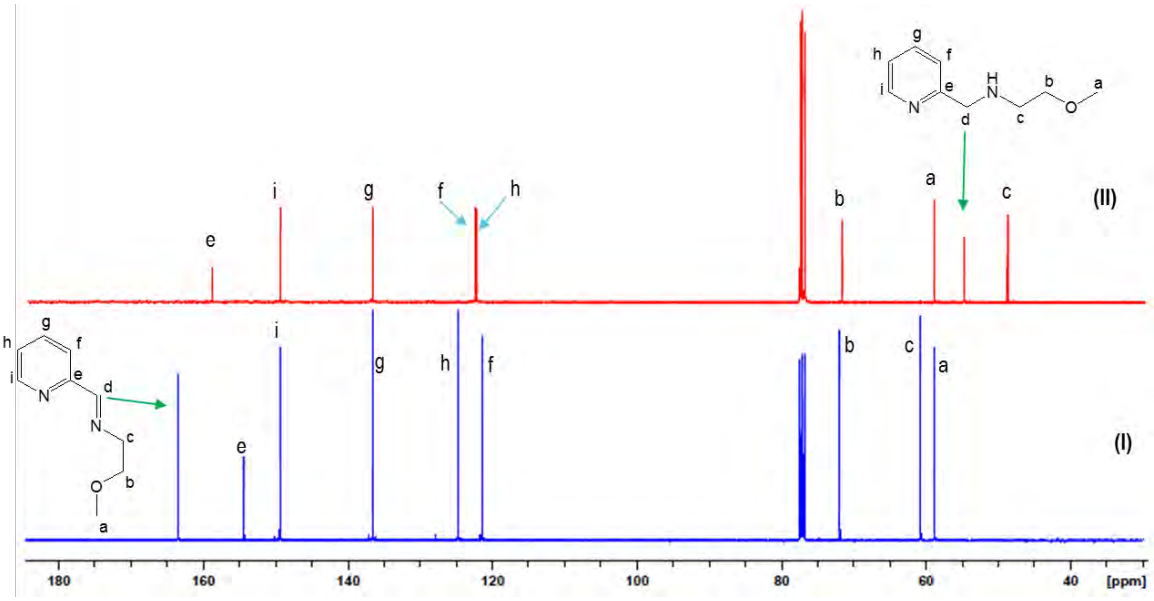

Figure 6.2: $^{13}C\{^{1}H\}$ NMR spectrum of ligands **L6** (I) and **L6a** (II) showing the shift of signature peaks upon reduction of ligand **L6** to **L6a**.

Moreover, IR stretching frequencies between 3278 and 3366 cm^{-1} for these (amino)pyridine ligands were indicative of the formation of secondary amines. Further analysis by mass spectrometry of **L5a**, **L6a**, **L8a** and **L10a** produced molecular ions associated with the formulae in Scheme 6.1. Elemental analyses data were in agreement with the proposed empirical formulae (Scheme 6.1) and confirmed the purity of these ligands.

Reactions of the (amino)pyridine ligands **L5a**, **L6a**, **L8a** and **L10a** with one equiv. of [$NiBr_2$(DME)] (Scheme 6.2) led to the formation of bis(chelated)nickel(II) complexes **18-21**, in good yields (75-83%). The formation of these bis(chelated)nickel(II) complexes could be attributed to thermodynamic stability due to chelate effect resulting from coordination of the second ligand unit.[27, 28] Complex **18** was obtained as a brown solid, complexes **19** and **20** as green solids while complex **21** was obtained as a violet solid. All the complexes **18-21** were hygroscopic.

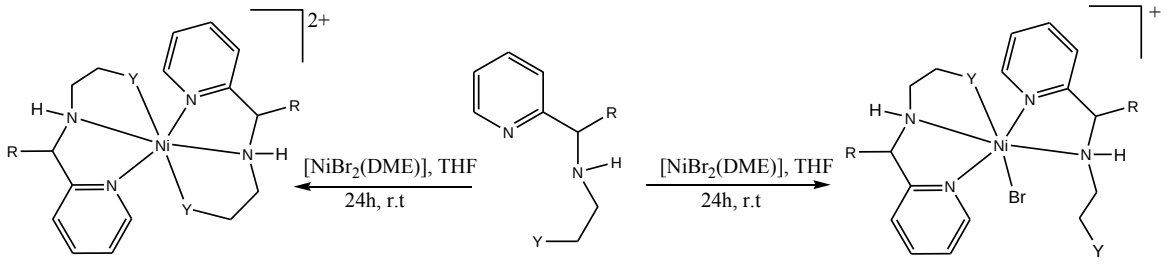

Scheme 6.2: Synthesis of (amino)pyridine nickel(II) complexes

Due to the paramagnetic nature of complexes **18-21**, NMR spectroscopy was not useful in their structural characterization. The complexes were thus characterized by magnetic moment measurements, elemental analyses, mass spectrometry and single crystal X-ray analysis for **19**

and **21**. The magnetic moments of the nickel(II) complexes **18-21** were recorded between 3.70-3.77 BM. These values were effectively higher than the predicted spin only value of 2.83 BM for nickel(II) complexes, but fall within the expected range for high spin nickel(II) complexes of 2.9-4.2 BM[29] when spin orbital contribution is considered.

Mass spectrometry data for all the complexes showed molecular fragmentation patterns that were consistent with the formation of bis(chelated)nickel(II) complexes (Figures 6.3 and 6.4). It is interesting to note that complexes **18-20** showed base peaks containing only one ligand unit; except for complex **21** (m/z = 361) associated with the bis(chelate)nickel(II) complex, and another peak at m/z = 290 [$(M-Br)^+$, 49%] attributed to one ligand unit.

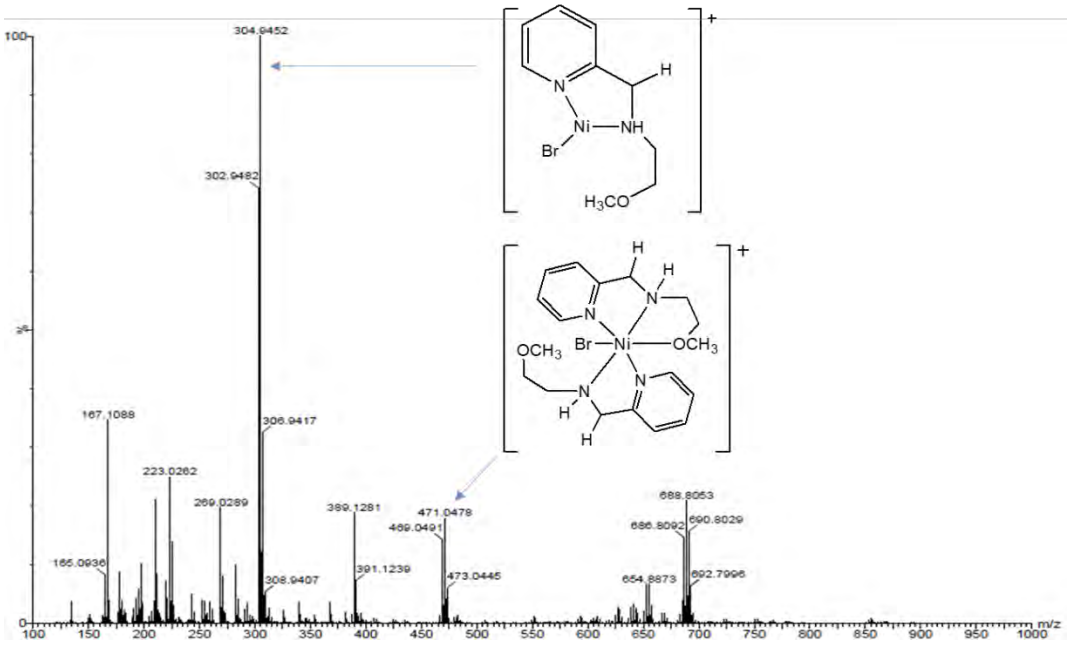

Figure 6.3: Mass spectrum of complex **19** showing base peak at m/z = 304 containing one ligand unit.

Mass spectral data of all the complexes point to possible dissociation of one ligand unit from the bis(chelated)nickel(II) complexes to form mono(chelated)nickel(II) complex species. This could be aided by possible steric strain around the metal centers of these complexes. The observed base peak at m/z = 361 corresponding to the bis(chelated) complex of **21** (Figure 6.4) could be attributed to reduced steric demand of the OH group. In addition, the stronger binding affinity of Ni to OH might also account for the enhanced stability of this bis(chelated) complex.

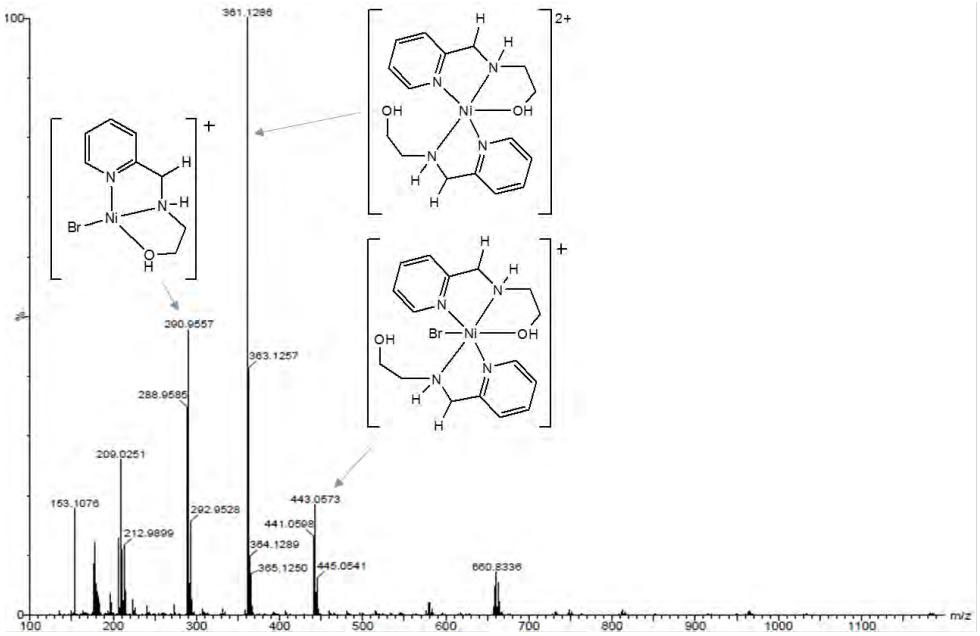

Figure 6.4: Mass spectrum of complex **21** showing a fragment, m/z = 361, associated with the bis(chelate) and m/z = 290 which is attributed to one ligand unit.

The formation of these bis(chelated)nickel(II) complexes was unambiguously proved by the crystal structures of complexes **19** and **21** (Figures 6.5 and 6.6). Furthermore, elemental analyses confirmed the purity and empirical formulae of these complexes, and were consistent with two ligand units per nickel(II) atom as proposed in Scheme 6.2.

6.3.2. Molecular structures of complexes 19 and 21

The solid state structure of compound **19** shows that it is a bis(pyridyl-amine) chelate. Interestingly, the coordination mode of each ligand is not equivalent. The first acts as a tridentate ligand with coordination to the nickel(II) ion through the pyridyl and secondary amine nitrogen as well as the methoxy oxygen atom. The second ligand coordinates in a bidentate manner through the pyridyl and amine nitrogen atoms only. The sixth coordination site is occupied by a bromide ligand, yielding a nominally octahedral coordination geometry. Both the secondary amines coordinated the metal ion without concomitant deprotonation; the chelate is therefore monocationic and was isolated as the bromide complex salt. The asymmetric unit of compound **19** is shown in Figure 6.5. The hydrogen bonding potential of the amine NH groups does not lead to an extended supramolecular structure; both showing direct hydrogen bonding to the bromide counter ion.

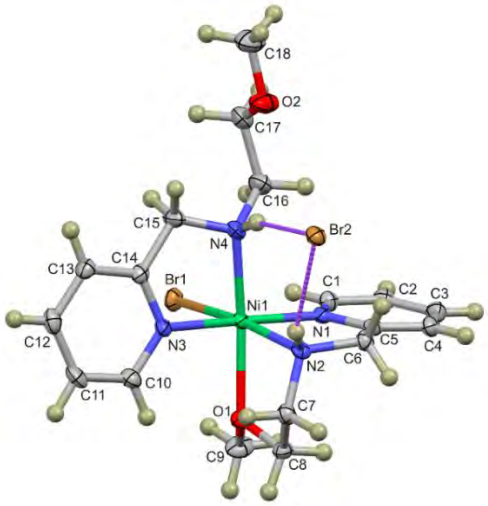

Figure 6.5: Labelled asymmetric unit of compound **19** with thermal ellipsoids rendered at the 50% probability level. The hydrogen atoms have been included as spheres of arbitrary radius. Hydrogen bonds between the two amine N–H groups and bromide ion are indicated as broken purple tubes.

Compound **21** shows an octahedral nickel(II) centre with two tridentate ligands coordinated (Figure 6.6). The secondary amine and hydroxyl units both coordinate without deprotonation. The molecule possesses crystallographically imposed inversion symmetry with the molecule crystallising in the triclinic space group *P*–1 with a single molecule in the unit cell i.e. $Z = 1$. The asymmetric unit of compound **21** comprises a half nickel(II) ion located on an inversion centre with a single (neutral) tridentate ligand coordinated and a single full site occupancy bromide ion and water molecule. The bond parameters describing the octahedral coordination spheres of compounds **19** and **21** are summarised in Table 6.2. The data in Table 6.2 clearly indicate the nominally octahedral geometry of both structures. The bond parameters show that the small bite angle of the ligands, which yield a five-membered chelation ring, are more acute than the ideal angle. Correspondingly, the bond angles which are not constrained by the ligand geometry are more obtuse.

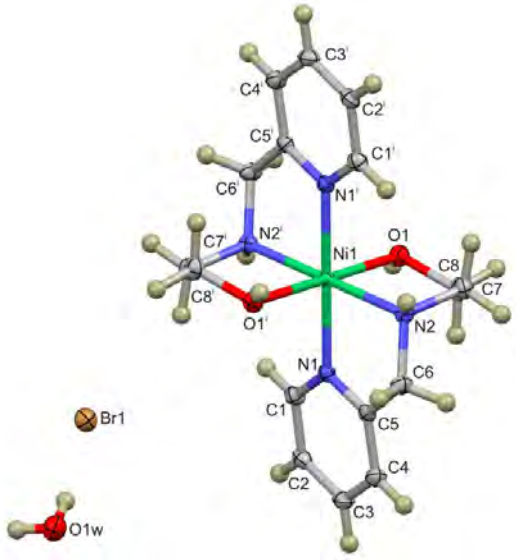

Figure 6.6: Symmetry-completed solid state structure of compound **21** with thermal ellipsoids rendered at the 50% probability level. The hydrogen atoms have been included as spheres of arbitrary radius. Symmetry code: (i) –x, –y, –z.

Table 6.1: Crystal data and structure refinement for complexes **19** and **21**

Parameter	**19**	**21**
Empirical formula	$C_{18}H_{26}Br_2N_4NiO_2$	$C_{16}H_{24}N_4NiO_2 \cdot 2(Br) \cdot 2(H_2O)$
Formula weight	550.97	558.91
Temperature(K)	100(2) K	100(2) K
Wavelength (Å)	0.71073 Å	0.71073 Å
Crystal system	Triclinic	Triclinic
Space group	P-1	P-1
a, b, c (Å)	9.2476(5), 9.8870(6), 12.5210(7)	8.1950(4), 8.3725(4), 8.9081(4)
α, β, γ (°)	92.876(3), 90.579(3), 110.439(4)	109.596(2), 98.327(2), 101.729(2)°
Volume($Å^3$)	1070.92(11)	548.55(5)
Z	2	1
Crystal size (mm)	0.19 × 0.11 × 0.04	0.19 × 0.08 × 004
Density (calculated) (Mg/m^3)	1.709	1.692
Absorption coefficient (mm^{-1})	4.66	4.55
F(000)	556	282
Number of reflections	4168	2119
Goodness-of-fit on F^2	1.13	1.09
R indices (all data)	$R_1 = 0.033$	$R_1 = 0.024$
	$wR_2 = 0.084$	$wR_2 = 0.063$
Largest diff. peak and hole($e.Å^{-3}$)	0.91 and -0.97	0.63 and -0.59

Table 6.2: Summary of the bond lengths (Å) and bond angles (°) describing the coordination spheres of compounds **19** and **21**.

19				**21**			
Bond lengths [Å]		**Angles [º]**		**Bond lengths [Å]**		**Angles [º]**	
Ni1–Br1	2.5394(5)	Br1–Ni1–N1	95.11(8)	Ni1–O1	2.116(2)	N1–Ni1–N2	81.29(7)
Ni1–O1	2.200(2)	N1–Ni1–N2	81.1(1)	Ni1–N1	2.079(3)	N1–Ni1–N2^{i}	98.71(8)
Ni1–N1	2.071(3)	N2–Ni1–N3	95.3(1)	Ni1–N2	2.081(3)	O1–Ni1–O1^{i}	180.0
Ni1–N2	2.112(2)	N3–Ni1–Br1	88.53(8)				
Ni1–N3	2.078(3)	N3–Ni–N4	81.01(1)				
Ni1–N4	2.106(3)	O1–Ni1–N4	169.2(1)				

Symmetry code: (i) –x, –y, –z

The solid state structure of compound **21** exhibits several hydrogen bonds. The bromide ion acts as an H-bond acceptor for three hydrogen bonds between the amine NH and two hydrogen atoms of the water molecule. Additionally, the water acts as an H-bond acceptor for the ligand O–H moiety. The result of this hydrogen bonding pattern is an infinite one-dimensional chain with adjacent metal cations bridged by two water molecules and two bromide ions, as shown in Figure 6.7. The hydrogen bond parameters are summarised in Table 6.3.

Although bond length does not necessarily correlate linearly with bond strength due to packing constraints in the lattice, the hydrogen bonds exhibited by both structure **19** and **21** are significantly shorter than the sum of the van der Waals radii. This, coupled with the fact that hydrogen bond lengths particularly those of compound **21** approach the ideal, suggests that the interactions are likely to be moderately strong.[30]

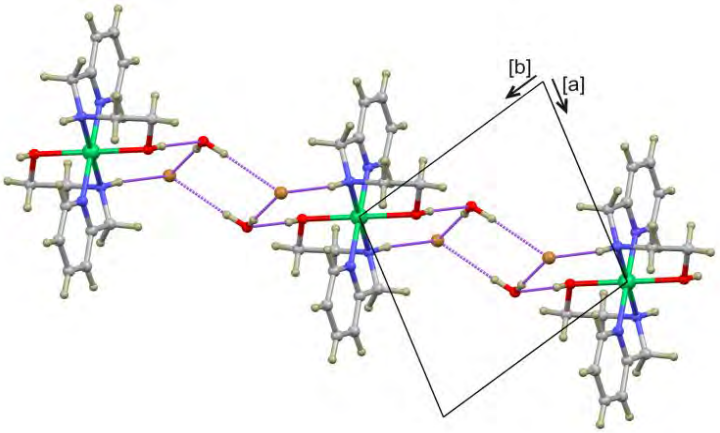

Figure 6.7: Infinite one-dimensional supramolecular structure, of **21**, supported by hydrogen bonds between the amine and hydroxyl moieties of the ligand (H-bond donors), water molecules (H-bond donor and acceptor) and the bromide ion (H-bond acceptor). The supramolecular structure is viewed down the *c*-axis, running transverse to the *ab* plane.

Table 6.3: Summary of the hydrogen bond parameters (Å and °) for compounds **19** and **21**.

	D–H	**H···A**	**D···A**	**D–H···A**
19				
N2–H101···Br2	0.82(4)	2.62(3)	3.360(2)	150(3)
N4–H102···Br2	0.95(4)	2.58(4)	3.501(2)	163(4)
21				
O1–H102···O1w	0.70(3)	1.99(3)	2.680(2)	175(4)
N2–H101···Br1	0.82(2)	2.56(2)	3.363(2)	169(2)
O1w–H1w···Br1	0.85(4)	2.46(4)	3.307(2)	175(4)
O1w–H2w···Br1	0.80(5)	2.48(5)	3.275(2)	172(5)

6.3.3. Ethylene oligomerization reactions

*6.3.3.1 Preliminary evaluation of complexes **18-21** as catalysts in ethylene oligomerization reactions*

Nickel(II) complexes **18-21** were evaluated as pre-catalysts in the oligomerization of ethylene using ethylaluminium dichloride ($EtAlCl_2$) and methylaluminoxane (MAO) as co-catalysts. In both cases, the complexes formed active catalysts in ethylene oligomerization reactions. The results of the oligomerization reactions are summarized in Table 6.4. All the complexes, upon activation with $EtAlCl_2$ or MAO, oligomerized ethylene to afford mainly C_4 and C_6 oligomers as well as some amounts of C_8 oligomers. The identities of these oligomerization products were established by a combination of GC and GC-MS (Figures 6.8 and 6.9).

The observed product distribution by complexes **18-21** is similar to those recently reported by Braunstein and co-workers using nickel(II) complexes chelated by bis(diphenylphosphino)(*N*-thioether)amine-type ligands.[31] In another study, Flapper *et al*.[32] bserved the formation of mainly C_4, and small amounts of C_6 and C_8 using nickel(II) complexes bearing pyridine-phosphine ligands and MAO as a co-catalyst. In contrast to our earlier findings, complexes **18-21** catalyzed ethylene oligomerization reactions using $EtAlCl_2$ co-catalyst to afford mainly butenes and hexenes without subsequent Friedel-Crafts alkylation of these oligomers by toluene solvent.[33-37]

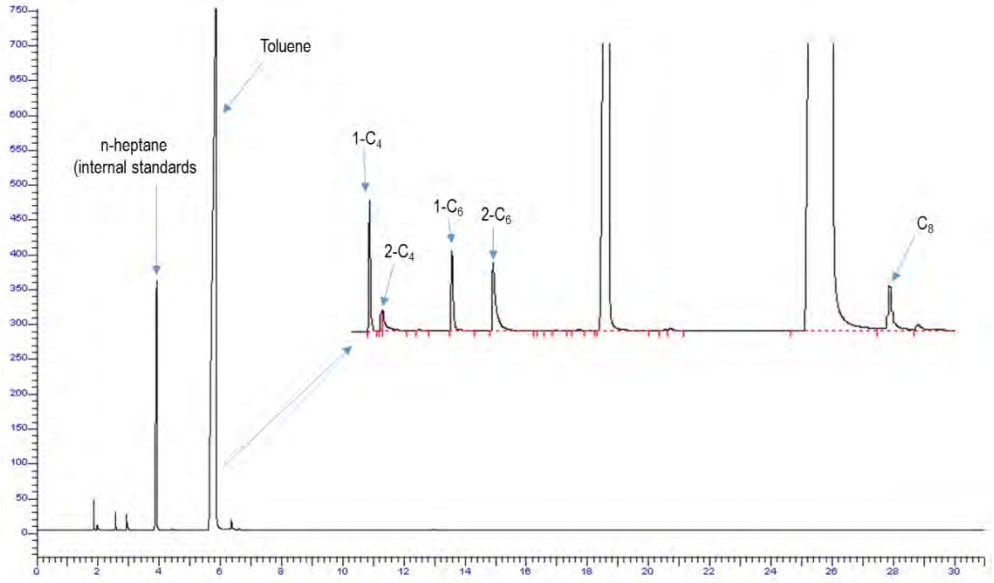

Figure 6.8: Gas chromatogram of products obtained catalyst **20**, Al:Ni ratio of 200:1, temperature = 30 °C, pressure = 10 bar, time = 1 h, solvent = toluene and n-heptane as internal standard, showing isomerization of C_4 and C_6 to internal olefins.

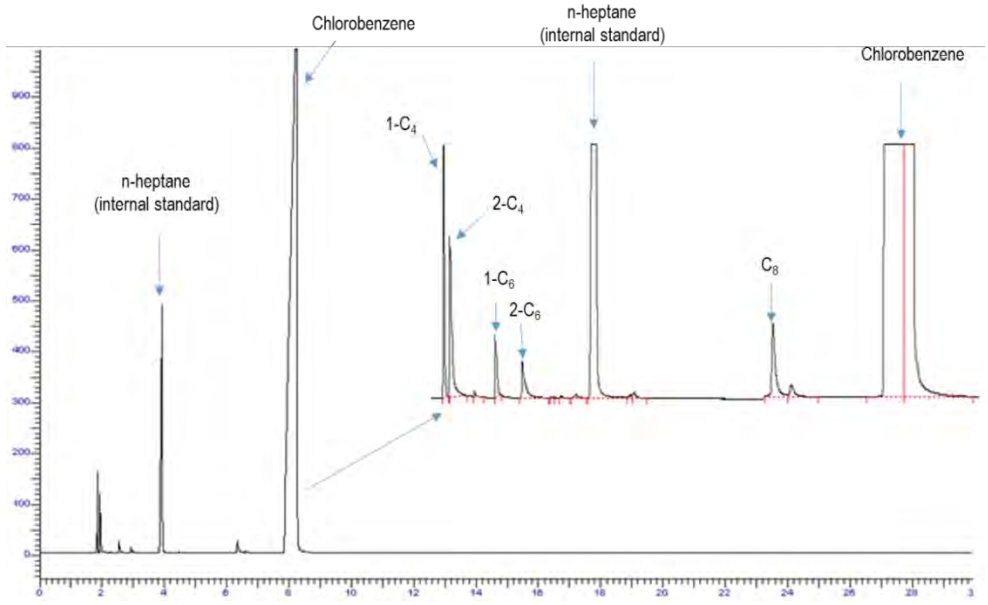

Figure 6.9: Gas chromatogram of products obtained catalyst **19**, Al:Ni ratio of 200:1, temperature = 30 °C, pressure = 10 bar, time = 1 h, solvent = chlorobenzene and n-heptane as internal standard, showing isomerization of C_4 and C_6 to internal olefins.

Table 6.4: Ethylene oligomerization data for **18-21** catalytic systems.[a]

Entry	Catalyst	Cocat.	Al:M	Yield (g)	Activity[b]	%Oligomer distribution[c]				
						C_4	**C_6**	**C_8**	**α-C_4**	**α-C_6**
1	**18**	$EtAlCl_2$	200	10.8	2 160	64	32	4	80	55
2	**19**	$EtAlCl_2$	200	11.9	2 380	61	35	4	72	52
3	**20**	$EtAlCl_2$	200	13.7	2 740	47	44	9	86	56
4	**21**	$EtAlCl_2$	200	9.3	1 860	54	40	6	75	52
5	**18**	MAO	1 000	9.4	1 880	77	15	8	94	56
6	**19**	MAO	1 000	8.5	1 700	74	16	10	88	51
7	**20**	MAO	1 000	11.2	2 240	71	18	11	91	58
8	**21**	MAO	1 000	9.8	1 960	72	18	10	86	56

[a]Reaction conditions: 5 µmol Ni; solvent, toluene, 80 mL; Pressure, 10 bar; Time, 1 h; temperature, 30 °C. [b]In kg oligomer.mol.$^{-1}$Ni.h^{-1}. [c]Determined by GC.

6.3.3.2. Effect of co-catalyst on ethylene oligomerization reactions by ***18-21***

In general, all the complexes exhibited higher catalytic activities upon activation using $EtAlCl_2$ compared to when using MAO. For example, using $EtAlCl_2$ co-catalyst, catalytic activities of up to 2 740 kg oligomer.mol.$^{-1}$Ni.h^{-1} were obtained while using MAO as the co-catalyst gave catalytic activities of up to 2 240 kg oligomer.mol.$^{-1}$Ni.h^{-1}. This observation is in agreement with previous ethylene oligomerization results using MAO and $EtAlCl_2$ activated nickel(II) complexes.[35, 38] This is, however, contrary to the report[39] on nickel(II) phosphinito-oxazoline complexes in which the MAO activated system generated more active catalysts for ethylene oligomerization reactions with activities of up to 2.30×10^5 h^{-1} compared to $EtAlCl_2$'s activities of up to 7.9×10^4 h^{-1}. The observed difference in activity as a function of the nature of co-catalyst may be attributed to the differences in the active species formed during activation using either MAO or $EtAlCl_2$.[40]

The nature of co-catalyst also affected product distribution. For example, activation using MAO displayed good selectivities towards butenes (71-77%) and octenes (8-11%) compared to activation using $EtAlCl_2$ in which the amount of butenes ranged from 47 to 64%. Moreover, the MAO systems exhibited higher selectivity for 1-butene (86-94%) compare to the $EtAlCl_2$ systems that afforded selectivity towards 1-butene in the range of 72 to 86%. In addition, there was marginal improvement on the production of octenes using MAO as co-catalyst (8-11%) compared to the $EtAlCl_2$ activated systems which recorded 4-9%. Change in product distribution due to the nature of co-catalyst has been previously reported for ethylene oligomerization reactions using MAO/$EtAlCl_2$ activated nickel(II) complexes.[41-43]

6.3.3.3. Influence of catalyst structure on ethylene oligomerization reactions

The effect of catalyst structure on the catalytic activities of complexes **18-21** was investigated at 10 bar ethylene pressure and reaction time of 1 h (Table 6.4). From the trend of catalytic activities by both the $EtAlCl_2$ and MAO systems, it is evident that the ligand environment influenced the catalytic performance of these nickel(II) complexes (**18-21**). For example, complex **18**, containing a methyl substituent on the ligand structure exhibited marginally lower catalytic activity of 2 160 kg oligomer.mol.$^{-1}$Ni.h^{-1}, compared to the unsubstituted complex **19** which gave catalytic activity of 2 380 kg oligomer.mol.$^{-1}$Ni.h^{-1} (Table 6.4, entries 1 and 2). A similar trend was also recorded using MAO as a co-catalyst. The electron donating ability of the methyl group in **18** is likely to decrease the positive charge on the nickel(II) metal center, thus limit ethylene coordination.[44-46] Hence, the enhanced catalytic activities of **19** relative to complex **18** could be attributed to greater electrophilicity of nickel(II) center in **19** compared to **18**.

The nature of the pendant donor group on the ligand was also noted to influence the activities of the resultant catalysts. For example, using $EtAlCl_2$ co-catalyst, substitution of a methoxy group in **19** by an amino group (**20**) led to increased catalytic activities from 2 380 kg oligomer.mol.$^{-1}$Ni.h^{-1} to 2 740 kg oligomer.mol.$^{-1}$Ni.h^{-1} respectively. A similar observation was recorded on using MAO as a co-catalyst. This is consistent with similar findings on nickel(II) complexes chelated by imino-imidazole ligands in which substitution of an ether group by an amino group resulted in improved catalytic activity.[38] A stronger coordination of the O to Ni (hard-soft acid base theory) thus slows down the generation of active species, and this would be responsible for this trend. This, consequently, must have limited the rate of ethylene coordination to the metal center in these complexes relative to complex **20**.

6.3.3.4. Effect of co-catalyst concentration and ethylene pressure on ethylene oligomerization reactions

Considering that the $EtAlCl_2$ activated nickel(II) systems catalyzed ethylene oligomerization with higher activity, $EtAlCl_2$ was chosen as the activator to probe the influence of reaction parameters such as Al/Ni ratio, time of the reaction and pressure on the catalytic behavior of complexes **18-21** using complex **19**. The oligomerization results are shown in Table 6.5.

The influence of the $EtAlCl_2$ concentration on the catalyst behavior was studied by varying the Al/Ni ratio from 100 to 300. Activation of nickel(II) pre-catalyst **19** with 100 equiv. of $EtAlCl_2$ gave a lower activity of 1 460 kg oligomer.mol.$^{-1}$Ni.h^{-1}, (Table 6.5, entry 1). This activity increased on using 200 equiv. to 2 380 kg oligomer.mol.$^{-1}$Ni.h^{-1} (entry 2). However, further increase of $EtAlCl_2$ concentration to 300 equiv. led to a reduction in catalytic activity to 2 680 kg oligomer.mol.$^{-1}$Ni.h^{-1}. This behavior has been largely associated with possible deactivation at higher $EtAlCl_2$ concentrations arising from higher amounts of impurities and ash/alumina content.[37]

Variation of Al/Ni ratio also had an effect on the selectivity of oligomers. Increasing the Al/Ni ratio from 100 to 300 resulted in a gradual decrease in C_4 selectivity from 65 to 57%, respectively, and was accompanied by marginal increase in the amount of hexenes produced from 31 to 38%. Moreover, it was observed that increasing the Al/Ni molar ratio from 100 to 300 (Table 6.5, entries 1−4) resulted in an increased of selectivity for 1-butene from 71 to 82%. A similar trend on α-olefin selectivity with increasing Al/Ni ration has previously been reported.[47-49]

Table 6.5: Ethylene oligomerization data for **19** using $EtAlCl_2$ as co-catalyst in toluene.[a]

Entry	Catalyst	Pressure (bar)	Al:Ni	Yield (g)	Activity[b]	%Oligomer distribution[c]				
						C_4	**C_6**	**C_8**	**α-C_4**	**α-C_6**
1	**19**	10	100	7.3	1 460	65	31	4	71	50
2	**19**	10	200	11.9	2 380	61	35	4	72	52
3	**19**	10	250	16.6	3 320	58	37	5	79	47
4	**19**	10	300	13.4	2 680	57	38	5	82	51
5	**19**	5	200	6.5	1 300	58	37	5	69	54
6	**19**	20	200	16.7	3 340	64	33	3	78	53
7	**19**	30	200	21.1	4 220	69	28	3	87	57
8[d]	**19**	10	200	21.5	4 300	77	17	6	54	52
9[d]	**21**	10	200	17.3	3 460	73	16	11	52	48

[a]Reaction conditions: 5 µmol Ni; solvent, toluene, 80 mL; temperature, 30 °C; Time, 1 h. [b]In kg oligomer.mol.$^{-1}$Ni.h^{-1}. [c]Determined by GC. [d]Solvent, chlorobenzene.

Oligomerization experiments using **19**/$EtAlCl_2$ system were conducted under different pressures of ethylene as shown in Table 6.5, entries 2 and 5-7. It was observed that increasing ethylene pressure considerably influenced the catalytic activity and selectivity of complex **19**. As would be expected, increase in pressure led to higher catalytic activity. For example, the activity increased from 1 300 kg oligomer.mol.$^{-1}$Ni.h^{-1} to 4 220 kg oligomer.mol.$^{-1}$Ni.h^{-1} at 5 bar and 30 bar, respectively. This is attributed to increased ethylene concentration in solution and hence higher monomer concentration around the active metal center at higher pressure.[35, 50] Moreover, selectivity for the butene fraction was enhanced with increase in ethylene pressure. For instance, the amount of butene increased from 58 to 69% with increase of pressure from 5 bar to 30 bar, respectively (Table 6.5, entries 5 and 7). Higher selectivity for 1-butene component within the butene fraction was also observed at higher pressures. This enhanced selectivity of α-olefins with increase in ethylene pressure is ascribed to rapid chain transfer relative to chain isomerization.[51-53]

Consistent with earlier reports,[19, 35, 37] reactions conducted in chlorobenzene solvent showed improved catalytic activities (Table 6.5, entries 8 and 9). For example, complex **19** in chlorobenzene recorded a catalytic activity of 4 300 kg oligomer.mol.$^{-1}$Ni.h^{-1}, which was higher compared to a corresponding reaction in toluene solvent (2 380 kg oligomer.mol.$^{-1}$Ni.h^{-1}). A similar trend was observed for complex **21**.

*6.3.3.5. Relative stabilities of complexes **19** and **21***

Catalyst lifetime/stability is a fundamental factor for feasible industrial considerations. Thus, using complexes **19** and **21**, and $EtAlCl_2$ as a co-catalyst, the effect of the reaction time on the catalytic activities of complexes **19** and **21** was investigated between 0.5 h to 2 h (Table 6.6).

Consistent with previous literature reports on nickel(II)-catalyzed ethylene oligomerization reactions,[35, 36, 40, 54, 55] prolonged reaction time resulted in a decrease in the observed catalytic activities. For example, catalytic activities of 1 560 kg oligomer.mol.$^{-1}$Ni.h^{-1} and 2 380 kg oligomer.mol.$^{-1}$Ni.h^{-1} were obtained at 0.5 h and 1 h, respectively, with complex **19**. This translates to an increase in catalytic activity of 53%. Complex **21**, on the other hand, recorded an increase in catalytic activity of 37% under a similar reaction time interval. However, on increasing the reaction period to 2 h, the catalytic activity of complex **19** decreased from 2 380 kg oligomer.mol.$^{-1}$Ni.h^{-1} at 1 h to 1 920 kg oligomer.mol.$^{-1}$Ni.h^{-1}, most likely due to catalyst deactivation. This corresponds to a decrease in catalytic activity of 19%, which is more than that observed for complex **21** of 13%. Thus, the relatively more active complex **19** exhibited lower stability, than complex **21**, over longer reaction times.

Table 6.6: Ethylene oligomerization data for **19** and **21** using $EtAlCl_2$ as co-catalyst in toluene.[a]

Entry	Complex	Time (h)	Yield (g)	Activity[b]
1	**19**	0.5	3.9	1 560
2	**19**	1	11.9	2 380
3	**19**	2	19.2	1 920
4	**21**	0.5	3.4	1 360
5	**21**	1	9.3	1 860
6	**21**	2	16.2	1 620

[a]Reaction conditions: 5 μmol Ni; solvent, toluene, 80 mL; temperature, 30 °C. [b]In kg oligomer.mol.$^{-1}$Ni.h^{-1}

It was also observed that longer reaction times resulted in a slight decline of the selectivity for butenes, varying from 66% (0.5 h) to 56% (2 h), but did not have a significant impact on the selectivity for α-olefins. Furthermore, a slight increase in the amount of C_6 from 30% (0.5 h) to

39% (2 h) was noted, which may be attributed to olefin reincorporation over longer reaction times.

6.3.4. Theoretical calculations of reactivity parameters for complexes 18-21

In order to gain insight into the catalytic trends of complexes **18-21**, DFT studies were performed using a split basis set LANL2DZ for nickel(II) and 6311G(dp) for the remaining atoms. The experimental data from the molecular structures of complexes **19** and **21** (Figures 6.7 and 6.8) were used to validate the data from the calculated geometries. Table 6.7 shows selected bond lengths related to the central nickel atom.

Table 6.7: Comparison of selected bond lengths for crystal structures of complexes **19** and **21** and calculated results

Bond lengths [Å]					
19			**21**		
	Experimental	Theoretical		Experimental	Theoretical
Ni1–Br02	2.5397(9)	ND[a]	**Ni1-N1[i]**	2.0795 (18)	2.0429
Ni1–O1	2.201(2)	2.6529	**Ni1-N1**	2.0795 (18)	2.0427
Ni1–N1	2.077 (3)	1.9411	**Ni1-N2[i]**	2.0818 (19)	2.0475
Ni1–N2	2.116 (2)	2.0214	**Ni1-N2**	2.0818 (19)	2.0473
Ni1–N3	2.077(3)	1.9477	**Ni1-O1[i]**	2.1156 (18)	2.5643
Ni1–N4	2.110(3)	2.0038	**Ni1-O1**	2.1157 (18)	2.5333

[a]The Ni-Br bond length was not determined since the optimized structures were drawn as proposed in Scheme 6.2, without a bromide ligand; and with both methoxy oxygen atoms coordinated to the Ni atom.

Table 6.8 shows the positive net charges of the nickel(II) metal centers of complexes **18-19**, Ni-Y bond lengths, as well as the HOMO-LUMO energy gaps (Δε) between the complexes and ethylene. The HOMO-LUMO energy gaps (Δε) [kcal/mol] were determined from the energy differences between the pre-catalysts' LUMO and ethylene's HOMO.

From the data in Table 6.7, it is evident that the calculated bond lengths were comparable to the experimental values obtained by X-ray crystallography, except for the Ni-O bonds that were longer than those of the crystal structures of both complexes **19** and **21**. Nonetheless, from both the experimental and theoretical data, the average Ni-O bond length in complex **21** was shorter compared to the Ni-O bond length in complex **19**, indicating strong coordination of OH to nickel(II) than OCH_3 to nickel(II).

Table 6.8: Theoretical data for complexes **18-21**

Complex	NBO charge (Ni)	Δε [kcal/mol]	Ni-Y (Å)	Activity[a]
18	1.201	83.10	2.6261	2 160
19	1.210	85.18	2.6529	2 380
20	1.242	84.69	2.8471	2 740
21	1.191	77.78	2.5336	1 860

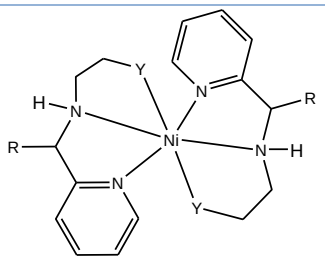

R = Me, Y= OMe, (**18**)
R = H, Y= OMe, (**19**)
R = H, Y= NEt_2, (**20**)
R = H, Y= OH, (**21**)

[a] In units of kg oligomer.mol.$^{-1}$Ni.h^{-1}

In order to investigate the ease of generation of the active species, the relationship between the average Ni-Y bond length and resultant catalytic activities of the complexes was studied. From the DFT results, a general increase in Pd-Y bond length was followed by an increase in catalytic

activity (Table 6.8 and Figure 6.10). For example, increase in Pd-Y bond length from 2.5336 Å (**21**) to 2.8471 Å (**20**) resulted in an increase in the catalytic activity from 1 860 to 2 740 kg oligomer.mol.$^{-1}$Ni.h^{-1}. This trend could be extrapolated to increased possibility of dissociation of one ligand unit in **20** compared to **21**, under ethylene pressure and in the presence of $EtAlCl_2$/MAO. This, thus, facilitates generation of the active species and subsequent coordination of ethylene to the nickel(II) leading to enhanced catalytic activity observed in **20** compared to **19**.

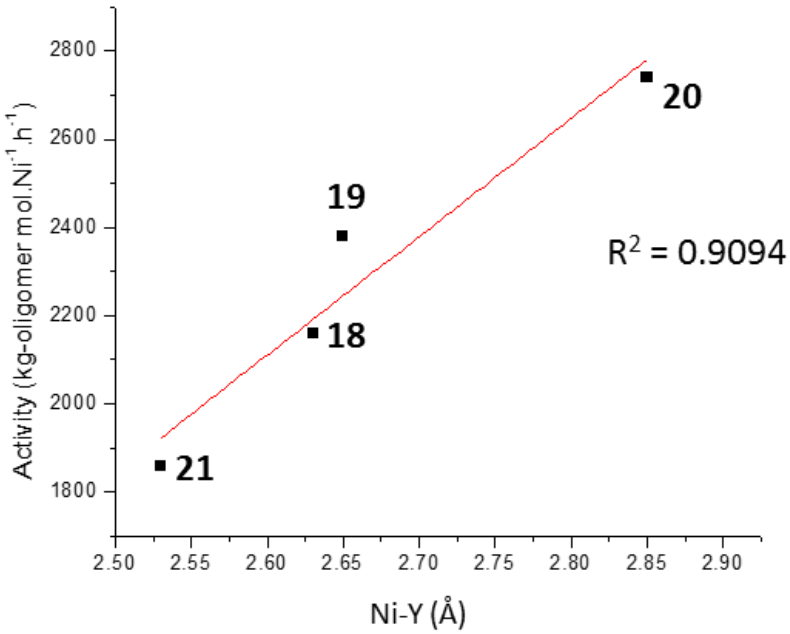

Figure 6.10: Plot of activity in kg oligomer.mol.$^{-1}$Ni.h^{-1} against Ni-Y (Å) depicting a correlation between catalytic activities and Ni-Y bond lengths.

A linear correlation between the NBO charges of the nickel(II) metal center and catalytic activity was also obtained (Figure 6.11). Generally, the catalytic activities increased with higher charge values which could be attributed to enhanced rate of ethylene coordination to the nickel(II) center. Indeed complex **20** exhibited the greatest NBO charge of 1.240 and concomitant highest catalytic activity of 2 740 kg oligomer.mol.$^{-1}$Ni.h^{-1}. This observation is consistent with a recent

report on a series of benzylidenequinolin nickel(II) complex systems whose catalytic activities were shown to increase with higher effective net charge values.[56]

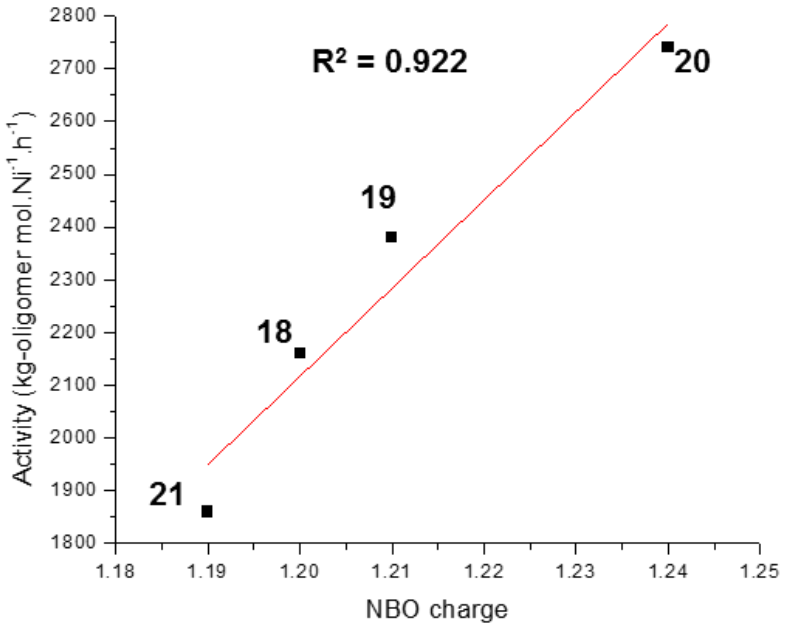

Figure 6.11: Plot of activity (kg oligomer.mol.$^{-1}$Ni.h^{-1}) against NBO charge illustrating the influence of NBO charge on catalytic activity.

HOMO-LUMO energy gaps were also investigated to study their relationships with catalytic activities (Table 6.8). The energy differences between pre-catalysts **18**-**21**'s LUMO and ethylene's HOMO were lower than the energy differences between pre-catalysts **18**-**21**'s HOMO and ethylene's LUMO. This is conceivable given that ethylene oligomerization is considered to be a nucleophilic reaction in which the ethylene monomer attacks the active metal species for electron addition.[56] Thus, the smaller the energy difference between HOMO and LUMO, the more favorable the orbital overlap, which promotes coordination to the metal center. From Figure 6.12, it is evident that the HOMO-LUMO energy gaps did not have a profound effect on the resultant catalytic activities of the complexes due to the weak correlation (R^2 = 0.568) observed. Moreover, the trend recorded contradicts the expected behaviour[57] since the catalytic

activities increased with higher energy gaps (Δε). However, this observation is consistent with a recent report,[56] and would suggest that ethylene coordination to the metal center is not the rate determining step in these ethylene oligomerization reactions.

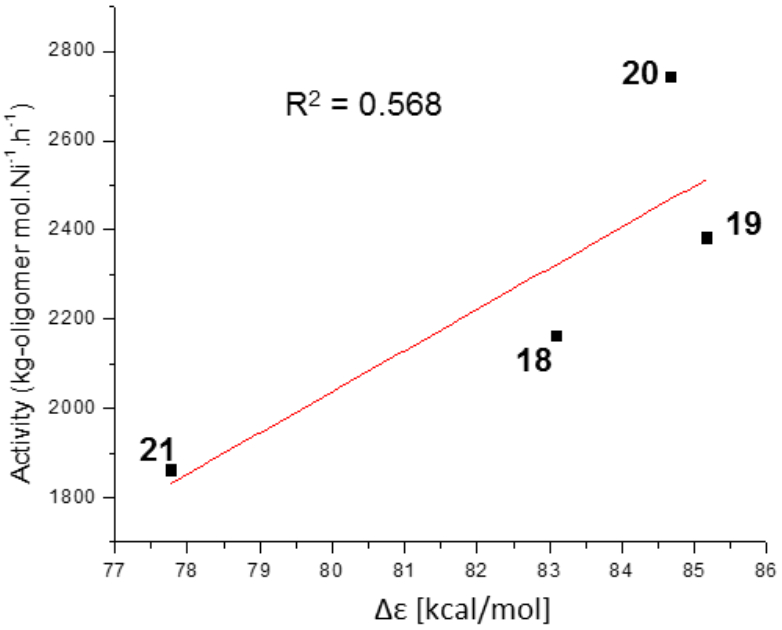

Figure 6.12: Plot of activity (kg oligomer.mol.$^{-1}$Ni.h^{-1}) against HOMO-LUMO energy gap (Δε) [kcal/mol] showing weak relationship between HOMO-LUMO energy gaps (Δε) and catalytic activity.

6.3.5. Postulated mechanism for ethylene oligomerization reactions by complexes 18-21.

Considering the results of these ethylene oligomerization studies and previous reports,[58-62] one possible pathway through which the catalytically active species could have been generated, from the bis(chelate)nickel(II) complexes **18-21**, could have been through the dissociation of the pendant arms (-OCH_3, -OH and -NEt_2) to form hemi-labile systems, as shown in Scheme 6.3. Thus, this dissociation would liberate a coordination site for the incoming ethylene monomer.

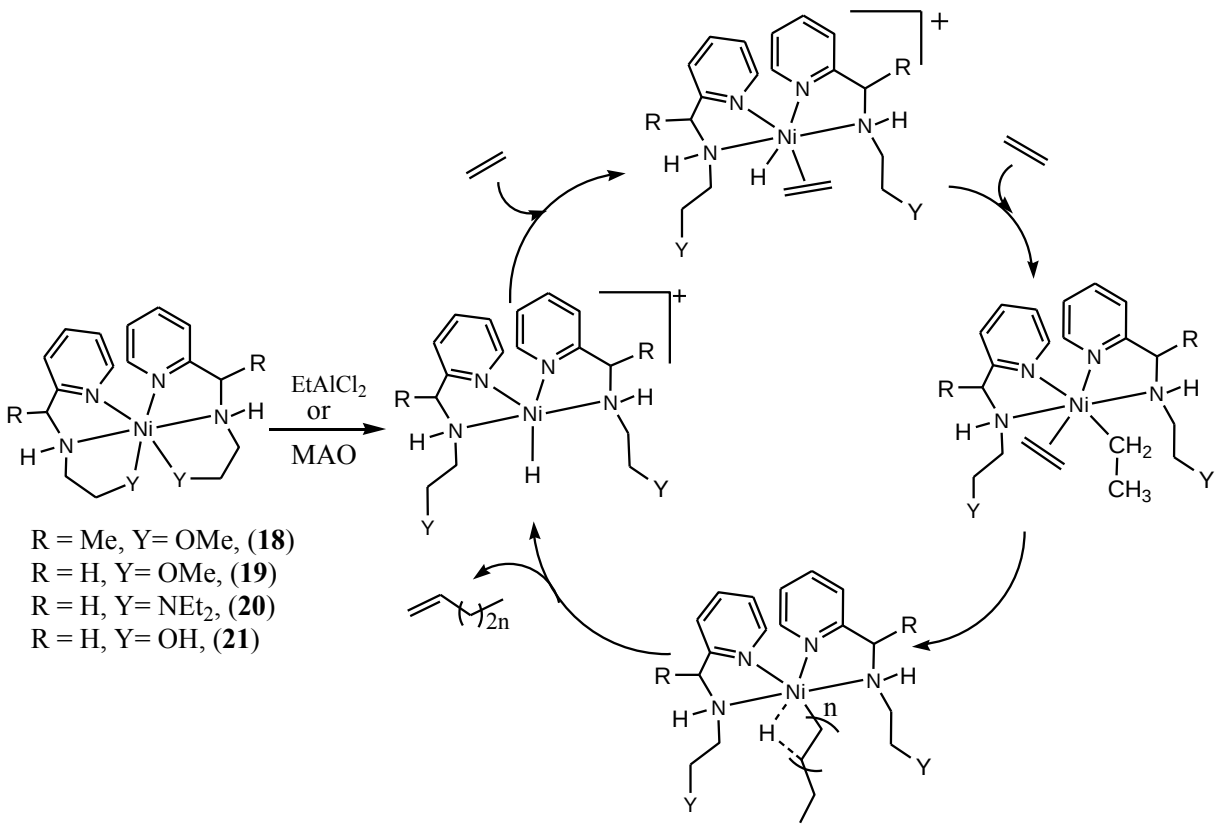

Scheme 6.3: Postulated mechanism for ethylene oligomerization by complexes **18-21**, upon activation with $EtAlCl_2$ or MAO co-catalyst, based on the hemi-lability of the pendant arm of the chelating ligand.

This postulation is supported by the molecular structure of complex **19** (Figure 6.5) in which one pendant arm is non-coordinated, with the sixth coordination position being occupied by a bromine ligand. In addition, the dependency of catalytic activities of complexes **18-21** on the Ni-Y (pendant arm, Y = OCH_3, OH and NEt_2) bond distance supports this activation pathway (Figure 6.10). Thus, a stronger/shorter Ni-Y bond as in complex **21** would result in a less active system (limit dissociation) and *vice versa*, consistent with its low catalytic activity observed in Table 6.8.

However, the mass spectroscopy data of complexes **18-21** point to generation of the active species of these complexes through a different pathway. From the mass spectral data, the complexes generally gave base peaks corresponding to one ligand unit, which shows that the active species of these complexes could be generated through the dissociation of one ligand unit as depicted in Scheme 6.4. This postulated ethylene oligomerization mechanism is in tandem with literature reports[60, 61] for bis(chelate)nickel(II) complexes.

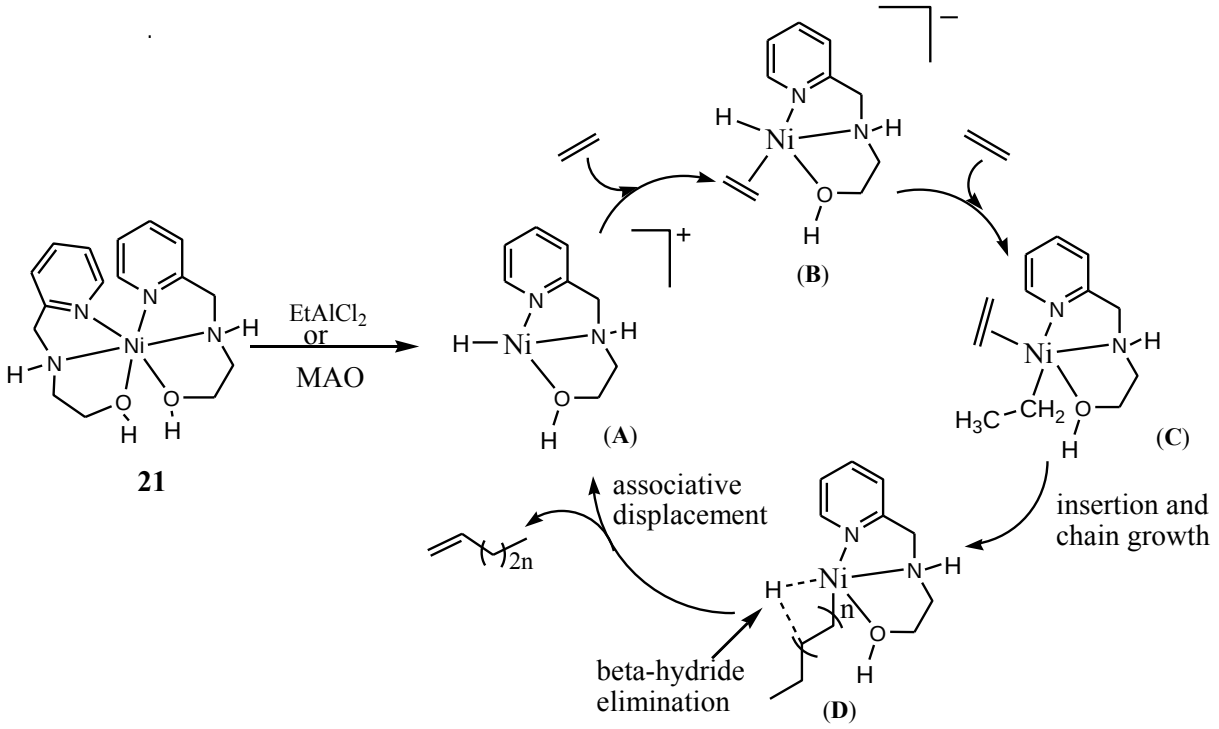

Scheme 6.4: Illustration (using complex **21**) of the possible mechanism for ethylene oligomerization by complexes **18-21** upon activation with $EtAlCl_2$ or MAO co-catalyst

From the mechanism, the active species **A** is generated, for example, by the reaction between complex **21** and $EtAlCl_2$ or MAO co-catalyst. Subsequently, coordination of the ethylene monomer to the nickel(II) metal center propagates the reaction. Thus, in complex **20**, greater

steric strain emanating from two sterically bulky diethylamine groups, could have facilitated easy dissociation of one ligand unit, hence giving the most active catalytic system.

6.4. Conclusions

A series of nickel(II) complexes containing (amino)pyridine ligands with pendant donor groups have been synthesized and structurally characterized. Consistent with elemental analyses data, single crystal X-ray diffraction studies of complexes **19** and **21** confirmed the tridentate coordination mode of the ligands as well as the formation of bis(chelated)nickel(II) complexes. Investigation of the catalytic activities of complexes **18-21** in the presence of $EtAlCl_2$ and MAO showed that they form active catalsyts in oligomerization of ethylene and display high catalytic activities. Activation using $EtAlCl_2$ exhibied higher activity compared to the MAO activated system, affording mainly butenes and hexenes as well as small quantities of octenes. However, the MAO activated systems registered better selectivities for butenes. Theoretical calculations showed a correlation between catalytic activities of complexes **18-21** and NBO charges and Ni-Y bond length. In addition, both the theoretical and mass spectral data point to the generation of the active species through dissociation of one ligand unit rather than through the displacement of the hemi-labile donor atoms.

6.5. References

1. J. Ye, B. Jiang, J. Wang, Y. Yang and Q. Pu, *J. Polym. Sci. Part A: Polym. Chem.*, 2014, **52**, 2748-2759.
2. P.-A. R. Breuil, L. Magna and H. Olivier-Bourbigou, *Catal. Lett.*, 2015, **145**, 173-192.

3. A. Forestière, H. Olivier-Bourbigou and L. Saussine, *Oil Gas Sci. Technol.*, 2009, **64**, 649-667.
4. D. Vogt, in *Applied Homogeneous Catalysis with Organometallic Compounds*, ed. B. C. a. W. A. Herrmann, WILEY-VCH, New York, 1996, vol. 2, ch. 2, pp. 240-252.
5. W. Keim, F. H. Kowaldt, R. Goddard and C. Krüger, *Angew. Chem. Int. Ed.*, 1978, **17**, 466-467.
6. J. Skupinska, *Chem. Rev.*, 1991, **91**, 613-648.
7. G. Mao, Y. Jiang, N. Li, Q. Wang, D. Zheng, M. Li and Y. Ning, *Chin. Sci. Bull.*, 2014, **59**, 2505-2512.
8. S. P. Netalkar, S. Budagumpi, H. H. Abdallah, P. P. Netalkar and V. K. Revankar, *J. Mol. Struct.*, 2014, **1075**, 559-565.
9. Y. Imanishi and N. Naga, *Prog. Polym. Sci.*, 2001, **26**, 1147-1198.
10. G. Wilke, *Angew. Chem. Int. Ed.*, 2003, **42**, 5000-5008.
11. R. Gao, W.-H. Sun and C. Redshaw, *Catal. Sci. Technol.*, 2013, **3**, 1172-1179.
12. W. Keim, A. Behr, B. Limbäcker and C. Krüger, *Angew. Chem. Int. Ed.*, 1983, **22**, 503-503.
13. D. P. Gates, S. A. Svejda, E. Oñate, C. M. Killian, L. K. Johnson, P. S. White and M. Brookhart, *Macromolecules*, 2000, **33**, 2320-2334.
14. L. K. Johnson, C. M. Killian and M. Brookhart, *J. Am. Chem. Soc.*, 1995, **117**, 6414-6415.
15. C. M. Killian, L. K. Johnson and M. Brookhart, *Organometallics*, 1997, **16**, 2005-2007.
16. X. Tang, W.-H. Sun, T. Gao, J. Hou, J. Chen and W. Chen, *J. Organomet. Chem.*, 2005, **690**, 1570-1580.
17. N. Fey, J. N. Harvey, G. C. Lloyd-Jones, P. Murray, A. G. Orpen, R. Osborne and M. Purdie, *Organometallics*, 2008, **27**, 1372-1383.

18. M. K. Ainooson, I. A. Guzei, L. C. Spencer and J. Darkwa, *Polyhedron*, 2013, **53**, 295-303.
19. C. Obuah, B. Omondi, K. Nozaki and J. Darkwa, *J. Mol. Catal. A: Chem.*, 2014, **382**, 31-40.
20. Bruker, APEX2, SAINT and SADABS. Bruker AXS Inc., Madison, Wisconsin, USA, 2012.
21. G. M. Sheldrick, *Acta Crystallogr. Sect. A: Found. Crystallogr.*, 2007, **64**, 112-122.
22. L. J. Farrugia, *Appl. Crystallogr.*, 2012, **45**, 849-854.
23. P. J. Hay and W. R. Wadt, *J. Chem. Phys.*, 1985, **82**, 270-283.
24. A. D. Becke, *J. Chem. Phys.*, 1993, **98**, 5648-5652.
25. C. Lee, W. Yang and R. G. Parr, *Phys. Rev. B*, 1988, **37**, 785-789.
26. M. J. T. Frisch, G. W.; Schlegel, H. B.; Scuseria, G. E.; Robb, M. A.; Cheeseman, J. R.; Scalmani, G.; Barone, V.; Mennucci, B.; Petersson, G. A.; Nakatsuji, H.; Caricato, M.; Li, X.; Hratchian, H. P.; Izmaylov, A. F.; Bloino, J.; Zheng, G.; Sonnenberg, J. L.; Hada, M.; Ehara, M.; Toyota, K.; Fukuda, R.; Hasegawa, J.; Ishida, M.; Nakajima, T.; Honda, Y.; Kitao, O.; Nakai, H.; Vreven, T.; Montgomery Jr., J. A.; Peralta, J. E.; Ogliaro, F.; Bearpark, M.; Heyd, J. J.; Brothers, E.; Kudin, K. N.; Staroverov, V. N.; Kobayashi, R.; Normand, J.; Raghavachari, K.; Rendell, A.; Burant, J. C.; Iyengar, S. S.; Tomasi, J.; Cossi, M.; Rega, N.; Millam, J. M.; Klene, M.; Knox, J. E.; Cross, J. B.; Bakken, V.; Adamo, C.; Jaramillo, J.; Gomperts, R.; Stratmann, R. E.; Yazyev, O.; Austin, A. J.; Cammi, R.; Pomelli, C.; Ochterski, J. W.; Martin, R. L.; Morokuma, K.; Zakrzewski, V. G.; Voth, G. A.; Salvador, P.; Dannenberg, J. J.; Dapprich, S.; Daniels, A. D.; Farkas, O.; Foresman, J. B.; Ortiz, J. V.; Cioslowski, J.; Fox, D. J., *GAUSSIAN 09 Revision A.1), Gaussian, Inc*., Wallingford CT, 2009.
27. F. Basolo and Y. T. Chen, *J. Am. Chem. Soc.*, 1954, **76**, 953-955.

28. F. Basolo and R. K. Murmann, *J. Am. Chem. Soc.*, 1952, **74**, 5243-5246.

29. A. F. Cotton, G. Wilkinson, M. Bochmann and C. A. Murillo, *Advanced inorganic chemistry*, Wiley, 1999.

30. M. P. Akerman and V. A. Chiazzari, *J. Mol. Struct.*, 2014, **1058**, 22-30.

31. A. Ghisolfi, C. Fliedel, V. Rosa, K. Y. Monakhov and P. Braunstein, *Organometallics*, 2014, **33**, 2523-2534.

32. J. Flapper, P. W. van Leeuwen, C. J. Elsevier and P. C. Kamer, *Organometallics*, 2009, **28**, 3264-3271.

33. M. K. Ainooson, S. O. Ojwach, I. A. Guzei, L. C. Spencer and J. Darkwa, *J. Organomet. Chem.*, 2011, **696**, 1528-1535.

34. A. Budhai, B. Omondi, S. O. Ojwach, C. Obuah, E. Y. Osei-Twum and J. Darkwa, *Catal. Sci. Technol.*, 2013, **3**, 3130-3135.

35. G. S. Nyamato, S. O. Ojwach and M. P. Akerman, *J. Mol. Catal. A: Chem.*, 2014, **394**, 274-282.

36. S. O. Ojwach, I. A. Guzei, L. L. Benade, S. F. Mapolie and J. Darkwa, *Organometallics*, 2009, **28**, 2127-2133.

37. G. S. Nyamato, M. G. Alam, S. O. Ojwach and M. P. Akerman, *J. Organomet. Chem.*, 2015, **783**, 64-72.

38. A. Boudier, P.-A. R. Breuil, L. Magna, H. Olivier-Bourbigou and P. Braunstein, *J. Organomet. Chem.*, 2012, **718**, 31-37.

39. P. Chavez, I. G. Rios, A. Kermagoret, R. Pattacini, A. Meli, C. Bianchini, G. Giambastiani and P. Braunstein, *Organometallics*, 2009, **28**, 1776-1784.

40. A. J. Swarts and S. F. Mapolie, *Dalton Trans.*, 2014, **43**, 9892-9900.

41. N. Ajellal, M. C. Kuhn, A. D. Boff, M. Hörner, C. M. Thomas, J.-F. Carpentier and O. L. Casagrande, *Organometallics*, 2006, **25**, 1213-1216.

42. L. L. de Oliveira, R. R. Campedelli, M. C. Kuhn, J.-F. Carpentier and O. L. Casagrande, *J. Mol. Catal. A: Chem.*, 2008, **288**, 58-62.

43. K. Song, H. Gao, F. Liu, J. Pan, L. Guo, S. Zai and Q. Wu, *Eur. J. Inorg. Chem.*, 2009, **2009**, 3016-3024.

44. A. J. Swarts, F. Zheng, V. J. Smith, E. Nordlander and S. F. Mapolie, *Organometallics*, 2014, **33**, 2247-2256.

45. B. Milani, A. Marson, A. Scarel, G. Mestroni, J. M. Ernsting and C. J. Elsevier, *Organometallics*, 2004, **23**, 1974-1977.

46. K. Ohno, A. Nagasawa and T. Fujihara, *Dalton Trans.*, 2015, **44**, 368-376.

47. W. Chai, J. Yu, L. Wang, X. Hu, C. Redshaw and W.-H. Sun, *Inorg. Chim. Acta*, 2012, **385**, 21-26.

48. Q.-s. Shi, X. Hao and C. Redshaw, *Chin. J. Polym. Sci.*, 2013, **31**, 769-777.

49. A. H. Ulbrich, R. R. Campedelli, J. L. S. Milani, J. H. dos Santos and O. d. L. Casagrande, *Appl. Catal. A: Gen.*, 2013, **453**, 280-286.

50. S. Liu, Y. Zhang, Q. Huo, S. He and Y. Han, *J. Spectrosc.*, 2015, **2015,** Article ID 310162, http://dx.doi.org/10.1155/2015/310162.

51. K. R. Birdwhistell and J. Lanza, *J. Chem. Educ.*, 1997, **74**, 579-581.

52. F. Speiser, P. Braunstein and L. Saussine, *Organometallics*, 2004, **23**, 2633-2640.

53. X. Tang, D. Zhang, S. Jie, W.-H. Sun and J. Chen, *J. Organomet. Chem.*, 2005, **690**, 3918-3928.

54. J. Lai, X. Hou, Y. Liu, C. Redshaw and W.-H. Sun, *J. Organomet. Chem.*, 2012, **702**, 52-58.

55. A. H. Ulbrich, A. L. Bergamo and O. d. L. Casagrande, *Catal. Commun.*, 2011, **16**, 245-249.

56. W. Yang, J. Yi and W. H. Sun, *Macromol. Chem. Phys.*, 2015, **216**, 1125-1133.

57. P. Huo, W. Liu, X. He, H. Wang and Y. Chen, *Organometallics*, 2013, **32**, 2291-2299.

58. C. Carlini, M. Isola, V. Liuzzo, A. M. R. Galletti and G. Sbrana, *Appl. Catal. A: Gen.*, 2002, **231**, 307-320.

59. C. Carlini, M. Marchionna, A. M. R. Galletti and G. Sbrana, *Appl. Catal. A: Gen.*, 2001, **206**, 1-12.

60. I. Kim, C. H. Kwak, J. S. Kim and C.-S. Ha, *Appl. Catal. A: Gen.*, 2005, **287**, 98-107.

61. L. Wang, C. Zhang and Z. X. Wang, *Eur. J. Inorg. Chem.*, 2007, **2007**, 2477-2487.

62. S. Wu and S. Lu, *J. Mol. Catal. A: Chem.*, 2003, **198**, 29-38.

CHAPTER 7

General concluding remarks and future prospects

7.1. General conclusions

In summary, this thesis presents the findings of the investigations on nitrogen-donor late transition metal complexes as ethylene oligomerization catalysts. The 2-(chloromethyl)-6-(pyrazol-1-ylmethyl)pyridine ligands (**L1** and **L2**) coordinate to the nickel(II), cobalt(II) and iron(II) metal centers in a bidentate manner giving rise to monometallic compounds. The 2-(chloromethyl)-6-(pyrazol-1-ylmethyl)pyridine nickel(II), cobalt(II) and iron(II) complexes **1-6** form active catalysts in ethylene oligomerization reactions when activated with either $EtAlCl_2$ or methylaluminoxane (MAO) as co-catalysts. The catalysts formed ethylene oligomers and Friedel-Crafts alkylated products depending on the co-catalyst and solvent used. While activation with $EtAlCl_2$ in toluene produce Friedel-Crafts toluene-alkylated products, the use of hexane and chlorobenzene give predominantly C_4 and C_6 oligomers. On the other hand, activation with MAO in toluene results in the formation of mainly C_4, C_6 and C_8 oligomers. The catalytic behaviour of these pre-catalysts is influenced by the complex structure and reaction conditions such as co-catalyst/complex ratio, time and pressure.

In Chapter 4, the N^N^O (pyrazolyl)-(phosphinoyl)pyridine ligands (**L3** and **L4**) used produced tridentate nickel(II), cobalt(II) and iron(II) complexes (**7-12**). Complexes **7-12** form active catalysts in ethylene oligomerization reactions upon activation with $EtAlCl_2$, methylaluminoxane (MAO) or trimethylaluminium ($AlMe_3$) as co-catalysts to produce C_4 as the

major product as well as C_6 and C_8 oligomers. The nature of solvent and co-catalyst significantly affected both the catalytic activities and product compositions of these catalysts.

In Chapter 5, a series of (imino)pyridine ligands (**L5-L9**) were used which coordinated to the palladium(II) metal centers in bidentate modes, forming monometallic complexes (**13-17**). Treatment of the neutral complexes **13-17** with one molar equivalent of $NaBAr_4$ led to *in situ* formation of the corresponding cationic compounds **13a-17a**. In the presence of ethylene, the neutral and cationic palladium(II) complexes exhibited modest catalytic activities in selective ethylene dimerization producing mainly butenes. The catalytic activities of the complexes were largely controlled by the ligand architecture and the pedant arms in the complexes allowed for coordination of the incoming ethylene monomer. From DFT calculations, the possible competition for coordination to the palladium(II) metal center between the ethylene monomer and the pendant moieties in the ligand framework controlled the catalytic activities of these systems.

Chapter 6 deals with attempts to circumvent hydrolysis of the (imino)pyridine ligands discussed in Chapter 5, when used to prepare their nickel(II) complexes, by reducing the imine ligands to their analogous amine compounds. The new (amino)pyridine ligands **L5a**, **L6a**, **L8a** and **L10a** coordinate to the nickel(II) metal center in a tridentate fashion, forming bis(chelated)nickel(II) complexes (**18-21**). All the nickel(II) complexes showed good catalytic activities towards ethylene oligomerization producing mostly C_4, and significant amounts of C_6 as well as trace amounts of C_8. These bis(chelate)nickel(II) complexes catalyzed ethylene oligomerization to butenes and hexenes without subsequent Friedel-Craft's alkylation of the preformed butenes and

hexenes to the toluene used as solvent, upon activation with $EtAlCl_2$ co-catalyst, contrary to the findings in Chapters 3 and 4.

7.2. Summary

The current work has demonstrated the role of ligand, metal center and nature of solvent in controlling the catalytic performance of late transition metal catalysts. In summary:-

i. Nickel(II) complexes exhibited higher catalytic activities than their corresponding iron(II) and cobalt(II) analogues.

ii. (Pyrazolyl)pyridine based complexes favored Friedel-Crafts alkylation of the pre-formed oligomers to toluene solvent, upon activation using $EtAlCl_2$, while (amino)pyridine containing systems formed exclusively oligomers.

iii. The nature of the solvent employed also controlled the catalytic activities and product distributions of these ethylene oligomerization reactions.

iv. (Amino)pyridine nickel(II) complexes generated highly active catalysts for ethylene oligomerization compared to their corresponding (imino)pyridine palladium(II) complexes.

v. Electronic properties of the ligand structure affected the electrostatic charge distribution of the metal centers, and ultimately had significant effect on the respective catalytic

activities. Catalytic activities increased with increasing effective net positive charge of the metal centers.

7.3. Future prospects

The findings of this study have significantly contributed towards the design and synthesis of active ethylene oligomerization catalysts. For example, the (amino)pyridine nickel(II) complexes studied in Chapter 6 showed great promise as homogeneous ethylene oligomerization catalysts. However, with regard to green chemistry principles such as organic solvents free processes, ease of separation of reaction medium, heterogeneous catalysis offers an attractive alternative. Thus, it would be interesting to extend the study of these (amino)pyridine nickel(II) catalysts to heterogeneous systems by use of supports such as MCM-41.

MCM-41 is a mesoporous material that has an ordered array of uniform channels, high surface area, thermal and chemical stability, and shape selectivity that belongs to a family called M41S discovered by scientists at Mobil in the 1990s. By synthesizing the nickel(II) complexes (Figure 7.1) with silanol groups (CPTMS and CPTES), for anchoring via covalent bonding, it would be of interest to investigate the potential of developing new(amino)pyridine nickel(II) heterogenized on mesoporous materials via anchoring with covalent bonds between the MCM-41 mesoporous support and the nickel(II) complexes.

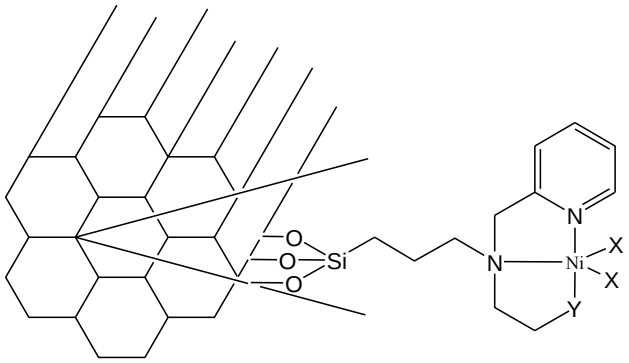

Mesoporous support

Y= OMe, NEt_2, OH
X = Br, Cl

Figure 7.1: Heterogeneous nickel(II) complexes

Moreover, considering the crucial role played by the ligand architecture, different ligand designs will be employed in the syntheses of the target pre-catalysts. For example, Scheme 7.1 illustrates a synthetic route for some of the heterogeneous nickel(II) and palladium(II) complexes that would be investigated as catalysts in ethylene oligomerization reactions.

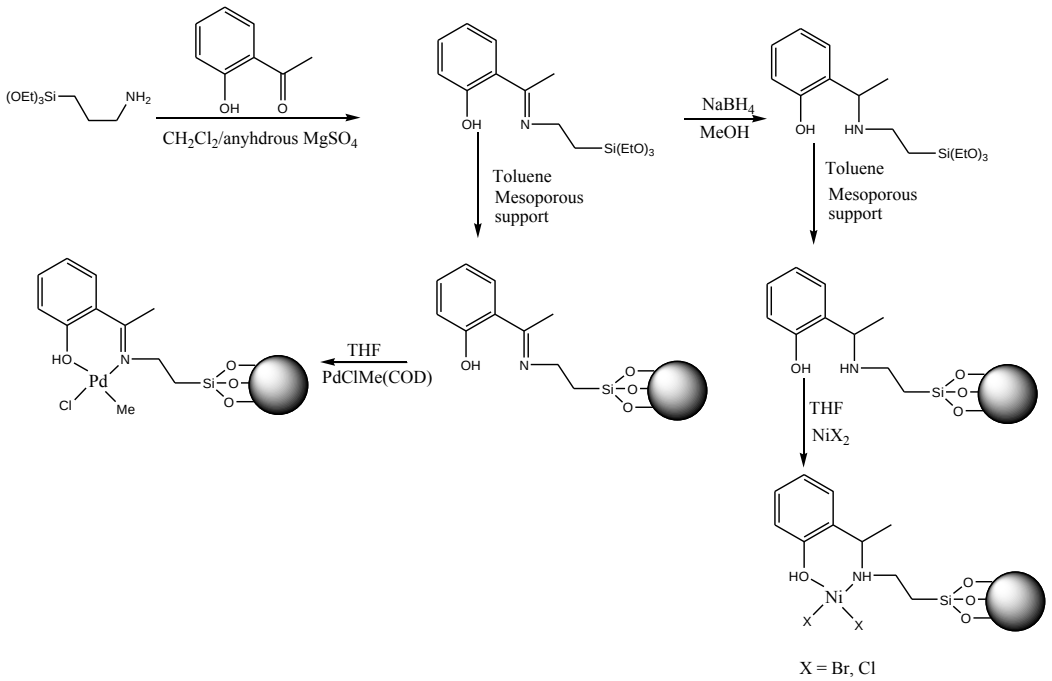

Scheme 7.1: Syntheses of heterogeneous nickel(II) and palladium(II) complexes based on N^O chelating agent